# Three Studies in Numerical Methods for Statistical Approximations

---

A thesis
submitted in partial fulfilment
of the requirements for the
Degree of
Doctor of Philosophy
in Statistics
by
Robert Ware

---

University of Canterbury

2003

# Contents

# Chapter 1

# Introduction

An explosive advance of numerical analysis techniques in recent years has paralleled the rapid increase and accessibility of computing power. This is not a coincidence. Many techniques that previously had been theoretical are now able to be applied. The most well-known of these is probably the Metropolis-Hastings algorithm which, although conceived in 1953, has only recently become practically applicable.

Numerical methods are required because it is not always possible to derive explicit probabilistic models and analytically compute their associated estimators. Two major classes of numerical problems that arise in statistical inference are optimisation problems and integration problems. Optimisation problems involve determining the 'best' solutions to mathematically defined problems. Integration problems involve obtaining a numerical approximation of an integral, for cases when the integral cannot be found explicitly. Optimisation is generally associated with the likelihood approach and integration with the Bayesian approach, although these are not strict classifications. Bootstrap methods, for example, are concerned with the integration of marginal distributions, but are not Bayesian methods. The statistical techniques that we shall be primarily concerned with are Bayesian methods and the inferences that can be drawn from their use. The approaches we shall focus on are customarily associated with integration problems. In two of the three parts of this thesis we shall focus on the fact that continuous statistical models are always only approximations for measurement processes that are necessarily discrete.

Numerical integration procedures provide almost unlimited scope for realistic statistical modelling. Until recently, acknowledging the full complexity and structure

in many statistical problems was difficult, and often resulted in the development of specific methodology and purpose-built software. The alternative was to formulate the problem in the, often over-simple, framework of an available method. Modern integration techniques provide a unifying framework within which many complex problems can be analysed using standard computer programs.

Recent numerical developments have unified researchers in all branches of applied statistics. Because traditional methods of analysis are not readily adaptable to all settings, researchers in individual disciplines have often developed original approaches for model fitting that are customised for their own problems. For example, the Metropolis-Hastings algorithm originated in the field of mechanical physics.

This Thesis is split into three main Chapters; each is concerned with some branch of numerical approximation. Chapter 2 considers how to calculate the probability that the sum of the product of variables assessed with a Normal distribution is negative. The analysis was motivated by a specific problem in electrical engineering. To resolve the problem, two distinct steps are required. First, we consider ways in which we can assess the distribution for the product of two Normally distributed variables. Three different methods are compared: a numerical methods approximation, which involves implementing a numerical integration procedure on MATLAB, a Monte Carlo construction and an approximation to the analytic result using the Normal distribution. The second step considers how to assess the distribution for the sum of the products of two Normally distributed variables by applying the Convolution Formula. To conclude Chapter 2 the two steps are combined to compute the distribution for the sum of products of Normally distributed variables, and thus to calculate the probability that this sum of products is negative. The problem is also approached directly, using a Monte Carlo approximation.

Chapter 3 investigates how well continuous conjugate theory can approximate real discrete mass functions in various measurement settings. All statistical measurements which represent the values of useful unknown quantities have a realm that is both finite and discrete. Thus our uncertainties about any measurement can be represented by discrete probability mass functions. Nonetheless, common statistical practice treats probability distributions as representable by continuous densities or mixture densities. Many statistical problems involve the analysis of sequences of

observations that the researcher regards exchangeably. Often we wish to find a joint probability mass function over $X_1, X_2, \ldots, X_n$, with interim interest in the sequence of updated probability mass functions $f(x_{i+1} \mid \mathbf{X}_i = \mathbf{x}_i)$ for $i = 1, 2, \ldots, n-1$.

We examine how well digital Normal mass functions and digital parametric mixtures are approximated by continuous Mixture Normal and Normal-Gamma Mixture Normal distributions for such items as $E(X_{i+1} \mid \mathbf{X}_i = \mathbf{x}_i)$ and $V(X_{i+1} \mid \mathbf{X}_i = \mathbf{x}_i)$. Digital mass functions are generated by specifying a finite realm of measurements for a quantity of interest, finding a density value of some specified function at each point, and then normalising the densities over the realm to generate mass values. Both a digitised prior mixing mass function and digitised information transfer function are generated and used, via Bayes' Theorem, to compute posterior mass functions. Approximating posterior densities using continuous conjugate theory are evaluated, and the two sets of results compared. The main achievement of this Chapter is to formalise a computing strategy that can be applied to many functional forms. An example is provided in the next Chapter

In Chapter 4 different approaches to flood frequency analysis are considered, with particular emphasis on estimating extreme hydrological events for a site, or group of sites. Flood risk has been the topic of a considerable number of publications over the last twenty years, yet there is still no consensus on how best to proceed. The problem is complicated by the need to estimate flood risk for return periods that exceed the length of observed record. Consequently much research has focused on methods emphasising data pooling. Chapter 4 begins with an examination of different frequentist approaches to flood estimation. We study at-site and regional estimates, and compare their accuracy and precision. Next, we assess flood exceedance quantiles using updated mixture mass functions as sequential forecasting distributions. These sequential forecasts are scored using three different scoring rules for distributions: the quadratic, logarithmic and spherical. The digital updating procedure is based on the work developed in Chapter 3. Both the frequentist methods and the digital forecasting procedures are applied to data collected from the Waimakariri River in Canterbury, New Zealand. We complete the Chapter by comparing the appropriateness of the frequentist and digital methods. It is found that the mixture distributions computed via the discrete digital method provide

much more uniform forecasts across an array of proposed distribution families than do the frequentist forecasting methods.

Before proceeding to the main body of work, we shall briefly introduce three different categories of numerical integration algorithms: non-Monte Carlo methods, non-iterative Monte Carlo methods and iterative Monte Carlo methods. Finally, the application of different methods of numerical approximation to the work contained in this Thesis will be discussed.

Numerical integration algorithms approximate the generation of random variables from a posterior distribution when this distribution cannot be directly computed. Non-Monte Carlo methods of numerical integration consist of algorithms based on Simpson's method. They do not require the input of a stream of (pseudo) random numbers. Whereas algorithms based on Simpson's method evaluate a function for a sequence of equally spaced points, Monte Carlo methods are types of numerical integration based on repeated simulations. Non-iterative Monte Carlo methods, also known as traditional Monte Carlo methods, are algorithms that require a stream of (pseudo) random numbers as input and produce a sample from the posterior density as output. Examples include importance sampling and accept-reject methods. Iterative Monte Carlo methods, or Markov chain Monte Carlo (MCMC) methods, are algorithms that require a random input stream and also require iteration to realise a sample from the posterior distribution of interest. Examples include the Gibbs sampling algorithm and the Metropolis-Hastings (M-H) algorithm.

Before we consider the differences between these three categories, we shall briefly introduce the Bayesian paradigm, illustrating the vital role of integration.

## 1.1 Bayesian Theory

Bayesian statistical theory is by now well developed and readily accepted by the scientific community, with many finding the Bayesian paradigm conceptually appealing. However, the need to evaluate often analytically intractable posterior integrals means that Bayesian methods are either avoided completely, reduced to simple assumptions (often unrealistically) or solved using sophisticated numerical integration

techniques. In recent years the availability of comparatively inexpensive, progressively faster computers has rapidly increased the popularity of computer-intensive statistical methods.

The key element of Bayesian inference is the distribution of $\theta$ conditional on observed data $x$, denoted $\pi(\theta \mid x)$ and called the posterior density. Suppose a sequence of data values is assessed with a mixture distribution through a conditional density $X \mid \theta \sim f(x \mid \theta)$, where $\theta \in \Theta$ is a mixing parameter. Bayes' Theorem relates prior information, specified as a prior distribution with density $\pi(\theta)$, to $\pi(\theta \mid x)$ by

$$\pi(\theta \mid x) = \frac{f(x \mid \theta)\pi(\theta)}{\int_\Theta f(x \mid \theta)\pi(\theta)\, d\theta}. \tag{1.1}$$

In other words $\pi(\theta)$ is updated to $\pi(\theta \mid x)$ through $f(x \mid \theta)$. Since the work of Fisher (1925) the function $f(x \mid \theta)$, considered as a function of $\theta$ from a specific observed value $x$, has been called the "likelihood function". In this thesis we shall often refer to it as the "information transfer function", to highlight its role in transferring information from an observation to forecasts of subsequent observations via Equation 1.1.

Bayesian inference, that is finding the posterior mean/variance, point estimates, is based on

$$E[m(\theta \mid x)] = \int_\Theta m(\theta)\pi(\theta \mid x) d\theta, \tag{1.2}$$

for suitable choices of $m(\cdot)$. This requires us to first obtain $\pi(\theta \mid x)$, which is often not available in closed form. A commonly desired density is $f(x_{i+1} \mid \mathbf{X}_i = \mathbf{x}_i) = \int_\Theta f(x_{i+1} \mid \theta, \mathbf{X}_i = \mathbf{x}_i)\pi(\theta \mid \mathbf{X}_i = \mathbf{x}_i)\, d\theta$, the updated predictive density for $X_{i+1}$ given observations $\mathbf{X}_i = \mathbf{x}_i$. The integration over all the parameters is often either very difficult, or impossible.

For a long time the computational drawback of the Bayesian approach was so great that it was rarely used. When it was used the favoured types of priors in Bayesian modelling were those allowing explicit computations, called conjugate priors. These are prior distributions for which the corresponding posterior distributions are members of the original prior family. Consequently the posterior density is found by simply updating parameters. Robert (2001) lists a series of conjugate priors for common sub-families within the exponential family.

The advent of powerful and accessible computing methods means that researchers do not need the rigid structures previously imposed by the need for analytical processing. Thus a researcher does not have to make a choice between describing an accurate model of a phenomenon, which often prevents the computation of explicit answers, or choosing a standard model which allows explicit computation, but may compromise the usefulness of the Bayesian inference.

As a result of the increased accessibility of Bayesian methods, the number of user-friendly, Bayesian software packages has blossomed. As yet there is no single, general purpose package, instead we have a number of packages designed for use in particular scenarios. Berger (2000) has compiled a list of available Bayesian software. As Bayesian software continues to develop, the advance of Bayesian methods into applied disciplines can be expected to continue apace.

## 1.2 Methods of Numerical Integration

### 1.2.1 Non-Monte Carlo Methods

Many approaches have been suggested to approximate integrals analytically. One of the simplest is Simpson's method, which approximates

$$I = \int_a^b h(\theta) d\theta \tag{1.3}$$

by splitting the domain of the integral into an even number of intervals and then using parabolic curves to approximate each successive pair of subintervals separately. The sum of these approximations serves as an estimate of the required integral. Simpson's rule is

$$\hat{I} = \frac{\delta}{3}\left\{h(a) + 4\sum_{i=1}^{n} h(\theta_{2i-1}) + 2\sum_{i=1}^{n} h(\theta_{2i}) + h(b)\right\}, \tag{1.4}$$

where the $\theta_i$'s constitute an ordered partition of $[a, b]$ and there are a number of equally spaced samples with $(\theta_{i+1} - \theta_i) = \delta$.

Numerous variants of Simpson's rule have been proposed, as have methods using orthogonal polynomials or splines. However, it seems that whichever numerical integration method is used, the accuracy dramatically decreases as the dimension of $\Theta$ increases. The error associated with numerical methods evolves as a power of the

dimension of $\Theta$, mainly because the size of the part of the space irrelevant for the computation of a given integral grows considerably with the dimension of the space. Although numerical integration methods keep improving over the years, an empirical rule of thumb is that most standard methods should not be used for integration in dimensions larger than four. The current state of numerical integration, as it pertains to Bayesian statistics, is discussed in Monahan and Genz (1996).

### 1.2.2 Non-iterative Monte Carlo Methods

Just as we can generate a sample from a given density, if we are given a sample we can approximately recreate that density. Non-iterative, or traditional, Monte Carlo integration draws samples from the required distribution and then forms sample averages to approximate expectations. Monte Carlo methods emerged at the time of the first computer. They are not operational without a computer, and correspond to some of the first computer programs written. A classic reference describing the problems of the day is *A Million Random Digits with 100,000 Normal Deviates* produced by the Rand Corporation (1955). There are a large number of different non-iterative Monte Carlo algorithms used to simulate values from the required, or target, density. To give a flavour of non-iterative Monte Carlo integration methods, we shall consider two of them, the traditional Monte Carlo integration method and importance sampling. Other well-known non-iterative Monte Carlo methods include the bootstrap and accept-reject methods.

#### Traditional Monte Carlo Integration

Consider the problem of evaluating the integral

$$\int_{\Theta} g(\theta) f(x \mid \theta) \pi(\theta) d\theta. \tag{1.5}$$

The Monte Carlo method, proposed by Metropolis and Ulam (1949) and von Neumann (1951), says that if random variables $\theta_1, \ldots, \theta_n$ can be generated from $\pi(\theta)$, the average

$$\frac{1}{n} \sum_{i=1}^{n} g(\theta_i) f(x \mid \theta_i) \tag{1.6}$$

converges almost surely to Expression 1.5 as $n \to \infty$, by the Strong Law of Large Numbers.

Similarly, since $f(x \mid \theta)\pi(\theta)$ is proportional to $\pi(\theta \mid x)$, if an *i.i.d.* sample of $\theta_i$'s can be generated from this density, then the average

$$\frac{1}{n}\sum_{i=1}^{n} g(\theta_i) \tag{1.7}$$

converges to

$$\frac{\int_\Theta g(\theta)f(x \mid \theta)\pi(\theta)d\theta}{\int_\Theta f(x \mid \theta)\pi(\theta)d\theta}. \tag{1.8}$$

To implement a Monte Carlo integration we must generate a large number of $\theta_i$ samples. This is achieved using a pseudo-random number generator from a computer. Draw $n$ (sufficiently large) *i.i.d.* samples from a uniform distribution, then transform the uniform variables into the variables of interest. Note that we refer to pseudo-random numbers rather than random numbers. A pseudo-random number generator is an algorithm which, starting from an initial value $\theta_0$ and a transformation $D$, produces a sequence of values. The generated values, $(\theta_1, \ldots, \theta_n)$, reproduce the behaviour of an *i.i.d.* sample when compared through a usual set of tests. The term "pseudo-random" is used since, given initial value $\theta_0$, the sample $(\theta_1 \ldots, \theta_n)$ is always the same. In other words, the validity of a random number generator is based on a single sample $\theta_1, \ldots, \theta_n$ when $n \to \infty$.

### Importance Sampling

The evaluation of Expression 1.5 based on simulation from $\pi(\theta)$ is not always optimal if we wish to minimise the variance of the estimator. In fact, it is always suboptimal! The main alternative to directly sampling from $\pi(\theta)$ is called importance sampling. Begin by rewriting Expression 1.5 as

$$\int_\Theta \frac{g(\theta)f(x \mid \theta)\pi(\theta)}{h(\theta)}h(\theta)d\theta, \tag{1.9}$$

where $h(\theta)$ is a probability density with $supp(h)$ including the support of $g(\theta)f(x \mid \theta)\pi(\theta)$. In this form, $h(\theta)$ is called the importance function. Generate a random sample from $h(\theta)$: $h(\theta_1), \ldots, h(\theta_n)$. Expression 1.5 can be approximated by

$$\frac{1}{n}\sum_{i=1}^{n} g(\theta_i)\omega_1(\theta_i), \tag{1.10}$$

with weights

$$\omega_i = \frac{f(x \mid \theta_i)\pi(\theta_i)}{h(\theta_i)}. \tag{1.11}$$

Similarly, an approximation to Expression 1.8 is given by

$$\frac{\sum_{i=1}^{n} g(\theta_i)\omega(\theta_i)}{\sum_{i=1}^{n} \omega(\theta_i)}, \tag{1.12}$$

since the numerator and denominator converge to $\int_\Theta g(\theta)f(x \mid \theta)\pi(\theta)d\theta$ and $\int_\Theta f(x \mid \theta)\pi(\theta)d\theta$ respectively.

The choice of $h(\theta)$ is important. It must be easy to simulate variables from $h(\theta)$ and $h(\theta)$ should be 'close' to the original integral. If $h(\theta)$ is not close enough then most of the weights, $\omega_i$, will be too small, while a few will be overly influential. See Chapter 6 of Robert (2001) for full details.

### 1.2.3 Iterative Monte Carlo Methods

Iterative, or Markov chain Monte Carlo, integration is a more general Monte Carlo method. MCMC methods have almost unlimited applicability, though their performance varies widely depending on the complexity of the problem. MCMC integration is essentially Monte Carlo integration using Markov chains. It derives its name from the idea that, to produce acceptable approximations to integrals, it is enough to generate a Markov Chain whose limiting distribution is the distribution of interest. Traditional Monte Carlo integration works by drawing samples from the target distribution; MCMC integration draws these samples by running a specially constructed Markov chain for a long time. MCMC methods have the advantage, over traditional Monte Carlo methods, that they do not require the precise construction of an importance function, but they take into account the characteristics of the posterior distribution.

There are many ways of constructing suitable Markov chains, but all of them are special cases of the general framework of Metropolis et al. (1953), who originally constructed them for use in mechanical physics, and (Hastings, 1970), who was the first to apply them in a statistical setting. The idea of using the limiting behaviour of a Markov chain came almost as early as the original Monte Carlo technique (Metropolis et al., 1953), but the computer power required was not available in those times.

Markov chains produced by MCMC methods are irreducible (average number of visits to an arbitrary set with positive measure is infinite) and ergodic (distribution

of $\theta_n$ converges to $\pi(\cdot \mid x)$ for almost any starting value of $\theta_0$ as $n \to \infty$). So for $n$ large enough, $\theta_n$ is approximately distributed $\pi(\theta \mid x)$, no matter what the starting value of $\theta_0$ is. A practical problem is how many simulations to run, that is, judging when the target distribution has reached equilibrium. The review article by Brooks and Roberts (1998) discusses proposed diagnostic criteria.

MCMC methods have almost unlimited applicability, although their performance can vary widely. The scale and scope of problems that can be dealt with has expanded, enhancing the position of statistics in most applied fields. The recent explosion of the range and number of Bayesian applications could not have happened without their increased use. The two most well-known MCMC algorithms are the Metropolis-Hastings algorithm and the Gibbs sampling algorithm.

### Metropolis-Hastings algorithm

The Metropolis-Hastings algorithm is a general purpose "black box" algorithm which does not require any assumptions on the target distribution, such as normality, unimodality etc. It does not depend on any approximation for the posterior density and does not require the precise construction of an importance function. The usefulness of the M-H algorithm increases as the number of dimensions of a problem increase, and as the calculations become more difficult.

To implement a M-H algorithm first define a "candidate-generating density", $q(\theta, \theta')$ and specify $\alpha_{\theta,\theta'}$, the "probability of move". When a process is at point $\theta$, the density will generate a new point, denoted $\theta'$. The process will move to this point with probability $\alpha_{\theta,\theta'}$.

The general M-H algorithm is:
Start with $\theta_0$ and repeat for $i = 1, 2, \ldots, n$.

1. Generate a candidate point $\theta'$ from $q(\theta_i, \cdot)$ and $u_i$ from $U(0, 1)$.

2. If $u_i \leq \alpha(\theta_i, \theta')$, set $\theta_{i+1} = \theta'$; else, set $\theta_{i+1} = \theta_i$,

Repeat steps (1) and (2) to generate $\theta_2, \theta_3, \ldots., \theta_n$.

After an initial "burning in" period, the draws are regarded as a sample from $\pi(\theta \mid x)$. The "burning in" period is the transient stage where the effect of $\theta_0$ is not yet small enough to be ignored. $\theta_0$ is taken from an approximation to the

prior (e.g. prior mode). An auspicious choice of starting value for $\theta_0$ will improve the rate of convergence, but the algorithm is usually robust enough to cope with a poor initial choice. The M-H algorithm is appealing for its universality, however the lack of connection between the proposed $q$ and the target distribution $\pi(\theta \mid x)$ may be detrimental to the convergence properties of the method and, in practise, may prevent convergence if the probability of reaching far away parts of distribution $\pi(\theta \mid x)$ is too small.

### Gibbs Sampler

The Gibbs sampler was introduced to the statistical community by Geman and Geman (1984), but it was the paper by Gelfand et al. (1990) that really sparked interest in Bayesian methods and stochastic processes through the use of statistical computing. Although the Gibbs sampler is a special case of the M-H algorithm (Müller, 1993), it was widely known among the statistical community before the M-H algorithm (Gilks et al., 1996).

The Gibbs sampler takes advantage of hierarchical structures within the Bayesian model, for example we can often decompose $\pi(\theta \mid x)$ as

$$\pi(\theta \mid x) = \int \pi_1(\theta \mid x, \lambda)\pi_2(\lambda \mid x)d\lambda. \tag{1.13}$$

To obtain $\pi(\theta \mid x)$ we simulate from joint distribution $\pi_1(\theta \mid x, \lambda)\pi_2(\lambda \mid x)$. When distributions $\pi_1(\theta \mid x, \lambda)$ and $\pi_2(\lambda \mid x)$ are known and can be simulated, we can apply a traditional Monte Carlo algorithm to achieve $\pi(\theta \mid x)$. But often the marginal distribution $\pi_2(\lambda \mid x)$ is not available either analytically of algorithmically. However, if both conditional posterior distributions, $\pi_1(\theta \mid x, \lambda)$ and $\pi_2(\lambda \mid x, \theta)$, can be simulated, then we can obtain $\pi(\theta \mid x)$ using only these conditional distributions.

One of the first Gibbs sampling techniques was introduced by Tanner and Wong (1987). They called it "data augmentation". It used the following algorithm:
Start with an arbitrary value $\lambda_0$.
Given $\lambda_{t-1}$, generate

1. $\theta_t$ according to $\pi_1(\theta \mid x, \lambda_{t-1})$
2. $\lambda_t$ according to $\pi_2(\lambda \mid x, \theta_t)$

If $\pi_1(\theta \mid x, \lambda) > 0$ on $\Theta$, the stationary distribution for sequence $\theta_n$, as $n \to \infty$, is $\pi(\theta \mid x)$. See Chapter 7 of Robert and Casella (1999) for a full introduction to the Gibbs sampler.

Although the Gibbs sampler was the first MCMC algorithm in widespread use, it has several disadvantages compared to the M-H algorithm. The M-H algorithm can be used to generate several parameters at one time, rather than iterating over one-dimensional complete conditionals, thus improving the rate of convergence. The Gibbs sampler is restricted to those cases where the complete joint posterior distribution is available. The more general nature of the M-H algorithm removes this restriction.

## 1.3 Discussion

All three numerical integration techniques studied can provide well-suited tools for most problems. There is considerable cross-over in the type of problem solvable by each method. It is often reasonable to use numerical integration methods when dealing with regular functions in small dimensions, as numerical integration methods tend to yield smaller errors with faster convergence. Existing scientific software, such as MATLAB or Maple, often provides highly efficient numerical procedures. In comparison, Monte Carlo simulation is implemented through pseudo-random generators, for the more common distributions, or specially written sub-routines, for more involved distributions, relying on weight of simulations for legitimacy.

Standard numerical methods do not take into account the probabilistic aspects of the problem, that is, that many of the functions involved in the computations are related to probability densities. Therefore a non-Monte Carlo numerical integration method may consider regions of a space which have zero (or low) probability under the distribution of the model, a phenomenon which does not usually occur when implementing Monte Carlo methods.

Monte Carlo methods have the advantage that, once the sample $\theta_1 \ldots, \theta_n$ is generated, it can be used repeatedly for all inferential purposes. Thus when the statistician needs to study the details of a posterior distribution, or needs to simultaneously estimate several features of the density, it may be preferable to use

a simulation based approach. Such an approach captures, if only approximately through the generated sample, the different characteristics of the density and thus allows, at little cost, extensions of the inferential scope to another test or estimate.

Although the popularity of MCMC methods cannot be denied, it is not the case that they are subsuming the more traditional methods of numerical integration. In some problems importance sampling will remain the method of choice, as will numerical integration in problems of low dimension — especially when extreme accuracy is required.

This thesis illustrates the difference between non-Monte Carlo numerical integration and Monte Carlo integration in Chapter 2, Section 3, in a real practical problem. The integral concerned is analytically intractable and is integrated over only one dimension. The non-Monte Carlo integration is completed quickly and accurately using pre-programmed routines in computer packages MATLAB and Maple. A Monte Carlo simulation achieved an integral of the same shape over the same domain, but it is far cruder even when the number of simulations is large.

In Section 5 of Chapter 2 we assess the density of the sum of various products of Normally distributed variables. This is done in two ways: by numerically integrating various products of Normally distributed variables then finding the density of the sum of these products using the convolution formula, and by using a Monte Carlo construction to simulate the density of the sums directly. Once again it is shown that, although both methods achieve densities with the same shape and similar statistics, the density approximated using non-Monte Carlo integration and convolutions is far more accurate. The work in Chapter 2 demonstrates that standard numerical methods can be superior to Monte Carlo methods, especially when the number of variables is small.

In Chapter 3 we investigate how well continuous conjugate theory can approximate real discrete mass functions when these are representable by digital Normal mass functions and digital parametric mixtures in various measurement settings. We compare the statistics of posterior mass functions with the posterior densities approximated through the use of conventional conjugate theory. So far in this Section, all discussion of Bayesian statistics has assumed that the prior distribution and information transfer, or likelihood, function are specified to be densities (and there-

fore continuous), and thus we are required to integrate to update $\pi(\theta)$ to $\pi(\theta \mid x)$. However, since unknown quantities have a discrete realm of possible measurement values, the exact computation of the updated posterior mass function requires the use of sums, rather than integrals. Traditionally these sums have been impractical to calculate for any non-trivial case, not because they are analytically difficult, but because the sheer number of them that need to be computed is overwhelming.

The work undertaken in Chapter 3 demonstrates how the advance of computing power now allows us to calculate posterior mass functions exactly. Previously researchers have been compelled to formulate their problems using the framework of conjugate theory, so that posterior calculations could be undertaken with relative ease. We show that, even if researchers feel their prior opinions can be accurately specified using a conjugate prior distribution, the corresponding posterior distribution may not be equivalent to the exact posterior mass function.

In Chapter 4, we consider the estimation of quantiles of extreme floods. This problem was first approached using a standard Bayesian format. Prior densities were specified, then a series of different Monte Carlo methods of numerical integration were implemented in an attempt to obtain the posterior density through information transfer, or likelihood, functions of various functional forms. However a number of complications occurred. In particular, whenever accept-reject methods were used the number of candidate points accepted was very low, and consequently convergence took a very long time. When MCMC methods were implemented the rate of convergence was also very slow, and on occasion the Markov chain would converge to different point estimates. As a consequence, Monte Carlo methods were put aside for the problem of estimating the quantiles of extreme floods. Work studied in Chapter 4 computes exact items by adapting the digital forecasting procedure introduced in Chapter 3 to the problem at hand. A procedure for scoring sequential forecasts of quantile estimates for extreme floods using digitised mass functions was developed, and compared with the conventional estimates used by frequentist statisticians.

Given the dependence on specific problem characteristics, no method of numerical approximation can claim superiority over another. Instead, it seems many statisticians use simulation based methods because they are within their field of expertise

and, comparatively, easily implemented. Experience acquired by the statistician in their everyday processing of stochastic models can be directly exploited in the implementation of simulation techniques, for example in the evaluation of the variation of the proposed estimators or of the stationarity of the resulting output. In comparison purely numerical techniques rely on branches of mathematics that are less familiar for many statisticians.

# Chapter 2

# Approximating the Distribution for Sums of Products of Normal Variables

## 2.1 Introduction

The work discussed in this chapter originated from a problem posed by Griffin (2000) who was interested in calculating the probability that the sum of the product of variables assessed with a Normal distribution was negative. Previous work involving the distribution of the product of two Normally distributed variables has been undertaken by Craig (1936), who was the first to determine the algebraic form of the moment-generating function of the product. Aroian et al. (1978) proved that, under certain conditions, the product of two Normally distributed variables approaches the standardised Pearson type III distribution. Cornwell et al. (1978) described the numerical evaluation of the product. Conradie and Gupta (1987) presented basic distributional results of the quadratic forms of $p$-variate complex Normal distributions. Their results were developed in terms of characteristic functions. However, these results were found to be too theoretical to be easily transferred to a problem as applied as the one under investigation.

While the work of Craig (1936) is relatively old, it is not at all well-known among statisticians. Indeed we did not even learn of it until we had rediscovered it

ourselves in developing this Thesis. At that time we also learned of the researches of Aroian et al. (1978) and Cornwell et al. (1978). Nonetheless, recent advances in computing power and graphics have allowed us to make several useful advances on the consulting problem that had been posed.

To calculate the probability that the sum of products of variables assessed as having a Normal distribution is negative, two distinct steps are required. The first step considers ways in which we can assess the distribution for the product of two Normally distributed variables. The second step involves identifying the distribution when summing a number of these products together.

In Section 2.2 of this Chapter, the process of differential continuous phase frequency shift keying is briefly introduced as it was studied by Griffin (2000). The relevance of the distribution of sums of products of Normally distributed variables is recognised. In Section 2.3 we assess the distribution for $Y = X_1X_2$, the product of two independent Normally distributed variables. We compare three different methods: a numerical methods approximation, which involves implementing a numerical integration procedure on MATLAB, a Monte Carlo construction and an approximation to the analytic result using the Normal distribution. The numerical integration procedure involves the joint distribution of $Y$ and $X_2$. We discover that $f(y, x_2)$ has a simple singularity at $(0, 0)$, and discuss the resulting consequences for the numerical integration. The numerical integration is implemented via MATLAB and Maple subroutines, eliminating the need for evaluation via statistical tables. New graphics are presented to aid understanding of the shape of the distribution $Y$. We undertake a specific analysis of the skewness of the product of two Normally distributed variables when the multiplicands are correlated. Section 2.4 considers how to assess the distribution for the sum of the products of two Normally distributed variables by applying the Convolution Formula. This technique is demonstrated using the products previously obtained via numerical integration. A computational procedure for approximating the required distribution using convolutions is developed. In Section 2.5 the methods of Sections 2.3 and 2.4 are combined to compute the distribution for the sum of products of Normally distributed variables, and thus to calculate the probability that this sum of products is negative. We also approach this problem directly, using a Monte Carlo approximation. Finally, in Section 2.6 a

summary of the chapter is presented.

## 2.2 Introduction to Differential Continuous Phase Frequency Shift Keying

Differential continuous phase frequency shift keying is a procedure for transmitting and decoding a signal that has been intentionally disturbed by noise. Interest centres on how accurately the receiver can decode the original signal.

In a typical encoding problem the original signal, called $s(t)$, is differentially encoded and then transmitted. During transmission over a channel, Gaussian noise, $w(t)$, is added to the signal so that the received signal, $y(t)$, is a combination of the transmitted signal and noise, i.e. $y(t) = s(t)+w(t)$. The ratio of $s(t)$ to the standard deviation of $w(t)$ is called the "signal to noise ratio". The estimate of the original signal is called the hypothesised signal, and is denoted $\hat{s}(t)$. The receiver uses a decoder to minimise the squared Euclidean distance between the transmitted signal and the hypothesised signal. The performance of the receiver can be characterised by the probability of error between $s(t)$ and $\hat{s}(t)$. As is common in problems of electrical engineering, the problem is expressed via complex valued functions and the practical solution is determined by the real component of the complex solution. In the problem posed by Griffin (2000), interest centres on the probability that the real component of the error metric between the transmitted and hypothesised signals is less than 0, that is, $P[Re(M_e(s, \hat{s})) < 0]$.

The transmitted signal consists of a finite number of received signals, say $N$ of them, so that

$$\mathbf{y} = \begin{bmatrix} y_{-\xi+1} \\ y_{-\xi+2} \\ \vdots \\ y_t \\ \vdots \\ y_{-\xi+N} \end{bmatrix} = \begin{bmatrix} s_{-\xi+1} + w_{-\xi+1} \\ s_{-\xi+2} + w_{-\xi+2} \\ \vdots \\ s_t + w_t \\ \vdots \\ s_{-\xi+N} + w_{-\xi+N} \end{bmatrix} = \mathbf{s} + \mathbf{w} \tag{2.1}$$

where $\xi$ is a positive integer. In the case of the problem posed, the error metric is

achieved as the real component of a complex expression and is representable as

$$M_e(s,\hat{s}) = 2\sum_{t=1}^{N\xi}\left(y_{R,t}y_{R,t-\xi}b_{R,t} + y_{R,t}y_{I,t-\xi}b_{I,t} - y_{I,t}y_{R,t-\xi}b_{I,t} + y_{I,t}y_{I,t-\xi}b_{R,t}\right). \quad (2.2)$$

The coefficients $b_{R,t}$ and $b_{I,t}$ are real constants, predetermined along with the means of $y_{R,t}$ and $y_{I,t}$ by the signal that is sent. Furthermore the added noise is constructed so that

$$\begin{bmatrix} y_{R,t} \\ y_{I,t} \\ y_{R,t-\xi} \\ y_{I,t-\xi} \end{bmatrix} \sim N\left(\begin{bmatrix} \mu_{R,t} \\ \mu_{I,t} \\ \mu_{R,t-\xi} \\ \mu_{I,t-\xi} \end{bmatrix}, \begin{bmatrix} \sigma_{\mathbf{w}}^2 & 0 & 0 & 0 \\ 0 & \sigma_{\mathbf{w}}^2 & 0 & 0 \\ 0 & 0 & \sigma_{\mathbf{w}}^2 & 0 \\ 0 & 0 & 0 & \sigma_{\mathbf{w}}^2 \end{bmatrix}\right).$$

The relative size of the different values of $\mu$ and $\sigma_{\mathbf{w}}^2$ are determined by the signal to noise ratio. For problems of this type it is usual practise to set all values of $\mu$ equal to 1, and then set $\sigma_{\mathbf{w}}^2$ to achieve the required signal to noise ratio for the problem under investigation. $N$ is usually given the value 2 or 3, $\xi$ is set to be some value of $2^k$, where $k \geq 0$, and $b_{R,t}$ and $b_{I,t}$ are both set to 1.

Our interest centres on finding the probability that the real component of the error metric is negative. In Sections 3 and 4 our focus will be on the shape of the distribution of the error metric. Thus, we shall disregard the coefficient "2" from Equation 2.2.

Essentially, the problem posed by $P\left[Re\left(M_e(s,\hat{s})\right) < 0\right]$ requires that we be able to compute probabilities for the sum of products of Normal variables. We now turn to a study of this problem in a general context.

## 2.3 The Simplest Problem of the Product of Two Normal Variables

The form of the simplest problem we consider is a bivariate Normal distribution with independent variables:

$$\begin{bmatrix} X_1 \\ X_2 \end{bmatrix} \sim N\left(\begin{bmatrix} \mu_1 \\ \mu_2 \end{bmatrix}, \begin{bmatrix} \sigma_1^2 & 0 \\ 0 & \sigma_2^2 \end{bmatrix}\right).$$

The joint density of $X_1$ and $X_2$ is

$$f(x_1,x_2) = \frac{1}{2\pi\sigma_1\sigma_2} e^{-\frac{1}{2}\left(\frac{x_1-\mu_1}{\sigma_1}\right)^2 - \frac{1}{2}\left(\frac{x_2-\mu_2}{\sigma_2}\right)^2} \qquad \text{for all} \quad x_1, x_2 \in \mathcal{R} \quad (2.3)$$

Our interest centres on the distribution of the product $X_1X_2$. To simplify notation, for the remainder of this chapter we let $Y = X_1X_2$.

### 2.3.1 A Numerical Methods Approximation

The conditional distribution of $Y \mid (X_2 = x_2)$, and the distribution of $X_2$, are:

$$\begin{aligned} Y \mid X_2 = x_2 &\sim N(x_2\mu_1, x_2^2\sigma_1^2), \\ X_2 &\sim N(\mu_2, \sigma_2^2). \end{aligned}$$

Thus we can find the joint density of $X_2$ and $Y$:

$$\begin{aligned} f(y, x_2) &= f(y \mid x_2)f(x_2) \\ &= \frac{1}{\sqrt{2\pi}|x_2|\sigma_1} e^{-\frac{1}{2x_2^2\sigma_1^2}(y-x_2\mu_1)^2} \frac{1}{\sqrt{2\pi}\sigma_2} e^{-\frac{1}{2\sigma_2^2}(x_2-\mu_2)^2} \\ &= \frac{1}{2\pi|x_2|\sigma_1\sigma_2} e^{-\frac{1}{2\sigma_1^2}\left(\frac{y}{x_2}-\mu_1\right)^2 - \frac{1}{2\sigma_2^2}(x_2-\mu_2)^2}. \end{aligned} \tag{2.4}$$

To find the marginal density $f(y)$, we need to integrate $f(y \mid x_2)f(x_2)$ with respect to $x_2$. In other words we solve

$$\begin{aligned} f(y) &= \int_{-\infty}^{\infty} f(y \mid x_2)f(x_2)dx_2 \\ &= \int_{-\infty}^{\infty} f(y, x_2)dx_2. \end{aligned} \tag{2.5}$$

This integration can be undertaken using the numerical integration procedure on the mathematical computer package MATLAB called "quad8", which works by using an adaptive recursive Newton Cotes 8 panel rule. A numeric value of $\int f(y, x_2)dx_2$ is obtained for an array of points in the domain of $Y$. These points are all extremely close to one another and essentially cover all realistic possibilities for $y$. We consider the density as essentially uniform on these tight intervals. These integrated values are then summed and normalised. The same numerical integration can be performed on the computer package Maple. The calling sequence "evalf(Int)" invokes a Clenshaw-Curtis quadrature method. As in MATLAB, a numeric value of $\int f(y, x_2)dx_2$ is obtained for an array of points in the domain of $Y$. We shall compare the results of these two integration procedures.

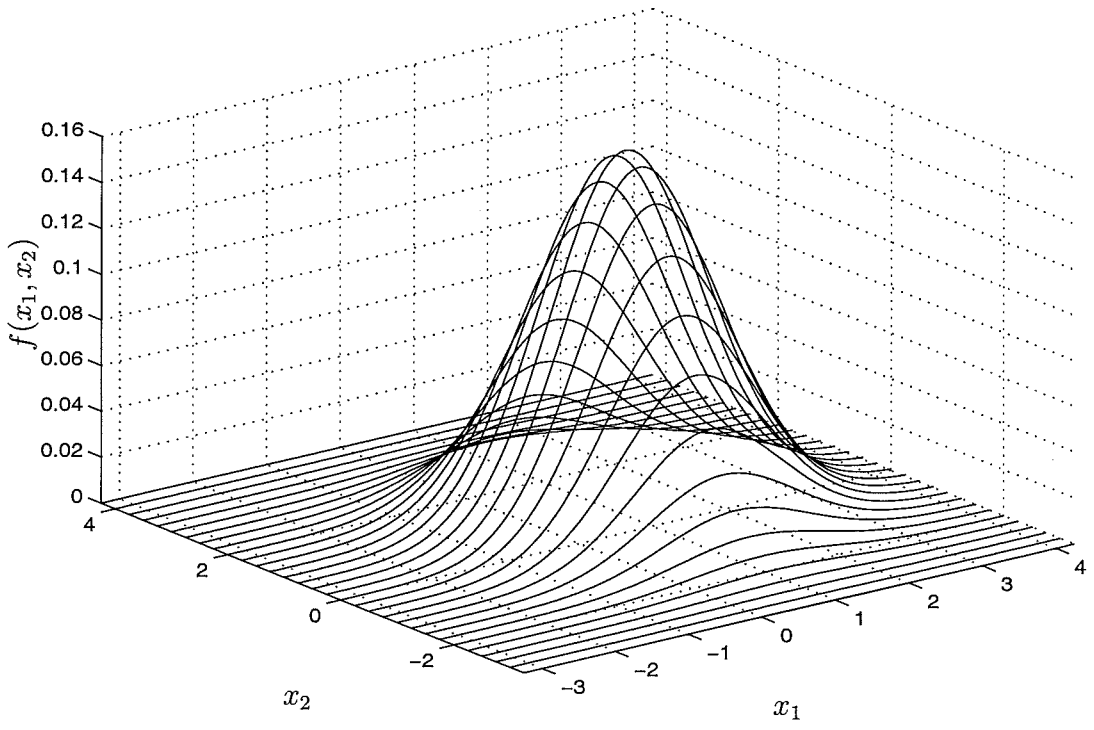


**Figure 2.1: Joint density of $X_1 \sim N(1,1)$ and $X_2 \sim N(0.5,1)$ displayed in three dimensions.**

**Case 1:** $\mu_1 = 1, \mu_2 = 0.5, \sigma^2 = 1, cov(X_1, X_2) = 0.$

Consider the case

$$\begin{bmatrix} X_1 \\ X_2 \end{bmatrix} \sim N\left( \begin{bmatrix} 1 \\ 0.5 \end{bmatrix}, \begin{bmatrix} 1 & 0 \\ 0 & 1 \end{bmatrix} \right).$$

The joint density of $X_1$ and $X_2$ is called a circular Normal density, and by Equation 2.3

$$f(x_1, x_2) = \frac{1}{2\pi} e^{-\frac{1}{2}\left(x_1^2 - 2x_1 + x_2^2 - x_2 + \frac{5}{4}\right)}. \tag{2.6}$$

We can view $f(x_1, x_2)$ in three dimensions, Figure 2.1, as well as by continuous contours in two dimensions, Figure 2.2. Figure 2.1 shows that $f(x_1, x_2)$ is a bivariate Normal surface with a maximum at $(1, 0.5)$. In Figure 2.2 the contours of constant probability density for $f(x_1, x_2)$ are drawn at 0.005, 0.055, 0.105 and 0.155. The isoproduct lines are shown for $\mathrm{x}_1 x_2 = \pm 1, \pm 2, \pm 3, \pm 4, \pm 5$.

The joint density $f(y, x_2)$ can be easily calculated. By Equation 2.4 we have

$$f(y, x_2) = \frac{1}{2\pi |x_2|} e^{-\frac{1}{2}\left(\frac{y^2}{x_2^2} - \frac{2y}{x_2} + x_2^2 - x_2 + \frac{5}{4}\right)}. \tag{2.7}$$

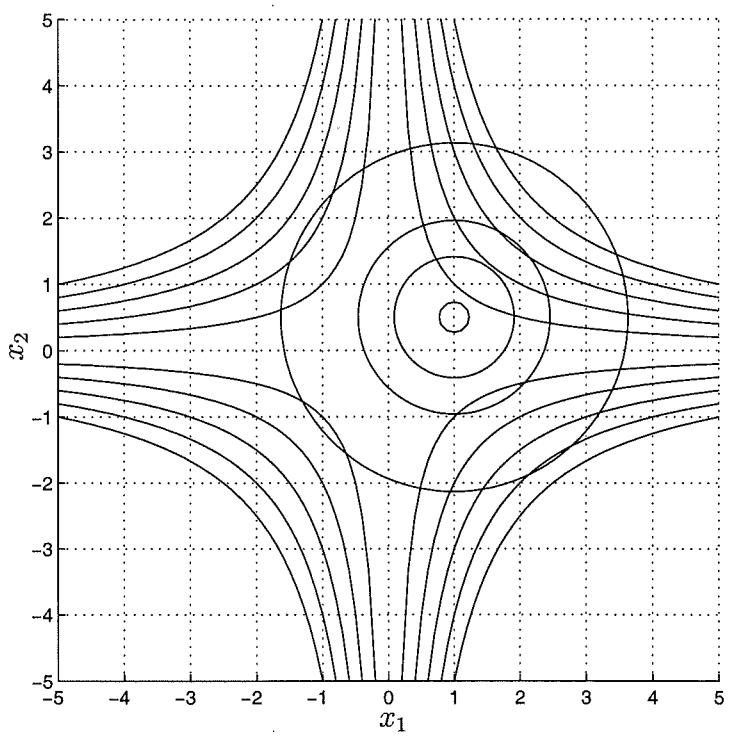


**Figure 2.2: Constant density contours for the joint density of $X_1 \sim N(1,1)$ and $X_2 \sim N(0.5,1)$ displayed in two dimensions, along with the isoproduct lines for $X_1X_2$.**

A study of $f(y, x_2)$ shows us that:

1. The domain for $(X_2, Y)$ is $\mathcal{R}^2 - \{(0, y) \mid y \neq 0\}$, because $y = x_1x_2$ and if $x_2 = 0$, $y$ must be 0.

2. When $x_2$ and $y$ are both large, $f(y, x_2) \approx 0$.

3. At pairs $(y, x_2) \neq (0, 0)$ the density will be what it is — varying real values.

4. The joint density has a simple singularity at $(y, x_2) = (0, 0)$. The direction from which the domain point $(y, x_2) = (c, 0)$ is approached does not affect the fact that $\lim_{x_2 \to 0} f(y, x_2)$ does not exist. To see this, let $y = kx_2$ for some real $k$. Then Equation 2.7 becomes

$$f(y, x_2) = \frac{1}{2\pi |x_2|} e^{-\frac{1}{2}\left(k^2 - 2k + x_2^2 - x_2 + \frac{5}{4}\right)}. \tag{2.8}$$

   In this form it is easy to see that $f(y, x_2) \to \infty$ as $x_2 \to 0$ for every real $k$. Moreover, it is evident directly from Equation 2.8 that for any fixed value of

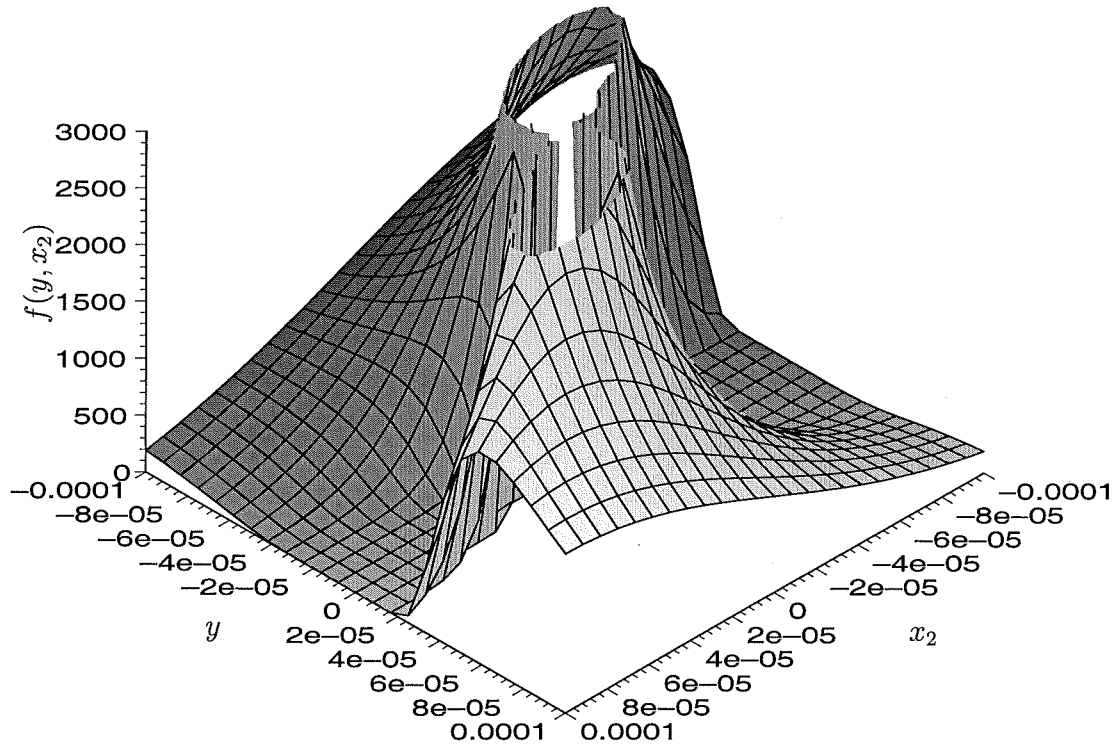


**Figure 2.3: The joint density $f(y, x_2)$ displayed in three dimensions for Case 1. For clarity the density is only displayed for $f(y, x_2) < 3000$.**

$y \neq 0$, $\lim_{x_2 \to 0} f(y, x_2) = 0$. (Remember that points $(y, x_2) = (y, 0)$ for $y \neq 0$ are missing from the domain of $(Y, X_2)$.)

Let us now examine the density $f(y, x_2)$ as produced by Maple in Figure 2.3 and MATLAB in Figure 2.4. Figure 2.3 displays a standard three dimensional picture of the function, while Figure 2.4 shows the isodensity contours. The larger contours correspond to low density values, the smaller contours correspond to high density values.

A consequence of $f(y, x_2)$ being undefined when $x_2 = 0$ and $y \neq 0$ is that to integrate $f(y, x_2)$ numerically we need to separate the integral into two domains for $X_2 : x_2 \in (-\infty, 0)$ and $x_2 \in (0, \infty)$. Once the positive and negative halves have been integrated individually, they are added together and normalised to give the marginal density $f(y)$. In MATLAB it took 10 minutes to complete this numerical integration using interval widths of 0.01. Figure 2.5 demonstrates that the marginal density is neither Normal or symmetric. Notice there is a slight fluctuation in $f(y)$ at $y \approx -2.3$. Similar, and far more marked, fluctuations occur in Case 2, and are

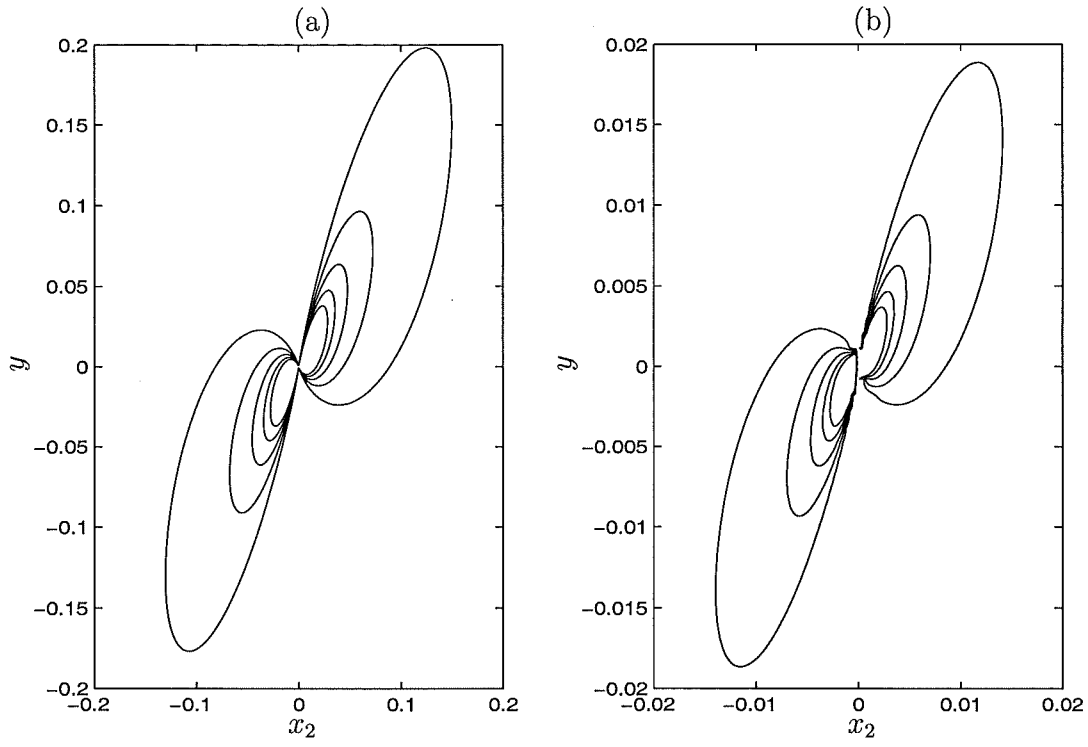


**Figure 2.4: Contours for the joint density $f(y, x_2)$ displayed in two dimensions for Case 1. In (a) contours are plotted at $f(y, x_2) = 1, 2, 3, 4, 5$. In (b) contours are plotted at $f(y, x_2) = 10, 20, 30, 40, 50$.**

discussed in the next subsection.

The density has an asymptote at $y = 0$, but of course we cannot display it graphically with the computer. There is a limit to how finely we can break up the domain of $X_2$ numerically. But because of our analysis of the $f(y, x_2)$ function we know that if we could do the numerical integration more finely, the area of the inner region around $y = 0$ would continue to increase. This is due to the simple singularity of $f(y, x_2)$ at $(y, x_2) = (0, 0)$.

**Case 2:** $\mu_1 = 5, \mu_2 = 2, \sigma^2 = 1, cov(X_1, X_2 = 0)$.

The density studied in the previous subsection was complicated by the extreme behaviour of $f(y, x_2)$ around the origin and the asymptote in $f(y)$ at $y = 0$. We shall now re-illustrate the method used in the previous subsection using values of $\mu$ that give a 'nicer' joint density $f(y, x_2)$.

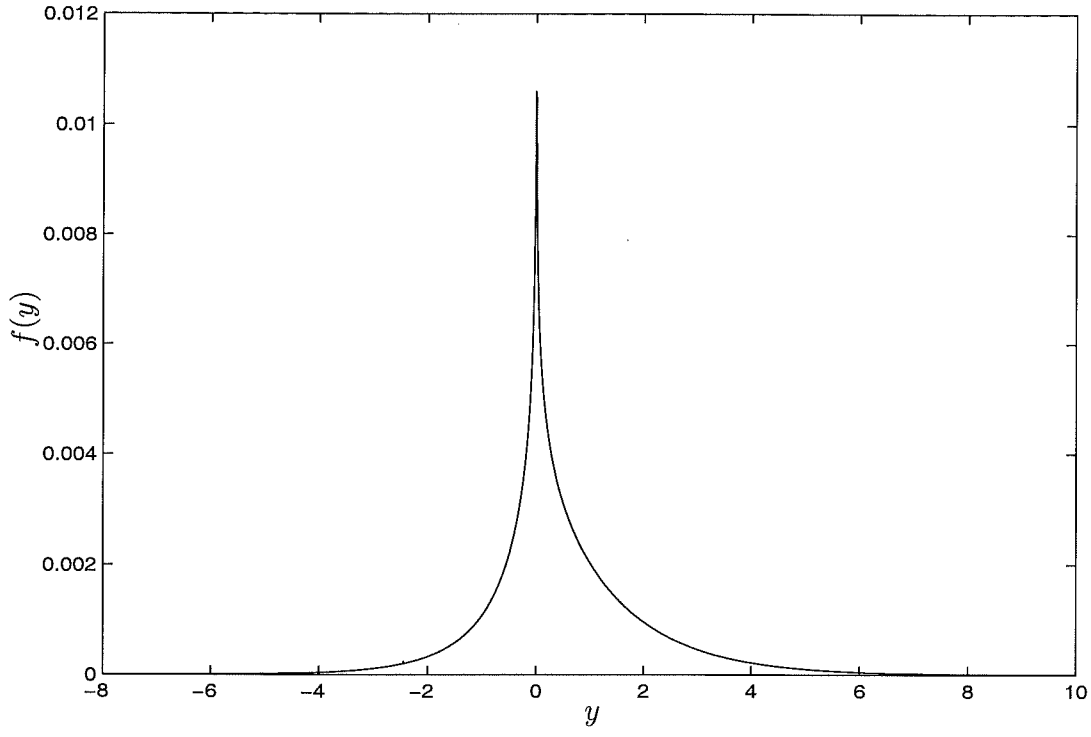


**Figure 2.5: The marginal density $f(y)$ obtained via numerical integration for Case 1. The function was integrated between $-13$ and 21, with interval widths of 0.01.**

We shall consider the case

$$\begin{bmatrix} X_1 \\ X_2 \end{bmatrix} \sim N\left(\begin{bmatrix} 5 \\ 2 \end{bmatrix}, \begin{bmatrix} 1 & 0 \\ 0 & 1 \end{bmatrix}\right).$$

From Equations 2.3 and 2.4 we calculate the joint densities $f(x_1, x_2)$ and $f(y, x_2)$ to be

$$f(x_1, x_2) = \frac{1}{2\pi} e^{-\frac{1}{2}\left(x_1^2 - 10x_1 + x_2^2 - 4x_2 + 29\right)} \tag{2.9}$$

and

$$f(y, x_2) = \frac{1}{2\pi\,|x_2|} e^{-\frac{1}{2}\left(\frac{y^2}{x_2^2} - \frac{10y}{x_2} + x_2^2 - 4x_2 + 29\right)}. \tag{2.10}$$

Of course Equation 2.9 shows the density $f(x_1, x_2)$ is a bivariate Normal surface which has a maximum at $(5, 2)$. The contours of $f(x_1, x_2)$ are circles.

The joint density $f(y, x_2)$ is displayed in three dimensions in Figure 2.6. We can see that, as in Case 1, there is a singularity at the origin. The analysis of the function we studied in Case 1 did not depend on the values of $\mu_1$ and $\mu_2$ at this point. Figure 2.7 displays $f(y, x_2)$ in two dimensions. Contour lines are drawn at

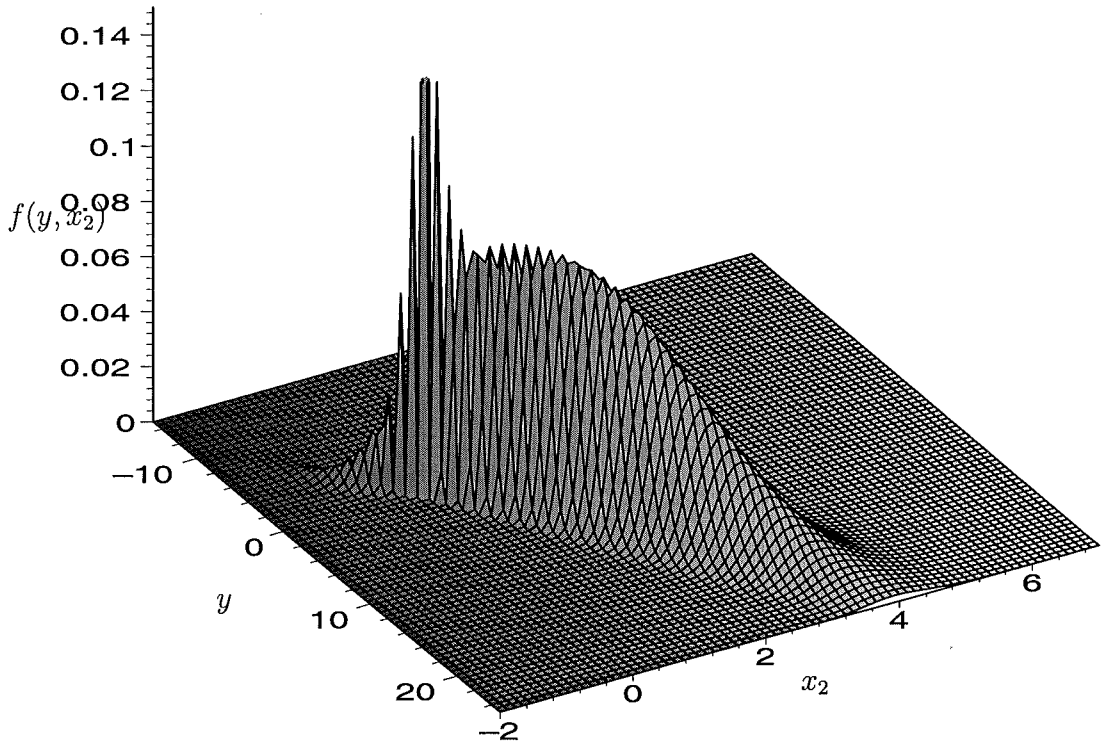


**Figure 2.6: The joint density $f(y, x_2)$ displayed in three dimensions for Case 2.**

$f(y) = 0.01, 0.03, 0.05, 0.07, 0.09$. The larger isodensity contours correspond to the lower density values and vice versa. Notice there are no contours lines displayed when $y > 0$ and $x_2 < 0$, or when $y < 0$ and $x_2 > 0$. The largest value of $f(y, x_2)$ in either of these quadrants is $7.9 \times 10^{-6}$.

To find the marginal density $f(y)$ we implement the same numerical integration procedure on MATLAB that was described in the previous subsection. We split $f(y, x_2)$ into negative and positive domains for $X_2$ and integrate the function over each domain separately. By combining the two domains and normalising, we can find a numerical approximation of $f(y)$. Figure 2.8 shows that although $f(y)$ is non-symmetric and non-Normal, it is far less so than in the previous problem. It took 200 minutes to complete the numerical integration with interval widths of 0.001.

When the numerical integration procedure was implemented on MATLAB results showed fluctuations near $y = 0$, $y \approx 4$, $y \approx 8$, $y \approx 12$, and $y \approx 17$. The fluctuations around $y = 0$ are shown in Figure 2.9, where $f(y)$ is evaluated at intervals of $10^{-5}$. Intuition, as well as our own analysis, suggests that these fluctuations are produced

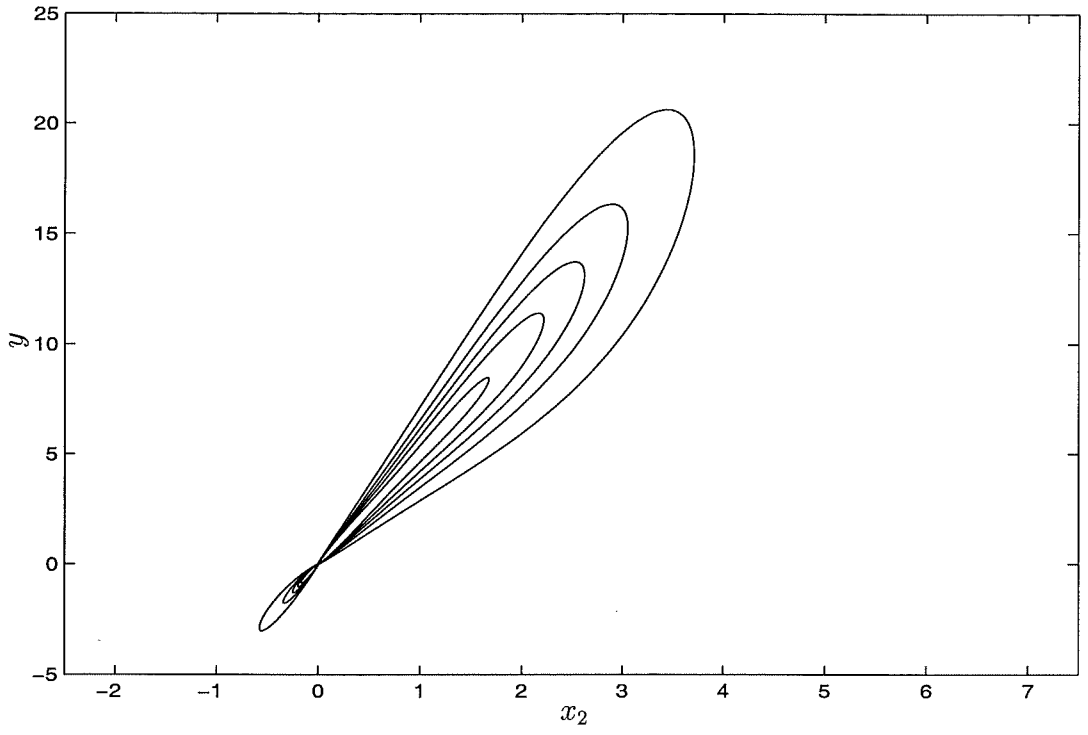


**Figure 2.7: Contours for the joint density $f(y, x_2)$ displayed in two dimensions for Case 2. Contours are plotted at $0.01, 0.03, 0.05, 0.07, 0.09$.**

due to the computational limitations of MATLAB and the discrete nature of the variable, rather than because they accurately represent the density $f(y)$. To test this speculation the same numerical integration was implemented on Maple. The Maple output for Case 2 is shown in Figure 2.10. The fluctuations did not occur in the Maple output. For practical purposes the fluctuations produced in the MATLAB output are irrelevant because the numerical results are so satisfactory. Moreover, as we shall soon see, they are quite accurate when compared to the crudeness of Monte Carlo methods.

### An Open Question

While I have resolved the computation of the density for the product of two Normal variables in a way that can be applied to any bivariate Normal, there is an open question that I have not had time to resolve. At what $(\mu_1, \mu_2)$ configurations does the density for $Y$ peak at $y = 0$ and at what configurations is it away from 0? Is it always unimodal?

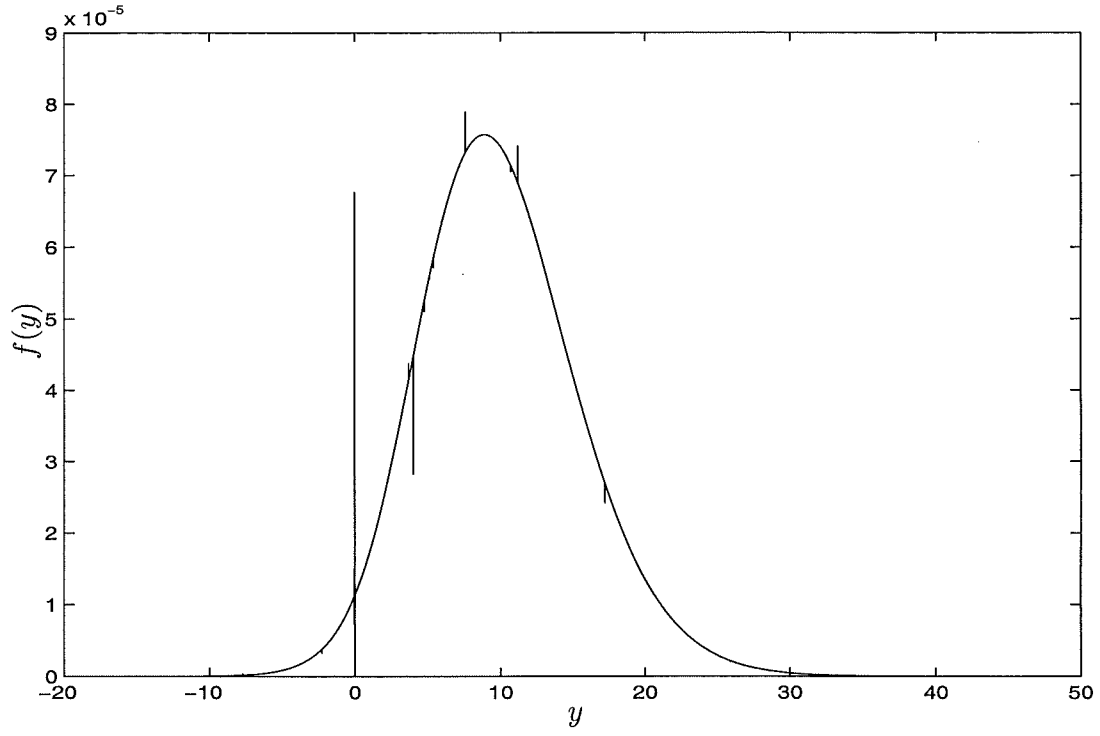


**Figure 2.8: The marginal density $f(y)$ obtained via numerical integration for Case 2. The function was integrated between $-15$ and 43, with interval widths of 0.001. Notice the fluctuations that occur at irregular intervals along $f(y)$.**

Rather than confront that question here, let us turn to a Monte Carlo resolution of the same specific problems we have already resolved.

### 2.3.2 A Monte Carlo Construction

A Monte Carlo method can be used to simulate $f(y)$. Generate two vectors, $\mathbf{X}_1$ and $\mathbf{X}_2$, each of length $N$, that consist of random variables drawn from $X_1 \sim N(\mu_1, \sigma_1^2)$ and $X_2 \sim N(\mu_2, \sigma_2^2)$. A new vector, $\mathbf{Y}$, can be obtained by multiplying $\mathbf{X}_1$ and $\mathbf{X}_2$ element-wise. The constituent elements of $\mathbf{Y}$ approximate a random sample from $f(y)$. To approximate the probability density function $f(y)$, sort the elements of $\mathbf{Y}$ into small, evenly spaced intervals and then normalise.

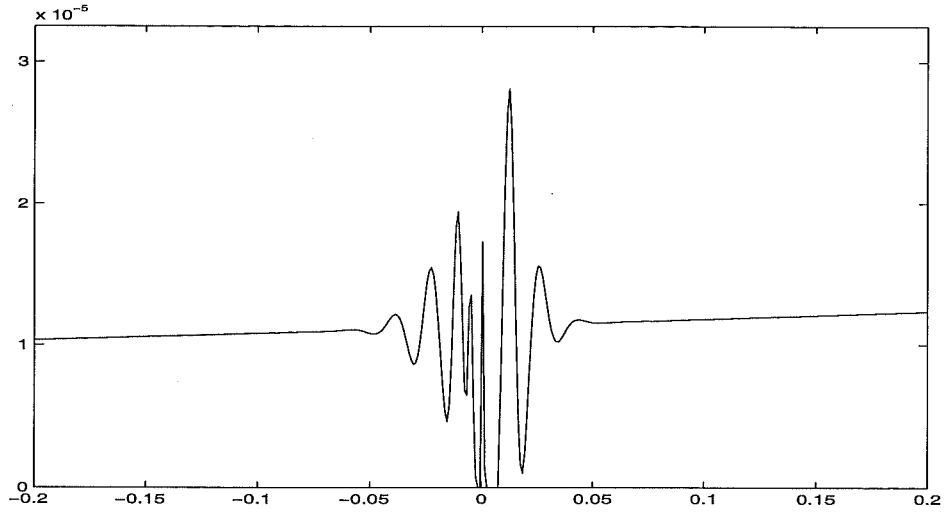


Figure 2.9: A close up view of $f(y)$ around $y = 0$ for Case 2. Notice the fluctuations near $y = 0$. The function was numerically integrated with interval widths of $10^{-5}$.

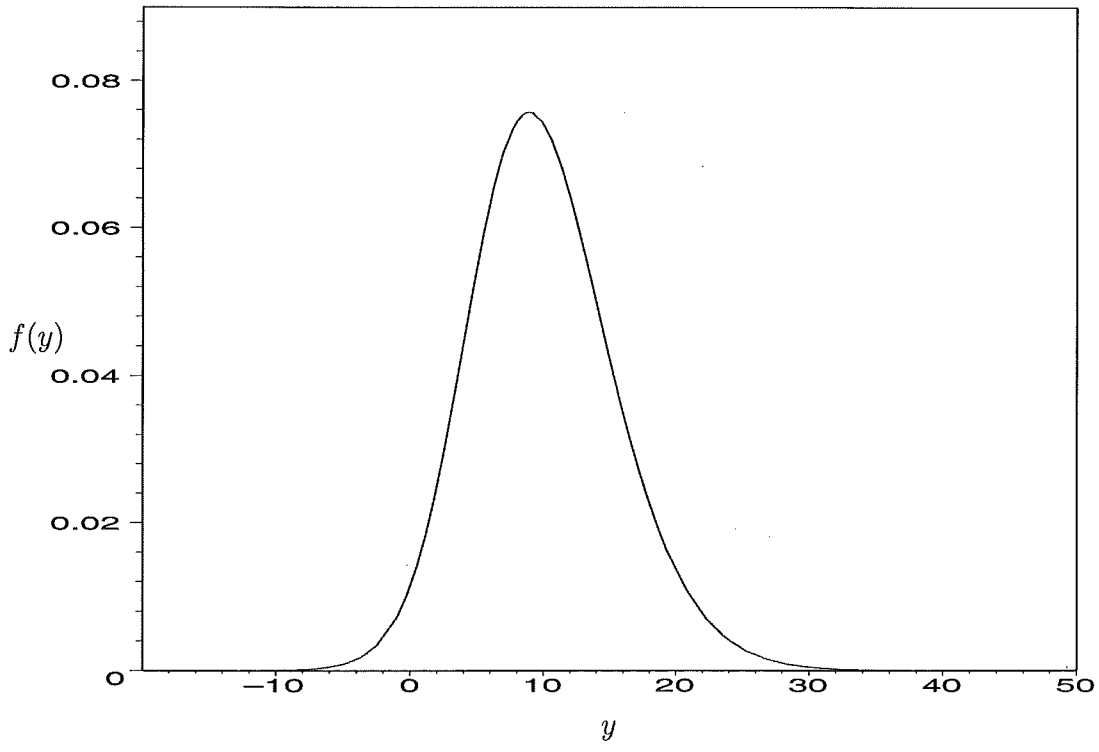


Figure 2.10: Numerically integrated density $f(y)$ produced using Maple for Case 2. Notice there is no irregular behaviour along $f(y)$.

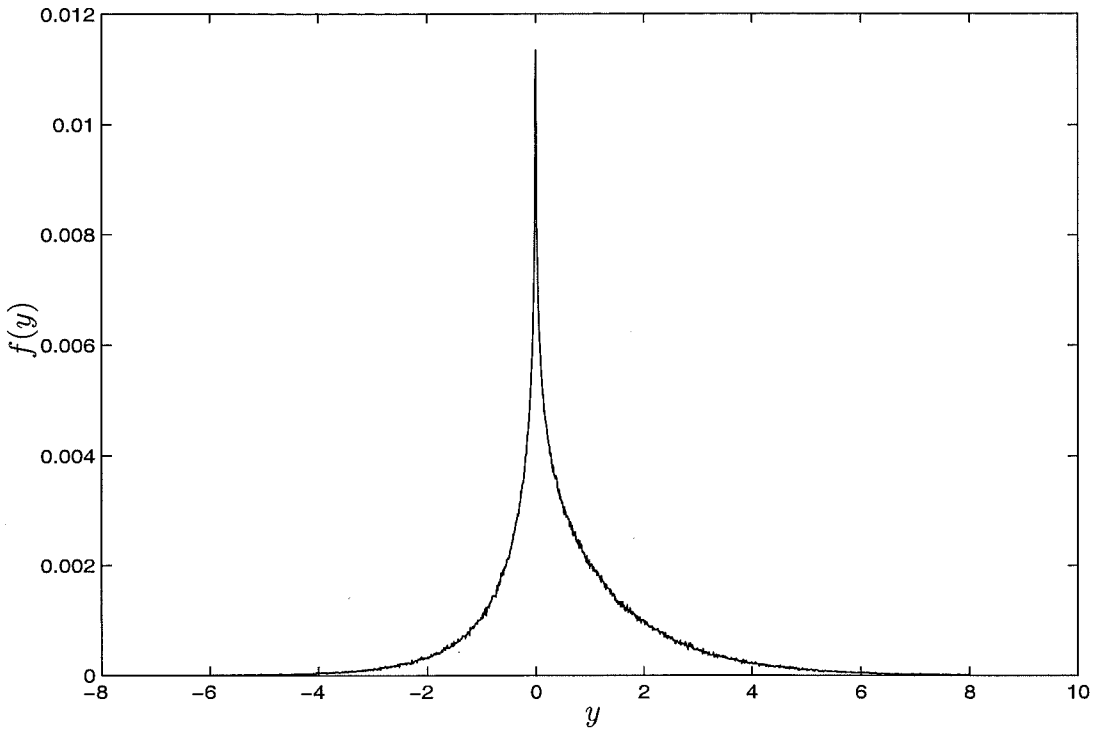


**Figure 2.11: The marginal density, $f(y)$, approximated using a Monte Carlo simulation for Case 1. The number of elements drawn to form $\mathbf{X}_1$ and $\mathbf{X}_2$ was $1,000,000$. The bins have width $0.01$**

**Case 1:** $\mu_1 = 1, \mu_2 = 0.5, \sigma^2 = 1, cov(X_1, X_2) = 0.$

Two vectors of length $1,000,000$ were obtained. The first contained elements drawn from $X_1 \sim N(1,1)$ and the second contained elements from $X_2 \sim N(0.5,1)$. The vectors were element-wise multiplied to form $\mathbf{Y}$, a vector of length $1,000,000$. The elements of $\mathbf{Y}$ constituted a random sample from $f(y)$. The elements were sorted into intervals of width 0.01. The resulting histogram is shown in Figure 2.11. The time taken to generate the histogram in MATLAB was approximately 5 seconds. It can be seen that Figure 2.5 and Figure 2.11 are approximately the same shape and cover the same domain, but that the Monte Carlo approximation is cruder than the numerical integration.

**Case 2:** $\mu_1 = 5, \mu_2 = 2, \sigma^2 = 1, cov(X_1, X_2) = 0.$

Two random vectors were generated and multiplied in a similar fashion to the previous subsection. The length of each vector was 1,000,000. The random samples were

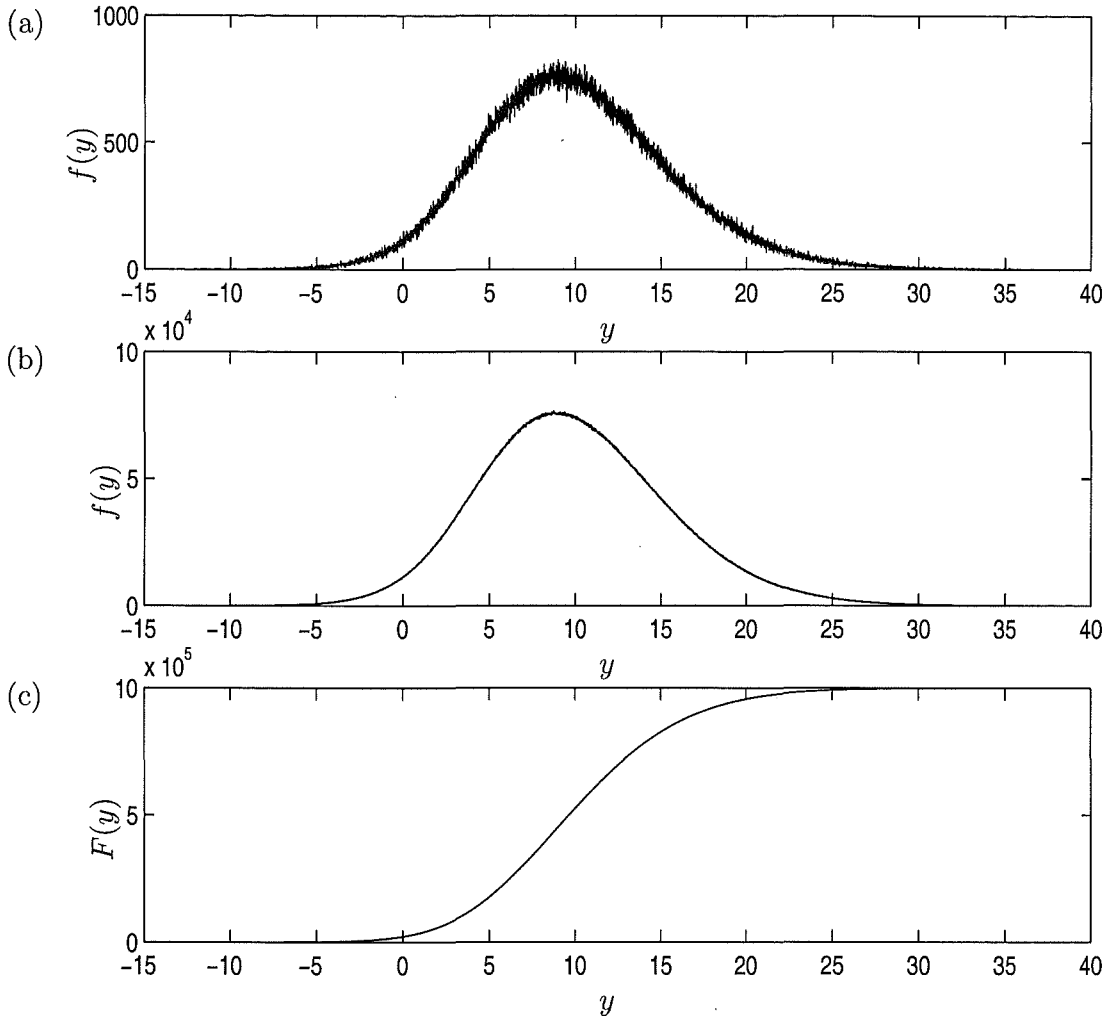


**Figure 2.12: The marginal density, $f(y)$, and marginal cumulative density, $F(y)$, obtained by Monte Carlo simulation for Case 2. $1,000,000$ ((a), (c)) and $100,000,000$ (b) elements were sorted into bins of width $0.01$.**

drawn from $X_1 \sim N(5,1)$ and $X_2 \sim N(2,1)$. After element-wise multiplication the elements of $\mathbf{Y}$ were sorted into intervals of width 0.01. A histogram representing $f(y)$ is shown in Figure 2.12(a). The largest negative non-zero value of $\mathbf{Y}$ was at $y = -16.65$, while the largest positive non-zero value was at $y = 47.74$.

Although the numerical integration and Monte Carlo method produce densities of similar shapes, it is clear the approximation displayed in Figure 2.12(a) is far cruder than that displayed in Figure 2.8.

The immediate difference between the two marginal densities obtained by a Monte Carlo method is that $f(y)$ has far higher variation in Case 2 than it does

in Case 1. The number of simulated random variables and the widths of the bins that the values are sorted into remain the same from case to case, but in Case 2 the non-zero domain of $Y$ is much larger. Consequently, in Case 2 there will be a smaller number of observations per interval width, and thus the variation between contiguous bins will be larger. A smoother Monte Carlo approximation can be obtained by increasing the number of elements drawn from $X_1$ and $X_2$ and/or increasing the bin width. To approximate $f(y)$ by a histogram containing $100,000,000$ observations took approximately 26 hours in MATLAB. The speed of the program was retarded by the size of the swap space on the computer system in the Department of Mathematics and Statistics, University of Canterbury, Christchurch. The resulting histogram is shown in Figure 2.12(b). Notice that the histogram comprising 100,000,000 observations is considerably smoother, but it still contains a surprising amount of fuzzy resolution compared to either Figure 2.8 or Figure 2.10, and these use bins that are ten times smaller!

Figure 2.12(c) shows the cumulative density function, $F(y)$, corresponding to the marginal density with $1,000,000$ elements. The cumulative density functions corresponding to $f(y)$ with $1,000,000$ and $100,000,000$ elements are more similar than their probability density functions are, as the fluctuations are 'evened out', e.g. compare the relative smoothness of Figure 2.12(a) and Figure 2.12(c).

### 2.3.3 An Approximation to the Analytic Result using the Normal Distribution

A third way to approximate $f(y)$ is by calculating the first two moments of $Y$, and then finding a distribution whose parameters match the moments of $Y$. We shall derive the moment-generating function for $Y$, and show that $Y$ can be approximated by a Normal curve under certain conditions.

#### The Product of Two Correlated Normally Distributed Variables

Craig (1936) was the first to study the form of the distribution of the product of two Normally distributed variables. He investigated the product $Z = \frac{X_1 X_2}{\sigma_1 \sigma_2}$, parameterising his results in terms of ratios $\delta_1 = \mu_1/\sigma_1$, $\delta_2 = \mu_2/\sigma_2$ and $\rho$, the correlation

coefficient, and determining the algebraic form of the moment-generating function. Aroian (1947) showed that $Z$ is asymptotically Normal if either $\delta_1$ or $\delta_2$ or both approach infinity. Aroian et al. (1978) distinguished six different cases for $Z$ depending on what is known about the parameters $\delta_1$, $\delta_2$ and $\rho$. The cases are: (1) $\delta_1 = 0$, $\delta_2$, $\rho$; (2) $\delta_1 = \delta_2$, $\rho$; (3) $\delta_1 = \delta_2 = 0$, $\rho$; (4) $\delta_1 = \delta_2 = \delta$, $\rho = 1$; (5) $\rho = 0$, and (6) $\delta_1 \neq \delta_2$, $\rho = 1$.

Aroian et al. (1978) also proved that if $\delta_1 = \delta_2 = \delta$, then as $\delta \to \infty$, the standardised distribution of $Z$ approaches the standardised Pearson type III distribution

$$f(z) = c\left(1 + \frac{\alpha_3 z}{2}\right)^{\left(-4/\alpha_3^2\right)-1} exp\left(-\frac{2z}{\alpha_3}\right), \qquad z \geq -\frac{2}{\alpha_3}, \tag{2.11}$$

where $\alpha_3$ is the measure of skewness and

$$c = \left(\frac{4}{\alpha_3^2}\right)^{\left(4/\alpha_3^2\right)-\frac{1}{2}} \left[\Gamma\left(\frac{4}{\alpha_3^2}\right)\right]^{-1} exp\left(-\frac{4}{\alpha_3^2}\right).$$

That is, if $W = (Z - \mu_Z)/\sigma_Z$, then as $\mu/\sigma$ increases to infinity, $F(w)$ approaches the standard Pearson type III distribution with mean zero and standard deviation one. Cornwell et al. (1978) describe the numerical evaluation of $Z$.

### The Moment-Generating Function of the Product of Two Correlated Normally Distributed Variables

Assume $X_1 \sim N(\mu_1, \sigma_1^2)$, $X_2 \sim N(\mu_2, \sigma_2^2)$ and that $X_1$ and $X_2$ have correlation $\rho$. Define $X_1 = X_0 + Z_1$ and $X_2 = X_0 + Z_2$, where

$$\begin{bmatrix} X_0 \\ Z_1 \\ Z_2 \end{bmatrix} \sim N\left(\begin{bmatrix} 0 \\ \mu_1 \\ \mu_2 \end{bmatrix}, \begin{bmatrix} \rho\sigma_1\sigma_2 & 0 & 0 \\ 0 & \sigma_1^2 - \rho\sigma_1\sigma_2 & 0 \\ 0 & 0 & \sigma_2^2 - \rho\sigma_1\sigma_2 \end{bmatrix}\right).$$

We have decomposed $X_1$ and $X_2$ into independent summands, one of which is shared between them.

To find the moment-generating function of $Y = X_1X_2 = (X_0 + Z_1)(X_0 + Z_2)$, we know that

$$\begin{aligned} M_Y(t) &= \int_{-\infty}^{\infty} e^{ty} f(y)dy \\ &= \int_{-\infty}^{\infty}\int_{-\infty}^{\infty}\int_{-\infty}^{\infty} e^{t(x_0+z_1)(x_0+z_2)} f(x_0, z_1, z_2)dx_0dz_1dz_2 \end{aligned}$$

$$= \frac{1}{\sqrt{2\pi\rho\sigma_1\sigma_2}} \frac{1}{\sqrt{2\pi\left(\sigma_1^2 - \rho\sigma_1\sigma_2\right)}} \frac{1}{\sqrt{2\pi\left(\sigma_2^2 - \rho\sigma_1\sigma_2\right)}}$$
$$\int_{-\infty}^{\infty}\int_{-\infty}^{\infty}\int_{-\infty}^{\infty} e^{t(x_0+z_1)(x_0+z_2) - \frac{1}{2}\frac{(x_0-0)^2}{\rho\sigma_1\sigma_2} - \frac{1}{2}\frac{(z_1-\mu_1)^2}{\sigma_1^2-\rho\sigma_1\sigma_2} - \frac{1}{2}\frac{(z_2-\mu_2)^2}{\sigma_2^2-\rho\sigma_1\sigma_2}} dx_0 dz_1 dz_2$$

$$= \left(\sqrt{(1-\rho\sigma_1\sigma_2 t)^2 - \sigma_1^2\sigma_2^2 t^2}\right)^{-1} e^{\frac{\mu_1\mu_2 t + \frac{1}{2}\left(\mu_1^2\sigma_2^2 + \mu_2^2\sigma_1^2 - 2\rho\mu_1\mu_2\sigma_1\sigma_2\right)t^2}{(1-\rho\sigma_1\sigma_2 t)^2 - \sigma_1^2\sigma_2^2 t^2}}. \quad (2.12)$$

See Appendix A for complete exposition.

An MGF of this form was found by Craig (1936), who calculated $M_Z(t)$, where $Z = \frac{X_1 X_2}{\sigma_1\sigma_2}$, to be

$$M_Z(t) = \left(\sqrt{[1-(1+\rho)t]\,[1+(1-\rho)t]}\right)^{-1} e^{\frac{2\delta_1\delta_2 t + \left(\delta_1^2 + \delta_2^2 - 2\rho\delta_1\delta_2\right)t^2}{2[1-(1+\rho)t][1+(1-\rho)t]}}, \quad (2.13)$$

Note that this result is written only in terms of the ratios $\delta_1$ and $\delta_2$, which are proportional to the reciprocals of the coefficient of variation, and $\rho$, the correlation coefficient.

To confirm the equivalence of Equations 2.12 and 2.13, observe that

$$\begin{aligned} M_Z(t) &= M_{\frac{X_1X_2}{\sigma_1\sigma_2}}(t) \\ &= M_Y\left(\frac{t}{\sigma_1\sigma_2}\right). \end{aligned} \quad (2.14)$$

By replacing every "$t$" in Equation 2.12 with "$\frac{t}{\sigma_1\sigma_2}$" it is soon seen that the two MGFs are identical.

### Moments of the Product of Two Correlated Normally Distributed Variables

The moment-generating function can be used to find moments about the origin of $Y$. By differentiating $M_Y(t)$ and evaluating at $t = 0$ we can find as many moments as required. These moments can be used to calculate the mean, variance and skewness of the product of two correlated Normal variables. Using Maple we find that:

$$E(Y) = \mu_1\mu_2 + \rho\sigma_1\sigma_2, \quad (2.15)$$

$$V(Y) = \mu_1^2\sigma_2^2 + \mu_2^2\sigma_1^2 + \sigma_1^2\sigma_2^2 + 2\rho\mu_1\mu_2\sigma_1\sigma_2 + \rho^2\sigma_1^2\sigma_2^2, \quad (2.16)$$

$$\alpha_3(Y) = \frac{6\sigma_1\sigma_2\left(\mu_1\mu_2\sigma_1\sigma_2\left(\rho^2+1\right) + \rho\left(\mu_1^2\sigma_2^2 + \mu_2^2\sigma_1^2\right)\right) + 2\rho\sigma_1^3\sigma_2^3\left(3+\rho^2\right)}{\left(\mu_1^2\sigma_2^2 + \mu_2^2\sigma_1^2 + \sigma_1^2\sigma_2^2\left(1+\rho^2\right) + 2\rho\mu_1\mu_2\sigma_1\sigma_2\right)^{3/2}} \quad (2.17)$$

Craig (1936) found equivalent moments, again using his $(\delta_1, \delta_2, \rho)$ parameterisation.

### Special Cases

We shall investigate three special cases for the product of two correlated Normal variables. First, we shall examine what happens when $\rho = 0$. In this case the Normal variables are independent. Second, we shall consider $\mu_1 = \mu_2 = 0$, $\sigma_1 = \sigma_2 = 1$ and $\rho = 1$. Here we are considering the square of a standard Normal distribution. Conventional theory tells us that we can expect to obtain the MGF and moments of a Chi-Square distribution. Finally, we examine what happens as the ratio of $\mu/\sigma$ changes over different values of $\rho$. This is achieved by setting $\mu_1$ and $\mu_2$ to $\mu$ and holding $\sigma_1$ and $\sigma_2$ constant at 1. $\rho$ varies between $-1$ and 1. Note that our three cases are equivalent to, in order, cases 5, 3 and 2 from Aroian et al. (1978).

**Case I:** $\rho = 0$

When $\rho = 0$, $X_1$ and $X_2$ are independent. The moment-generating function of $Y$ can be written as

$$M_Y(t) = \left(\sqrt{1 - \sigma_1^2\sigma_2^2t^2}\right)^{-1} e^{\frac{\mu_1\mu_2t + \frac{1}{2}\left(\mu_1^2\sigma_2^2 + \mu_2^2\sigma_1^2\right)t^2}{1-\sigma_1^2\sigma_2^2t^2}}. \tag{2.18}$$

The mean, variance and skewness are:

$$E(Y) = \mu_1\mu_2, \tag{2.19}$$

$$V(Y) = \mu_1^2\sigma_2^2 + \mu_2^2\sigma_1^2 + \sigma_1^2\sigma_2^2, \tag{2.20}$$

$$\alpha_3(Y) = \frac{6\mu_1\mu_2\sigma_1^2\sigma_2^2}{\left(\mu_1^2\sigma_2^2 + \mu_2^2\sigma_1^2 + \sigma_1^2\sigma_2^2\right)^{3/2}}. \tag{2.21}$$

The moments of $Y$ can be found more quickly by observing that $E(Y^r) = E(X_1^r)E(X_2^r)$, and the moments of the Normal distribution are well-known. The values of $E(Y)$, $V(Y)$ and $\alpha_3(Y)$ obtained using this method are the same as the values produced using the moment-generating function; see Appendix A.1 for details. The distribution of the product of two independent Normal variables corresponds to Cases 1 and 2 as discussed in the previous subsections, where we had $cov(X_1, X_2) = 0$, and as such we shall consider this problem in greater depth in Section 2.3.3.

**Case II:** $\mu_1 = \mu_2 = 0$, $\sigma_1 = \sigma_2 = 1$, $\rho = 1$

When two perfectly correlated standard Normal variables are multiplied together, the moment-generating function, mean, variance and skewness of their product, $Y$,

can be written as:

$$M_Y(t) = (1-2t)^{-\frac{1}{2}}, \tag{2.22}$$

$$E(Y) = 1, \tag{2.23}$$

$$V(Y) = 2, \tag{2.24}$$

$$\alpha_3(Y) = 2\sqrt{2}. \tag{2.25}$$

It is well known that if $U_1, U_2, \ldots, U_\nu$ are independent standard Normal variables, then $\sum_{i=1}^{\nu} U_i^2$ has a Chi-square distribution with $\nu$ degrees of freedom. Thus it is no surprise that the MGF and moments are identical to those from a Chi-Square distribution with one degree of freedom.

Note that when $\rho = -1$, we obtain

$$M_Y(t) = (1+2t)^{-\frac{1}{2}}, \tag{2.26}$$

the MGF of a "negative Chi-square" distribution with one degree of freedom.

**Case III:** $\mu_1 = \mu_2 = \mu$, $\sigma_1 = \sigma_2 = 1$

In this case the moment-generating function of $Y$ can be written as

$$M_Y(t) = \left(\sqrt{(1-\rho t)^2 - t^2}\right)^{-1} e^{\frac{\mu^2 t(1+t-\rho t)}{(1-\rho t)^2 - t^2}}. \tag{2.27}$$

The expected value of $Y$ is

$$E(Y) = \mu^2 + \rho. \tag{2.28}$$

Observe that for any distinct value of $\rho$, $E(Y)$ increases at an increasing rate as ratio $\mu/\sigma$ increases absolutely. However, for any specific value of $\mu/\sigma$, $E(Y)$ increases linearly on $\rho \in [-1, 1]$. Both Case I and Case II occur as special cases in Figure 2.13. When $\rho = 0$ we observe that the expected value of $Y$ is $\mu^2$, which is the value given in Equation 2.19 with $\mu_1 = \mu_2 = \mu$. Remember that for Case III we have set $\sigma^2 = 1$, so when $\mu = 0$ and $\rho = 1$ we have the Chi-square case. From Figure 2.13 we can see that this gives an expected value of 1. Note that if the graph were to include values of $\mu$ that are less than zero, the graph would be symmetric about $\mu = 0$. Note that for Case III we could write any "$\mu$" or "$\mu/\sigma$" term as "$\delta$", but for the sake of clarity we shall retain "$\mu$" for the remainder of this subsection.

The variance of $Y$ is

$$V(Y) = 2\mu^2(1+\rho) + \rho^2 + 1. \tag{2.29}$$

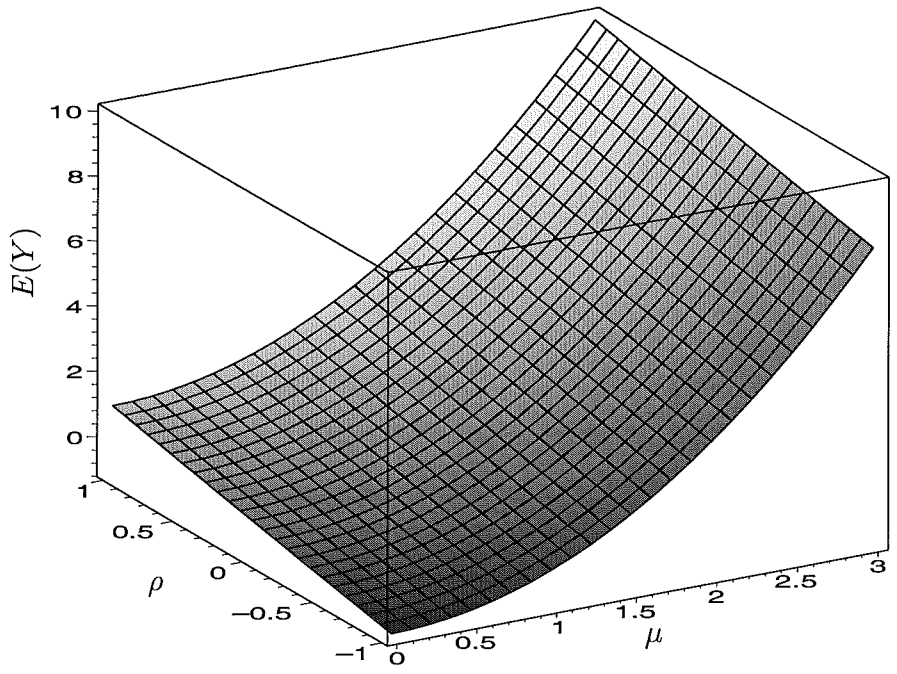


**Figure 2.13: Expected value of $Y$ for Case III.**

Figure 2.14 shows how $V(Y)$ changes as $\mu/\sigma$ varies over different values of $\rho$. As ratio $\mu/\sigma$ increases the variance will get larger increasingly quickly, except for when $\rho = -1$, when this is the case the variance is always 2. If $\mu/\sigma$ is held constant, the variance increases as $\rho$ increases; the larger $\mu/\sigma$ is specified to be, the faster $V(Y)$ increases. As with the expected value, if the graph was plotted over negative values of $\mu$, it would be symmetric about $\mu = 0$.

The skewness of $Y$ is

$$\alpha_3(Y) = \frac{6\mu^2(\rho+1)^2 + 2\rho(3+\rho^2)}{(2\mu^2(\rho+1) + \rho^2 + 1)^{3/2}}. \tag{2.30}$$

Figure 2.15 shows how the skewness changes as $\mu/\sigma$ varies over different values of $\rho$. Observe that when $\rho = 0$, $\alpha_3(Y) = 0$ when $\mu/\sigma = 0$, but as the ratio increases the skewness rises rapidly, until it is at its maximum when $\mu/\sigma = 1$, as the ratio continues to increase $\alpha_3(Y)$ gradually decreases to 0. When $\mu = 0$ and $\rho = 1$ the skewness is $2\sqrt{2}$, and when $\mu = 0$ and $\rho = -1$ the skewness is $-2\sqrt{2}$. In general, $\alpha_3 \to 0$ as $\mu/\sigma \to \infty$. This is because in Equation 2.30 we have a $\mu^2$ term over a $\mu^3$ term. The closer $\mid \rho \mid$ is to one the slower the approach of $\alpha_3(Y)$ to 0. The sole exception to this limit is when $\rho = -1$, whenever this is the case the skewness is a constant $-2\sqrt{2}$. As with $E(Y)$ and $V(Y)$, if $\alpha_3(Y)$ had been plotted over negative

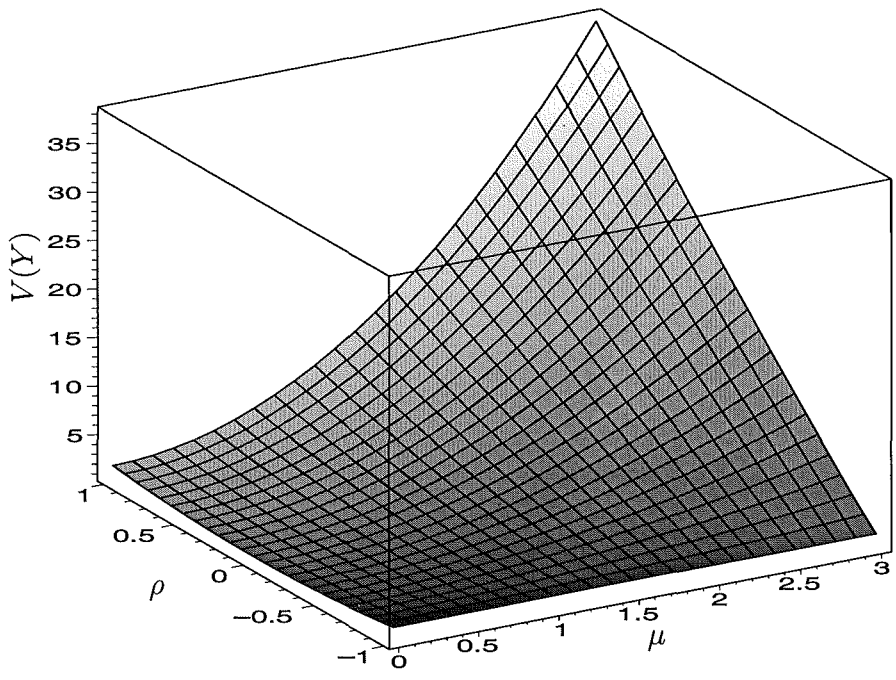


**Figure 2.14: Variance of $Y$ for Case III.**

values of $\mu$ it would be symmetric about $\mu = 0$.

### The Product Of Two Independent Normally Distributed Variables

After investigating the distribution of the product of two correlated Normally distributed variables we now turn our attention back to Case I, where the variables are independent. Remember that in both Case 1 and Case 2 of Sections 2.3.1 and 2.3.2 we had $cov(X_1, X_2) = 0$.

We know that the MGF of $W \sim N(\mu, \sigma^2)$ is

$$M_W(t) = e^{\mu t + \frac{1}{2}\sigma^2 t^2}, \tag{2.31}$$

giving $E(W) = \mu$ and $V(W) = \sigma^2$. A study of Equation 2.18 shows that as $\delta_1 \to \infty$ and $\delta_2 \to \infty$, the coefficient of the exponential term will have a decreasing influence on $M_Y(t)$. In fact, as $\delta_1$ and $\delta_2$ increase,

$$M_Y(t) \to e^{\mu_1\mu_2 t + \frac{1}{2}\left(\mu_1^2\sigma_2^2 + \mu_2^2\sigma_1^2\right)t^2}. \tag{2.32}$$

We recognise that as $\delta_1$ and $\delta_2$ both increase without bound, $M_Y(t)$ converges to a Normal moment-generating function of $Y$ with mean $\mu_1\mu_2$ and variance $\mu_1^2\sigma_2^2 + \mu_2^2\sigma_1^2$. In Equation 2.18 it was shown that the analytic result of the product of two

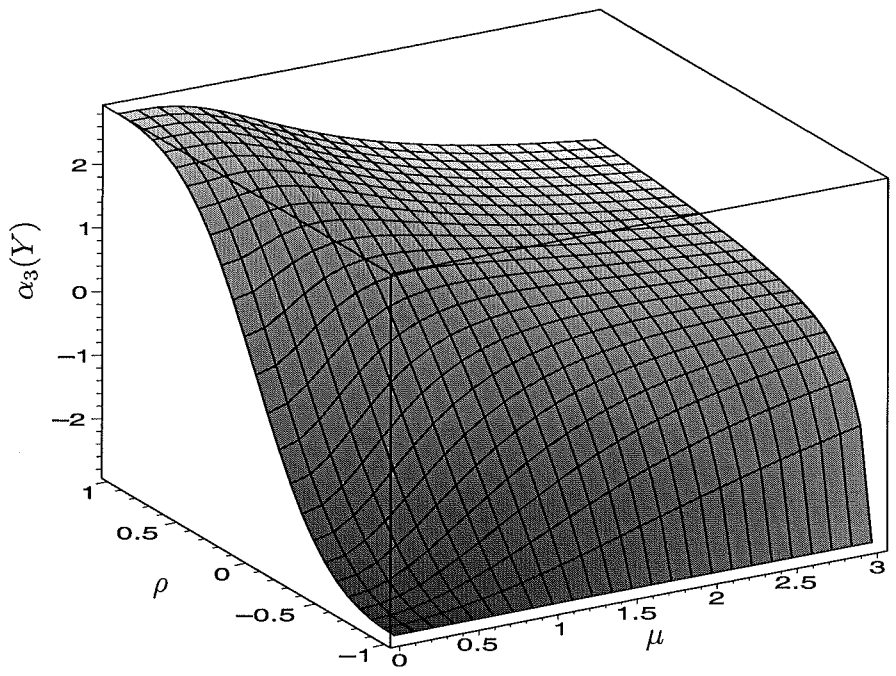


**Figure 2.15: Skewness of $Y$ for Case III.**

Normal distributions is not a Normal distribution, however Equation 2.32 shows that the limit of $M_Y(t)$ is Normally distributed. In other words, the product of $X_1 \sim N(\mu_1, \sigma_1^2)$ and $X_2 \sim N(\mu_2, \sigma_2^2)$ tends towards a $N(\mu_1\mu_2, \mu_1^2\sigma_2^2 + \mu_2^2\sigma_1^2)$ distribution as $\delta_1$ and $\delta_2$ increase.

This knowledge allows us to investigate a third approximation method in our quest to assess the distribution for the product of two independent Normal variables. When $\delta_1$ and $\delta_2$ are large, the distribution of the product of two independent Normal variables will be approximately Normal. Since the Normal distribution is fully specified by its first two moments, we can calculate the mean and the variance of $Y$ and approximate $f(y)$ by forming a Normal density with these parameters.

As we have already seen, the mean and variance for Case I are:

$$\begin{aligned} E(Y) &= \mu_1\mu_2, \\ V(Y) &= \sigma_1^2\sigma_2^2 + \mu_1^2\sigma_2^2 + \mu_2^2\sigma_1^2 \\ &= \sigma_1^2\sigma_2^2\left(1 + \delta_1^2 + \delta_2^2\right). \end{aligned} \tag{2.33}$$

The expression for $V(Y)$ obtained in Equation 2.33 differs from the variance of $Y$ deduced from Equation 2.32. In Equation 2.33 an analytic result was calculated, while in Equation 2.32 we took the limit of $M_Y(t)$ as $\delta_1 \to \infty$ and $\delta_2 \to \infty$. It is clear

that under these conditions the $\sigma_1^2\sigma_2^2$ term becomes negligible. In the two Cases we shall consider in this Section we assume that $X_1$ and $X_2$ have equal variance, that is, $\sigma^2 = \sigma_1^2 = \sigma_2^2$, so

$$\begin{aligned} V(Y) &= \sigma^2\left(\sigma^2 + \mu_1^2 + \mu_2^2\right) \\ &= \sigma^4\left(1 + \delta_1^2 + \delta_2^2\right). \end{aligned} \tag{2.34}$$

We can approximate the distribution of the product of two independent Normally distributed variables with a $N(\mu_1\mu_2, \sigma^4\left(1 + \delta_1^2 + \delta_2^2\right))$ distribution. The approximation will improve as $\delta_1$ and $\delta_2$ become large, since the limit of the distribution is $N(\mu_1\mu_2, \sigma^4\left(\delta_1^2 + \delta_2^2\right))$.

Before moving on we shall briefly consider what happens to $M_Y(t)$ as $\delta_1$ and $\delta_2$ decrease to 0. Now the moment-generating function of $Y$ is certainly not Normal. A study of $M_Y(t)$ shows us that as $\delta_1 \to 0$ and $\delta_2 \to 0$,

$$M_Y(t) \to \left(1 - \sigma_1^2\sigma_2^2t^2\right)^{-1/2}. \tag{2.35}$$

A quick study of $M_Y(t)$ shows that all its odd moments are equal to zero. Consequently $Y$ is symmetric about the origin. Also $V(Y) \to \sigma_1^2\sigma_2^2$ and the kurtosis of the limit of $Y$ is 9.

### The Skewness of the Analytic Result for Independent Variables

One way to predict the adequacy of the Normal approximation is by considering the skewness of $Y$ from the analytic result. We know the skewness of Case I is

$$\begin{aligned} \alpha_3(Y) &= \frac{6\mu_1\mu_2\sigma_1^2\sigma_2^2}{\left(\sigma_1^2\sigma_2^2 + \mu_1^2\sigma_2^2 + \mu_2^2\sigma_1^2\right)^{3/2}} \\ &= \frac{6\delta_1\delta_2}{\left(\sigma_1\sigma_2\right)^{-3}\left(\sigma_1^2\sigma_2^2 + \mu_1^2\sigma_2^2 + \mu_2^2\sigma_1^2\right)^{3/2}}. \end{aligned} \tag{2.36}$$

The skewness of $Y$ depends on the ratios $\delta_1$ and $\delta_2$. Clearly $\alpha_3(Y) \to 0$ as $\delta_1 \to \infty$ and $\delta_2 \to \infty$. The adequacy of the approximating Normal curve is related to the size of $\alpha_3(Y)$ for large $\delta_1$, $\delta_2$ values. As the skewness decreases the approximation improves. Note that $\alpha_3(Y)$ will always be skewed in the direction of the mean of $Y$, $\mu_1\mu_2$. The skewness will be largest when $\frac{d\alpha_3(Y)}{d\delta_1} = \frac{d\alpha_3(Y)}{d\delta_2} = 0$. Differentiating $\alpha_3(Y)$ with respect to $\delta_1$ and $\delta_2$, setting the two derivatives to zero and solving

simultaneously we find that $\alpha_3(Y)$ has extreme points at $(\delta_1, \delta_2) = (\pm 1, \pm 1)$. By differentiating again we find that the maximum value of $\alpha_3(Y)$ occurs at $(-1, -1)$ and $(1, 1)$. The maximum value of $\alpha_3(Y)$ is 1.15 (2dp). The minimum value of $\alpha_3(Y)$, which is $-1.15$ (2dp), occurs at $(-1, 1)$ and $(1, -1)$. Thus the skewness of $Y$ is largest when $\mu_1 = \sigma_1$ and $\mu_2 = \sigma_2$. When $X_1$ and $X_2$ have equal variance the skewness will be largest when $\mu_1 = \mu_2 = \sigma$.

The advantage of this method of approximation compared to the methods studied in Section 2.3.1 and Section 2.3.2 is that it is far quicker. Calculating the two numbers that represent $\mu$ and $\sigma$ using straightforward formulae is simpler and faster than either numerically integrating a function over narrow interval widths, or running a Monte Carlo simulation a large number of times.

**Case 1:** $\mu_1 = 1, \mu_2 = 0.5, \sigma^2 = 1, cov(X_1, X_2) = 0.$

In this Case $\delta_1 = 1$, $\delta_2 = 0.5$ and $\alpha_3(Y) = 0.\dot{8}$. The small size of $\delta_1$ and $\delta_2$ result in $f(y)$ being significantly skewed. This suggests that it is not appropriate to approximate $f(y)$ with a Normal density for Case 1. This suspicion is reinforced by a study of Sections 2.3.1 and 2.3.2, where it is demonstrated that the density of $Y$ is clearly not Normal. In fact, since $\alpha_3(Y) = 0.\dot{8}$ and $\mu_1 = \sigma_1$, this is one of the least suitable $(\delta_1, \delta_2)$ configurations for us to approximate with a Normal distribution.

The parameters of our Normal approximation to the analytic result are:

$$\begin{aligned} \mu &= \mu_1 \mu_2 \\ &= 0.5 \qquad (2.37) \\ \text{and} \qquad \sigma^2 &= \sigma^2 \left(\mu_1^2 + \mu_2^2 + \sigma^2\right) \\ &= 2.25. \qquad (2.38) \end{aligned}$$

To approximate $f(y)$ we could use a $N(0.5, 2.25)$ density but in this case that approximation would clearly be inappropriate.

**Case 2:** $\mu_1 = 5, \mu_2 = 2, \sigma^2 = 1, cov(X_1, X_2) = 0.$

In Case 2 we have $\delta_1 = 5$, $\delta_2 = 2$ and $\alpha_3(Y) = 0.37$ (2dp). The skewness here is less than the skewness in Case 1 so, although the approximation to $f(y)$ is non-Normal, it is far closer to being Normal than in Case 1. The parameters of the

approximating Normal distribution are $\mu = 10$ and $\sigma^2 = 30$. To approximate $f(y)$ we use a $N(10, 30)$ density. This is shown by the green line in Figure 2.16.

### An Open Question

In this Subsection it has been shown that the limiting distribution of the product of two independent Normal distributions is also a Normal distribution. However the question remains: When is the ratio of mean to variance large enough for $f(y)$ to be adequately approximated by a Normal density? Is it the individual ratios $\mu_1/\sigma$ and $\mu_2/\sigma$ that determine the adequacy of the Normal approximation to $f(y)$, or is the combined ratio $\mu_1\mu_2/\sigma^2$ more important? Is there a critical value of $\alpha_3(Y)$ below which a Normal approximation is justified when ratios $\mu_1/\sigma$ and $\mu_2/\sigma$ are large?

Rather than confront those questions here, we shall put the Normal approximation aside until Section 2.5.

## 2.3.4 Comparison of Approximation Methods

The distribution of the product of two independent Normal densities has been approximated using three different methods. In Section 2.3.1, Section 2.3.2 and Section 2.3.3 we approximated the density of $Y$ by numerical integration, by a Monte Carlo construction and via a Normal distribution. These three approximation methods were studied for the Cases where $(\mu_1, \mu_2)$ was equal to $(1, 0.5)$, Case 1, and $(5, 2)$, Case 2. For each Case we set $\sigma^2 = 1$.

In Case 1 the approximations of $f(y)$ produced by numerical integration and Monte Carlo simulation are of the same shape and cover similar domains — compare Figure 2.5 and Figure 2.11. Remember that the numerical integration has interval widths of 0.01 and for the Monte Carlo simulation $N = 1,000,000$. The major difference between the two methods is that the Monte Carlo approximation is far cruder than the approximation attained through numerical integration. The Normal approximation, a $N(0.5, 2.25)$ curve, is clearly a different shape to the other two $f(y)$ approximations. The shape difference of the Normal approximation is not surprising considering the high value of $\alpha_3(Y)$.

In Case 2 the similarity of the approximations obtained via numerical integra-

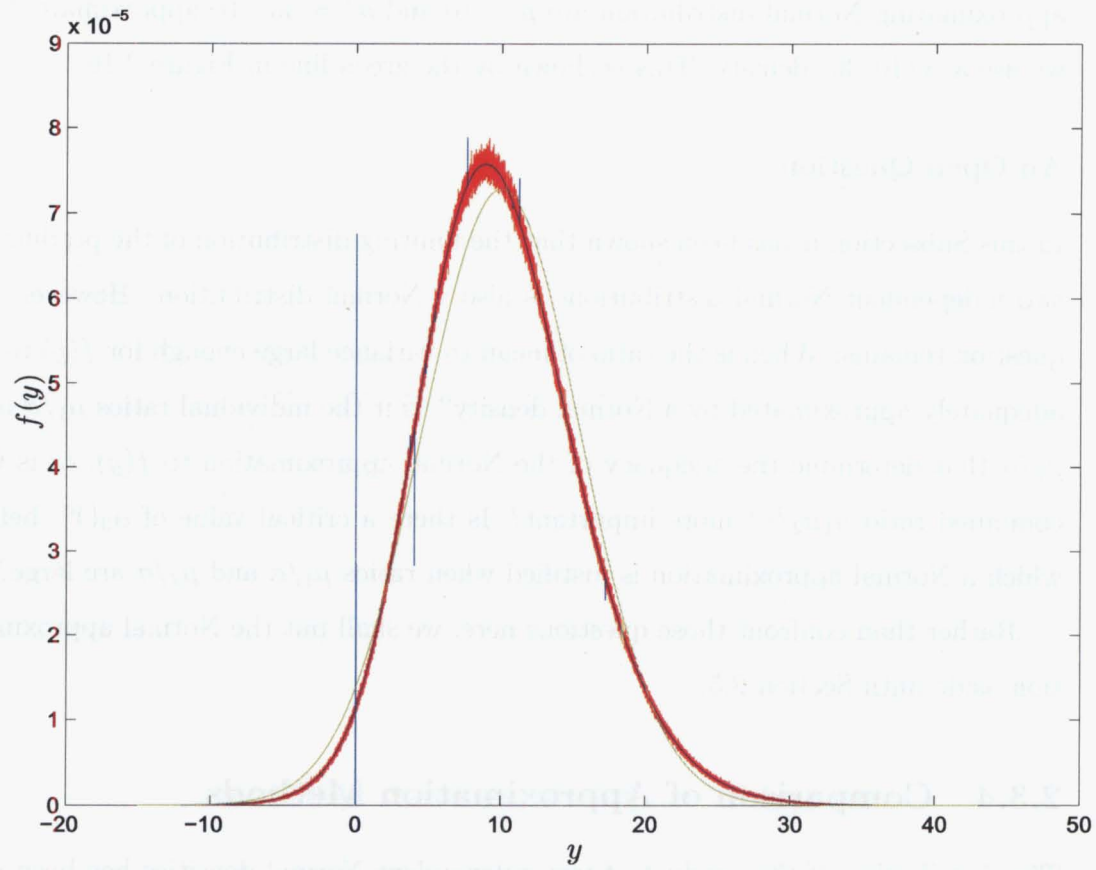


**Figure 2.16: A comparison of the three different approximations of $f(y)$ for Case 2. The Monte Carlo (red) and numerical integration (blue) approximations have interval widths of 0.001. The Normal approximation to the analytic result is green.**

tion, blue, and Monte Carlo simulation, red, can be seen in Figure 2.16. The numerical integration has interval widths of 0.001 and for the Monte Carlo simulation $N = 100,000,000$. Notice how much more accurate the numerical integration is. The Normal approximation, green, is much closer to the other two approximations than it was in Case 1. We expect that as $\mu_1$ and $\mu_2$ increase relative to $\sigma^2$ the approximations of $f(y)$ obtained via numerical integration and Monte Carlo methods will become increasingly similar to a $N(\mu_1\mu_2, \sigma^2(\mu_{X_1}^2 + \mu_{X_2}^2 + \sigma^2))$ density.

Table 2.1 shows that in both Cases the mean and variance calculated from $f(y)$ are very similar. This is true for Case 1 even though the shape of the Normal approximation is very different to the shape of the other two approximations. In both Cases the skewness of the numerical integration and Monte Carlo approximations is

| Case | Method of Approximation | Mean | Variance | Skewness |
|---|---|---|---|---|
| Case 1 | Numerical Integration | 0.5004 | 2.2522 | 0.8894 |
| | Monte Carlo | 0.4978 | 2.2418 | 0.8941 |
| | Normal | 0.5 | 2.25 | 0 |
| | Exact Moment Values | 0.5 | 2.25 | 0.8889 |
| Case 2 | Numerical Integration | 10.0000 | 29.9943 | 0.3649 |
| | Monte Carlo | 9.9992 | 29.9952 | 0.3653 |
| | Normal | 10 | 30 | 0 |
| | Exact Moment Values | 10 | 30 | 0.3651 |

**Table 2.1: A comparison of the mean and variance of the three approximate distributions. The exact known values of the first three moments of the product distribution are included for comparison. The Normal approximation uses the exact known values of the first two moments of the product distribution. Values are recorded to 4dp.**

very close to the exact known skewness of the product distribution. The skewness of the Normal approximation will always be zero, suggesting that in both of these two Cases it is a comparatively poor method of approximation.

In Case 1 there is more difference between the three different mean and variance estimates than there is in Case 2. If the numerical integration takes place using interval widths of 0.001 rather than 0.01, the approximate values of $E(Y)$ and $V(Y)$ are 0.5000 and 2.2499 respectively. If the Monte Carlo simulation takes place with a larger value of $N$, say with $100,000,000$ simulations rather than $1,000,000$, then $E(Y) = 0.4999$ and $V(Y) = 2.2500$.

## 2.4 Sums of Products of Two Normal Variables

To calculate the error metric, $M_e(\mathbf{s}, \hat{\mathbf{s}})$, we need to investigate the density for a sum of several products of Normal variables. In Section 2.3 we found how to obtain the density for the product of two Normal variables. In this section we shall consider how to find the density for the sum of several products. One way is to use the theory of convolutions.

### 2.4.1 Convolutions of Numerical Integration

The theory of convolutions is one method that can be used to find the distribution of a sum of random variables. If we have two random variables, $Y_1$ and $Y_2$, whose joint density is given by $f(y_1, y_2)$, we can write the joint density of $Z = Y_1 + Y_2$ and $Y_2$ as

$$f(z, y_2) = f(y_1, y_2) \left| \frac{dy_1}{dz} \right|. \tag{2.39}$$

Since

$$\left| \frac{dy_1}{dz} \right| = 1, \tag{2.40}$$

Equation 2.39 becomes

$$f(z, y_2) = f(z - y_2, y_2). \tag{2.41}$$

Summing over $y_2$ gives

$$f(z) = \sum_{y_2} f(z - y_2, y_2). \tag{2.42}$$

Formula 2.42 is called the Convolution Formula. In the case of independent variables, as we study here, Equation 2.42 reduces to

$$f(z) = \sum_{y_2} f(z - y_2) f(y_2). \tag{2.43}$$

In practical terms, the Convolution Formula involves obtaining vectors which contain a grid of possible values of $Y_1$ and $Y_2$ along with the density valuations at each respective point. Computationally the procedure for implementing this convolution process is as follows,

1. Select a value of $Z$.

2. Find pairs of $(y_1, y_2)$ that sum to $z$.

3. Evaluate $f(\mathbf{y}_1)$ and $f(\mathbf{y}_2)$ over the vectors $\mathbf{y}_1$ and $\mathbf{y}_2$ that support the sum.

4. Flip the vector $f(\mathbf{y}_2)$, so the orders of $\mathbf{y}_1$ and $\mathbf{y}_2^F$ are appropriate to generate the sum in each component.

5. Find the component product of $f(\mathbf{y}_1)$ and the flipped $f(\mathbf{y}_2)$.

6. Sum the product vector.

Once this process is repeated for all possible values of $Z$, the vector containing $f(z)$ values is normalised. The resulting mass function is an approximation of the density.

**Case 1:** $\mu_1 = 1, \mu_2 = 0.5, \sigma^2 = 1, cov(X_1, X_2) = 0.$

In Section 2.3.1 we used numerical integration to obtain an approximation of the marginal density $f(y)$, where $X_1 \sim N(1,1)$, $X_2 \sim N(0.5,1)$ and $cov(X_1, X_2) = 0$. The resultant density was shown in Figure 2.5. The problem we address here is how to determine the density for the sum of $N$ independent generations of such a variable $Y$. This is achieved sequentially by first convoluting $f(y)$ with itself, and then convoluting $f(y)$ with the achieved density for the convoluted sum. The density $f(y)$ can be convoluted either with itself or with another density any number of times. To display quickly how the distribution of the sum converges to a Normal we shall convolute the sum densities with themselves a few times.

We shall convolute $Y_i \sim f_{Y_i}(y)$ with itself. The densities $f_{Z_j}(z) = f_{\left[\sum_{i=1}^{2^j-1} Y_i\right]}(z)$, $j = 1, \ldots, 5$, obtained through a series of convolutions are demonstrated in Figure 2.17. The top panel displays the unadulterated $f_{Z_1}(z) = f_Y(y)$ density for comparison. Note the density featured in the top panel is the density displayed in Figure 2.5. The second panel displays $f_{Z_2}(z)$. The density still retains a maximum at 0, but the curve is noticeably less 'peaked'. The third panel demonstrates $f_{Z_3}(z) = f_{\sum_{i=1}^{4} Y_i}(y)$. The density now has a mode greater than 0, and although it is still slightly skewed, it looks much more like a Normal density. The fourth and fifth panels show $f_{Z_4}(z) = f_{\sum_{i=1}^{8} Y_i}(y)$ and $f_{Z_5}(z) = f_{\sum_{i=1}^{16} Y_i}(y)$. We can see that as the number of summed variables increases, $f_Z(z)$ approaches normality, even though the original $f_Y(y)$ is far from a Normal density. Of course such is expected from the Central Limit Theorem. However the convolution procedure allows us to compute

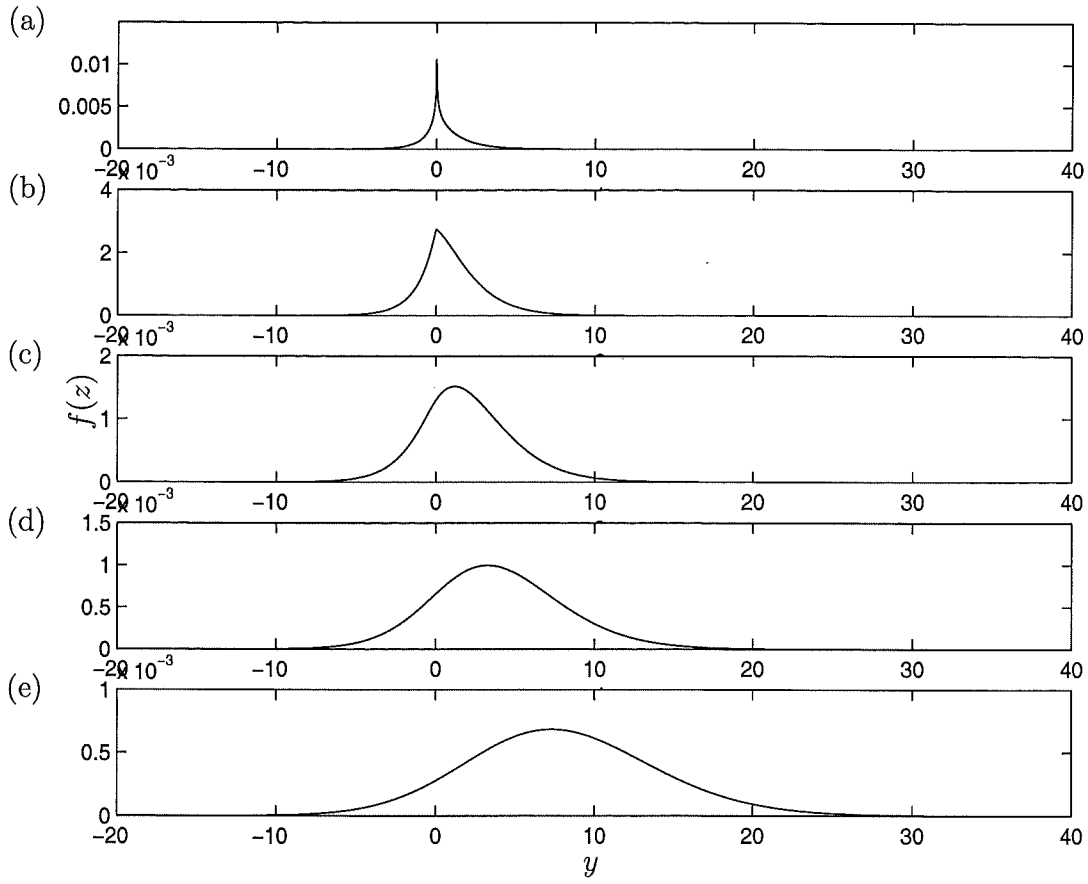


**Figure 2.17: A sequence of convolutions based on the numerical integration obtained in Section 2.3.1. The panels represent $f_{Z_i}(z)$ for $i = 1, \ldots, 5$.**

exact distribution values for non-Normal distributions of sums of fewer variables. The only non-Normal parts of $f_{Z_5}(z)$ are the extreme tails, in the top and bottom 2%.

**Case 2:** $\mu_1 = 5, \mu_2 = 2, \sigma^2 = 1, cov(X_1, X_2) = 0.$

In Section 2.3.1 we used a numerical integration procedure to attain an approximation of the marginal density $f(y)$, where $X_1 \sim N(5,1)$, $X_2 \sim N(2,1)$ and $cov(X_1, X_2) = 0$. The density is displayed in Figure 2.8. Figure 2.18 displays a series of convolutions $f_{Z_j}(z)$, $j = 1, \ldots, 5$. Note that $f_{Z_1}(z) = f(y)$. The density in the top panel is the approximation of the marginal density which was attained in Section 2.3.1. As with Case 1, which was described in the previous Subsection, $f(y)$ is convoluted with itself $1, 2, 4, 8$ and 16 times. Once again, although $f(y)$ is clearly

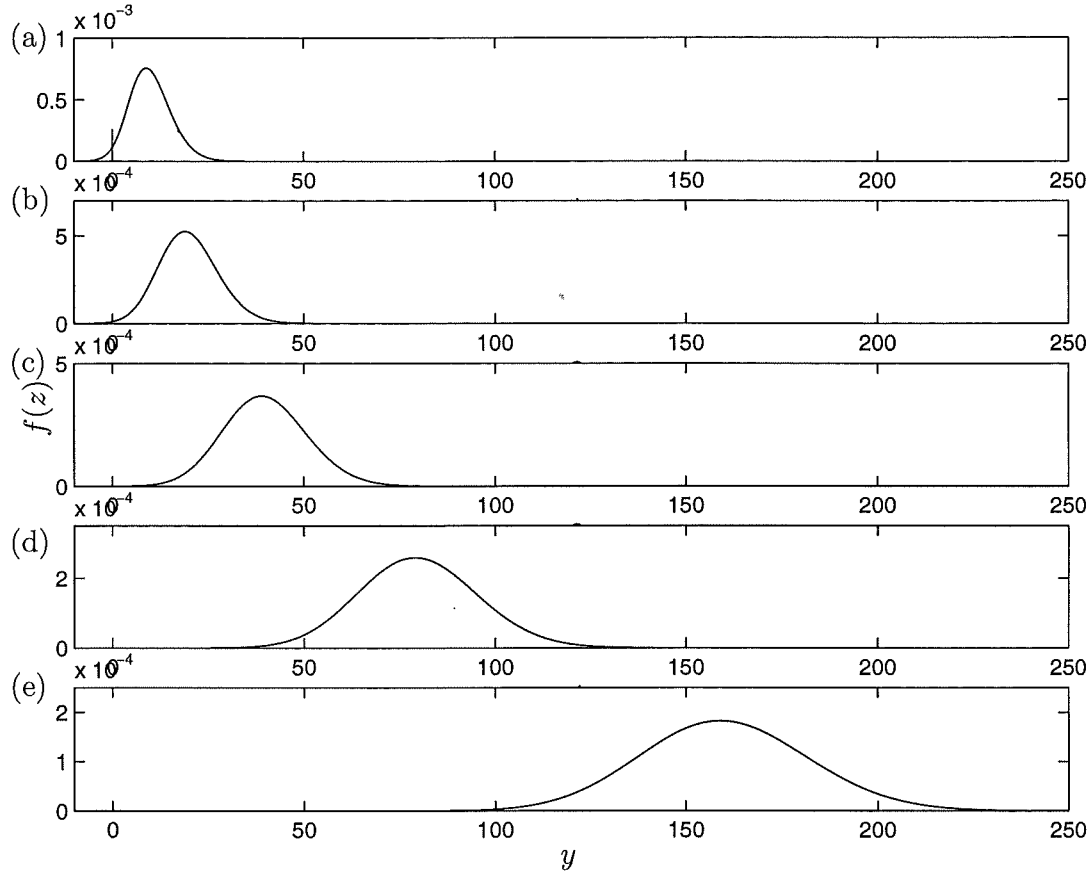


**Figure 2.18: A sequence of convolutions based on the numerical integration obtained in Section 2.3.1. The panels represent $f_{Z_i}(z)$ for $i = 1, \ldots, 5$.**

non-Normal, $f_{Z_j}(z)$ quickly approaches normality as $j$ increases.

## 2.5 Calculation of the Error Metric

The problem that instigated this research involves finding the probability that the real component of the error metric between transmitted and hypothesised signals is negative. See Section 2.2 for full details. The form of the error metric that we shall concern ourselves with for the remainder of this chapter is

$$M_e(s, \hat{s}) = \sum_{t=1}^{N\xi} (y_{R,t}y_{R,t-\xi}b_{R,t} + y_{R,t}y_{I,t-\xi}b_{I,t} - y_{I,t}y_{R,t-\xi}b_{I,t} + y_{I,t}y_{I,t-\xi}b_{R,t}) . \quad (2.44)$$

Calculation of $M_e(s, \hat{s})$ involves computing the density for the sum of four or more products of variables, each assessed as having a Normal distribution.

We investigate three procedures to approximate the error metric. One way to

obtain $M_e(s, \hat{s})$ is by computing the densities of products of independent Normally distributed variables via numerical integration and then using the Convolution Formula to identify the density of the sum of a series of these products, that is, by combining the processes introduced in Sections 2.3.1 and 2.4. Another way to approximate $M_e(s, \hat{s})$ is to implement a Monte Carlo simulation. A third way to approximate the distribution of the error metric is with a Normal distribution whose parameters are set to the mean and variance of $M_e(s, \hat{s})$. This approximation is only appropriate when $\alpha_3(Y)$ is small.

### 2.5.1 Properties of the Error Metric

#### Correlation of Products of Normal Variables

In Section 2.4 we studied the distribution of sums of products of independent Normal variables, where each product is uncorrelated with any other product. However, a study of Equation 2.44 shows us that when calculating the distribution of the error metric, some of the products of Normal variables will be correlated. In fact, if we assess

$$\begin{bmatrix} Y_0 \\ Y_1 \\ Y_2 \end{bmatrix} \sim N\left( \begin{bmatrix} \mu_0 \\ \mu_1 \\ \mu_2 \end{bmatrix}, \begin{bmatrix} \sigma_0^2 & 0 & 0 \\ 0 & \sigma_1^2 & 0 \\ 0 & 0 & \sigma_2^2 \end{bmatrix} \right),$$

then the covariance of $Y_0Y_1$ and $Y_1Y_2$ is

$$\begin{aligned} cov(Y_0Y_1, Y_1Y_2) &= E[(Y_0Y_1 - \mu_0\mu_1)(Y_1Y_2 - \mu_1\mu_2)] \\ &= E(Y_0Y_1^2Y_2) - \mu_0\mu_1E(Y_1Y_2) - \mu_1\mu_2E(Y_0Y_1) + \mu_0\mu_1^2\mu_2 \\ &= \int_{-\infty}^{\infty} y_0 f(y_0)dy_0 \int_{-\infty}^{\infty} y_1^2 f(y_1)dy_1 \int_{-\infty}^{\infty} y_2 f(y_2)dy_2 \\ &\quad -\mu_0\mu_1 \int_{-\infty}^{\infty} y_1 f(y_1)dy_1 \int_{-\infty}^{\infty} y_2 f(y_2)dy_2 \\ &\quad -\mu_1\mu_2 \int_{-\infty}^{\infty} y_0 f(y_0)dy_0 \int_{-\infty}^{\infty} y_1 f(y_1)dy_1 + \mu_0\mu_1^2\mu_2 \\ &= \mu_0\left(\mu_1^2 + \sigma_1^2\right)\mu_2 + \mu_0\mu_1^2\mu_2 - \mu_0\mu_1^2\mu_2 - \mu_0\mu_1^2\mu_2 \\ &= \sigma_1^2\mu_0\mu_2, \end{aligned} \tag{2.45}$$

which is non-zero when both $\mu_0 \neq 0$ and $\mu_2 \neq 0$.

### Mean and Variance of the Error Metric

Standard distribution theory tells us that for random variables $X_0$ and $X_1$, $E(X_0 + X_1) = E(X_0) + E(X_1)$ and $V(X_0 + X_1) = V(X_0) + V(X_1) + 2cov(X_0, X_1)$. Since, from Section 2.3.3, $E(Y_t Y_{t+1}) = \mu_t \mu_{t+1}$ and $V(Y_t Y_{t+1}) = \sigma_1^2\sigma_2^2 + \mu_1^2\sigma_2^2 + \mu_2^2\sigma_1^2$, we have

$$\begin{aligned}
E\left(M_e(s,\hat{s})\right) &= E\left(\sum_{t=1}^{N\xi}\left(y_{R,t}y_{R,t-\xi}b_{R,t} + y_{R,t}y_{I,t-\xi}b_{I,t} - y_{I,t}y_{R,t-\xi}b_{I,t} + y_{I,t}y_{I,t-\xi}b_{R,t}\right)\right) \\
&= \sum_{i=1}^{N\xi}\left(b_{R,t}E(Y_{R,t}Y_{R,t-\xi}) + b_{I,t}E(Y_{R,t}Y_{I,t-\xi}) - b_{I,t}E(Y_{R,t-\xi}Y_{I,t})\right. \\
&\quad \left. + b_{R,t}E(Y_{I,t}Y_{I,t-\xi})\right) \\
&= \sum_{t=1}^{N\xi}\left(\mu_{R,t}\mu_{R,t-\xi}b_{R,t} + \mu_{R,t}\mu_{I,t-\xi}b_{I,t} - \mu_{I,t}\mu_{R,t-\xi}b_{I,t} + \mu_{I,t}\mu_{I,t-\xi}b_{R,t}\right) \quad (2.46)
\end{aligned}$$

and

$$\begin{aligned}
V\left(M_e(s,\hat{s})\right) &= V\left(\sum_{t=1}^{N\xi}\left(y_{R,t}y_{R,t-\xi}b_{R,t} + y_{R,t}y_{I,t-\xi}b_{I,t} - y_{I,t}y_{R,t-\xi}b_{I,t} + y_{I,t}y_{I,t-\xi}b_{R,t}\right)\right) \\
&= \sum_{t=1}^{N\xi}\Big(b_{R,t}^2V(Y_{R,t}Y_{R,t-\xi}) + b_{I,t}^2V(Y_{R,t}Y_{I,t-\xi}) \\
&\quad + b_{I,t}^2V(Y_{I,t}Y_{R,t-\xi}) + b_{R,t}^2V(Y_{I,t}Y_{I,t-\xi}) \\
&\quad + 2b_{R,t}b_{I,t}\left(cov(Y_{R,t}Y_{R,t-\xi}, Y_{I,t-\xi}Y_{R,t}) + cov(Y_{R,t}Y_{I,t-\xi}, Y_{I,t-\xi}Y_{I,t})\right. \\
&\quad \left. - cov(Y_{R,t}Y_{R,t-\xi}, Y_{R,t-\xi}Y_{I,t}) - cov(Y_{I,t}Y_{R,t-\xi}, Y_{I,t-\xi}Y_{I,t})\right) \\
&\quad + 2b_{R,t}b_{R,t+\xi}(cov(Y_{R,t}Y_{R,t-\xi}, Y_{R,t+\xi}Y_{R,t}) + cov(Y_{I,t}Y_{I,t-\xi}, Y_{I,t+\xi}Y_{I,t})) \\
&\quad + 2b_{R,t}b_{I,t+\xi}(cov(Y_{I,t}Y_{I,t-\xi}, Y_{I,t}Y_{R,t+\xi}) - cov(Y_{R,t}Y_{R,t-\xi}, Y_{R,t}Y_{I,t+\xi})) \\
&\quad + 2b_{I,t}b_{R,t+\xi}(cov(Y_{R,t}Y_{I,t-\xi}, Y_{R,t}Y_{R,t+\xi}) - cov(Y_{R,t-\xi}Y_{I,t}, Y_{I,t}Y_{I,t+\xi})) \\
&\quad + 2b_{I,t}b_{I,t+\xi}(-cov(Y_{I,t-\xi}Y_{R,t}, Y_{R,t}Y_{I,t+\xi}) - cov(Y_{R,t-\xi}Y_{I,t}, Y_{I,t}Y_{R,t+\xi}))\Big) \\
&= \sum_{t=1}^{N\xi}\Big(b_{R,t}^2\left(\sigma_{R,t-\xi}^2\sigma_{R,t}^2 + \mu_{R,t-\xi}^2\sigma_{R,t}^2 + \mu_{R,t}^2\sigma_{R,t-\xi}^2 + \sigma_{I,t-\xi}^2\sigma_{I,t}^2\right. \\
&\quad \left. + \mu_{I,t-\xi}^2\sigma_{I,t}^2 + \mu_{I,t}^2\sigma_{I,t-\xi}^2\right) + b_{I,t}^2\left(\sigma_{R,t}^2\sigma_{I,t-\xi}^2 + \mu_{R,t}^2\sigma_{I,t-\xi}^2\right. \\
&\quad \left. + \mu_{I,t-\xi}^2\sigma_{R,t}^2 + \sigma_{R,t-\xi}^2\sigma_{I,t}^2 + \mu_{I,t}^2\sigma_{R,t-\xi}^2 + \mu_{R,t-\xi}^2\sigma_{I,t}^2\right) \\
&\quad + 2b_{R,t}b_{I,t}\left(\sigma_{R,t}^2\mu_{R,t-\xi}\mu_{I,t+\xi} + \sigma_{I,t-\xi}^2\mu_{R,t}\mu_{I,t}\right. \\
&\quad \left. - \sigma_{R,t-\xi}^2\mu_{R,t}\mu_{I,t} - \sigma_{I,t}^2\mu_{R,t-\xi}\mu_{I,t-\xi}\right) \\
&\quad + 2b_{R,t}b_{R,t+\xi}\left(\sigma_{R,t}^2\mu_{R,t-\xi}\mu_{R,t+\xi} + \sigma_{I,t}^2\mu_{I,t-\xi}\mu_{I,t+\xi}\right) \\
&\quad + 2b_{R,t}b_{I,t+\xi}\left(\sigma_{I,t}^2\mu_{I,t-\xi}\mu_{R,t+\xi} - \sigma_{R,t}^2\mu_{R,t-\xi}\mu_{I,t+\xi}\right)
\end{aligned}$$

$$+2b_{I,t}b_{R,t+\xi}\left(\sigma^2_{R,t}\mu_{I,t-\xi}\mu_{R,t+\xi} - \sigma^2_{I,t}\mu_{R,t-\xi}\mu_{I,t+\xi}\right)$$
$$+2b_{I,t}b_{I,t+\xi}\left(-\sigma^2_{R,t}\mu_{I,t-\xi}\mu_{I,t+\xi} - \sigma^2_{I,t}\mu_{R,t-\xi}\mu_{R,t+\xi}\right)\Big). \quad (2.47)$$

When $\mu_{R,t} = \mu_{I,t} = \mu$, $b_{R,t} = b_{I,t} = 1$ and $\sigma^2_{R,t} = \sigma^2_{I,t} = \sigma^2$ for all $t$, the expectation and variance of the error metric reduce to

$$E\left(M_e(s,\hat{s})\right) = 2N\xi\mu^2 \quad (2.48)$$

$$\text{and} \quad V\left(M_e(s,\hat{s})\right) = 4N\xi\sigma^2\left(\sigma^2 + 2\mu^2\right) \quad (2.49)$$

### 2.5.2 Calculation of the Error Metric using Numerical Integration and Convolutions

To use numerical integration and convolutions to identify the density of the error metric via the processes discussed in the preceding Sections, each product must be uncorrelated with any other product. A study of Equation 2.44 shows that we cannot rearrange $M_e(s,\hat{s})$ so that this will be the case. However, an inspection of Equations 2.48 and 2.49 shows that, whether we are summing independent or correlated variables, the expectation and variance of the error metric will be the same. Simulations suggest that this relationship does not hold for any higher moments. Thus, although we cannot expect the approximation of the error metric attained by using our numerical integration and convolution procedure to be as accurate as a Monte Carlo approximation, the two methods should produce densities that are reasonably similar. This is because, as $N\xi$ increases, both distributions will approach Normality (by the Central Limit Theorem) and will have the same mean and variance (by Equations 2.48 and 2.49).

A study of Equation 2.44 shows that to assess the distribution for the error metric, we first need to find the density of the product of two Normally distributed variables via numerical integration. Then we convolute $N\xi$ of these individual densities of products of Normal variables. Since each of our $Y_{R,t}$ and $Y_{I,t}$ terms is Normally distributed with mean $\mu$ and variance $\sigma^2$, we merely find the density for the product of two $N(\mu,\sigma^2)$ densities using numerical integration, and then use the Convolution Formula to find the density of the sum of $N\xi$ of these products. Finally, we calculate $P(M_e(s,\hat{s})) < 0$ by forming the cumulative sum of $M_e(s,\hat{s})$ and finding

its value at 0.

### 2.5.3 Calculation of the Error Metric using a Monte Carlo Construction

A Monte Carlo construction can be used to simulate the error metric directly from Equation 2.44. We can approximate the distribution of the error metric by implementing Monte Carlo simulations on either MATLAB or WinBUGS. A value of $M_e(s, \hat{s})$ can be calculated for any set of received $Y$ values. If a large number of sets of $Y$ values are randomly drawn, and if $M_e(s, \hat{s})$ is calculated for each of the sets, then we have a large number of random samples drawn from the distribution of the error metric, our target distribution. An estimate of $P[M_e(s, \hat{s}) < 0]$ is obtained by counting the number of random samples which have taken on a negative value, and dividing by the total number of samples.

The density of the error metric is approximated by sorting the samples into intervals and normalising. Scott (1992) showed that the shape of a histogram estimate depends on how the bins are defined. The smaller the bin widths, the more accurate the estimates are. However, narrow bins tend to introduce extra variability. In Section 2.3.2 we discussed how finely inaccurate the Monte Carlo approximation is compared to the numerically integrated and convoluted approximation, viz. Figures 2.5 and 2.11. This is a common problem for researchers who are interested in studying the density of the target distribution (Hoti et al., 2002). One way to alleviate this is to 'smooth' the data using the average of $M$ different histograms, all based on the same bin width, $h$, but using different equally spaced sideways shifts (Scott, 1985). When the number of histograms is increased to infinity the bin width of the averaged shifted histogram vanishes (since $h/M \to 0$ as $M \to \infty$) and the estimate becomes the kernel density estimator (KDE),

$$\hat{f}_{KDE}(x) = \frac{1}{nh} \sum_{i=1}^{n} K\left(\frac{x - X_i}{h}\right), \tag{2.50}$$

where $K(u)$ is a kernel smoothing function, $n$ is the number of draws from the target density and $h > 0$ is a smoothing parameter. The smoothing parameter plays a role similar to that of the bin widths of the histogram. When comparing

the approximated histogram with the KDE, we can view the KDE as the average of infinitely many histograms with bin width $h$.

MATLAB programs to implement kernel density estimates are available from the Rolf Nevanlinna Institute's internet site[1]. The smoothing function used in Examples 1 and 2 is $K(u) = (1 - |u|)_+$, where $(u)_+ = u$ if $u > 0$ and zero otherwise. This is known as the triangle kernel function. To compare the approximated histogram with the KDE, we can view the KDE as the average of infinitely many histograms with bin width $h$.

The density of the error metric can be directly simulated using WinBUGS. $Y$ values are generated and the relevant statistics are directly obtained. If the variable under investigation is assessed as continuous, as it is in this case, WinBUGS automatically plots a smoothed KDE of the target density. The KDE is calculated using a default $h$ value of 0.2.

### 2.5.4 Calculation of the Error Metric using Normal Approximations

If the values of $\alpha_3(Y)$ are sufficiently small we can assess the distribution of the error metric by approximating the product of two Normal distributions as another Normal distribution. This approximation will improve as $N\xi$ increases, since the Central Limit Theorem tells us that the distribution of the error metric will become increasingly Normal as the number of sums of products increases. In Section 2.5.1 we showed that, for our problem, the mean and variance of $M_e(s, \hat{s})$ are $2N\xi\mu^2$ and $4N\xi\sigma^2(\sigma^2 + 2\mu^2)$ respectively.

[1] www.rni.helsinki.fi/~fjh

### 2.5.5 Example 1

To illustrate the discussion of the previous two subsections, and to show how to calculate $P[M_e(s,\hat{s}) < 0]$ in practice, let $N = 2$, $\xi = 1$, $b_{R,i} = b_{I,i} = [1 \quad 1]$ and

$$\begin{bmatrix} Y_{R,0} \\ Y_{I,0} \\ Y_{R,1} \\ Y_{I,1} \\ Y_{R,2} \\ Y_{I,2} \end{bmatrix} \sim N\left( \begin{bmatrix} 1 \\ 1 \\ 1 \\ 1 \\ 1 \\ 1 \end{bmatrix}, \begin{bmatrix} 1 & 0 & 0 & 0 & 0 & 0 \\ 0 & 1 & 0 & 0 & 0 & 0 \\ 0 & 0 & 1 & 0 & 0 & 0 \\ 0 & 0 & 0 & 1 & 0 & 0 \\ 0 & 0 & 0 & 0 & 1 & 0 \\ 0 & 0 & 0 & 0 & 0 & 1 \end{bmatrix} \right).$$

The form of the error metric is, from Equation 2.44,

$$\begin{aligned} M_e(s,\hat{s}) &= \sum_{t=1}^{2} (y_{R,t}y_{R,t-1}b_{R,t} + y_{R,t}y_{I,t-1}b_{I,t} - y_{I,t}y_{R,t-1}b_{I,t} + y_{I,t}y_{I,t-1}b_{R,t}) \\ &= y_{R,0}y_{R,1} + y_{R,1}y_{I,0} - y_{R,0}y_{I,1} + y_{I,0}y_{I,1} + y_{R,1}y_{R,2} + y_{R,2}y_{I,1} \\ &\quad -y_{R,1}y_{I,2} + y_{I,1}y_{I,2}. \end{aligned} \tag{2.51}$$

#### Example 1: Numerical Integration and Convolutions

We use numerical integration, as described in Section 2.3.1, to approximate the density of the product of two $N(1,1)$ distributions. Each product is integrated between limits of -8.0005 and 17.0005, with interval width 0.001.

To compute density $M_e(s,\hat{s})$, we sum the eight products of Normal variables using the Convolution Formula. $M_e(s,\hat{s})$ has values recorded on the interval $(-82.004, 118.004)$. In Figure 2.19 this approximation of $M_e(s,\hat{s})$ is represented by the smooth blue line.

#### Example 1: Monte Carlo using MATLAB

By directly using a Monte Carlo construction we can approximate the density of the error metric. To simulate the $Y$ vectors needed we randomly select $15,000,000$ observations for each $Y_{R,t}$ and $Y_{I,t}$, $t = 0, 1, 2$. We chose to select $15,000,000$ observations because that is the maximum number that can currently be stored in the memory of a computer operating in the Department of Mathematics and Statistics, University of Canterbury. A value of the error metric is calculated for each of these

$15,000,000$ sets of $Y$ values. By sorting these values into fine intervals we obtain an approximation of the density of the error metric. The simulated values of $M_e(s,\hat{s})$ were sorted into bins of width 0.001. Figure 2.19 shows this approximation as the jagged red line. To estimate $P[M_e(s,\hat{s}) < 0]$ we calculate the proportion of our $15,000,000$ simulations that produce a negative value of $M_e(s,\hat{s})$.

The KDE was computed using a smoothing parameter of $h = 0.4$. It is displayed in Figure 2.19 as the smooth black line. As expected the KDE bisects the approximating histogram.

### Example 1: Monte Carlo using WinBUGS

The density of the error metric can be directly simulated using WinBUGS. $5,000,000$ sets of $Y$ values were generated and the mean, variance, skewness and $P[M_e(s,\hat{s}) < 0]$ were directly obtained. These statistics are displayed in Table 2.2. The KDE computed using WinBUGS has the same shape and coverage as the KDE generated using MATLAB.

### Example 1: Normal Approximation

In the previous section we showed that, for our examples, the expectation and variance of the error metric can be represented as $E\left(M_e(s,\hat{s})\right) = 2N\xi\mu^2$ and $V\left(M_e(s,\hat{s})\right) = 4N\xi\sigma^2\left(\sigma^2+2\mu^2\right)$. Since $Y_{R,t} \sim N(1,1)$ and $Y_{I,t} \sim N(1,1)$ for $t = 0,1,2$, $N = 2$ and $\xi = 1$, the density of the error metric is approximated by a Normal density with mean 4 and variance 24.

Recall that in Section 2.3.3 we found that the skewness of the product of two independent Normal variables, $\alpha_3(Y_1Y_2)$, is greatest when $\mu_1 = \sigma_1$ and $\mu_2 = \sigma_2$. In this example each individual $\alpha_3(Y)$ value is the largest possible. Although the Central Limit Theorem tells us that the distribution of $M_e\left(s,\hat{s}\right)$ will approach Normality as the number of summed variables increases, in this case we are only summing eight products of Normals. Thus, although the resulting density is less non-Normal than the original product, it is still far from Normal itself.

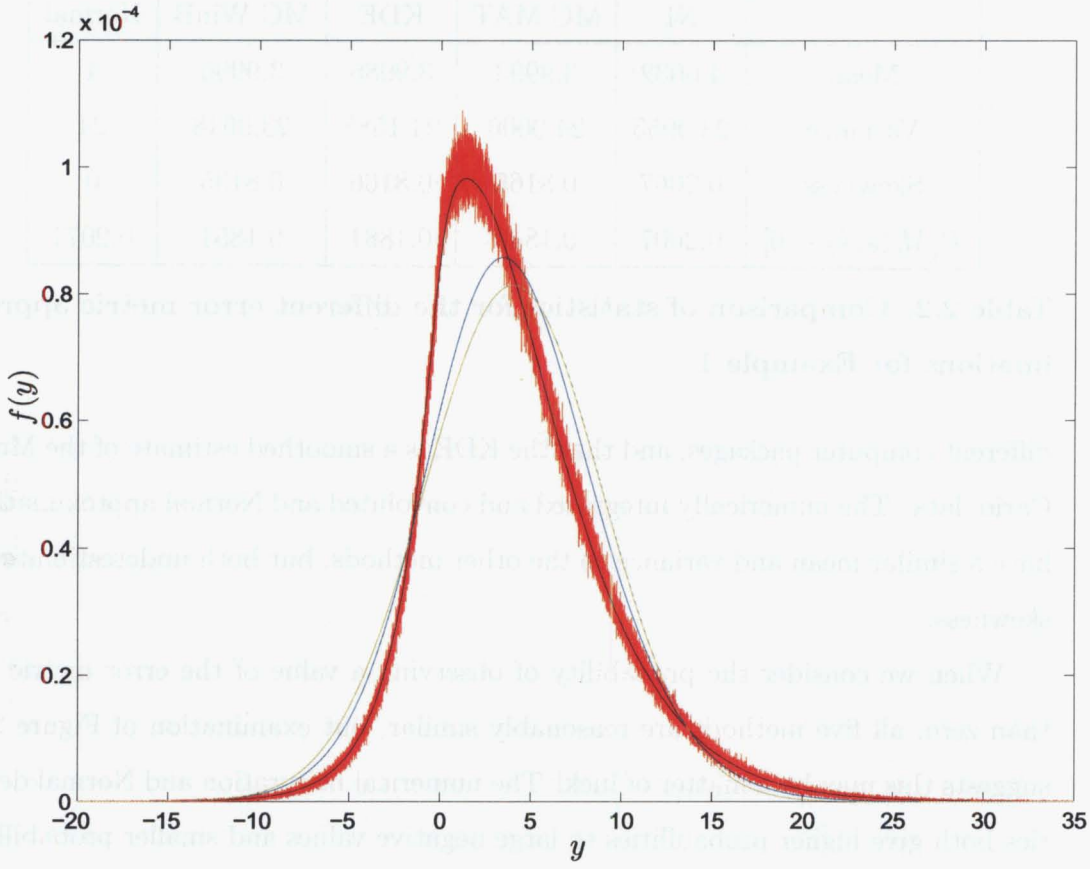


**Figure 2.19: The density of the error metric approximated by numerical integration and convolutions (blue), a Monte Carlo method (red), a kernel density estimate (black) and a Normal density (green) for Example 1.**

**Example 1: Results**

Figure 2.19 displays the four densities produced by our different approximation methods. The density of the error metric is clearly non-Normal. The KDE (black) is a smoothed version of the Monte Carlo (red), and both of these densities are quite different from the numerically integrated and convoluted (blue) and Normal (green) densities. Given the high skewness of each product of Normal variables this is hardly surprising.

Table 2.2 shows that the mean, variance and skewness for the error metric, and the probability of observing a value less than 0, are very similar for both Monte Carlo approximations and the smoothed KDE. Again, this is not a surprise when we consider that both Monte Carlo estimates were formed using the same process on

| | NI | MC MAT | KDE | MC WinB | Normal |
|---|---|---|---|---|---|
| Mean | 4.0032 | 3.9993 | 3.9985 | 3.9996 | 4 |
| Variance | 23.9955 | 24.0006 | 24.1588 | 23.9648 | 24 |
| Skewness | 0.2067 | 0.8165 | 0.8166 | 0.8135 | 0 |
| $P[M_e(s,\hat{s}) < 0]$ | 0.2007 | 0.1840 | 0.1881 | 0.1851 | 0.2071 |

**Table 2.2: Comparison of statistics for the different error metric approximations for Example 1.**

different computer packages, and that the KDE is a smoothed estimate of the Monte Carlo data. The numerically integrated and convoluted and Normal approximations have a similar mean and variance to the other methods, but both underestimate the skewness.

When we consider the probability of observing a value of the error metric less than zero, all five methods are reasonably similar, but examination of Figure 2.19 suggests this may be a matter of luck! The numerical integration and Normal densities both give higher probabilities to large negative values and smaller probabilities to values slightly below zero.

### 2.5.6 Example 2

In the second example we assume that $N = 2$, $\xi = 1$, $b_{R,i} = b_{I,i} = [1 \quad 1]$ and

$$\begin{bmatrix} Y_{R,0} \\ Y_{I,0} \\ Y_{R,1} \\ Y_{I,1} \\ Y_{R,2} \\ Y_{I,2} \end{bmatrix} \sim N\left( \begin{bmatrix} 1 \\ 1 \\ 1 \\ 1 \\ 1 \\ 1 \end{bmatrix}, \begin{bmatrix} 0.1 & 0 & 0 & 0 & 0 & 0 \\ 0 & 0.1 & 0 & 0 & 0 & 0 \\ 0 & 0 & 0.1 & 0 & 0 & 0 \\ 0 & 0 & 0 & 0.1 & 0 & 0 \\ 0 & 0 & 0 & 0 & 0.1 & 0 \\ 0 & 0 & 0 & 0 & 0 & 0.1 \end{bmatrix} \right).$$

The form of the error metric is the same as in Equation 2.51,

$$\begin{aligned} M_e(s,\hat{s}) \;=\; & y_{R,0}y_{R,1} + y_{R,1}y_{I,0} - y_{R,0}y_{I,1} + y_{I,0}y_{I,1} + y_{R,1}y_{R,2} + y_{R,2}y_{I,1} \\ & -y_{R,1}y_{I,2} + y_{I,1}y_{I,2}. \end{aligned}$$

### Example 2: Numerical Integration and Convolutions

Numerical integration is used to identify the density of the product of two $N(1, 0.1)$ distributions. The product is integrated between limits $-1$ and 4 with interval widths of 0.001, and is convoluted to produce an approximate density for $M(s, \hat{s})$. This is displayed in Figure 2.20 as the smooth blue line.

### Example 2: Monte Carlo using MATLAB

A Monte Carlo construction can be used to simulate an error metric directly. 15,000,000 values were simulated for each of the six Normally distributed variables. An approximating histogram is shown in Figure 2.20 as the jagged red line. A KDE, displayed as a smooth black line, was computed using $h = 0.2$.

### Example 2: Monte Carlo using WinBUGS

WinBUGS was used to directly obtain the density of the error metric. $5,000,000$ sets of $Y$ values were generated and the mean, variance, skewness and $P[M_e(s, \hat{s}) < 0]$ were calculated. They are displayed in Table 2.3.

### Example 2: Normal Approximation

Equations 2.48 and 2.49 tell us that $E(M(s, \hat{s})) = 4$ and $V(M(s, \hat{s})) = 1.68$. We approximate the density of the error metric with a $N(4, 1.68)$ density. This is shown in Figure 2.20 as the green line.

On this occasion we expect the Normal approximation will more accurately reflect the density of the error metric. Each individual product of Normals is less skewed than in Example 1, since $\mu = \frac{1}{\sqrt{10}}\sigma$.

### Example 2: Results

Figure 2.20 shows that the densities produced have much more in common than they did in the previous example. The approximations obtained through numerical integration and convolutions and the Normal density are very similar. Although they are still noticeably different from the Monte Carlo and KDE approximations, the four densities are much more similar than they were in Example 1. This is due

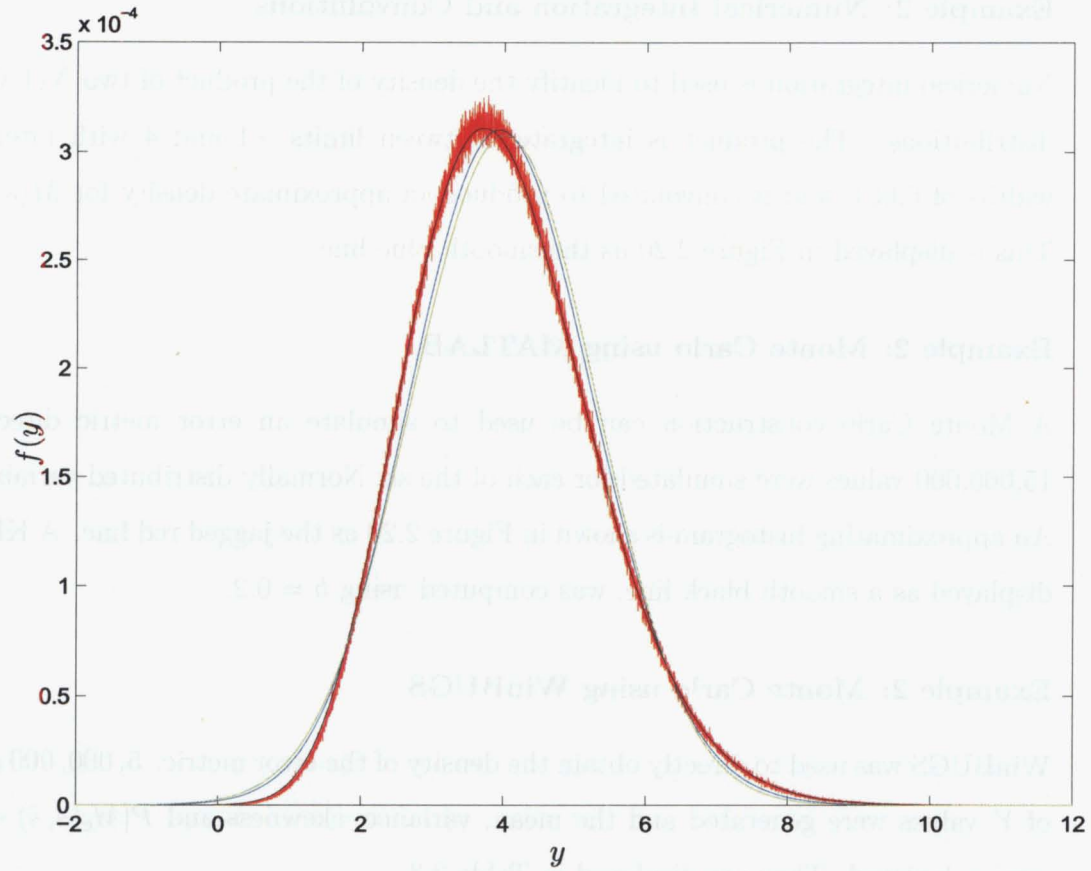


**Figure 2.20: The density of the error metric approximated by numerical integration and convolutions (blue), a Monte Carlo method (red), a kernel density estimate (black) and a Normal density (green) for Example 2.**

to the individual densities of products of two $N(1, 0.1)$ variables being more Normal themselves, since the $\mu/\sigma$ ratio is larger.

In both of the examples we have studied $N\xi$ has been small. In fact it has been 2, the smallest specification possible. In an example with a larger value of $N\xi$, which contains more densities to sum, we can expect the different approximation methods to produce increasingly similar results.

Table 2.3 shows how similar the statistics for the different approximations are. As expected, the difference between the different means and variances is small. The KDE and the two Monte Carlo approximations are still more skewed, but the skewness is roughly half what it was in Example 1. For all approximation methods $P[M_e(s, \hat{s}) < 0]$ is very small, although the numerically integrated and convoluted

| | NI | MC MAT | KDE | MC WinB | Normal |
|---|---|---|---|---|---|
| Mean | 4.0023 | 4.0002 | 3.9993 | 3.9993 | 4 |
| Variance | 1.6755 | 1.6805 | 1.8463 | 1.6810 | 1.68 |
| Skewness | 0.1183 | 0.4404 | 0.4393 | 0.4396 | 0 |
| $P[M_e(s,\hat{s}) < 0]$ | 0.0007 | 0.0002 | 0.0001 | 0.0002 | 0.0010 |

**Table 2.3: Comparison of statistics for the different error metric approximations for Example 2.**

and Normal approximations still give higher probabilities to negative values.

## 2.6 Summary

We began this chapter by briefly introducing the process of Differential Continuous Phase Frequency Shift Keying. The error metric was introduced and we stated our problem in full detail. We discovered that the calculation of the error metric involves two distinct steps: we must assess the distribution for the product of two Normally distributed variables, and we must identify the distribution of the sum of a number of these products of Normal distributions. Sections 2.3 and 2.4 discuss these two processes in depth.

In Section 2.3 the density of the product of two independent Normal variables is approximated using three different methods. We considered a numerical methods approximation, which consisted of implementing numerical integration procedures on both MATLAB and Maple. We considered a Monte Carlo construction. We investigated the moment generating function of the product of two correlated Normal variables, and showed how the mean, variance and skewness change for three special cases. We also showed that as the ratio of $\mu$ to $\sigma$ increases, the distribution of the product of two independent Normal variables tends towards a Normal distribution. These three approximation methods were compared over two examples. It was shown that although both the numerical integration and the Monte Carlo simulation produced densities of the same shape, and similar statistics, the numerical integration was finely accurate compared to the crudeness of the Monte Carlo method. It was shown that it is inappropriate to use a Normal density as an

approximation when $\mu/\sigma$ is small.

Section 2.4 considered how to identify the density of the sum of the products of two Normal variables. The Convolution Formula was introduced, and the computational steps used to identify the density of a sum of random variables outlined. The technique was demonstrated using the product Normal densities obtained in Section 2.3.

In Section 2.5 the theory of the preceding Sections was combined. The density of the error metric was approximated using numerical integration and the Convolution Formula, and $P[M_e(s, \hat{s}) < 0]$ was computed. A Monte Carlo method was used to approximate the density of the error metric, as was a Normal density. The densities were shown to have the same shape and similar statistics, but the density of $(M_e(s, \hat{s}))$ approximated using numerical integration and convolutions is more accurate.

# Chapter 3

# Approximation of Posterior Means and Variances of the Digitised Normal Distribution using Continuous Normal Approximation

## 3.1 Introduction

It is well-known that all statistical measurements which represent the values of useful unknown quantities have a finite and discrete realm of possible measurement values. We denote these as $\mathbf{R}(X) = \{x_1, x_2, \ldots, x_K\}$. Thus our uncertainties about any measurements, if expressed via asserted probability distributions, are represented by discrete probability mass functions. For various historical reasons, common statistical practice treats probability distributions as representable by continuous densities or mixture densities such as the Normal-Gamma mixture-Normal distribution.

If the conditional distribution of $X$, given $\mu$ and $\sigma^2$, is Normally distributed with mean $\mu$ and variance $\sigma^2$, and if $\mu$ is also distributed Normally with mean $\mu_0$ and variance $\tau^2$, independent of $\sigma^2$, then conventional conjugate mixture-Normal theory

tells us that, for a single case, the conditional distribution of $X$ given $\sigma^2$, derived by

$$f(x \mid \sigma^2) = \int_{-\infty}^{\infty} f(x \mid \mu, \sigma^2) f(\mu \mid \sigma^2) d\mu, \tag{3.1}$$

is Normal with mean $\mu_0$ and variance $\sigma^2 + \tau^2$. The distribution of $\mu$ given $(X = x)$, whose density will be denoted by $f(\mu \mid x, \sigma^2)$, is also Normal. It has mean $x - \frac{\sigma^2}{\sigma^2+\tau^2}(x - \mu_0)$ and variance $\frac{\sigma^2\tau^2}{\sigma^2+\tau^2}$. To summarise this situation symbolically,

$$\mu \mid \sigma^2 \sim N\left(\mu_0, \tau^2\right) \tag{3.2}$$

$$X \mid \mu, \sigma^2 \sim N\left(\mu, \sigma^2\right) \tag{3.3}$$

$$X \mid \sigma^2 \sim N\left(\mu_0, \sigma^2 + \tau^2\right) \tag{3.4}$$

and

$$\mu \mid X = x, \sigma^2 \sim N\left(x - \frac{\sigma^2}{\sigma^2 + \tau^2}(x - \mu_0), \frac{\sigma^2\tau^2}{\sigma^2 + \tau^2}\right). \tag{3.5}$$

If we are to consider these equations in a Bayesian framework we say that $f(\mu \mid \sigma^2)$ is the prior density for $\mu$, $f(x \mid \mu, \sigma^2)$ is the information transfer (or likelihood) function when understood as a function of $\mu$ for a fixed value of $X$, $f(x \mid \sigma^2)$ is the predictive density for $X$ and $f(\mu \mid X = x, \sigma^2)$ is the posterior density for $\mu$.

The purpose of this Chapter is to investigate how well this continuous conjugate theory, and its extension when $\sigma^2$ has an inverted Gamma mixture, can approximate real discrete mass functions when these are representable by digital Normal mass functions and digital parametric mixtures in various measurement settings. The development of large computer memories now allows us to resolve these approximation questions quite accurately for any range of scenarios we may choose.

Digital Normal mass functions are generated by specifying a finite realm of measurements for a quantity of interest, evaluating a Normal density at each point in the realm, and then normalising the density values to generate 'digitised' Normal mass values. Both a digitised prior mixing mass function and a digitised information transfer function are generated and used, via Bayes' Theorem, to compute posterior mass functions. Approximating posterior densities using continuous conjugate theory are evaluated, and the two sets of results compared.

Many statistical problems involve the analysis of sequences of observations that the researcher regards exchangeably. In many cases it is of interest to find a joint probability mass function over $X_1, X_2, \ldots, X_n$, with interim interest in the sequence

of updated probability mass functions $f(x_{i+1} \mid \mathbf{X}_i = \mathbf{x}_i)$ for $i = 1, \ldots, n-1$. The bold symbol $\mathbf{X}_i$ denotes the vector of quantities $(X_1, \ldots, X_i)$. The lower case $\mathbf{x}_i$ is the vector of their realised values, $(x_1, \ldots, x_i)$. In this context we are interested in the approximate adequacy of the continuous conjugate theory for such items as $E(X_{i+1} \mid \mathbf{X}_i = \mathbf{x}_i)$ and $V(X_{i+1} \mid \mathbf{X}_i = \mathbf{x}_i)$.

This Chapter begins with an extended description of the programming strategy used to solve a very simplified problem. Once we are clear on the setup and structure of the procedure we can address more involved mixture problems using a notation that will have become concise. In Section 2 we consider our problem when the prior density is fully specified. In Section 3 we consider the same problem when a hierarchical Bayes model is assessed. Each of these two main Sections begins with an investigation into how we can construct useful parametric families of discrete mass functions by 'digitising' well-known continuous distributions in the context of problems that are now conventionally set up as mixture-Normal distributions (Section 2), or Normal-Gamma mixture-Normal distributions (Section 3). We then show how we can use Bayes' Theorem to compute means and variances of posterior mass functions. We review how conventional conjugate theory is used to generate approximate posterior densities. Finally, we apply the theories of the previous subsections to both the mixture-Normal and Normal-Gamma mixture-Normal distributions. Different parameter values are used to compare results obtained from the use of digitised distributions and results gathered through the use of conventional conjugate theory. The final Section contains a summary of the work.

The computational procedure constructed in this Chapter can be applied to other distributions as well, as we shall see. In Chapter 4 of this Thesis this procedure is applied to various families of extreme value distributions, relying on this present Chapter for a more detailed discussion of construction details. We begin with a complete analysis of the simplest case in all its details.

## 3.2 Approximation of Posterior Means and Variances when a One-Stage Prior Distribution is Specified

One way of constructing useful parametric families of discrete mass functions is to 'digitise' well-known continuous distributions, such as the Normal, in the context of problems that are now conventionally set up as mixture-Normal distributions as described above. The construction procedure amounts to evaluating a specified Normal density over the finite realm of discrete possible values of the measured quantities, and normalising to make the density values sum to 1. We now consider how this can work.

### 3.2.1 Discrete Mass Functions Characterised as Digitised Normal Densities

The simplest problem of the form described above arises when the prior density is fully specified. We assume that the variance parameter of the conditional distribution of observations is known, and is $\sigma^2$. We assume that the mean parameter is unknown, and we assess it as being Normally distributed with mean $\mu_0$ and variance $\tau^2$. In this case we need only work with the probability mass functions $f(x \mid \mu, \sigma^2)$ and $f(\mu \mid \sigma^2)$, which we want to characterise as digitised Normal densities. We begin by specifying a finite realm of measurements for a quantity of interest, evaluating the density at each point in that realm and then normalising the density values to generate the probability mass function.

#### Forming Matrices of Mass Values

To generate the digitised spaces with which we are concerned we start by defining two realms. One will represent the possible measurement values of $X$, and will be denoted $\mathbf{R}(X)$. The elements of $\mathbf{R}(X)$ are determined by the measuring device used to identify $X$. The other realm will represent the location of the digitised mixture function with parameter $\mu$, and is denoted $\mathbf{R}(\mu)$. We shall delimit the elements

of $\mathbf{R}(\mu)$ only to a degree of fineness that really interests us. We must be careful to ensure that each realm includes every possible value that realistically could be attained by its subject. We shall specify a general computing structure for such spaces that will allow a range of specific situations by varying the distance between the elements within each of the two realms. For the purposes of this Chapter both $\mathbf{R}(X)$ and $\mathbf{R}(\mu)$ will be confined to being symmetric about 0.

Once we have identified each of these realms we use them to form a matrix of mass values for $f(x \mid \mu, \sigma^2)$. The matrix has rows corresponding to the candidate $X$ values and columns corresponding to the possible values for $\mu$. At each grid-point on our matrix we evaluate $f(x \mid \mu, \sigma^2)$ from the density corresponding to the $\mu$ of that column. In this current setup the value of $\sigma^2$ is fixed. The columns are normalised to sum to 1, as later they are used in the computation of the posterior mass function $f(\mu \mid X = x, \sigma^2)$. Each column is a digital Normal mass function for $X$ conditioned on the corresponding value of $\mu$.

The second task is to construct a matrix of mass values to represent the prior mixing mass function. To aid our later computations, matrices $f(x \mid \mu, \sigma^2)$ and $f(\mu \mid \sigma^2)$ should be the same size. We want to characterise $f(\mu \mid \sigma^2)$ as a digital $N(\mu_0, \tau^2)$ curve. Note that $\mu_0$ and $\tau^2$ are preselected values. At each element contained in $\mathbf{R}(\mu)$ we evaluate $f(\mu \mid \sigma^2)$. This vector of density values is then normalised to produce a digital mass function. Note that the length of the row vector $f(\mu \mid \sigma^2)$ is equal to the number of columns in matrix $f(x \mid \mu, \sigma^2)$. Finally, row vector $f(\mu \mid \sigma^2)$ is replicated and tiled to produce a matrix which is the same size as $f(x \mid \mu, \sigma^2)$. The vector $f(\mu \mid \sigma^2)$ is not removed from the memory of the computer, as it is required for use further on in our computations.

### The Information Transfer Function

An information transfer function (ITF) is used to update our uncertain knowledge about $X_{i+1}$ given we know that $\mathbf{X}_i = \mathbf{x}_i$ has occurred. The common parlance for what we call an ITF is a "likelihood function". We prefer the use of the term "information transfer function" to accentuate the realisation that there really is no "true value of $\mu$" to be estimated, only sequential values of $X$'s to be observed. In the context of opinions expressed by the exchangeable distribution, the ITF is the

form in which the observation of one $X$ allows us to infer something about the next — thus the name "information transfer function". (See Lad, 1996, pp. 397–399 for further discussion.)

The ITF can be calculated for each potential observation value. Each row of matrix $f(x \mid \mu, \sigma^2)$ corresponds to the ITF for one candidate $X$ value. Thus for any observed value of $X = x$, we merely read the corresponding row of the $f(x \mid \mu, \sigma^2)$ matrix of mass values as the ITF.

### Generating Sequences of Observation Values

We want to generate $\mathbf{X}_N$, a vector of length $N$ whose elements represent observations from a distribution. These observations will be used, via the ITF, to compute such items as $E(X_{i+1} \mid \mathbf{X}_i = \mathbf{x}_i)$ and $V(X_{i+1} \mid \mathbf{X}_i = \mathbf{x}_i)$.

To simulate an observation vector we randomly select elements from $\mathbf{R}(X)$. For the purpose of generating observations we assume that $\mu$ is known to us. The variance parameter, $\sigma^2$, is also a predetermined value. To generate a sequence of observation values we follow these steps:

1. Extract the column of $f(x \mid \mu, \sigma^2)$ which corresponds to the chosen $\mu$. This is a mass function characterised as a digitised $N(\mu, \sigma^2)$ density. The number of elements in the mass function is the same as the size of the realm of $X$.

2. Form a cumulative mass function, $F(x \mid \mu, \sigma^2)$, using the mass function from the preceding step.

3. Generate $\mathbf{U}_N$, a vector of size $N$ consisting of $U(0, 1)$ random variables.

4. Find the smallest element of $\mathbf{R}(X)$ for which $F(x \mid \mu, \sigma^2) > U_i$ is true. This is $X_i$. Each element of $\mathbf{U}_N$ corresponds to a constituent of the cumulative mass function, and thus to a member of the realm of $X$.

5. Repeat steps 1–4 until the sequence of observations, $\mathbf{X}_N$, is complete.

To this point we have constructed:

(a) $\mathbf{R}(X)$, a vector to represent the realm measurement values of $X$,

(b) $\mathbf{R}(\mu)$, a vector to represent the realm of the location of the digitised mixture function with parameter $\mu$,

(c) $f(x \mid \mu, \sigma^2)$, a matrix of mass values whose columns correspond to conditional probability mass functions for $X$ given different values of $\mu$, and whose rows correspond to ITF's for the various observation values of $X$,

(d) $f(\mu \mid \sigma^2)$, a matrix of mass values with identical rows, each of which designates a digitised Normal mass function. The size of this matrix is equal to that of $f(x \mid \mu, \sigma^2)$,

(e) $\mathbf{X}_N$, an observation vector whose elements have been generated randomly from digitised Normal mass function $f(x \mid \mu, \sigma^2)$, where $\mu$ has been assumed known.

In the course of this study we shall perform this routine using different values of $\mu$. Remember that our objective is, via ITF's, to see how closely continuous conjugate theory can approximate real discrete mass functions in various measurement settings. We can do this by comparing the sequential predictive distributions for components of $\mathbf{X}_N$ attained through using conjugate theory and through using real digital mass function computations. We can also compare the posterior means and variances of the posterior digitised Normal mixtures with approximate values that we compute using standard conjugate methods. In other words, how do the means and variances of $X_{i+1} \mid (\mathbf{X}_i = \mathbf{x}_i)$ compare using exact and approximate methods?

### 3.2.2 Computing Posterior Means and Variances of Posterior Discrete Densities

To find exact values for $E(X_{i+1} \mid \mathbf{X}_i = \mathbf{x}_i)$ and $V(X_{i+1} \mid \mathbf{X}_i = \mathbf{x}_i)$ for the discrete mass functions characterised as digitised Normal densities we should compute

$$f\left(x_{i+1} \mid \mathbf{X}_i = \mathbf{x}_i, \sigma^2\right) = \sum_{\mu} f\left(x_{i+1} \mid \mu, \mathbf{X}_i = \mathbf{x}_i, \sigma^2\right) f\left(\mu \mid \mathbf{X}_i = \mathbf{x}_i, \sigma^2\right). \quad (3.6)$$

The first function in this sum of products of functions does not change. It is always represented by the columns of the matrix $f(x \mid \mu, \sigma^2)$ we have just discussed. The second function is the sum of Equations corresponding to (3.2) and (3.3) and changes

with each observed value of $\mathbf{X}_i = \mathbf{x}_i$ according to Bayes' Theorem. This implies

$$f(\mu \mid \mathbf{X}_i = \mathbf{x}_i, \sigma^2) = \frac{f(\mathbf{X}_i = \mathbf{x}_i \mid \mu, \sigma^2) f(\mu \mid \sigma^2)}{\sum\limits_{\mu} f(\mathbf{X}_i = \mathbf{x}_i \mid \mu, \sigma^2) f(\mu \mid \sigma^2)} \qquad \text{for} \quad i = 1, 2, \ldots, N-1. \tag{3.7}$$

Bayes' Theorem is a computational formula for determining posterior probability distributions conditional upon observing the data $\mathbf{X}_i = \mathbf{x}_i$. The posterior probability distribution reflects our revised mixing function over values of $\mu$ in light of the knowledge that $\mathbf{X}_i = \mathbf{x}_i$ has occurred.

To compute $E(X_{i+1} \mid \mathbf{X}_i = \mathbf{x}_i)$ and $V(X_{i+1} \mid \mathbf{X}_i = \mathbf{x}_i)$ we merely compute the mean and variance of the appropriate $f_{X_{i+1}}(x \mid \mathbf{X}_i = \mathbf{x}_i, \sigma^2)$ that has been computed from the observed data. The formulae

$$E\left(X_{i+1} \mid \mathbf{X}_i = \mathbf{x}_i\right) = \sum_x x f_{X_{i+1}}\left(x \mid \mathbf{X}_i = \mathbf{x}_i, \sigma^2\right) \tag{3.8}$$

and

$$V\left(X_{i+1} \mid \mathbf{X}_i = \mathbf{x}_i\right) = \sum_x x^2 f_{X_{i+1}}\left(x \mid \mathbf{X}_i = \mathbf{x}_i, \sigma^2\right) - \left[\sum_x x f_{X_{i+1}}\left(x \mid \mathbf{X}_i = \mathbf{x}_i, \sigma^2\right)\right]^2, \tag{3.9}$$

are implemented by multiplying the elements of the realm of $X$ (in Equation 3.9 the elements of $\mathbf{R}(X)$ are squared) element-wise with $f(x_{i+1} \mid \mathbf{X}_i = \mathbf{x}_i, \sigma^2)$ and then summing the products.

It is easy to find $E(X_1)$ and $V(X_1)$. The matrices $f(\mu \mid \sigma^2)$ and $f(x \mid \mu, \sigma^2)$ both reside in the computer via the calculations described in Section 2.1. Use Equation 3.6 to find $f(x_1 \mid \sigma^2)$ and then apply Equations 3.8 and 3.9.

To find items $E(X_{i+1} \mid \mathbf{X}_i = \mathbf{x}_i)$ and $V(X_{i+1} \mid \mathbf{X}_i = \mathbf{x}_i)$, where $i \geq 1$, we 'observe' $X_i$ and use the information this observation gives us to form the ITF and implement Bayes' Theorem, thus finding the updated mixing function $f(\mu \mid \mathbf{X}_i = \mathbf{x}_i, \sigma^2)$. We are now in position to re-apply Equation 3.6 and compute the updated predictive mass function, and thus find $E(X_{i+1} \mid \mathbf{X}_i = \mathbf{x}_i)$ and $V(X_{i+1} \mid \mathbf{X}_i = \mathbf{x}_i)$ exactly! In particular, to find $E(X_2 \mid X_1 = x_1)$ and $V(X_2 \mid X_1 = x_1)$:

1. Observe $X_1 = x_1$.

2. Extract the row corresponding to $X_1$ from the matrix $f(x \mid \mu, \sigma^2)$. This is the ITF through $\mu$ from $X_1 = x_1$ to $X_2$.

3. Implement Bayes' Theorem to update the mixing function, $f(\mu \mid X_1 = x_1, \sigma^2)$. This involves multiplying vectors $f(X_1 = x_1 \mid \mu, \sigma^2)$ and $f(\mu \mid \sigma^2)$ element-wise, and normalising.

4. Replicate and tile vector $f(\mu \mid X_1 = x_1, \sigma^2)$ to form a matrix which has the same dimensions as matrix $f(x \mid \mu, \sigma^2)$.

5. Calculate $f(x_2 \mid X_1 = x_1, \sigma^2)$, the updated predictive mass function, according to Equation 3.6. Matrix $f(x \mid \mu, \sigma^2)$ is multiplied element-wise with the updated mixing function matrix, and the columns are summed. The resulting vector has length equal to the size of $\mathbf{R}(X)$.

6. Compute $E(X_2 \mid X_1 = x_1)$ and $V(X_2 \mid X_1 = x_1)$ using Equations 3.8 and 3.9.

Repeat Steps 1–6 as many times as required to obtain $E(X_{i+1} \mid \mathbf{X}_i = \mathbf{x}_i)$ and $V(X_{i+1} \mid \mathbf{X}_i = \mathbf{x}_i)$.

Note that for the purpose of this Chapter the term "vector" refers to a one-dimensional array of size $a \times 1 \times 1$ where $a > 1$. The term "matrix" refers to a two-dimensional array of size $a \times b \times 1$ where $a, b > 1$. The term "array" refers to a three-dimensional array of size $a \times b \times c$ where $a, b, c > 1$.

### 3.2.3 Conventional Conjugate Mixture-Normal Theory

Conventional conjugate mixture-Normal theory tells us that if $\mu \mid \sigma^2 \sim N(\mu_0, \tau^2)$ and $X \mid \mu, \sigma^2 \sim N(\mu, \sigma^2)$, then $X \mid \sigma^2 \sim N(\mu_0, \sigma^2 + \tau^2)$. In fact the joint exchangeable distribution for the entire sequence of $X$'s is multivariate Normal:

$$\begin{pmatrix} X_1 \\ X_2 \\ X_3 \\ \vdots \\ X_K \end{pmatrix} \sim N\left( \begin{bmatrix} \mu_0 \\ \mu_0 \\ \mu_0 \\ \vdots \\ \mu_0 \end{bmatrix}, \begin{bmatrix} \sigma^2+\tau^2 & \tau^2 & \tau^2 & \cdots & \tau^2 \\ \tau^2 & \sigma^2+\tau^2 & \tau^2 & \cdots & \tau^2 \\ \tau^2 & \tau^2 & \sigma^2+\tau^2 & & \tau^2 \\ \vdots & \vdots & & \ddots & \\ \tau^2 & \tau^2 & \tau^2 & & \sigma^2+\tau^2 \end{bmatrix} \right). \quad (3.10)$$

Which can be written in the form $\mathbf{X}_K \sim N_K(\mu_0 \mathbf{1}_K, \sigma^2 \mathbf{I}_K + \tau^2 \mathbf{1}_{K,K})$. For any individual $X_i$, the mean is equal to $\mu_0$, the variance equals $\sigma^2 + \tau^2$ and the covariance with any other $X_j$ equals $\tau^2$.

Standard multivariate Normal theory says that we assert $\mathbf{X}_K \sim N_K(\mu_\mathbf{0}, \Sigma)$, and if the $K$-dimensional vector $\mathbf{X}$ is partitioned into two sub-vectors $\mathbf{X}_1$ and $\mathbf{X}_2$, where $(\mathbf{X}_1, \mathbf{X}_2)$ is any partition of $\mathbf{X}$ into its first $K_1$ and remaining $K_2$ components, then the conditional distribution for $\mathbf{X}_2 \mid (\mathbf{X}_1 = \mathbf{x}_1)$ is

$$\mathbf{X}_2 \mid (\mathbf{X}_1 = \mathbf{x}_1) \sim N_{K_2}\left[\mu_{\mathbf{0}2} + \Sigma_{21}\Sigma_{11}^{-1}(\mathbf{x}_1 - \mu_{\mathbf{0}1}), \Sigma_{22} - \Sigma_{21}\Sigma_{11}^{-1}\Sigma_{12}\right]. \tag{3.11}$$

Applying this multivariate Normal result to the exchangeable Normal distribution tells us that the conditional density for $\mathbf{X}_2 \mid (\mathbf{X}_1 = \mathbf{x}_1)$ can be assessed as

$$\mathbf{X}_2 \mid (\mathbf{X}_1 = \mathbf{x}_1) \sim N_{K_2}\left[\frac{\sigma^2\mu_0 + \tau^2 \sum_{i=1}^{K_1} x_{1_i}}{(\sigma^2 + K_1\tau^2)}\mathbf{1}_{K_2}, \sigma^2\mathbf{I}_{K_2} + \frac{\sigma^2\tau^2}{(\sigma^2 + K_1\tau^2)}\mathbf{1}_{K_2,K_2}\right]. \tag{3.12}$$

For details see the text of Lad (1996, pp. 375–376, 387–388).

In the specific application to our problem involving the forecast of $X_{i+1}$ given $(\mathbf{X}_i = \mathbf{x}_i)$ these general results apply with the partitioned vector $\mathbf{X}_1$ equal to the condition vector $(\mathbf{X}_i = \mathbf{x}_i)$ and the partitioned vector $\mathbf{X}_2$ equal to the quantity $X_{i+1}$. The two items that we are most interested in are the posterior conditional expectation of $X_{i+1}$ given the observations $(\mathbf{X}_i = \mathbf{x}_i)$, and the posterior conditional variance of $X_{i+1}$ given the observations $(\mathbf{X}_i = \mathbf{x}_i)$.

The conditional expectation reduces to

$$E\left(X_{i+1} \mid \mathbf{X}_i = \mathbf{x}_i\right) = \left(\sigma^2 + i\tau^2\right)^{-1}\left(\sigma^2\mu_0 + i\tau^2\bar{x}_i\right), \tag{3.13}$$

where $\bar{x}_i$ is the average of the observed $\mathbf{X}_i$. We observe that as the number of observations increases, the relative weight on the prior mean, and on each individual observation value, decreases. However, the relative weight on the observed mean, $\bar{x}_i$, increases, that is, $E\left(X_{i+1} \mid \mathbf{X}_i = \mathbf{x}_i\right) \to \bar{x}_i$ as $i \to n$. In other words, as the number of observations increases, the relative importance of any specific observation value diminishes, but the overall importance of the average of all observations increases.

The conditional variance reduces to

$$V\left(X_{i+1} \mid \mathbf{X}_i = \mathbf{x}_i\right) = \sigma^2 + \sigma^2\tau^2(\sigma^2 + i\tau^2)^{-1}. \tag{3.14}$$

Note that $V\left(X_{i+1} \mid \mathbf{X}_i = \mathbf{x}_i\right)$ reduces monotonically towards $\sigma^2$ as the number of observations increase. In this application the posterior conditional variance decreases toward the variance of the ITF as $i$ increases.

### 3.2.4 Case 1: $X \mid \mu, \sigma^2 \sim N_{dig}(\mu, 1)$ and $\mu \mid \sigma^2 \sim N_{dig}(0, 1)$

In the first example we shall consider the case where we have a one-stage prior mass function. The use of a one-stage prior mass function means that we feel our uncertain opinion about the conditional distribution of $X$ can be fully specified by the moments that are described by one distribution, in this case the Normal. We choose our parameters to be $\mu_0 = 0$, $\sigma^2 = 1$ and $\tau^2 = 1$, so that

$$\mu \mid \sigma^2 \sim N_{dig}(0, 1) \tag{3.15}$$

$$\text{and} \qquad X \mid \mu, \sigma^2 \sim N_{dig}(\mu, 1). \tag{3.16}$$

We identify realms $\mathbf{R}(X)$ and $\mathbf{R}(\mu)$ as having an interval width of 0.08. $\mathbf{R}(X)$ must cover every possible value that could realistically be generated as a measurement for $X$. We shall characterise the standard measurements of $X$ as fully between $-4$ and 4. We shall also include a few extreme values $(\pm 5, \pm 6, \pm 7, \pm 8)$ to represent possible extreme measurements. Thus the size of $\mathbf{R}(X)$ is 109.

Extreme measurements are often measured more crudely, either because the measurement device is not calibrated to record extreme observations with the same degree of fineness as it is for commonly observed values, or because the researchers may not regard measurement precision to be as important for less common observation values. In Chapter 4 we encounter a situation where it is not possible to measure extreme observations to the normal level of fineness.

The elements of $\mathbf{R}(\mu)$ should cover every value of the mixing location parameter $\mu$. In this case the realm will have a minimum value of $-2$ and a maximum value of 2, with the same spacing in the grid of possibilities as for $X$, 0.08. Thus the size of $\mathbf{R}(\mu)$ is 51.

We shall study the closeness of the conjugate Normal approximation to the precise computation based on the digitised Normal distribution under three different observational scenarios. The 'observed' $X$ values shall be sampled from mass functions corresponding to the digitised $N(0, 1)$, $N(2, 1)$ and $N(4, 1)$ densities. When we sample from mass function $N_{dig}(0, 1)$ we expect the mode of our sampled values to be equal to the mode of the prior location mixing mass function, $\mu = 0$. When we sample from mass function $N_{dig}(2, 1)$, we obtain a sequence of observations that our prior mixing mass function suggests is unlikely. When we take a sample from

mass function $N_{dig}(4,1)$, we obtain a sequence of observations that our prior mixing mass function suggests is surprising.

### Computation of $f(x \mid \mu, \sigma^2)$ and $f(\mu \mid \sigma^2)$

Our immediate aim is to form matrices $f(x \mid \mu, \sigma^2)$ and $f(\mu \mid \sigma^2)$. The number of rows in each matrix is equal to the size of $\mathbf{R}(X)$, and the number of columns is equal to the size of $\mathbf{R}(\mu)$. In this case the size of matrices $f(x \mid \mu, \sigma^2)$ and $f(\mu \mid \sigma^2)$ is $109 \times 51$. Matrix $f(x \mid \mu, \sigma^2)$ has rows corresponding to the elements of $\mathbf{R}(X)$ (i.e. from $-8$ to 8) and columns corresponding to elements of $\mathbf{R}(\mu)$ (i.e. from $-2$ to 2). We evaluate density $f(x \mid \mu, \sigma^2)$ at each grid-point, and then normalise the columns. Each column of $f(x \mid \mu, \sigma^2)$ is a mass function characterised as a digitised Normal density conditioned on the corresponding value of $\mu$. For example the first column is $N_{dig}(-2,1)$, the second column is $N_{dig}(-1.92,1)$, and so on. A bar graph of each column shows that they look as if they are truncated digital Normal mass functions. Figure 3.1 shows two of these columns, corresponding to $N_{dig}(0,1)$ and $N_{dig}(2,1)$, as well as the bar graph of the mass function corresponding to a digitised $N(4,1)$ density.

The bar graphs of the mass functions appear truncated because the range of $\mathbf{R}$(X) is less than the range of the non-zero values of the Normal densities that the mass functions are based on. A bar graph of the 26th column, $N_{dig}(0,1)$, does look as if it has a Normal shape because, although there are no points less than $-4$ or greater than 4 included in the computation of the mass function, these values have negligible mass when $\mu = 0$ and $\sigma^2 = 1$. A bar graph of the 51st column looks obviously truncated because $\mathbf{R}$(X) only has elements fully recorded on the interval from $-4$ to 4. Observe there is positive mass placed on $X = 5$ (see Figure 3.1(b)). This effect is demonstrated even more clearly by Figure 3.1(c), a bar graph of $N_{dig}(4,1)$, where it appears the mass function has only been fully recorded on half its range. There are extreme elements with noticeable positive mass recorded at $X = 5, 6, 7$.

The prior mixing mass function is characterised as $N_{dig}(0,1)$. To form matrix $f(\mu \mid \sigma^2)$ evaluate the standard Normal density for each constituent element of $\mathbf{R}(\mu)$, and normalise. We now have $f(\mu \mid \sigma^2)$, a $1 \times 51$ vector. Replicate and tile this vector so that it becomes a matrix with 109 rows.

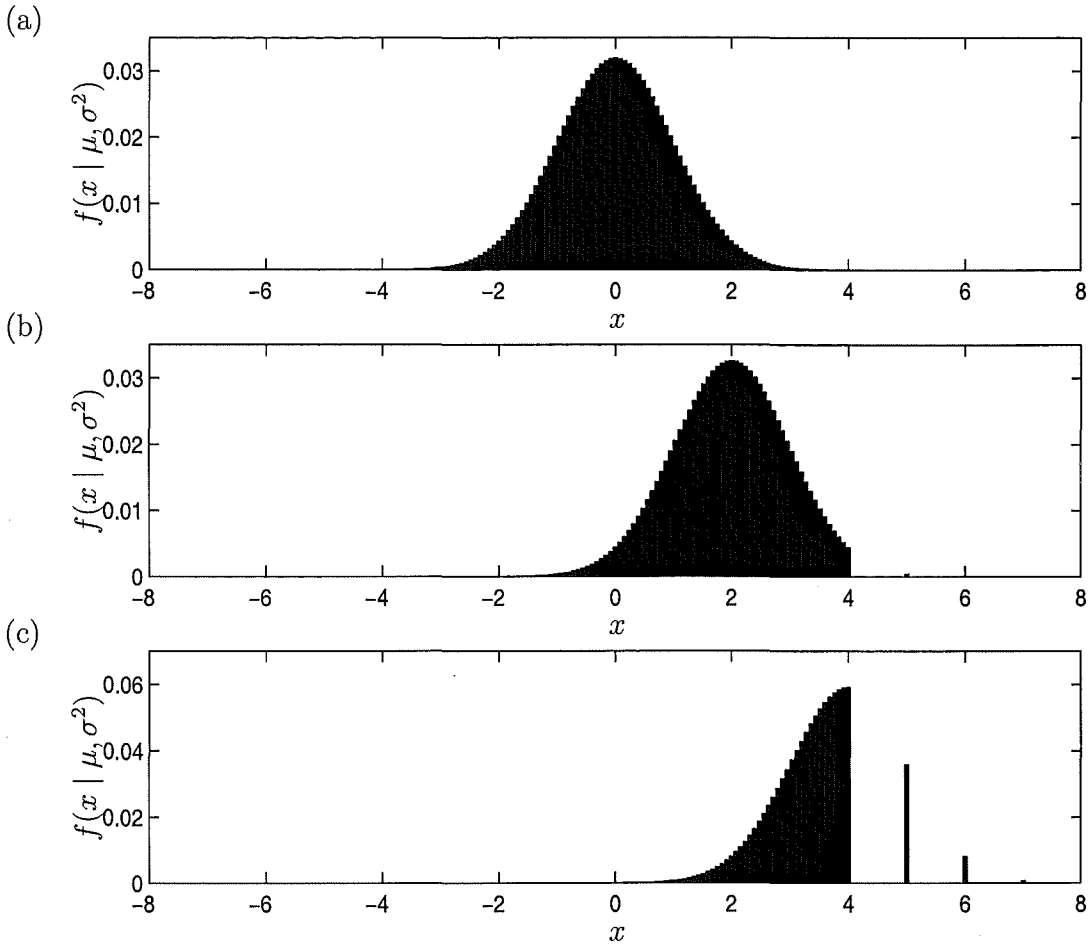


**Figure 3.1: Bar graph of the digitised Normal mass functions evaluated at (a) $\mu = 0$, (b) $\mu = 2$ and (c) $\mu = 4$. Positive mass values are recorded for elements of $\mathrm{R}(X)$ only. Note that the scale along the $y$-axis in (c) is double that of (a) or (b).**

### Computation of Conditional Moments for $f(x \mid \mu, \sigma^2)$

To compute conditional moments for the columns of $f(x \mid \mu, \sigma^2)$ we use the formulae,

$$E(X \mid \mu, \sigma^2) = \sum_x x f\left(x \mid \mu, \sigma^2\right) \tag{3.17}$$

$$\text{and} \qquad V\left(X \mid \mu, \sigma^2\right) = E(X^2 \mid \mu, \sigma^2) - \left[E\left(X \mid \mu, \sigma^2\right)\right]^2. \tag{3.18}$$

The expected value for each column of matrix $f(x \mid \mu, \sigma^2)$ can be computed using Equation 3.17. The expected values are symmetric about 0 and range from near $-2$, for $E(X \mid \mu = -2)$, to near 2, for $E(X \mid \mu = 2)$. Figure 3.2 shows the magnitude of error in $E(X \mid \mu, \sigma^2)$ when using continuous conjugate approximations rather than

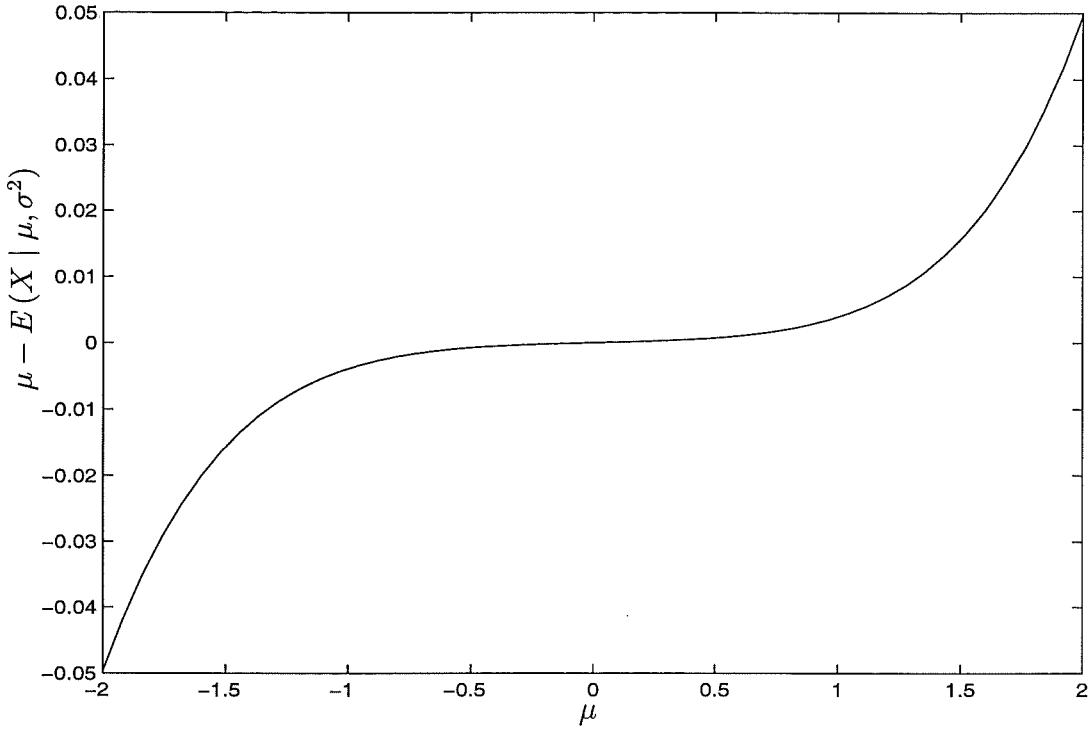


**Figure 3.2: Magnitude of error in $\mathbf{E}(X \mid \mu, \sigma^2)$ using continuous conjugate methods rather than actual digital computations. Note that these errors are calculated directly from $f(x \mid \mu, \sigma^2)$.**

the actual computed values obtained using digital mass functions.

The calculation of $E(X \mid \mu = 2)$ produces a value of 1.95 (2dp) compared to the continuous conjugate approximation of $E(X \mid \mu = 2) = 2$. This is because, although $\mathbf{R}(X)$ is symmetric, the 51st column of the $f(x \mid \mu, \sigma^2)$ matrix, $f(x \mid \mu = 2, \sigma^2 = 1)$ is not. The 51st column of $f(x \mid \mu, \sigma^2)$ is symmetric about $\mu$ within the range $[0, 4]$. Beyond this range there are more components of $\mathbf{R}(X)$ below 0 than above 4. Consequently, the positive mass on $f(X < 0 \mid \mu = 2)$ is greater than the mass on $f(X > 4 \mid \mu = 2)$, and so $E(X \mid \mu = 2) < 2$. In contrast the conjugate approximation specifies complete symmetry about $\mu = 2$. Thus when Equation 3.17 is computed the actual digital calculation is smaller than the conjugate approximation. In fact the conjugate approximation will always be larger absolutely than the digital computation, except for $E(X \mid \mu = 0)$, when the conjugate approximation and digital computation are equal. Figure 3.2 illustrates that as $|\mu|$ decreases towards 0, $|E(X \mid \mu, \sigma^2) - \mu|$ decreases. This is because as $\mu$ decreases the range of values

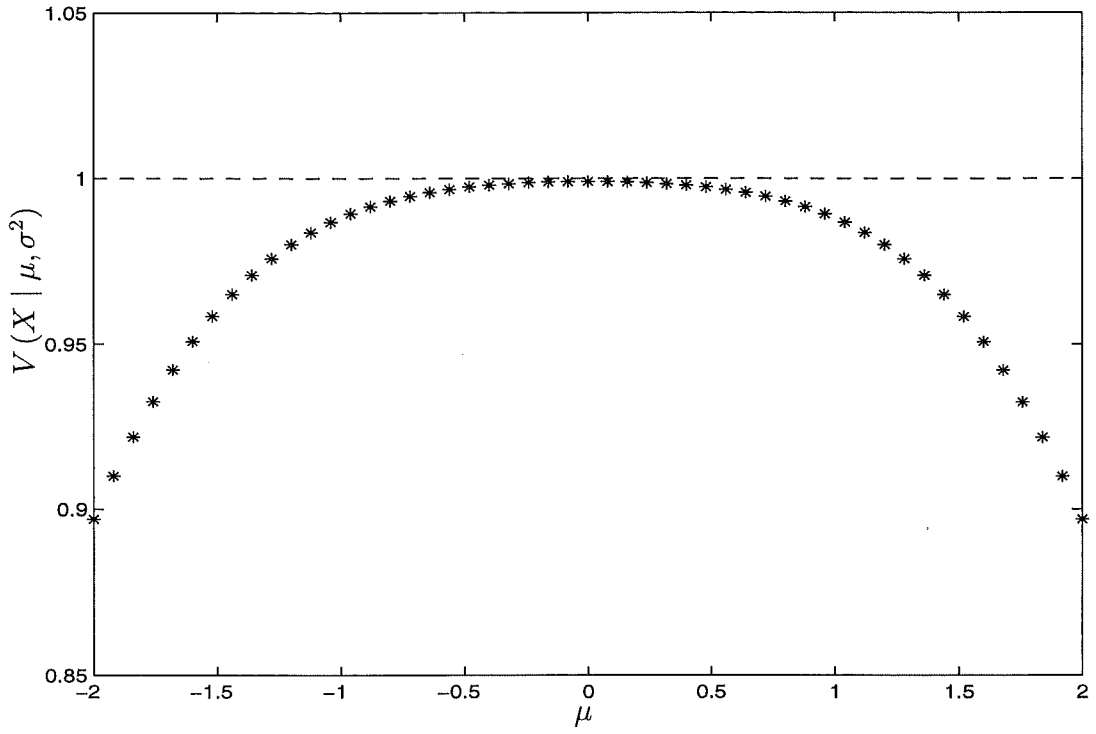


**Figure 3.3: Values of $\mathbf{V}(X \mid \mu, \sigma^2)$ obtained using digital computation (marked by "$*$") and conjugate approximation (marked by "$--$"). Note that continuous conjugate theory specifies constant variance over all values of $\mu$, while digital computations show the variance is dependent on $\mu$.**

in $\mathbf{R}(X)$ that are symmetric about $\mu$ increase.

Values of $V(X \mid \mu, \sigma^2)$ range even more widely over the possible values of $\mu$, as is shown in Figure 3.3. Whereas the conjugate continuous specification is of a variance constant over the different values of $\mu$, the digitised conditional moments have smaller variances when located about $\mu$ values away from 0. As with the conditional expectation, this is because, as we move away from 0, the number of $X$ values: (a) for which the mass of $N(\mu, 1)$ is non-negligible, and (b) are not included in $\mathbf{R}(X)$, increases.

### Case 1A: Observations Generated from $\mathbf{X}_N \sim N_{dig}(0, 1)$

**Case 1A: Digital Mass Functions.** Now that matrices $f(x \mid \mu, \sigma^2)$ and $f(\mu \mid \sigma^2)$ have been computed we are in position to consider the three examples. We begin with observations generated from $N_{dig}(0, 1)$. We generated 25 observations using

the procedure described in Section 3.2.1. In this case the mean of the prior mixing function is equal to the mean of the mass function we used to generate our observations.

We want to find the series of items $E(X_{i+1} \mid \mathbf{X}_i = \mathbf{x}_i)$ and $V(X_{i+1} \mid \mathbf{X}_i = \mathbf{x}_i)$. Section 3.2.2 has detailed how this process can be undertaken: use Bayes' Theorem to update the prior mixing function, compute the updated predictive mass function and then calculate the conditional moments. This process can be repeated as many times as required, which in this case is until we have found values for $E(X_{i+1} \mid \mathbf{X}_i = \mathbf{x}_i)$ and $V(X_{i+1} \mid \mathbf{X}_i = \mathbf{x}_i)$ for $i = 0, \ldots, 24$.

**Case 1A: Conjugate Theory.** A study of Equation 3.10 shows that the distribution of $\mathbf{X}_N$ can be written in the form

$$\mathbf{X}_N \sim N\left(\begin{bmatrix} 0 \\ 0 \\ 0 \\ \vdots \\ 0 \end{bmatrix}, \begin{bmatrix} 2 & 1 & 1 & \cdots & 1 \\ 1 & 2 & 1 & \cdots & 1 \\ 1 & 1 & 2 & & 1 \\ \vdots & \vdots & & \ddots & \\ 1 & 1 & 1 & & 2 \end{bmatrix}\right). \tag{3.19}$$

It follows from Equations 3.13 and 3.14 that the posterior mean of the $(i+1)th$ observation, conditional on observing the first $i$ observations is

$$E\left(X_{i+1} \mid \mathbf{X}_i = \mathbf{x}_i\right) = \frac{\sum_i x_i}{i+1}. \tag{3.20}$$

The posterior variance of the $(i+1)th$ observation, conditional on observing the first $i$ observations is

$$V\left(X_{i+1} \mid \mathbf{X}_i = \mathbf{x}_i\right) = \frac{i+2}{i+1}. \tag{3.21}$$

**Case 1A: Results.** Figure 3.4 shows the result of a typical example for the case where 25 observations are generated via a digitised $N(0,1)$ density. In this case the prior mixing function is the same as the conditional distribution of observations, $\mathbf{X}_{25}$, so it is not surprising that the conditional expectation of the digital computations and the conjugate approximations are very similar. The only slight disparity occurs for the first few observations. The conditional expectations are plotted in the top panel of Figure 3.4.

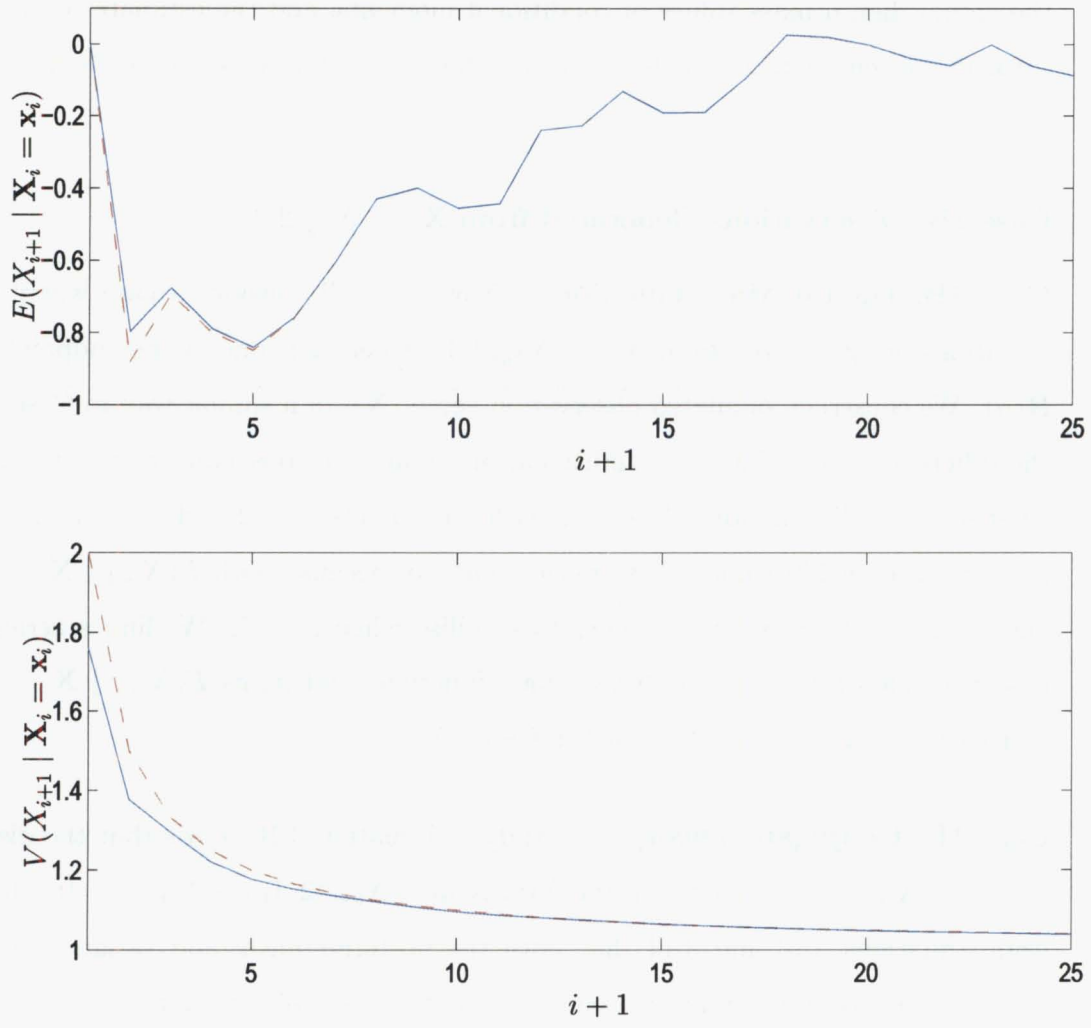


**Figure 3.4: Conditional Expectations and Variances of the Digital Mass Function (solid blue line) and Conventional Conjugate Theory (dashed red line) when $\mathbf{X}_{25} \sim N_{dig}(0, 1)$.**

The two different conditional variances we calculate are very similar for $i \geq 5$. The first few conditional variances have larger values for the conjugate approximation than they do for the digital computation. The value of $V(X_1)$ is 1.760, but conjugate theory approximates it as 2. If $\mathbf{R}(\mu)$ had have been wider, that is, contained more extreme elements, then we could reasonably expect the digital mass value and conjugate approximation to be closer. As $i$ increases the two types of conditional variance modelled become more similar.

We have just investigated the case where the conditional distribution of observations is the same as the mode of the prior mixing mass function. We have seen that

the actual digital mass values of conditional moments, and the estimates obtained through conventional conjugate theory for the same conditional moments, are very similar.

**Case 1B: Observations Generated from $\mathbf{X}_N \sim N_{dig}(2,1)$.**

**Case 1B: Digital Mass Functions.** Now we shall consider a case where observations are generated from $\mathbf{X}_N \sim N_{dig}(2,1)$, where 2 is one of the endpoints of $\mathbf{R}(\mu)$. We construct simulated observation vector $\mathbf{X}_N$ in a similar way to Case 1A, the difference being that the conditional distribution of observations is now characterised as a digital Normal density with parameters $\mu = 2$ and $\sigma^2 = 1$. In this case we observe 100 values of $X$, rather than 25, because both $E(X_{i+1} \mid \mathbf{X}_i = \mathbf{x}_i)$ and $V(X_{i+1} \mid \mathbf{X}_i = \mathbf{x}_i)$ take longer to stabilise when $\mu = 2$. We find a series of posterior mass functions, predictive mass functions and items $E(X_{i+1} \mid \mathbf{X}_i = \mathbf{x}_i)$ and $V(X_{i+1} \mid \mathbf{X}_i = \mathbf{x}_i)$ as described in Case 1A.

**Case 1B: Conjugate Theory.** A study of Equation 3.10 shows that the distribution of $\mathbf{X}_{100}$ can be written in the form $\mathbf{X}_{100} \sim N_{100}(\mathbf{2}, \mathbf{I}_{100} + \mathbf{1}_{100,100})$. It follows from Equations 3.13 and 3.14 that both the posterior mean and variance of the $(i+1)th$ observation, conditional on observing the first $i$ observations, are the same as in Case 1A, viz:

$$E(X_{i+1} \mid \mathbf{X}_i = \mathbf{x}_i) = \frac{\sum_i x_i}{i+1} \tag{3.22}$$

and

$$V(X_{i+1} \mid \mathbf{X}_i = \mathbf{x}_i) = \frac{i+2}{i+1}. \tag{3.23}$$

**Case 1B: Results.** The conditional expectation of $E(X_{i+1} \mid \mathbf{X}_i = \mathbf{x}_i)$ is plotted in the upper panel of Figure 3.5 for a typical example when 100 observations are generated from a digitised $N(2,1)$ distribution. The equivalent conditional variance is shown in the lower panel of Figure 3.5. The generating value of $\mu$ has been selected as one of the most extreme possibilities of $\mathbf{R}(\mu)$. There is a larger difference between the conditional expectations calculated using digital mass functions and conventional conjugate theory than in Case 1A. It is of the order of 0.1 relative to the actual expectation of approximately 1.9. The approximate values of

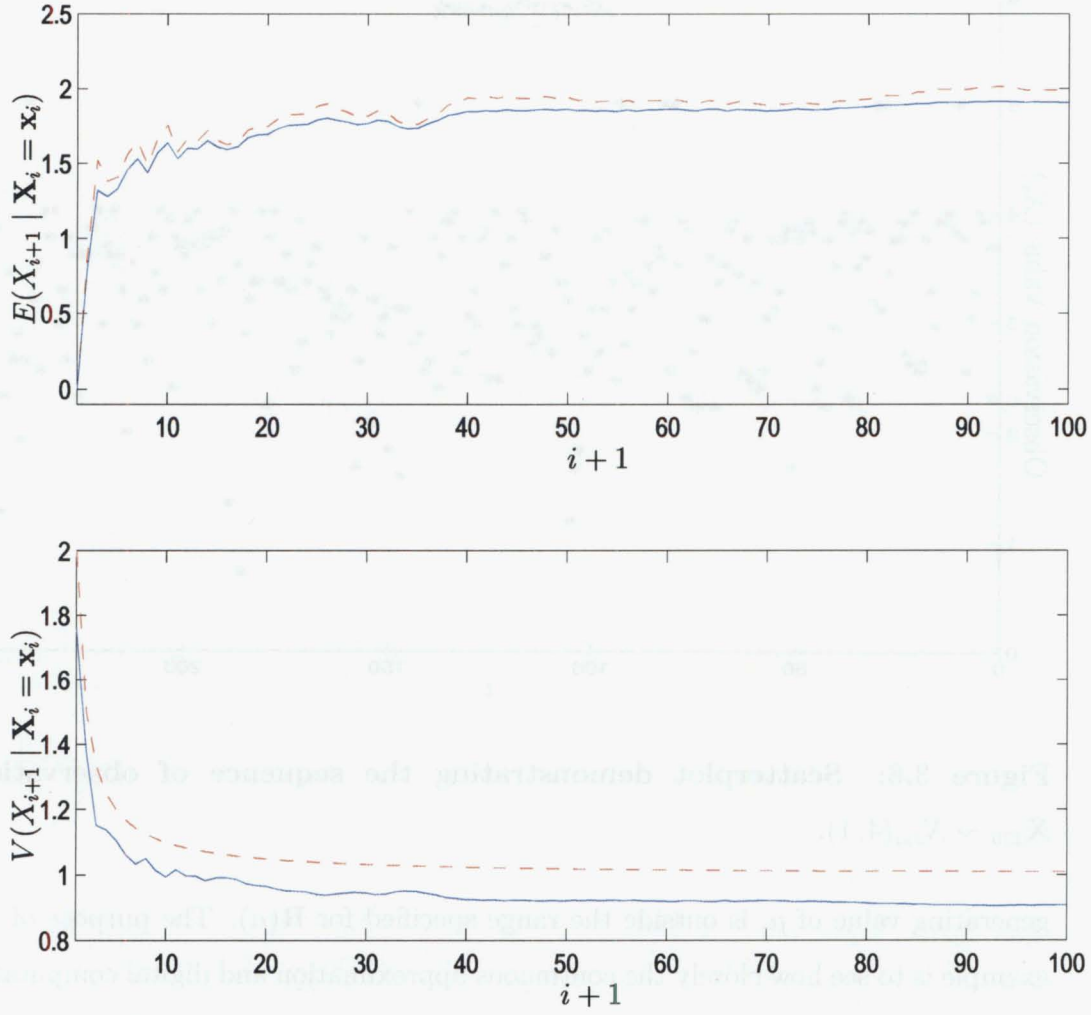


**Figure 3.5: Conditional Expectations and Variances of the Digital Mass Function (solid blue line) and Conventional Conjugate Theory (dashed red line) when $\mathbf{X}_{100} \sim N_{dig}(2,1)$.**

$E(X_{i+1} \mid \mathbf{X}_i = \mathbf{x}_i)$ obtained by conjugate theory are always higher than the equivalent computed digital values. A corresponding observation can be made for the values of $V(X_{i+1} \mid \mathbf{X}_i = \mathbf{x}_i)$. The actual conditional variance is approximately 0.9 and the relative difference is about 0.1.

### Case 1C: Observations Generated from $\mathbf{X}_N \sim N_{dig}(4,1)$.

**Case 1C: Digital Mass Functions.** Our final example in this Section considers the case where observations are generated from $N_{dig}(4,1)$. Notice that 4, the

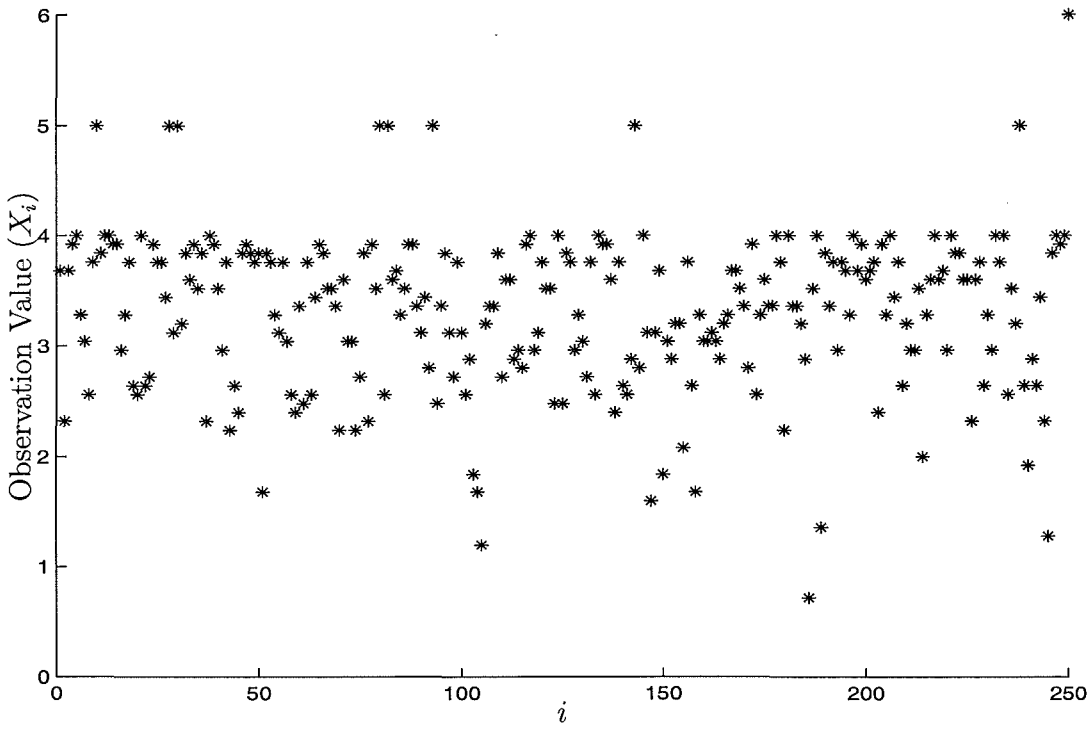


**Figure 3.6: Scatterplot demonstrating the sequence of observations $\mathbf{X}_{250} \sim N_{dig}(4, 1)$.**

generating value of $\mu$, is outside the range specified for $\mathbf{R}(\mu)$. The purpose of this example is to see how closely the continuous approximation and digital computation cohere when the generating value of $\mu$ has been selected to be far from our prior specification of $\mu$. The observation vector is generated, and a series of updated mixing functions, updated predictive mass functions and items $E(X_{i+1} \mid \mathbf{X}_i = \mathbf{x}_i)$ and $V(X_{i+1} \mid \mathbf{X}_i = \mathbf{x}_i)$ are found, as in the two previous examples. In this case 250 observations were generated.

**Case 1C: Conjugate Theory.** A study of Equation 3.12 shows that the formulae for $E(X_{i+1} \mid \mathbf{X}_i = \mathbf{x}_i)$, and $V(X_{i+1} \mid \mathbf{X}_i = \mathbf{x}_i)$ are the same as in the previous two examples.

**Case 1C: Results.** A typical sequence of observations generated from a digitised $N(4, 1)$ distribution are shown in Figure 3.6. As we expect, the most commonly selected elements of $\mathbf{R}(X)$ are those close to 4. In the sequence of 250 observations we only observe $(X_i > 4)$ on 9 occasions. Because the (non-digitised) $N(4, 1)$ density

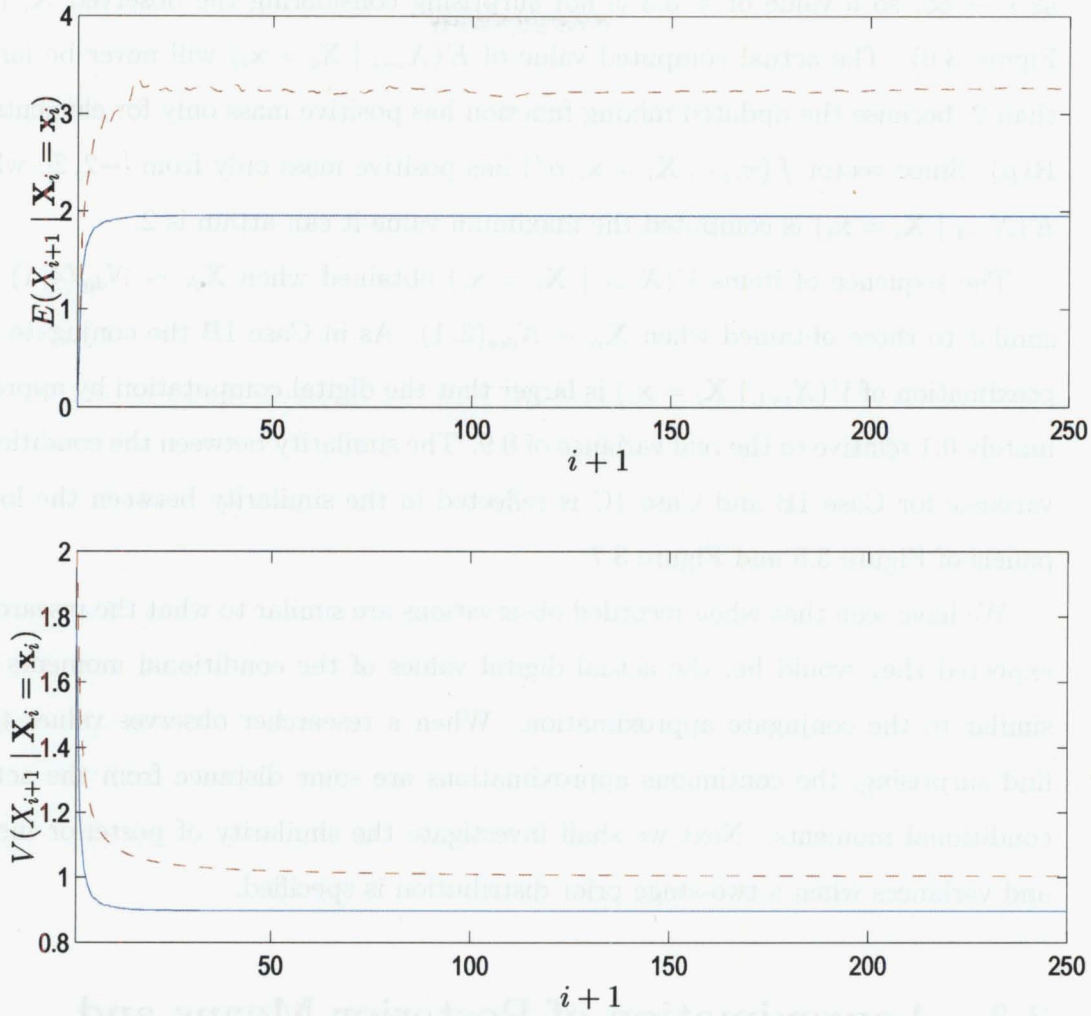


**Figure 3.7: Conditional Expectations and Variances of the Digital Mass Function (solid blue line) and Conventional Conjugate Theory (dashed red line) when $\mathbf{X}_{250} \sim N_{dig}(4,1)$.**

is symmetric about 4 it is reasonable to expect that the number of times we observe $X_i = 3$ and $X_i = 5$, and the number of times we observe $X_i = 2$ and $X_i = 6$ will be approximately the same. In this case we observe $X_i = 3$ on 9 occasions compared to $X_i = 5$ on 8 occasions.We observe $X_i = 2$ and $X_i = 6$ once each.

Figure 3.7 shows the conditional expectation and variance for a typical example when we have 250 observations. $E\left(X_{i+1} \mid \mathbf{X}_i = \mathbf{x}_i\right)$ is plotted in the upper panel of Figure 3.7. It shows a large difference between the conjugate approximation (which is approximately 3.3) and the actual digital computation ($\approx$ 1.95). The limit of the conjugate approximation approaches the arithmetic mean of the $i$ observations

as $i \rightarrow \infty$, so a value of $\approx 3.3$ is not surprising considering the observed $\mathbf{X}_i$ (see Figure 3.6). The actual computed value of $E(X_{i+1} \mid \mathbf{X}_i = \mathbf{x}_i)$ will never be larger than 2, because the updated mixing function has positive mass only for elements of $\mathbf{R}(\mu)$. Since vector $f(x_{i+1} \mid \mathbf{X}_i = \mathbf{x}_i, \sigma^2)$ has positive mass only from $[-2, 2]$, when $E(X_{i+1} \mid \mathbf{X}_i = \mathbf{x}_i)$ is computed the maximum value it can attain is 2.

The sequence of items $V(X_{i+1} \mid \mathbf{X}_i = \mathbf{x}_i)$ obtained when $\mathbf{X}_N \sim N_{dig}(4, 1)$ are similar to those obtained when $\mathbf{X}_N \sim N_{dig}(2, 1)$. As in Case 1B the conjugate approximation of $V(X_{i+1} \mid \mathbf{X}_i = \mathbf{x}_i)$ is larger that the digital computation by approximately 0.1 relative to the real variance of 0.9. The similarity between the conditional variance for Case 1B and Case 1C is reflected in the similarity between the lower panels of Figure 3.5 and Figure 3.7.

We have seen that when recorded observations are similar to what the researcher expected they would be, the actual digital values of the conditional moments are similar to the conjugate approximation. When a researcher observes values they find surprising, the continuous approximations are some distance from the actual conditional moments. Next we shall investigate the similarity of posterior means and variances when a two-stage prior distribution is specified.

## 3.3 Approximation of Posterior Means and Variances when a Two-Stage Prior Distribution is Specified

So far in this Chapter we have considered how well conventional conjugate mixture-Normal theory can approximate real discrete mass functions, represented by digital Normal mass functions, when the prior distribution is fully specified. In this Section we shall extend this approach and investigate how well Normal-Gamma mixture-Normal conjugate theory approximates measurements obtained through the use of real discrete mass functions when they are representable by digital Normal mass functions and digital Gamma mass functions.

If we assert that the precision of the $X$ observations, $\pi$, has a Gamma distribution with parameters $\alpha$ and $\beta$, the conditional distribution of $\mu$, given $\pi$, is a Normal

distribution with mean $\mu_0$ and precision $\tau\pi$, and that $X$, conditioned on $\mu$ and $\pi$, is distributed Normally with mean $\mu$ and precision $\pi$. Then using an extension of Equation 3.1, the density for $X$ can be derived by

$$f(x) = \int_{-\infty}^{\infty}\int_{-\infty}^{\infty} f(x \mid \mu,\pi) f(\mu \mid \pi) f(\pi) d\mu d\pi \tag{3.24}$$

$$= \int_{-\infty}^{\infty} f(x \mid \mu) f(\mu) d\mu. \tag{3.25}$$

Conventional conjugate theory tells us that, for a single case, $X$ has a general $t$-distribution with location parameter $\mu_0$, scale parameter $\tau\alpha/(1+\tau)\beta$ and shape parameter $2\alpha$. To summarise this situation symbolically,

$$\pi \sim \Gamma(\alpha,\beta) \tag{3.26}$$

$$\mu \mid \pi \sim N(\mu_0, \tau\pi) \tag{3.27}$$

$$X \mid \mu,\pi \sim N(\mu,\pi) \tag{3.28}$$

and

$$X \sim t(2\alpha, \mu_0, \tau\alpha/(1+\tau)\beta). \tag{3.29}$$

Under a Bayesian framework we say $f(\pi)$ is the prior density for $\pi$, $f(\mu \mid \pi)$ is the prior density for $\mu$, $f(x \mid \mu,\pi)$ is the ITF and $f(x)$ is the predictive density for $X$. $f(\pi)$ and $\pi$ are often called the hyperprior and hyperparameter respectively. This form of distribution is known as an hierarchical Bayes model.

In the previous section the one-stage prior, $f(\mu \mid \sigma^2)$, was used. That is, we assumed the spread was known, and had the value $\sigma^2$, but that the location of the prior was unknown, and was distributed Normally with parameters $\mu_0$ and $\tau^2$. Now we are including an additional level of prior modeling by assuming that both the location, conditioned on the spread and represented by $\mu$, and the spread, represented by $\pi$, of the observations are unknown, and placing a prior distribution on each of them. We assess the distribution of $\mu \mid \pi$ as in Case 1, but now we also need to assess the distribution of $\pi$. This is an example of a two-stage prior distribution.

Notice that a major difference in this Section is that we now parameterise the Normal distribution by its precision, $\pi$, rather than its variance, $\sigma^2 \equiv \pi^{-1}$. The only time in the remainder of Section 3 that we shall refer to variance is in the calculation of item $V(X_{i+1} \mid \mathbf{X}_i = \mathbf{x}_i)$.

### 3.3.1 Discrete Mass Functions Characterised as Digitised Normal and Digitised Gamma Densities

This Section will involve working with probability mass functions $f(x \mid \mu, \pi)$ and $f(\mu \mid \pi)$, which are characterised as digitised Normal densities, and $f(\pi)$, which is characterised as a digitised Gamma density. To compute the predictive mass function of $X$ we follow a procedure similar to that described in Section 3.2. In that case we worked with the mass functions $f(x \mid \mu, \sigma^2)$ and $f(\mu \mid \sigma^2)$, and created two matrices of equal dimensions. Now we need to consider three mass functions. To account for the extra mass function we shall represent $f(x \mid \mu, \pi)$, $f(\mu \mid \pi)$ and $f(\pi)$ in array form. The three arrays constructed will be of equal size

Before we can form the three arrays needed to undertake the required computations we must define realms for $X$, $\mu$ and $\pi$.

#### Forming Arrays of Mass Values

To generate the digitised space we are interested in, we first identify realms $\mathbf{R}(X)$, $\mathbf{R}(\mu)$ and $\mathbf{R}(\pi)$, which represent the possible measurement values of $X$, and mixing possibilities for $\mu$ and $\pi$ respectively. The specification of $\mathbf{R}(X)$ and $\mathbf{R}(\mu)$ has been discussed previously. $\mathbf{R}(\pi)$ will represent the spread of the digitised mixture function with parameter $\pi$, and should include every value of $\pi$ that could be relevant to its subject.

After identifying the three realms of interest, we form an array of mass values for $f(x \mid \mu, \pi)$. The array will have height corresponding to the candidate $X$ values, width corresponding to the candidate $\mu$ values and depth corresponding to the possible values for $\pi$. Evaluate density $f(x \mid \mu, \pi)$ at each grid-point. Normalise the columns for later use, when they will aid in the computation of the posterior mass function $f(\mu \mid X = x, \pi)$.

Arrays $f(\mu \mid \pi)$ and $f(\pi)$ also have height corresponding to the size of $\mathbf{R}(X)$, width corresponding to the size of $\mathbf{R}(\mu)$ and depth corresponding to the size of $\mathbf{R}(\pi)$. To construct $f(\mu \mid \pi)$, form a matrix whose dimensions correspond to candidate $\mu$ and $\pi$ values. Evaluate density $f(\mu \mid \pi)$ at each grid-point. Replicate and tile the matrix until it is the same size as $f(x \mid \mu, \pi)$. Note that every plane corresponding

to a member of $\mathbf{R}(X)$ will be identical.

To construct array $f(\mu)$ a similar method is used. First, evaluate $f(\pi)$ for each element of $\mathbf{R}(\pi)$. The resulting vector represents a mass function characterised as a digitised Gamma density. Replicate and tile the vector along both the $X$ and $\mu$ dimensions. Values in this array will vary in the $\pi$ dimension only. All three arrays will now be the same size.

#### Generating Sequences of Observation Values

A vector of length $N$ containing observation values is generated by following the sequence of steps outlined in Section 3.2.1. The only difference is that the mass function the $X$'s are drawn from is parameterised by $\mu$ and $\pi$, rather than by $\mu$ and $\sigma^2$. To this point we have constructed realms $\mathbf{R}(X)$, $\mathbf{R}(\mu)$ and $\mathbf{R}(\pi)$, arrays $f(x \mid \mu, \pi)$, $f(\mu \mid \pi)$ and $f(\pi)$ and $\mathbf{X}_N$, a vector containing $N$ observation values.

### 3.3.2 Computing Posterior Means and Variances of Posterior Discrete Densities

To find exact values for $E(X_{i+1} \mid \mathbf{X}_i = \mathbf{x}_i)$ and $V(X_{i+1} \mid \mathbf{X}_i = \mathbf{x}_i)$ for the discrete mass functions characterised as digitised Normal and digitised Gamma densities, we compute

$$f(x_{i+1} \mid \mathbf{X}_i = \mathbf{x}_i) = \sum_{\mu} \sum_{\pi} f(x_{i+1} \mid \mu, \mathbf{X}_i = \mathbf{x}_i, \pi) f(\mu, \pi \mid \mathbf{X}_i = \mathbf{x}_i), \tag{3.30}$$

which is an extension of Equation 3.6. The first function in this sum of products does not change. It is always represented by array $f(x \mid \mu, \pi)$. The second function is a combination of Equations 3.26, 3.27 and 3.28. After each observed value of $(\mathbf{X}_i = \mathbf{x}_i)$, it is updated via Bayes' Theorem, a consequence of which is

$$f(\mu, \pi \mid \mathbf{X}_i = \mathbf{x}_i) = \frac{f(\mathbf{X}_i = \mathbf{x}_i \mid \mu, \pi) f(\mu, \pi)}{\sum_{\mu} \sum_{\pi} f(\mathbf{X}_i = \mathbf{x}_i \mid \mu, \pi) f(\mu, \pi)} \qquad \text{for} \quad i = 1, 2, \ldots, N-1. \tag{3.31}$$

Before we can implement Bayes' Theorem we must calculate the joint mass function for $(\mu, \pi)$. It is widely known that

$$f(\mu, \pi) = f(\mu \mid \pi) f(\pi). \tag{3.32}$$

Thus to obtain $f(\mu, \pi)$ we merely multiply array $f(\mu \mid \pi)$ element-wise with array $f(\pi)$. Once $f(\mu, \pi)$ is found we follow similar steps to those outlined in Section 3.2.2 on page 76:

1. Observe $X_i = x_i$.
2. Extract the matrix corresponding to $X_i$ from array $f(x \mid \mu, \pi)$. This is the ITF through $\mu$ and $\pi$ from $X_i = x_i$ to $X_{i+1}$.
3. Implement Bayes' Theorem and thus obtain the updated mixing function, matrix $f(\mu, \pi \mid \mathbf{X}_i = \mathbf{x}_i)$. Replicate and tile this matrix so it has the same size as array $f(x \mid \mu, \pi)$.
4. Calculate $f(x_{i+1} \mid \mathbf{X}_i = \mathbf{x}_i)$ by Equation 3.30.
5. Compute $E(X_{i+1} \mid \mathbf{X}_i = \mathbf{x}_i)$ and $V(X_{i+1} \mid \mathbf{X}_i = \mathbf{x}_i)$.

Repeat steps 1–5 as many times as required.

### 3.3.3 Conventional Conjugate Normal-Gamma Mixture-Normal Theory

A multivariate Normal distribution that treats the components of $\mathbf{X}$ independently can be identified by parameters $\mu$ and $\pi$. The density function for a vector of quantities $\mathbf{X} \in \mathcal{R}^K$ is

$$f(\mathbf{x}) = \int_{-\infty}^{\infty} \int_{-\infty}^{\infty} (2\Pi)^{-K/2} \pi^{K/2} \exp\left[-\pi \sum_{i=1}^{K} (x_i - \mu)^2 / 2\right] dM(\mu, \pi), \qquad (3.33)$$

where $\Pi$ denotes the real number pi. We use the capital letter $\Pi$ for the real number pi, rather than the usual lower case letter, in an attempt to avoid confusion with the mixing parameter $\pi = (\sigma^2)^{-1}$. We say $f(\mathbf{x})$ is a mixture of conditionally independent Normal densities with mixing parameters $\mu$ and $\pi$ and mixing distribution function $M$, and it is denoted by $\mathbf{X} \sim M\text{-}N_K(\mu, \pi)$.

The product of a conditional density function and a marginal density is a joint density function. If the conditional density function, denoted $(\mu \mid \pi)$, is Normal with

parameters $\mu_0$ and $\tau\pi$, and if the marginal density, $\pi$, is Gamma with parameters $\alpha$ and $\beta$, then the joint density function for $(\mu, \pi)$ is

$$f(\mu,\pi) \propto (\tau\pi)^{1/2} \exp\left[-\tau\pi\left(\mu-\mu_0\right)^2/2\right] \pi^{\alpha-1}\exp\left(-\beta\pi\right) \qquad ((\mu,\pi)\in(\mathcal{R},\mathcal{R}^+)), \tag{3.34}$$

and we say the joint density is a member of the Normal-Gamma family of distributions, denoted $(\mu, \pi) \sim N\Gamma(\mu_0, \tau, \alpha, \beta)$.

Suppose the components of $\mathbf{X}$ are regarded exchangeably and that $\mathbf{X} \sim M\text{-}N_K(\mu, \pi)$ with $M(\mu, \pi)$ specified as $N\Gamma(\mu_0, \tau, \alpha, \beta)$. If $\mathbf{X}$ is partitioned into $\mathbf{X}_1$ and $\mathbf{X}_2$, of sizes $K_1$ and $K_2$ respectively, then $\mathbf{X}_2 \mid (\mathbf{X}_1 = \mathbf{x}_1) \sim M\text{-}N_{K_2}(\mu, \pi)$, with the conditional mixing function $M(\mu, \pi \mid \mathbf{X}_1 = \mathbf{x}_1)$ in the Normal-Gamma form

$$N\Gamma\left[\frac{\tau\mu_0 + K_1\bar{x}_{K_1}}{\tau+K_1}, \tau+K_1, \alpha+\frac{K_1}{2}, \beta+\left(\frac{K_1}{2}\right)s_{K_1}^2+\frac{\tau K_1\left(\bar{x}_{K_1}-\mu_0\right)^2}{2\left(K_1+\tau\right)}\right], \tag{3.35}$$

where $\bar{x}_{K_1}$ is the arithmetic mean of $\mathbf{X}_1$ and $s_{K_1}^2$ is the average squared difference, $K_1^{-1}\sum_{i=1}^{K_1}(x_i-\bar{x})^2$. For details see the text of Lad (1996, pp. 395–397, 408–412).

In this application involving the forecast of $X_{i+1}$ given $(\mathbf{X}_i = \mathbf{x}_i)$, we are interested in the case when $\mathbf{X}_1 = (\mathbf{X}_i = \mathbf{x}_i)$ and $\mathbf{X}_2 = X_{i+1}$. The conditional expectation reduces to

$$E(X_{i+1} \mid \mathbf{X}_i = \mathbf{x}_i) = \frac{\tau\mu_0 + i\bar{x}_i}{\tau+i}. \tag{3.36}$$

Initially the conditional expectation depends solely on $\mu_0$, but as $i$ increases the weighting given to $\mu_0$ steadily decreases. $E(X_{i+1} \mid \mathbf{X}_i = \mathbf{x}_i)$ will be increasingly strongly influenced by the arithmetic mean of the observed quantities. As more observations are recorded each individual observation, and the prior mean, will be less influential, but the arithmetic mean of the observed quantities will be more influential.

The conditional variance is

$$V(X_{i+1} \mid \mathbf{X}_i = \mathbf{x}_i) = \frac{(\tau+i+1)\left[2\beta+is_i^2+\tau i\left(\bar{x}_i-\mu_0\right)^2/\left(i+\tau\right)\right]}{(\tau+i)\left[2\alpha+i-2\right]}. \tag{3.37}$$

The conditional variance is initially equal to the prior variance, $\beta(1+\tau)/\tau(\alpha-1)$. As $i \to \infty$, $V(X_{i+1} \mid \mathbf{X}_i = \mathbf{x}_i) \to s_i^2$, where $s_i^2$ is the average squared difference of the conditioning observations from their mean. That is, as the number of observations

increases, each individual observation becomes less important, but the overall importance of $s_i^2$ increases in determining the predictive variance for the next quantity $X_{i+1}$.

### 3.3.4 Case 2: $\pi \sim \Gamma_{dig}(2,2)$, $\mu \mid \pi \sim N_{dig}(0,\pi)$ and $X \mid \mu, \pi \sim N_{dig}(\mu,\pi)$

The examples in this Section consider the case where we have a digitised two-stage prior mass function. We shall study the closeness of the conjugate Normal-Gamma mixture-Normal approximation to the precise computation based on the digitised Gamma and digitised Normal distributions under different scenarios. Parameters are chosen to be $\alpha = 2$, $\beta = 2$, $\mu_0 = 0$ and $\tau = 1$, so that

$$\pi \sim \Gamma_{dig}(2,2) \tag{3.38}$$

$$\mu \mid \pi \sim N_{dig}(0,\pi) \tag{3.39}$$

$$\text{and} \qquad X \mid \mu, \pi \sim N_{dig}(\mu,\pi). \tag{3.40}$$

The 'observed' $X$'s shall be sampled from mass functions corresponding to digitised Normal distributions with parameters $\mu = 0, 2, 4$ and $\pi = 0.25, 0.4, 1$. Note that the $\mu$ values we shall use are the same as in Case 1.

We identify realms $\mathbf{R}(X)$, $\mathbf{R}(\mu)$ and $\mathbf{R}(\pi)$ as having as interval width of 0.08. We characterise the standard measurements of $X$ as fully between $-6$ and 6, with summary extreme values $(\pm 7, \pm 8, \pm 9, \pm 10)$ to represent possible extreme measurements. The size of $\mathbf{R}(X) = 159$. The realm of $\mu$ has the same endpoints as in Case 1, $-2$ and 2, meaning the size of $\mathbf{R}(\mu)$ is 51. $\mathbf{R}(\pi)$ should cover every reasonable value of interest for the mixing spread parameter $\pi$. In this case the realm of $\pi$ will have a minimum value of 0.4 and a maximum value of 2. Thus the size of $\mathbf{R}(\pi)$ is 21.

#### Computation of $f(x \mid \mu, \pi)$, $f(\mu \mid \pi)$ and $f(\pi)$

Before we can compute any of our desired items we must form arrays $f(x \mid \mu, \pi)$, $f(\mu \mid \pi)$ and $f(\pi)$. All three arrays will be size $159 \times 51 \times 21$. The only array whose entries are all distinct is $f(x \mid \mu, \pi)$. Entries along its height, which we call

the $X$-axis, correspond to elements of $\mathbf{R}(X)$. Elements along its width, the $\mu$-axis, correspond to the elements of $\mathbf{R}(\mu)$ and elements along its depth, the $\pi$-axis, correspond to the elements of $\mathbf{R}(\pi)$. A combination of any single element from $\mathbf{R}(\mu)$ and any single element from $\mathbf{R}(\pi)$ will have a related vector of mass values, corresponding to each element of $\mathbf{R}(X)$. Each of these mass functions is characterised as a digitised $N(\mu, \pi)$ density. For example, if the value of $\mu$ is chosen to be $-2$ and the value of $\pi$ is chosen to be 0.4, then the corresponding mass function, denoted by the values along the $X$-axis, is characterised as a digitised Normal density with mean $-2$ and precision 0.4. If we move one place along the $\mu$-axis, to $\mu = -1.92$, the corresponding mass function is characterised as a digitised Normal density with mean $-1.92$ and precision 0.4.

To construct array $f(\mu \mid \pi)$, first form a matrix of size $51 \times 21$. The values along the $\mu$-axis correspond to elements of $\mathbf{R}(\mu)$. This has length 51. Values along the $\pi$-axis correspond to elements of $\mathbf{R}(\pi)$. This has length 21. At each gridpoint evaluate the mass of a $N(0, \pi)$ distribution at value $\mu$. Normalise along the dimension corresponding to $\mathbf{R}(\mu)$. Replicate and tile the matrix along the $X$-axis until it has height 109.

Array $f(\mu)$ is constructed from a mass function which corresponds to a digitised Gamma$(2, 2)$ density. The mass function is evaluated for each member of $\mathbf{R}(\pi)$, and is then replicated and tiled along both the $X$-axis and $\mu$-axis.

### Case 2A: Observations Generated from $\mathbf{X}_N \sim N_{dig}(0, 1)$

**Case 2A: Digital Mass Functions** Now that arrays $f(x \mid \mu, \pi)$, $f(\mu \mid \pi)$ and $f(\pi)$ have been computed we are in a position to consider our examples. We generate 500 observations from $N_{dig}(0, 1)$ and find the sequence of items $E(X_{i+1} \mid \mathbf{X}_i = \mathbf{x}_i)$ and $V(X_{i+1} \mid \mathbf{X}_i = \mathbf{x}_i)$ by following the steps described in Section 3.3.2 for $i + 1 = 1, \ldots, 500$.

**Case 2A: Conjugate Theory** It follows from Equations 3.36 that the posterior mean of the $(i + 1)th$ observation, conditional on observing the first $i$ observations, is

$$E(X_{i+1} \mid \mathbf{X}_i = \mathbf{x}_i) = \frac{i\bar{x}_i}{i + 1}. \tag{3.41}$$

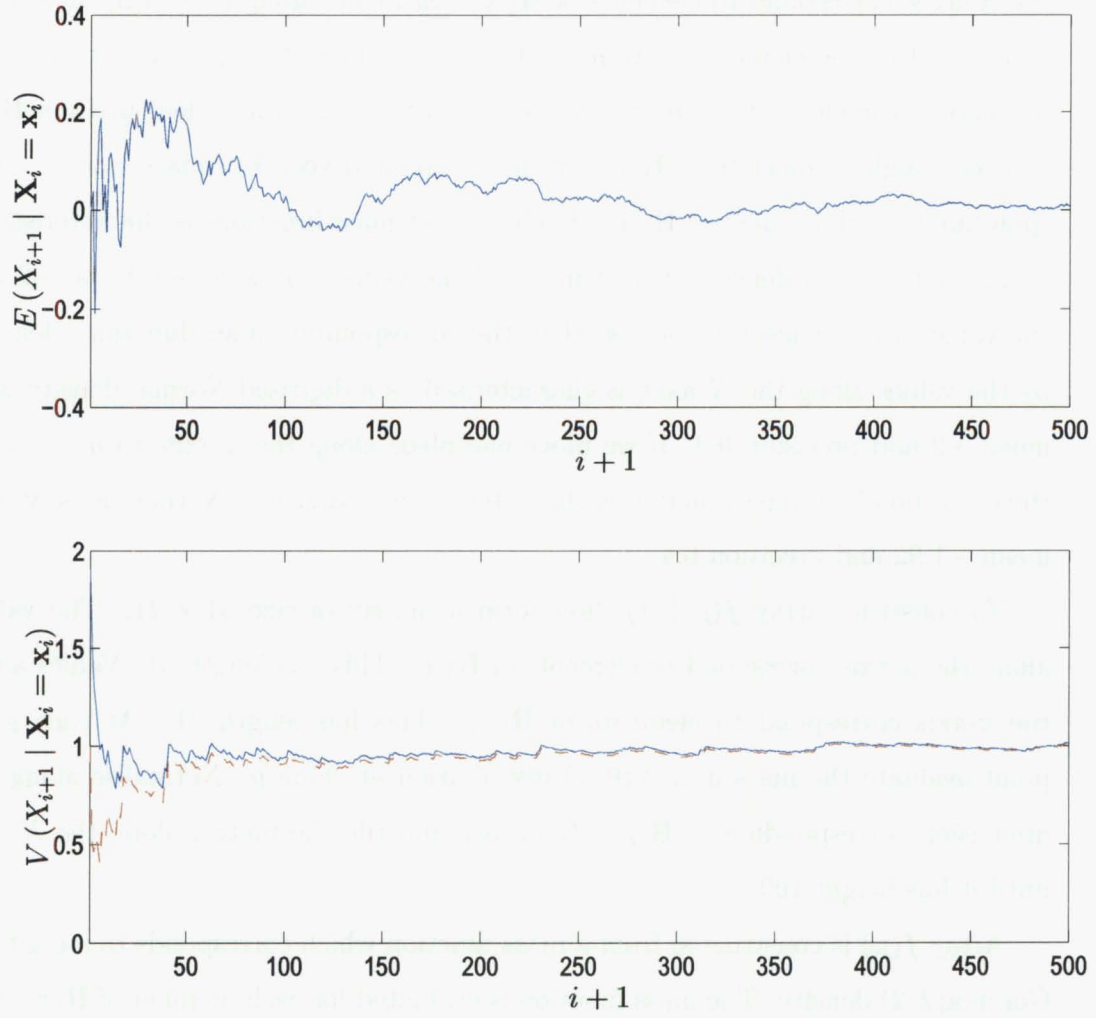


**Figure 3.8: Conditional Expectations and Variances of the Digital Mass Function (blue line) and Conventional Conjugate Theory (red line) when $\mathbf{X}_{500} \sim N_{dig}(0,1)$. The conditional expectations are indistinguishable.**

As $i$ increases, the conditional expectation tends toward the arithmetic mean of $\mathbf{X}_i$.

Equation 3.37 implies that the posterior variance of the $(i+1)th$ observation, conditional on observing the first $i$ observations, is

$$V(X_{i+1} \mid \mathbf{X}_i = \mathbf{x}_i) = \frac{4 + is_i^2 + i\bar{x}_i^2/(i+1)}{(i+1)}. \tag{3.42}$$

As the number of observations increase we expect $V(X_{i+1} \mid \mathbf{X}_i = \mathbf{x}_i)$ to tend to $s_i^2$.

**Case 2A: Results.** Figure 3.8 shows the result of a typical example when $\mathbf{X}_{500} \sim N_{dig}(0,1)$. The mode of the prior distribution is the same as the mode

of the conditional distribution of observations $\mathbf{X}$. Consequently it is not surprising that the conditional expectations for the digital computations and conjugate approximation are almost identical for all values of $i$.

The two conditional variances are closely linked. Neither conditional variance decreases monotonically, unlike in Case 1. Notice how similar the fluctuations in $V(X_{i+1} \mid \mathbf{X}_i = \mathbf{x}_i)$ are. The difference between the digital computation and the conjugate approximation steadily decreases until they are almost identical whenever $i > 150$.

### Case 2B: Observations Generated from $\mathbf{X}_N \sim N_{dig}(0, 0.4)$

**Case 2B: Digital Mass Functions.** The items required, $E(X_{i+1} \mid \mathbf{X}_i = \mathbf{x}_i)$ and $V(X_{i+1} \mid \mathbf{X}_i = \mathbf{x}_i)$, can be found in the manner outlined in Case 2A.

**Case 2B: Conjugate Theory.** A study of Equations 3.36 and 3.37 show the conditional posterior mean and variance remain the same as in Case 2A.

**Case2B: Results.** Figure 3.9 shows the result of a typical example when $\mu = 0$, $\pi = 0.4$ (equivalent to $\sigma^2 = 2.5$) and $n = 5000$. As in Case 2A, the conditional expectations for the digital computations and conjugate approximation are almost identical for all values of $i$. Interestingly, the conjugate approximation of the conditional expectation appears to be slightly more unstable than the digital computation, most noticeably when $2000 < i$. Notice that the conjugate approximation fluctuates slightly above and below the digital computation, which seems to be constant.

The two conditional variances are similar. Note that when $i < 1000$ the conjugate approximation fluctuates considerably more than the digital computation. The conditional variance of the digital computation appears to reach stability at $i \approx 3000$. The variance of the conjugate approximation is larger than the variance of the digital computation before stability is reached. The approximate variance decreases gradually until by $i \approx 4250$ the two conditional variances are very similar, nevertheless the conjugate approximation remains slightly larger.

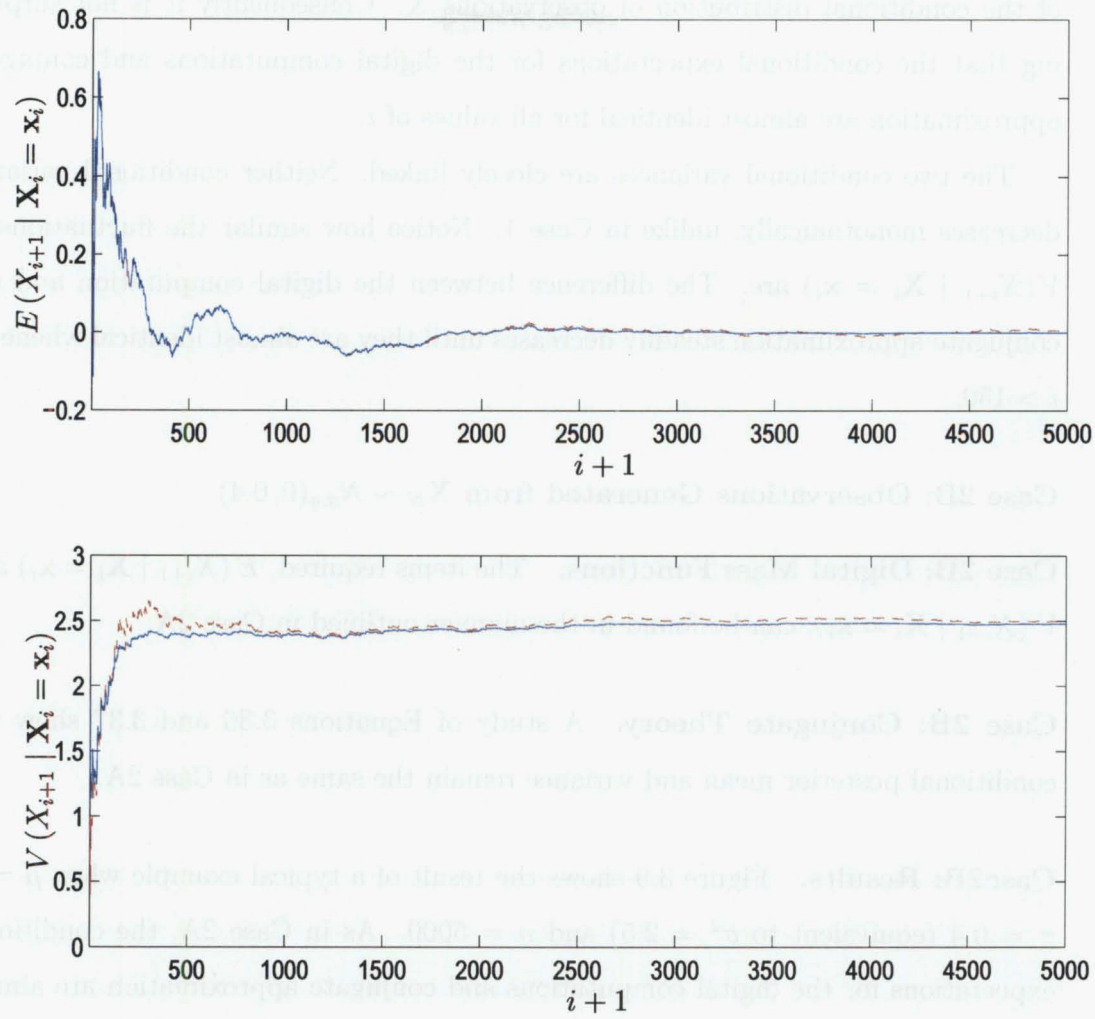


**Figure 3.9: Conditional Expectations and Variances of the Digital Mass Function (solid blue line) and Conventional Conjugate Theory (dashed red line) when $\mathbf{X}_{5000} \sim N_{dig}(0, 0.4)$.**

**Case 2C: Observations Generated from $\mathbf{X}_N \sim N_{dig}(0, 0.25)$**

For Case 2C the observations are generated from a mass function characterised as a Normal density with mean equal to zero, which is also the value of the prior mean. The generating value of $\pi$ is 0.25, which is outside the range of $\mathbf{R}(\pi)$. If a researcher, who had specified the same prior mixture mass function as we have, observed these values, they would notice that the observations were centred around 0, which is as they would expect, but would be surprised by how widely the data was spread.

The result of a typical example when $\mu = 0$, $\pi = 0.25$ and $n = 5000$ is shown in

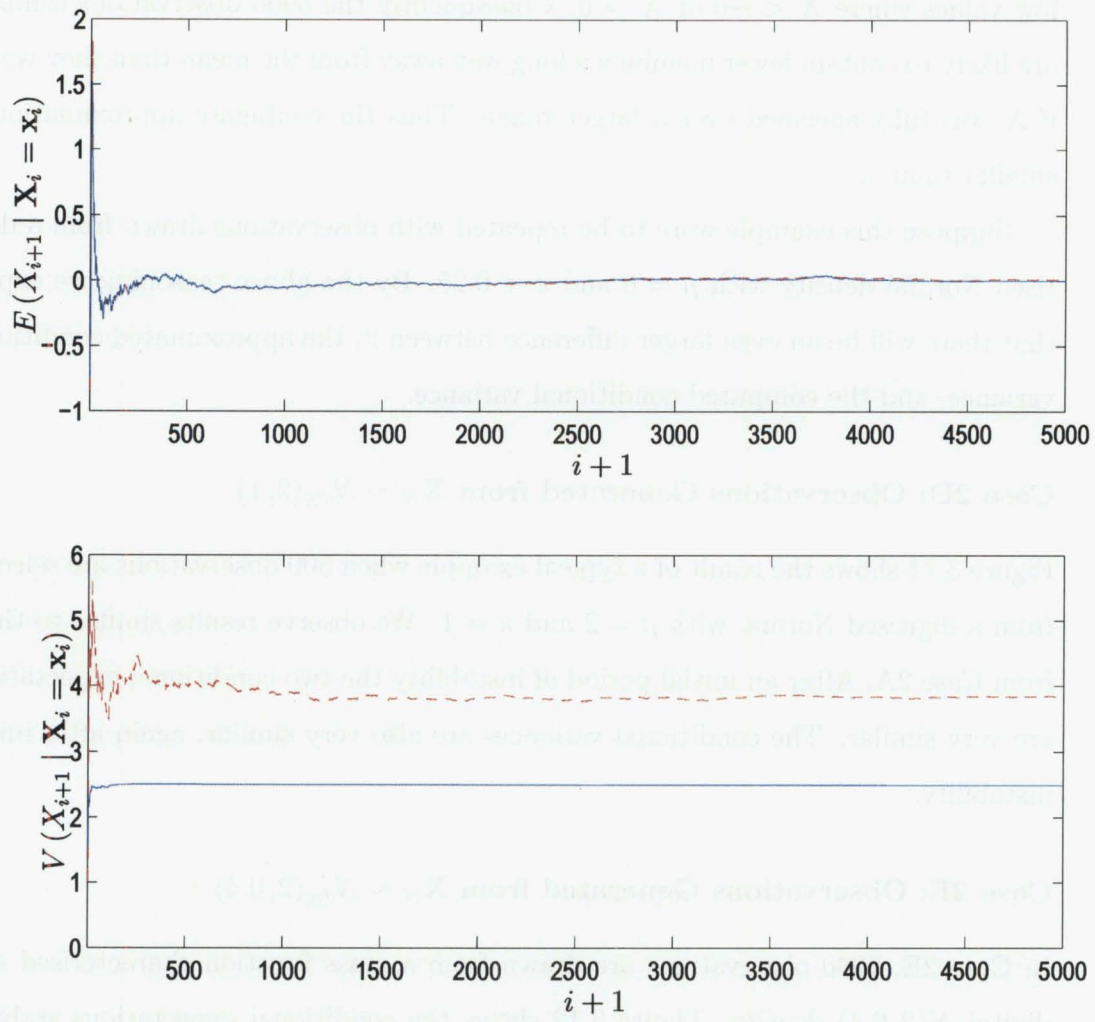


**Figure 3.10: Conditional Expectations and Variances of the Digital Mass Function (solid blue line) and Conventional Conjugate Theory (dashed red line) when $\mathbf{X}_{5000} \sim N_{dig}(0, 0.25)$.**

Figure 3.10. As in the previous two cases, the conditional expectation for the digital computation and conjugate approximation are almost identical for all values of $i$.

The two conditional variances are quite different. Due to the range of $\mathbf{R}(\pi)$, the conditional variance of the digital computation cannot take a value higher than 2.5. Remember that $\sigma^2 = 2.5$ is equivalent to $\pi = 0.4$. Although the observations are selected from a digitised Normal density with $\pi = 0.25$ ($\equiv \sigma^2 = 4$), the conditional variance of the conjugate approximation stays slightly below 4, $V(X_{i+1} \mid \mathbf{X}_i = \mathbf{x}_i) \approx 3.8$. This is because $\mathbf{R}(X)$, the realm that contains all possible $X$ values, is only fully specified on $[-6, 6]$. Thus the selection of $\mathbf{X}$ is likely to contain

few values where $X < -6$ or $X > 6$. Consequently the 5000 observations sampled are likely to contain fewer members a long way away from the mean than they would if $X$ was fully specified over a larger range. Thus the conjugate approximation is smaller than 4.

Suppose this example were to be repeated with observations drawn from a digitised Normal density with $\mu = 0$ and $\pi < 0.25$. By the above reasoning we expect that there will be an even larger difference between $\pi$, the approximated conditional variance, and the computed conditional variance.

### Case 2D: Observations Generated from $\mathbf{X}_N \sim N_{dig}(2, 1)$

Figure 3.11 shows the result of a typical example when 500 observations are selected from a digitised Normal with $\mu = 2$ and $\pi = 1$. We observe results similar to those from Case 2A. After an initial period of instability the two conditional expectations are very similar. The conditional variances are also very similar, again after initial instability.

### Case 2E: Observations Generated from $\mathbf{X}_N \sim N_{dig}(2, 0.4)$

In Case 2E, 5000 observations are drawn from a mass function characterised as a digital $N(2, 0.4)$ density. Figure 3.12 shows the conditional expectations stabilise to the same value. Again the conjugate approximation is more unstable than the digital computation.

The conjugate approximation of the conditional variance is slightly larger than the digital computation. As the precision increases relative to $\mu$, we expect to see more of a difference between the two conditional variances. Since we expect the range of possible $X$ values specified by conjugate theory to be beyond the range in which $\mathbf{R}(X)$ is fully specified.

### Case 2F: Observations Generated from $\mathbf{X}_N \sim N_{dig}(2, 0.25)$

Figure 3.13 shows the results of a typical case when the generating values of $\mu$ and $\pi$ are 2 and 0.25 respectively. The number of observations drawn is 5000. The two conditional expectations are both similar, and are approximately equal to 1.9. In

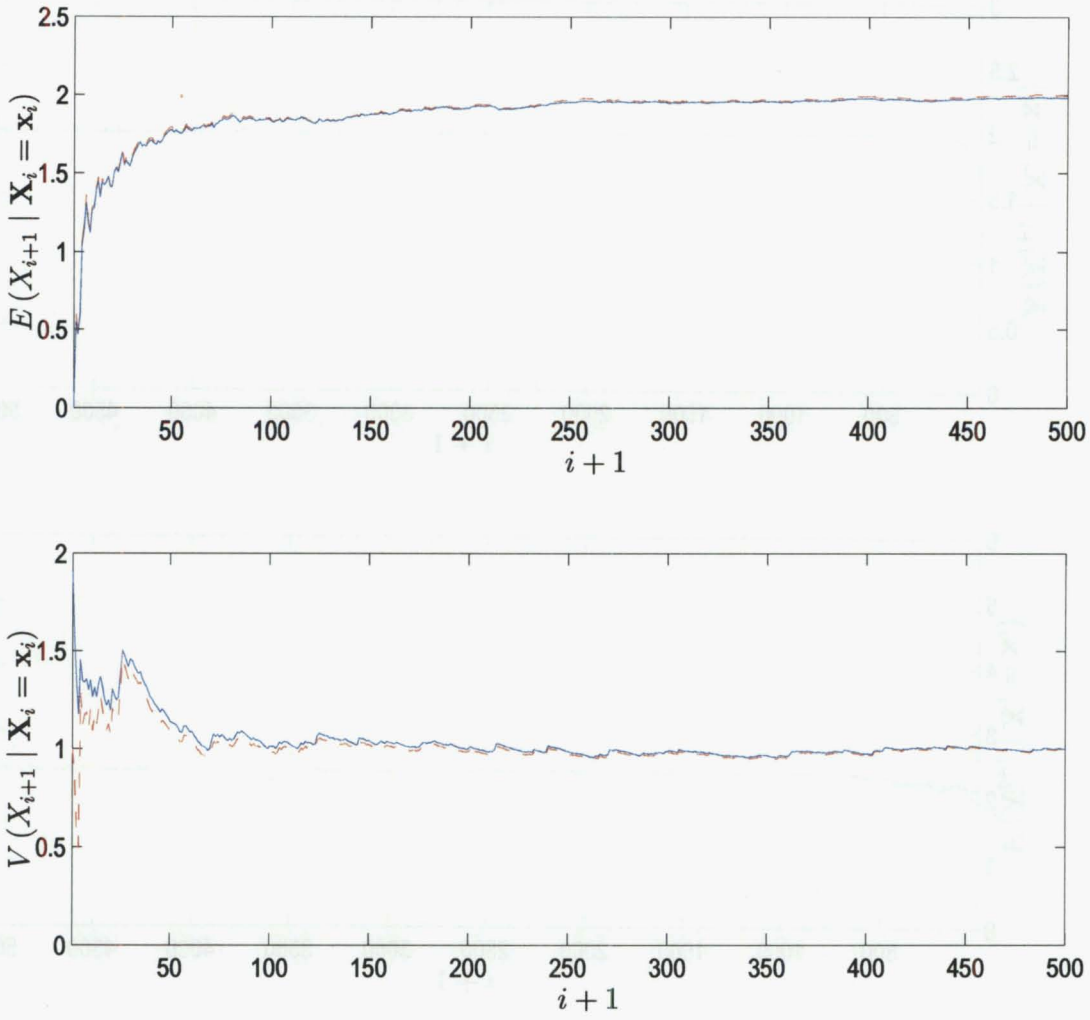


**Figure 3.11: Conditional Expectations and Variances of the Digital Mass Function (solid blue line) and Conventional Conjugate Theory (dashed red line) when $\mathbf{X}_{500} \sim N_{dig}(2,1)$.**

this case the mean of the conditional distribution of observations is 2, but both the computed and approximated conditional values of $E\left(X_{i+1} \mid \mathbf{X}_i = \mathbf{x}_i\right)$ are less than 2. This is because the range of $\mathbf{R}(X)$ means it is unlikely there will be any observations greater than 6, in fact $P(X > 6) = 0.0009$ (4dp). Whereas we are comparatively more likely to observe a value of $X_i$ less than $-2$ since $P(X < -2) = 0.0243$ (4dp).

The approximation of the conditional variance is larger than the variance attained through digital computations, and both are less than 4. The computed conditional variance is approximately 2.5, as expected considering the maximum value of $\mathbf{R}(\mu)$ is 2.5. The conjugate approximation gives a conditional variance of

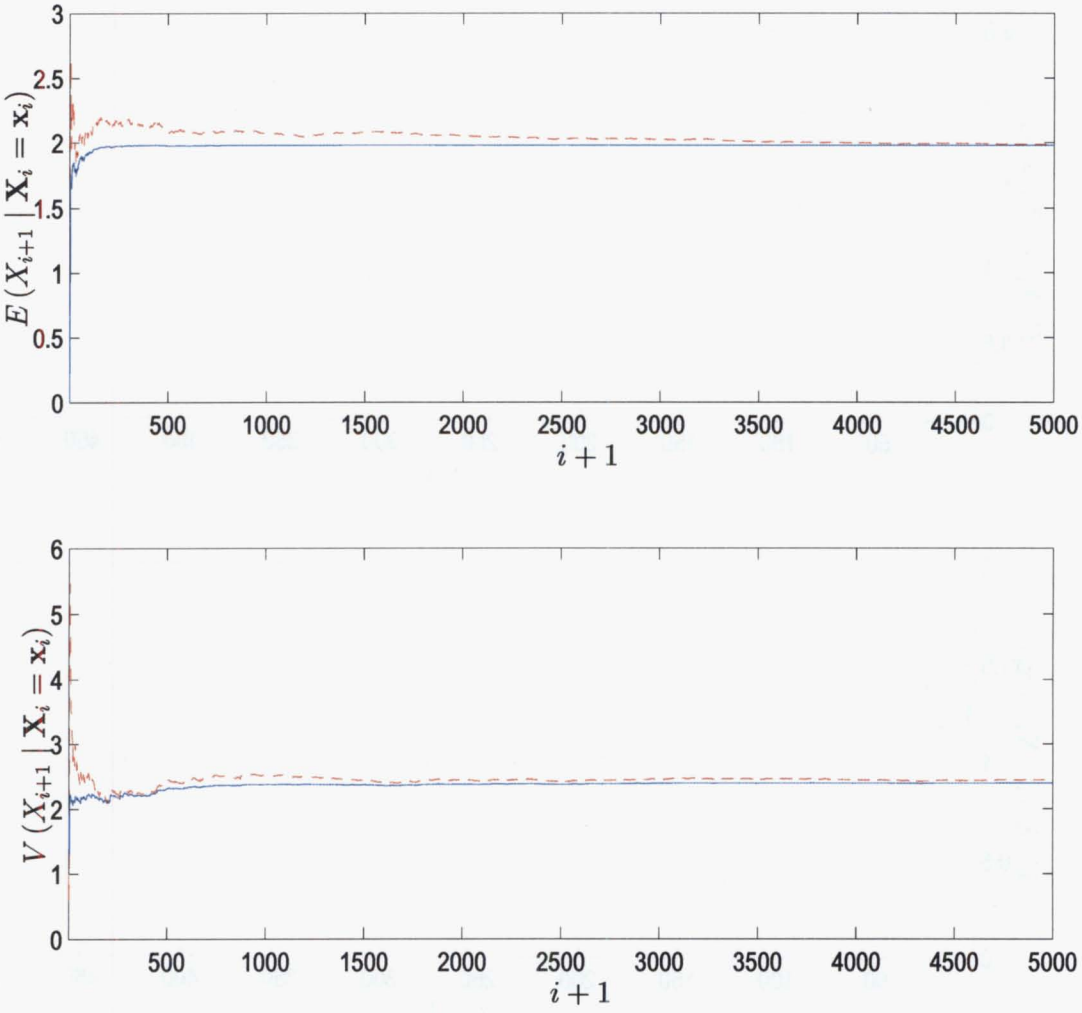


**Figure 3.12: Conditional Expectations and Variances of the Digital Mass Function (solid blue line) and Conventional Conjugate Theory (dashed red line) when $\mathbf{X}_{5000} \sim N_{dig}(2, 0.4)$.**

3.6, significantly less than the approximation of 3.9 attained in Case 1C. The two components of the conjugate approximation of $V(X_{i+1} \mid \mathbf{X}_i = \mathbf{x}_i)$ whose value will alter from Case 2C to Case 2F are $s_i^2$ and $\bar{x}_i$, both of these components will have lower values in Case 2F than Case 2C. Thus is because, although $\pi = 0.25$ in both cases, the number of distinct elements of $\mathbf{R}(X)$ that we could reasonably expect to observe is smaller in this case, as discussed in the paragraph above.

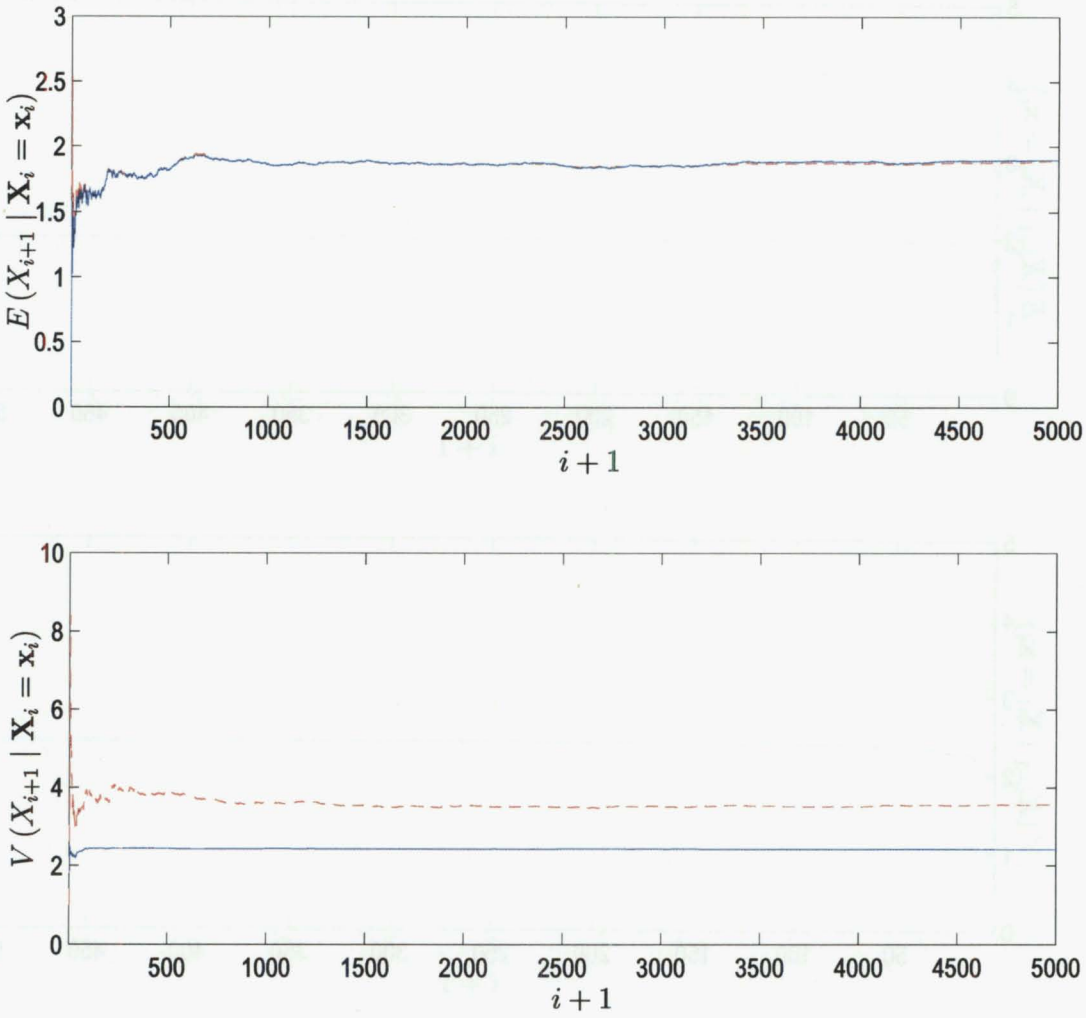


**Figure 3.13: Conditional Expectations and Variances of the Digital Mass Function (solid blue line) and Conventional Conjugate Theory (dashed red line) when $\mathbf{X}_{5000} \sim N_{dig}(2, 0.25)$.**

**Case 2G: Observations Generated from $\mathbf{X}_N \sim N_{dig}(4, 1)$**

Figure 3.14 shows the result of a typical example when 500 observations were generated from a digitised Normal mass function with parameter values of $\mu = 4$ and $\pi = 1$. The generating value of $\mu$ is not an element of $\mathbf{R}(\mu)$. Thus, if a researcher specified the prior mixture mass function considered in this Section, they would be surprised by the location of this set of observations.

The values of the conditional expectations are unsurprising. The two expectations have both reached stability more quickly than in either Case 2A or Case 2D.

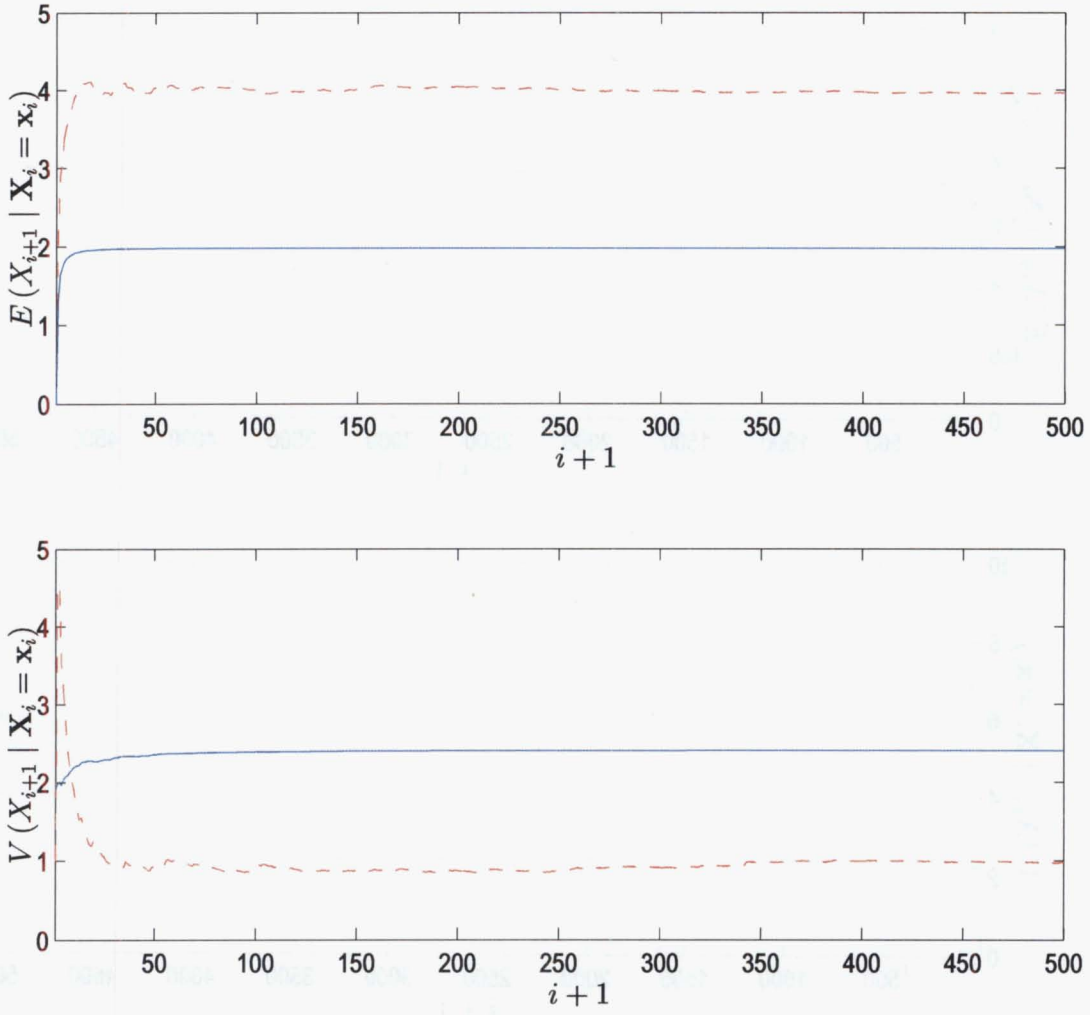


**Figure 3.14: Conditional Expectations and Variances of the Digital Mass Function (solid blue line) and Conventional Conjugate Theory (dashed red line) when $\mathbf{X}_{500} \sim N_{dig}(4,1)$.**

$E(X_{i+1} \mid \mathbf{X}_i = \mathbf{x}_i)$ for the conjugate approximation is just below 4, the mean of the conditional distribution of $X$ values. The computed expectation is practically 2, the maximum value of $\mathbf{R}(\mu)$.

An interesting point to note is that in Case 1C, where we dealt with a one-stage prior and $\mathbf{R}(X)$ was fully specified on $[-4,4]$, observations were also selected from a $N_{dig}(4,1)$ mass function. The conjugate approximation was approximately 3.3. Now $\mathbf{R}(X)$ is fully specified on $[-6,6]$, thus the observations drawn will have larger variance. If we were to rerun Case 2G with $\mathbf{R}(X)$ fully specified on $[-4,4]$, we would obtain the conjugate approximation $E(X_{i+1} \mid \mathbf{X}_i = \mathbf{x}_i) = 3.32$.

| $\mu$ | Digital Computation of Conditional Variance | Conjugate Approximation of Conditional Variance |
|---|---|---|
| 2.0 | 1.0553 | 1.0269 |
| 2.1 | 1.0592 | 1.0271 |
| 2.2 | 1.0593 | 1.0264 |
| 2.3 | 1.0721 | 1.0044 |
| 2.4 | 1.1395 | 1.0039 |
| 2.5 | 1.2296 | 1.0035 |
| 2.6 | 1.3743 | 1.0018 |
| 2.7 | 1.5300 | 1.0240 |
| 2.8 | 1.6200 | 1.0024 |
| 2.9 | 1.7901 | 1.0008 |
| 3.0 | 1.9743 | 0.9972 |
| 3.1 | 2.1567 | 0.9944 |
| 3.2 | 2.3486 | 0.9895 |
| 3.3 | 2.4052 | 0.9855 |
| 3.4 | 2.4052 | 0.9789 |
| 3.5 | 2.4052 | 0.9682 |
| 3.6 | 2.4052 | 0.9616 |
| 3.7 | 2.4052 | 0.9495 |
| 3.8 | 2.4052 | 0.9366 |
| 3.9 | 2.4052 | 0.9057 |
| 4.0 | 2.4052 | 0.8910 |

**Table 3.1: Digital computations and conjugate approximations of $V(X_{10000} \mid \mathbf{X}_{9999} = \mathbf{x}_{9999})$ when $X_{9999} \sim N_{dig}(\mu, 1)$.**

The conditional variance is much larger than it was in Case 2D, when $\mathbf{X}_N \sim N_{dig}(2, 1)$. To see how $V(X_{i+1} \mid \mathbf{X}_i = \mathbf{x}_i)$ changes as $\mu$ increases, $V(X_{10000} \mid \mathbf{X}_{9999} = \mathbf{x}_{9999})$ was calculated for cases when observations were generated for selected digitised $N(\mu, 1)$ distributions. Results are listed in Table 3.1.

The approximated conditional variance decreases increasingly rapidly as $\mu$ increases. This is expected because as $\mu$ increases the possibility that an observation value could come from part of $\mathbf{R}(X)$ that is not fully specified increases. If we were to plot a bar graph of observations drawn from $N_{dig}(2, 1)$ they would appear as if they are drawn from a Normal mass function, but if we were to plot the observations from $N_{dig}(4, 1)$, the bar graph would be clearly truncated. This idea was investigated

as part of Section 3.2.4, see Figure 3.1 for illustration.

In contrast the digitally computed conditional variance increases as $\mu$ increases. $V(X_{i+1} \mid \mathbf{X}_i = \mathbf{x}_i)$ is close to one when $\mu = 2$. As $\mu$ increases from 2.3 to 3.3 the increase is particularly rapid. When $\mu = 3.3$ the conditional variance has become as large as the elements of $\mathbf{R}(\mu)$ and $\mathbf{R}(\pi)$ will allow it to.

### Case 2H: Observations Generated from $\mathbf{X}_N \sim N_{dig}(4, 0.4)$

Case 2H, where 5000 observations are generated from $N_{dig}(4, 0.4)$, produces similar results to Case 2G. The computed conditional expectation is still approximately 2, but the approximate expectation has dropped to 3.75, reflecting the non-symmetrical nature of the observations about 4 due to the smaller precision, see Section 3.2.4 for comments and Figure 3.16 for illustration.

The lower panel of Figure 3.15 demonstrates that the computed conditional variance is slightly smaller than 2.5, the maximum value allowable by $\mathbf{R}(\pi)$. The approximate variance has dropped to approximately 1.9.

### Case 2I: Observations Generated from $\mathbf{X}_N \sim N_{dig}(4, 0.25)$

The conditional expectation and variance of a typical example when 5000 observations are generated from $N_{dig}(4, 0.25)$ are similar to results from Case 2H, as shown in Figure 3.16. A researcher who had specified the prior mass functions, $f(\mu \mid \pi) \sim N(0, \pi)$ and $f(\pi) \sim \Gamma(2, 2)$, would be very surprised to observe this data. For the conjugate conditional approximation $E(X_{i+1} \mid \mathbf{X}_i = \mathbf{x}_i) \approx 3.5$ and $V(X_{i+1} \mid \mathbf{X}_i = \mathbf{x}_i) \approx 2.8$. Neither of these values are surprising considering the range of observations values that are likely to be observed.

## 3.4 Summary

In this Chapter we have investigated how well continuous conjugate theory can approximate real discrete mass functions in various measurement settings We have described a procedure for assessing the value of conjugate continuous approximations in real problems where mixture digital mass functions can be specified.

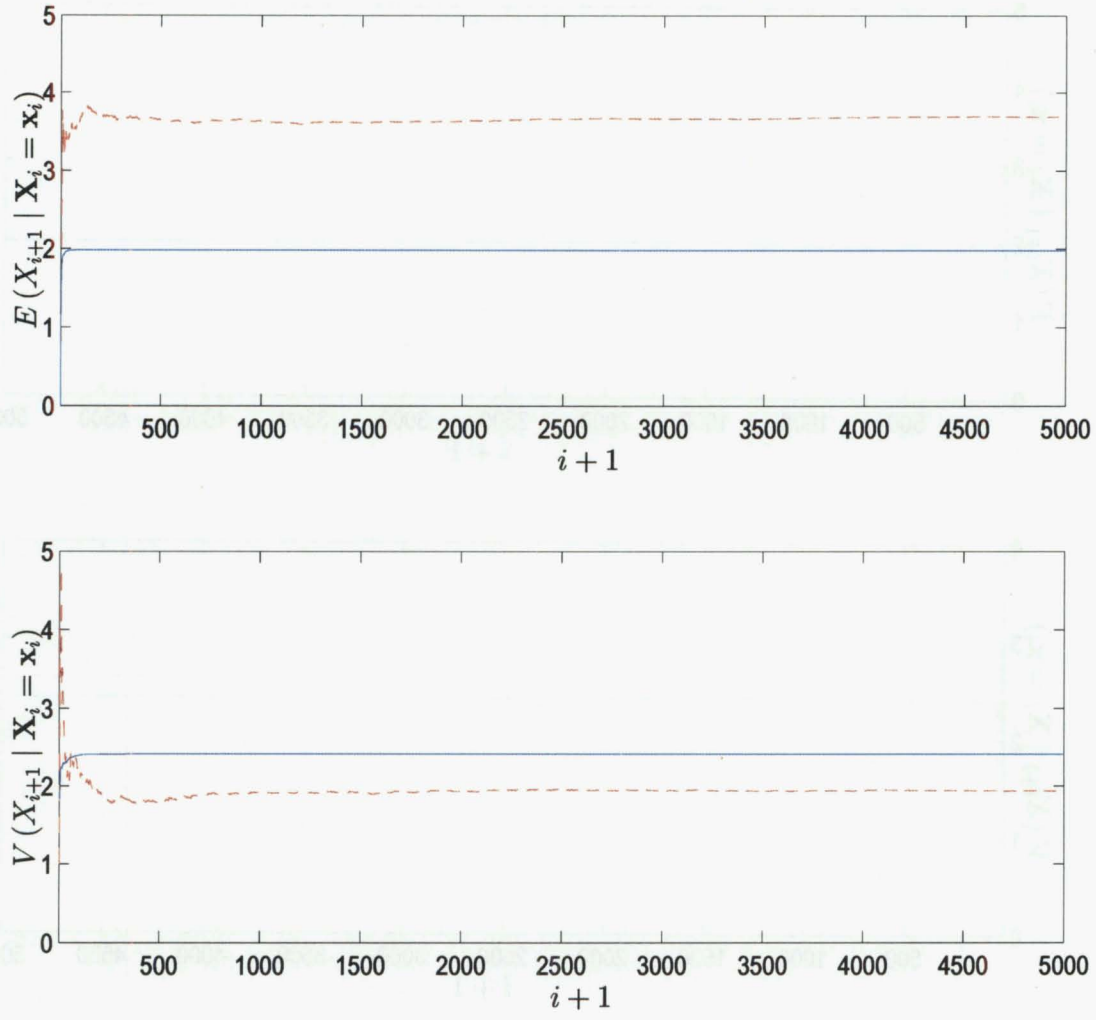


**Figure 3.15: Conditional Expectations and Variances of the Digital Mass Function (solid blue line) and Conventional Conjugate Theory (dashed red line) when $\mathbf{X}_{5000} \sim N_{dig}(4, 0.4)$.**

Well known continuous distributions were digitised, and the means and variances of their posterior mass functions computed. Conventional conjugate theory was used to approximate the means and variances of posterior densities. Our interest has centred on how well digital Normal mass functions and digital parametric mixtures are approximated by continuous mixture-Normal and Normal-Gamma mixture-Normal distributions for such items as $E(X_{i+1} \mid \mathbf{X}_i = \mathbf{x}_i)$ and $V(X_{i+1} \mid \mathbf{X}_i = \mathbf{x}_i)$.

We have observed that when the researcher records observation values that are similar to what they have expected to observe, the discrete digital calculations and continuous approximations are very similar. That is, if the mode of the observations

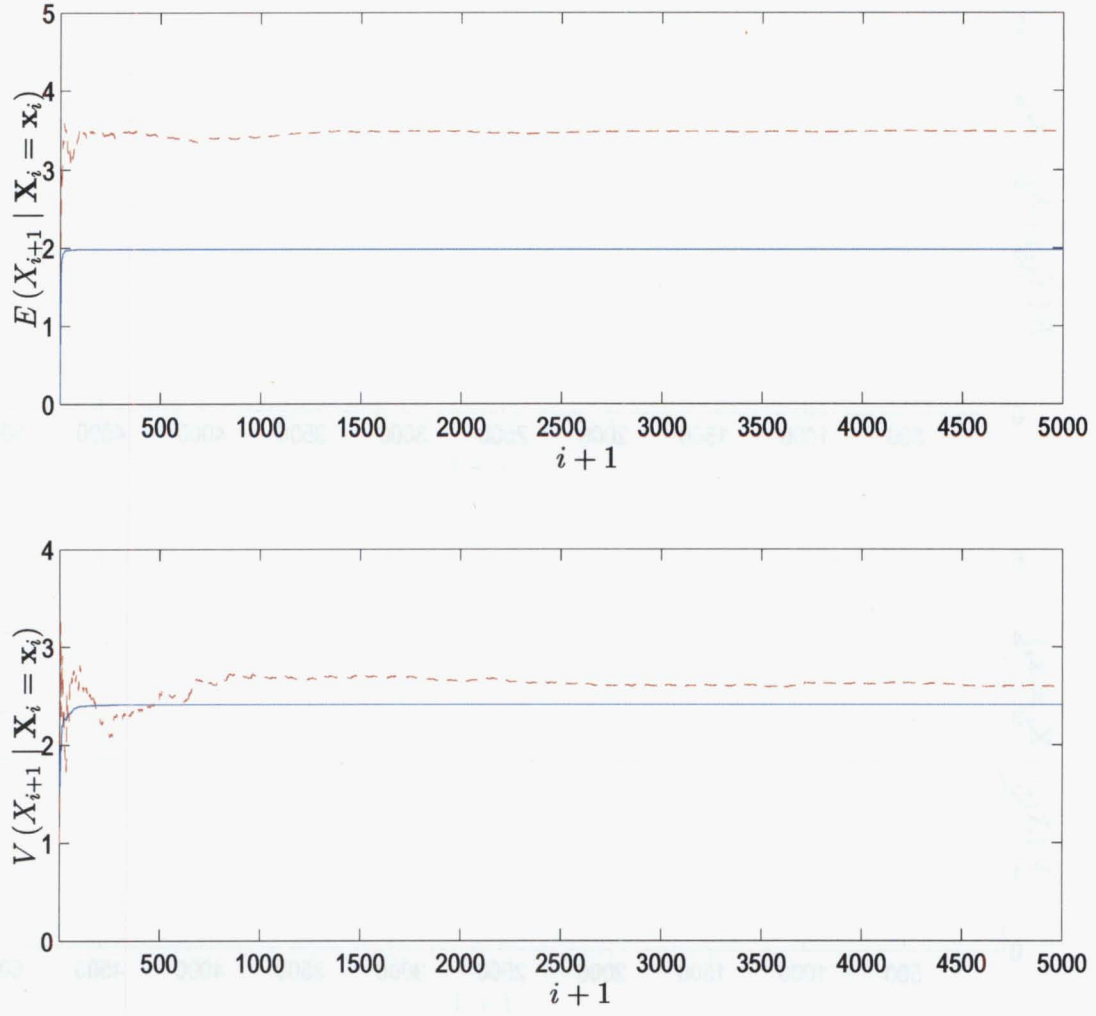


**Figure 3.16: Conditional Expectations and Variances of the Digital Mass Function (solid blue line) and Conventional Conjugate Theory (dashed red line) when $\mathbf{X}_{5000} \sim N_{dig}(4, 0.25)$.**

is close to the mode of the prior mixing mass function, and if the variance is small relative to the range of $\mathbf{R}(X)$, the actual calculations and the approximations are almost indistinguishable. When a researcher records observations they would be surprised by, for example, the cases when we defined the generating value of $\mu$ to be close to the extremities of $\mathbf{R}(\mu)$, the continuous approximations are larger (absolutely) than the digital calculations. When observations are such that the researcher is really surprised, the approximated conditional moments do not work at all well.

# Chapter 4

# Flood Frequency Analysis of the Waimakariri River

## 4.1 Introduction

A common problem in many areas of environmental engineering is that of estimating the return period of rare geophysical events, such as extreme floods, for a site or group of sites. A large volume of work considering the estimation of flood risk has appeared in the last 20 years. Approaches have ranged from arcane mathematical formulations to operational institutional guidelines. Despite the large number of publications there is no consensus on how best to proceed. The problem is complicated by the necessity of evaluating flood risk for return periods that exceed the length of the observed record.

Modern flood frequency theory is typical of much conventional statistical theory, in that most effort is expended in determining an appropriate form to model the "underlying distribution" of floods, and then estimating the parameters of this underlying distribution. Conventional estimates of flood exceedance quantiles are highly dependent on the form of the portion of the underlying flood frequency distribution (the right tail) which is most difficult to estimate from observed data. Currently there is no compelling theory on which to base the distributional form of the right hand tail.

This Chapter will begin with an introduction to flood frequency estimation. We

introduce the process undertaken to measure river flow, concentrating on details specific to the Waimakariri River. In Section 3 we examine different frequentist approaches to estimating flood exceedance quantiles. We study both at-site and regional estimates, and compare their accuracy and precision. In Section 4 we develop a procedure for forecasting exceedance quantiles of floods. Different sets of results are obtained and their scores computed. This work is based on the digital updating procedure introduced and studied in Chapter 3. In Section 5 the results obtained through the frequentist and digital methods are compared. First, we use subjective methods, scoring the conditional expectation and variance for both the Waimakariri River data and a simulated data set. Then we use an objectivist method to compare the accuracy and precision of the two methods for a simulated data set. Finally, a summary of this Chapter is presented in Section 6.

Note that although the word "exceedance" is not found in the Oxford English Dictionary, it is commonly used in environmental engineering, particularly when the analysis of extreme events is studied. It is probably based on "excedent", meaning "The portion or quantity in excess", as this the meaning regularly attached to it. Nonetheless it is commonly spelled "exceedance" in the general engineering literature that uses the word. See, for example, the standard work of Metcalfe (1997).

## 4.2 River Flow Records

Measurements of instantaneous river flow can be produced by combining measures of flow velocity and cross-sectional area of the river. This Section will detail the process taken to measure river flow, concentrating on procedures used specific to the Waimakariri River. First, we describe the process undertaken in New Zealand to obtain river flow measurements. Second, we introduce the Waimakariri River in depth, and outline its measurement history. We conclude this Section by detailing the problem of estimating flood exceedance quantiles.

### 4.2.1 River Flow Measurement in New Zealand

Throughout New Zealand there are a number of government funded authorities responsible for recording river flow. Prior to amalgamation in 1989, each local

catchment board was responsible for keeping records about rivers within its catchment. Records for the Waimakariri River were gathered by the North Canterbury Catchment Board. Since amalgamation, water records have become the responsibility of district councils, regional councils and branches of the National Institute of Water and Atmospheric Research (NIWA). For example, records for the Waimakariri River are held by the Canterbury Regional Council (known for promotional purposes as Environment Canterbury), records for the Rakaia River are held by NIWA-Christchurch and records for the Waihopai River are held by the Marlborough District Council.

River flow is measured by combining measurements of a river's water flow velocity and cross-sectional area. A "stage-discharge rating curve relationship" is used to combine these two measures. Stage-discharge rating curves have been constructed for every New Zealand river whose flow is of interest, and are used to estimate the volume of flow in a given time period. The units used are cubic metres per second, or cumecs. The annual maximum instantaneous flood peak is the name given to the largest of these measures of volume in one calendar year. A sequence of these maximum flow values is called an annual maxima series (AMS).

To measure the cross-sectional area of water, two components are needed: the water level and river bed profile. Today, the water level of many New Zealand rivers, including the Waimakariri, is recorded mechanically. The standard interval between recordings is fifteen minutes. The river bed profile of each river whose flow is of interest is mapped on irregular occasions. This cross-section is re-mapped whenever the river's controlling authority suspects the profile may have changed. Re-mapping usually occurs directly after a notable flood event, or "fresh". There are approximately 10–15 freshes each year in the Waimakariri River, although the bed profile is not re-mapped after every one.

Water velocity is recorded at a number of points across a river. Water velocity was originally recorded either by standing in the river holding a current meter, or by dropping a current meter over the side of a boat. Now, velocity is measured electronically, from a boat that is being driven back and forth across a river. Relationships between average cross-sectional velocities and water level are developed, to allow for extrapolation to large events. It is known hydraulically and through

measurement how velocity increases to an asymptotic limit with increasing depth. Since it is not safe to use a boat to undertake an accurate measure of water velocity while a flood is in progress, a more informal process may be used to record the measurement. During extreme floods, the flow velocity can instead be measured from a bridge or cableway, or flow may be measured indirectly, by using standard water depth-velocity relationships. Consequently the measure of water velocity will be less accurate than it is when the river is flowing at a normal level. This a real example of a problem we commented on in Section 2.4 of Chapter 3, where a measurement device is unable to measure extreme values to the same level of fineness with which it is able to measure commonly recorded values. In assessing the measurement process for river flows it must be recognised that the precision of the process is higher for normal flows than for extreme flows.

The complete river flow measurement process consists of a series of approximations. Flood flow records for large rivers, including the Waimakariri, are recorded in units of $10m^3/sec$ (that is, "ten cumecs"), reflecting the lack of accuracy resulting from the series of approximations inherent within each of the measures in the series. It is standard for NIWA to assume that their flow measures are within $\pm 8\%$ of the "true flow" 95% of the time. It is conventional statistical practice to presume that the recorded measurement is equal to the true measurement value plus some unknown (and unobservable) measurement error, or, symbolically, $X = \mu + \epsilon$. Although in this Thesis we treat such a viewpoint as, in practice, meaningless, it is nevertheless interesting to know with what precision NIWA regard their measurements, particularly when defining the width between successive values in the realms of $X$ and the characterising parameters.

### 4.2.2 The Waimakariri River

The Waimakariri River is located in the Canterbury region of the South Island of New Zealand. It is classified as a "Main Divide" river, meaning that it has a catchment which drains from the ranges east of the Main Divide of the South Island. It has a catchment area of $3210km^2$, the largest of any river in Canterbury. The Waimakariri River flows through the northern outskirts of Christchurch. Flood

protection works have been constructed to protect most of urban Christchurch and Kaiapoi.

The daily flow of the Waimakariri River has been recorded since 1930 at the site of the Old State Highway One bridge. The site is $5.4km$ from the mouth of the river, and consequently the water level is effected by the tide. The Waimakariri River is also measured at a site in the Waimakariri Gorge. When records of river levels do not exist, for example if the mechanical recorder is broken or if the flow records have been lost, flow records are estimated based on water levels at the Waimakariri Gorge recording site. Studies of the relationship between recorded flow levels at these two sites show this to be a reasonable resolution to the "missing data problem". Recent Waimakariri River flows can be viewed on the Canterbury Regional Council's internet site[1].

Between 1930 and 1966 water levels at the Old State Highway One bridge site were recorded visually at irregular intervals. The AMS series for this period was calculated retrospectively using slope-area calculations and records from the Waimakariri Gorge site. "Slope-area gaugings" are post-flood event measurements. They take into account the highest water level mark, the associated cross-sectional area of the channel, slope of the channel bed, and likely velocities of the flow as read from a standard water depth-flow velocity relationship table. It is widely recognised that slope-area gaugings are less precise than records obtained via conventionally recorded flow levels. In 1966 a mechanical recorder was installed to record the water level every 15 minutes.

Flow measurements for years 1960 through 1966 were complicated by the constant change of the river-bed profile due to large amounts of shingle being removed from the river bed for use in construction of Christchurch's Northern motorway. During the period on record there has been a small ($< 10$ cumecs) amount of upstream water diversion. This is an insignificant amount considering the level of measurement precision.

The highest mechanically measured discharge for the Waimakariri River is $3070m^3/sec$ (1979), a value exceeded twice in the recorded period (1940 and 1957). AMS values range between $710m^3/sec$ (1939) and $3990m^3/sec$ (1957) with mean

[1] www.crc.govt.nz/Water/Rivers-Rainfall/graphist.asp?site_no=66401

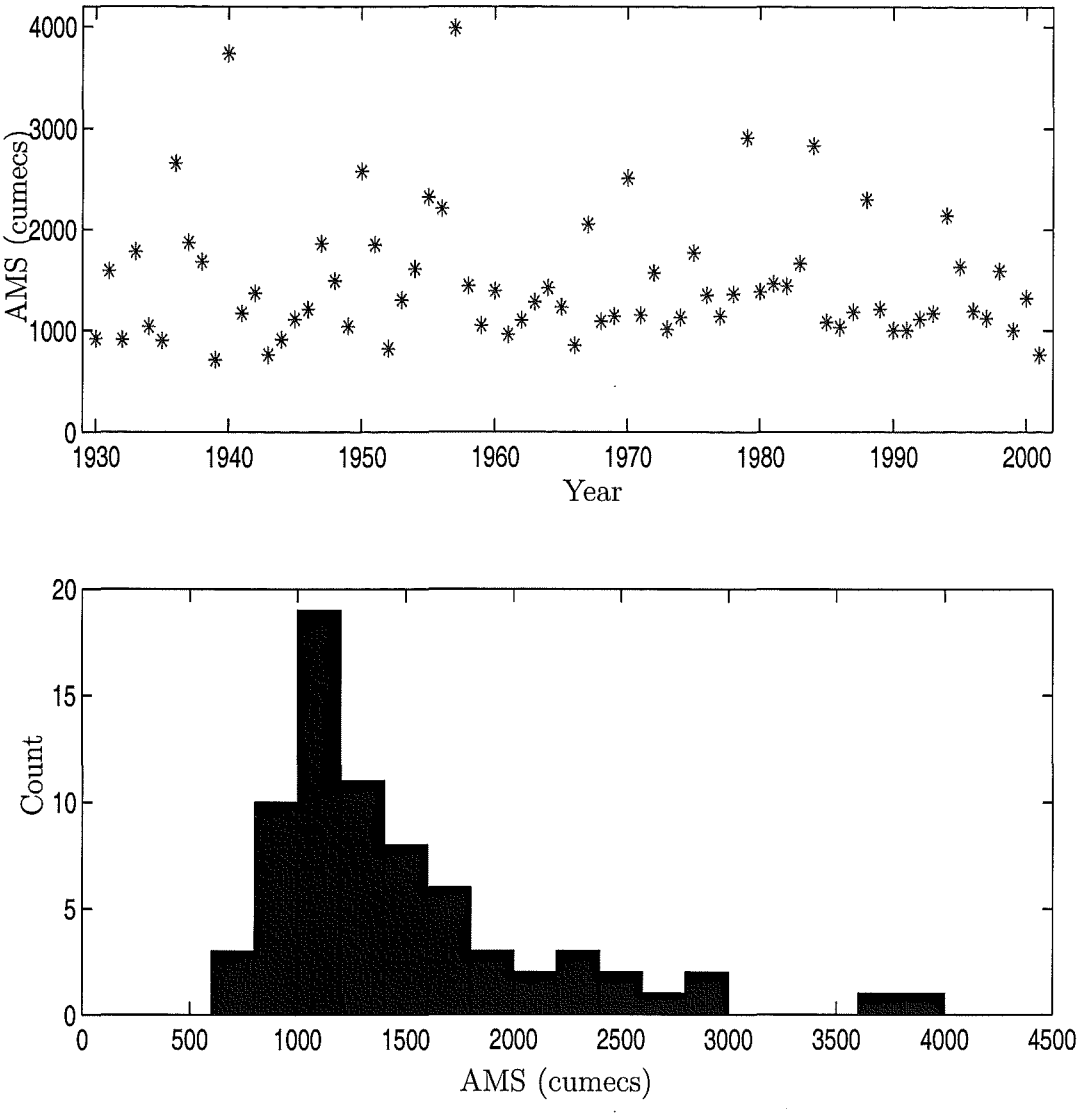


**Figure 4.1: AMS recorded for the Waimakariri River.**

$1485m^3/sec$, standard deviation $632m^3/sec$ and skewness 1.77. The upper panel of Figure 4.1 shows a scatterplot of the recorded AMS for the Waimakariri River. The lower panel shows a histogram of the observations, sorted into bins of width $200m^3/sec$.

### 4.2.3 Problem Statement

The problem assessed in this Chapter concerns the characterisation of extreme floods. At each site $i$ we want to estimate the $Fth$ quantile of non-exceedance probability, denoted $Q_i(F)$, $0 \leq F \leq 1$. Denoting by $X_i$ the annual maximum instanta-

neous flood peak at site $i$, the quantile $Q_i(F)$ is the value we expect $X_i$ to exceed with probability $(1-F)$ during the year of interest. That is, $P(X_i \leq Q_i(F)) = F$ for the year of interest.

$Q(F)$ is interpreted to mean that, in any year, we expect that there is a $F\%$ chance that $X$ will be less than $Q(F)$. Conversely there is a $(1-F)\%$ chance that $X$ will exceed $Q(F)$. The "return period" of a flood exceedance is defined to be the reciprocal of the probability of exceedance in one year, $1/(1-F)$. It is the expected time between exceedances of the size of $Q(F)$.

$Q(F)$ is commonly (and misleadingly) referred to as a "one in $1/(1-F)$ year flood" See, for example, Metcalfe (1997). For instance $Q(0.95)$ is the value that we expect $X$ to exceed, during the course of a year, with probability 0.05. The implication of the phrase "one in twenty year flood" is that $Q(0.95)$ will only be exceeded once in the next twenty years. However, a standard binomial calculation shows that the probability of the flow exceeding $Q(0.95)$ in at least one of the next twenty years is almost $\frac{2}{3}$. If we define $Y$ to be the number of years that $Q(0.95)$ is exceeded in a twenty year period, then the probability of observing at least one exceedance in that twenty year time period is

$$\begin{aligned} P(Y \geq 1) &= 1 - P(Y = 0) \\ &= 1 - \prod_{i=1}^{20} P(X_i = 0) \\ &= 1 - (0.95)^{20} \\ &= 0.64 \quad (2\text{dp}). \end{aligned} \tag{4.1}$$

Table 4.2.3 displays the actual probabilities that $Q(0.95)$ is exceeded in $Y$ separate years over a twenty year period. Notice that the chance of $Q(0.95)$ being exceeded in one of the twenty years is 0.3774 – which differs considerably from the implication of "one in twenty year flood". Nonetheless the terminology "one in $1/(1-F)$ year

| $Y$ | 0 | 1 | 2 | 3 | 4 | 5 | 6+ |
|---|---|---|---|---|---|---|---|
| $P(Y)$ | 0.3585 | 0.3774 | 0.1887 | 0.0596 | 0.0133 | 0.0022 | 0.0003 |

**Table 4.1: The probability that $Q(0.95)$ will be exceeded in $Y$ years over a twenty year period.**

flood" is standard within the engineering community, and we shall follow it here.

## 4.3 Frequentist Approach to Estimating Flood Exceedance Quantiles

Conventional frequentist flood estimation theory has centred around estimating the parameters of the "underlying distribution" of the floods. This underlying distribution is believed to be a stochastic generating structure that produces a random outcome which is of interest to the researcher. The aim of frequentist estimation is to find the characterising parameter values of this, unobservable, underlying distribution. An opposing view is that there is no "correct" functional form that stochastically generates random outcomes — the observations are what they are, nothing more or less. People are uncertain about what values subsequent observations will be, and probabilities represent their informed knowledge. For the majority of this Thesis this is the paradigm that is followed. However for the remainder of this Section we shall assume that the underlying distribution exists as a meaningful concept, as a frequentist statistician does at all times.

### 4.3.1 At-Site Flood Frequency Analysis

The simplest flood estimation methods involve collecting AMS data for a site, and using this data to estimate the characterising parameters of the underlying distribution, the functional form of which is assumed known. Popular estimation techniques include the method of moments and maximum likelihood estimation. The method of moments is notoriously unreliable for fitting extreme value distributions due to the poor sampling properties of second and higher order sample moments. The method of maximum likelihood has been used when dealing with extreme values, however it doesn't work well when the sample size is small to moderate. Moreover its computational aspects are based on iterative procedures which require reasonable starting values. For the parameter estimation undertaken in this Chapter we shall use the method of L-moments, a linear extension of the conventional method of moments. L-moments have been widely used in recent studies of extreme phenomenon. For a

taste of the breadth of current research see Kjeldsen et al. (2002), Kroll and Vogel (2002) and Park et al. (2001) to see L-moments applied in studies in South Africa, the United States of America and South Korea. The theory of L-moments is introduced in Section 4.3.3. Three popular candidates for underlying flood distribution are introduced in Section 4.3.4

### 4.3.2 Regional Flood Frequency Analysis

Recent research into flood frequency estimation has focused on developing and evaluating regionally derived flood frequency estimates. In regional flood frequency analysis it is assumed that the data from all gauged sites in a region can be combined in such a way as to produce a single regional flood frequency curve. This curve is applicable, after appropriate rescaling, anywhere in that region. Regionalisation allows us to pool data from $m$ sites. Each site has $n_i$ years of recorded measures, where $n_i$ can be of any length.

Conventional regionalisation techniques identify a fixed set of recording sites which adjoin each other. Each region is identified by considering which sites are 'close' to each other. Proximity can be assessed using statistical measures (e.g. coefficient of variation ($CV$) or ratio of mean flow to drainage area) or spatial measures (e.g. longitude and latitude of each site).

The biggest advantage of regional estimation is seen to be the increase in record length. A regional approach is necessary when estimating floods at sites with no observed data. Many studies (e.g. Lettenmaier et al., 1987; Hosking, 1990) have shown that flood estimates based on regional information are more accurate (have less absolute error) and are more stable (have less variance) than those based solely on at-site records. The most commonly used regionalisation techniques are based on the index flood approach.

#### The Index Flood Approach

The index flood approach was first introduced by Dalrymple (1960), and has since been implemented on a regular basis. See the review article by Stedinger and Lu (1995) for examples. It was developed as a way of deriving a regional frequency

curve. The underlying flood frequency distribution at each site is assumed to be identical, except for a scale factor. Consequently we are able to use a straightforward pooling approach. First, the data at each site are normalised by the index flood (details of this procedure will be described shortly). Next, the parameters of a dimensionless regional flood frequency curve are estimated. Finally, the parameters are rescaled at the site of interest by a local estimate of the scaling factor, usually the at-site mean.

The key assumption of an index flood procedure is that the region is homogeneous, that is, the frequency distributions of the $N$ sites in a region are identical, apart from a site-specific scaling factor. The distribution common to all sites in the region is called the regional frequency distribution. It is dimensionless and defined by its (regional) quantiles, $q(F)$, $0 \leq F \leq 1$. It is usually assumed that the form of $q(F)$ is known apart from $p$ undetermined parameters $\theta_1, \ldots, \theta_p$. The site-specific scaling factor is called the index flood, denoted $\mu_i$ at site $i$ (see Hosking and Wallis, 1993). The index flood is usually taken to be the sample mean of the frequency distribution at site $i$, although any location parameter of the frequency distribution may be used instead. For example, Smith (1989) uses the quantile $Q(0.9)$. Thus we can write

$$Q_i(F) = \mu_i q(F), \qquad i = 1, \ldots, N, \tag{4.2}$$

where $Q_i(F)$ is the quantile of non-exceedance probability $F$ at site $i$.

A standard scaled data approach is the simplest index flood method. This involves dividing each measure by its at-site sample mean, and then treating all the scaled data points as if they were observations from the regional frequency distribution. Parameter estimates are found and the estimated regional flood distribution is then multiplied by the at-site mean of the site under investigation.

A more advanced index flood procedure was outlined by Hosking and Wallis (1993).

1. Estimate the mean at each site, $\hat{\mu}_i$, by the sample mean at site $i$.

2. Rescale the data, $x'_{ij} = x_{ij}/\hat{\mu}_i$, $j = 1, \ldots, n_i$, $i = 1, \ldots, n$, as the basis for estimating $q(F)$. Remember that $n_i$ is the number of years of record at site $i$ and the region consists of $n$ sites.

3. Estimate the parameters separately at each site. Denote the site $i$ estimate of $\theta_k$ by $\hat{\theta}_k^{(i)}$.

4. Combine the at-site estimates to give regional estimates:

$$\hat{\theta}_k^{(R)} = \frac{\sum_{i=1}^{n} n_i \hat{\theta}_k^{(i)}}{\sum_{i=1}^{n} n_i}. \tag{4.3}$$

   Each estimated regional parameter is a weighted average. The site $i$ estimate is given weight proportional to $n_i$, since for regular statistical models the variance of $\hat{\theta}_k^{(i)}$ is inversely proportional to $n_i$.

5. Substitute estimates $\hat{\theta}_k^{(1)}, \ldots, \hat{\theta}_k^{(n)}$ into $q(F)$ to give $\hat{q}(F)$, the estimated regional quantile of non-exceedance probability.

6. The site $i$ quantile estimates are obtained by combining the estimates of $\mu_i$ and $q(F)$:

$$\hat{Q}_i(F) = \hat{\mu}_i \hat{q}(F). \tag{4.4}$$

Both the scaled data and the index flood methods are applied to the Waimakariri River AMS data in Section 4.3.5.

### Hierarchical Regional Flood Frequency Approach

Regional flood frequency analysis assumes that all sites in the defined region are homogeneous, that is, all moments ($> 1$) are assumed to be identical after correction for scale, for each of the $n$ sites in the region. This assumption is highly unlikely to be true, especially when the size of the catchment areas in a region varies. See Stedinger (1983), who showed that $CV$ varies with the size of the drainage area and other basin characteristics.

The more homogeneous a region is, the more accurate the regional approach is. However the reverse is also true: as the heterogeneity among sites increases, the regional approach becomes less accurate. Lettenmaier and Potter (1985) showed that the performance of index flood methods gets worse as either the regional mean $CV$, or the site-to-site variation in the $CV$ increases. Homogeneity would be expected to increase as regions are defined to include a smaller number of sites. However the performance of regional estimators also declines as smaller and smaller regions are

defined, on account of the increasing variance of parameter estimates. This suggests that a compromise is required. This can be achieved by recognising that different key characteristics of flood behaviour are approximately constant over different spatial scales. By measuring different flood characteristics at different scales we can maximise the benefits of pooling data while minimising the consequences of defining too large a region.

An hierarchical approach to regional flood frequency analysis is one where different key characteristics of flood behaviour are assumed to be approximately constant over different spatial scales. For example, Gabriele and Arnell (1991) developed a hierarchical regional flood frequency estimation procedure which estimates different moments from different, but nested, subsets of data. The higher-order moments are estimated on a regional basis, while the lower-order moments are estimated on a subregional basis. The location of the annual maximum flow is estimated at-site.

The practical value of adopting an hierarchical approach arises because of sampling uncertainties associated with short record lengths. The higher the order of the moment that is to be estimated, the greater the number of observations, and thus the greater the number of sites, we need to record to estimate that moment with the same degree of accuracy. In other words, more samples of a given size are needed to estimate regional skewness to an acceptable level of accuracy than are needed to estimate the regional $CV$ to the same level of accuracy.

Each of the different estimation methods outlined above relies on accurate parameter estimations methods. In flood frequency analysis the current estimation method of choice is the method of L-moments.

### 4.3.3 L-moments

L-moments were introduced by Hosking (1990) as expectations of linear combinations of order statistics. L-moments have been widely used in flood frequency analysis, both overseas (see Stedinger and Lu (1995) for a summary of these investigations) and in New Zealand (Pearson, 1991, 1993; Madsen et al., 1997).

L-moments can be defined for any random variable whose mean exists. They form the basis of a general theory which covers the summarisation and description of

theoretical probability distributions and observed data samples, and the estimation of parameters and quantiles of probability distributions. L-moments are analogous to conventional moments. However, a distribution may be specified by its L-moments even if some of its conventional moments do not exist. Such a specification is always unique.

If $X$ is a (real) random variable with cumulative distribution function $F(x)$ and quantile function $x(F)$, and if $X_{1:n} \leq X_{2:n} \leq \ldots \leq X_{n:n}$ are the order statistics of a random sample of size $n$ drawn from the distribution of $X$, then the L-moments of $X$ are defined to be the quantities

$$\lambda_r \equiv r^{-1} \sum_{k=0}^{r-1} (-1)^k \binom{r-1}{k} EX_{r-k:r}, \qquad r = 1, 2, \ldots \tag{4.5}$$

To standardise the higher L-moments, $\lambda_r$, $r \geq 3$, so that they are independent of the units of measurement of $X$, the L-moment ratios of X are defined as the quantities

$$\tau_r = \lambda_r / \lambda_2, \qquad r = 3, 4, \ldots \tag{4.6}$$

In particular, $\lambda_1$ is the mean of the distribution; $\lambda_2$ is a measure of the scale or dispersion; and $\tau_3$ and $\tau_4$ are measures of skewness and kurtosis respectively. The L-$CV$, $\tau = \lambda_2/\lambda_1$, is analogous to the usual coefficient of variation.

As we have just seen, a common problem in flood frequency analysis is estimating, from a random sample of size $n$, a probability distribution whose specification involves unknown parameters, $\theta_1, \ldots, \theta_p$. The method of L-moments obtains parameter estimates by equating the first $p$ sample L-moments to the corresponding population quantities, just as the traditional method of moments does. For an ordered sample $x_1 \leq x_2 \leq \ldots \leq x_n$, estimates of the first few L-moments are:

$$l_1 = \sum_{i=1}^{n} x_i / n, \tag{4.7}$$

$$l_2 = \sum_{i>j} (x_i - x_j) / n(n-1), \tag{4.8}$$

$$l_3 = \sum_{i>j>k} 2(x_i - 2x_j + x_k) / n(n-1)(n-2). \tag{4.9}$$

General formulae are given in Hosking (1990). $l_1$ is the usual sample mean. L-$CV$ and L-skewness are estimated by $t = l_2/l_1$ and $t_3 = l_3/l_2$ respectively. They can be used to judge which distributions are consistent with a given data sample. They can

also be used to estimate the parameters when fitting a distribution to the sample, by equating the sample and population L-moments.

L-moments are linear combinations of Probability Weighted Moments (PWMs), which were defined by Greenwood et al. (1979), and used in flood frequency estimation by Landwehr et al. (1979); Greis and Wood (1981); Hosking et al. (1985); Hosking and Wallis (1987); McKerchar and Pearson (1990). Procedures based on PWMs and on L-moments are equivalent. However L-moments are more easily interpretable as measures of distributional shape.

### 4.3.4 Candidate Distributions

The choice of the functional form of the underlying flood frequency distribution has a large effect on the flood quantile estimates, especially since the quantiles that interest us are those in the extreme right hand tail of the distribution. Many underlying distributions have been proposed, but none has met with universal approval. The three most common candidates, the Generalised Extreme Value distribution, the Generalised Logistic Distribution and the Lognormal distribution are now introduced.

#### The Generalised Extreme Value Distribution

The Generalised Extreme Value (GEV) Distribution was introduced by Jenkinson (1955). It combines into a single form the three possible types of limiting distribution for extreme values, as derived by Fisher and Tippett (1928). The GEV is probably the most widely used distribution when measuring AMS of river flow. It has been recommended for this purpose in the UK Flood Studies Report (National Environment Research Council, 1975). A typical application consists of fitting one type of extreme value limiting distribution to the series of annual maxima.

The distribution function is

$$F(x) = \begin{cases} exp\left[-\left\{1-k\left(\frac{x-\xi}{\alpha}\right)\right\}^{1/k}\right], & k \neq 0, \\ exp\left[-exp\left\{-\left(\frac{x-\xi}{\alpha}\right)\right\}\right], & k = 0, \end{cases} \tag{4.10}$$

where $X$ is bounded by $(\xi+\alpha/k)$ from above if $k > 0$ and from below if $k < 0$. $\xi$ is the location parameter, $\alpha$ $(> 0)$ is the scale parameter and $k$ is the shape parameter. The

shape parameter determines which type of extreme value distribution is represented.

The type I GEV distribution (EV1), also known as the Gumbel distribution, corresponds to $k = 0$. The type II GEV distribution (EV2), also known as the Fréchet distribution, corresponds to $k < 0$. The type III GEV distribution (EV3) corresponds to $k > 0$. Note that if $X$ is assessed to be distributed EV3, then $-X$ has a Weibull distribution. The Weibull distribution is often used in hydrology to analyse extreme low river flows.

The GEV inverse distribution function is

$$x(F) = \begin{cases} \xi + \frac{\alpha}{k}\left\{1 - (-log\ F)^k\right\}, & k \neq 0, \\ \xi - \alpha\ log\ (-log\ F), & k = 0, \end{cases} \tag{4.11}$$

and the GEV probability density function is

$$f(x) = \begin{cases} \frac{\left(1-\frac{k}{a}(x-\xi)\right)^{1/k} exp\left[-\left(1-\frac{k}{a}(x-\xi)\right)^{1/k}\right]}{\alpha\left(1-\frac{k}{a}(x-\xi)\right)}, & k \neq 0, \\ \alpha^{-1}\ e^{-(x-\xi)/\alpha}\ exp\left[-e^{-(x-\xi)/\alpha}\right], & k = 0. \end{cases} \tag{4.12}$$

In practice it is usually assessed that $k$ is between $-0.5$ and 0, so we most often deal with an EV2 distribution. The EV2 distribution has expectation

$$E(X) = \xi + \frac{\alpha}{k}\left(1 - \Gamma(1+k)\right) \tag{4.13}$$

and variance

$$V(X) = \left(\frac{\alpha}{k}\right)^2 \left(\Gamma(1+2k) - \Gamma^2(1+k)\right). \tag{4.14}$$

Although the EV2 distribution is bounded below by $\xi + \alpha/k$, of course we cannot actually observe a negative flow. In practice this sub-zero lower bound is rarely a problem. For example, of the ten rivers we analyse in the next Section, the most mass that any of their estimated density functions places on negative values of $X$ is less than $10^{-3}$.

Hosking (1990) used L-moments to show that point estimates of the GEV distribution can be obtained using:

$$z = \frac{2}{(3+t_3)} - \frac{log\ 2}{log\ 3}, \tag{4.15}$$

$$\hat{k} \approx 7.8590z + 2.5994z^2, \tag{4.16}$$

$$\hat{\alpha} = \frac{l_2\hat{k}}{\left(1-2^{-\hat{k}}\right)\Gamma\left(1+\hat{k}\right)}, \tag{4.17}$$

$$\hat{\xi} = l_1 + \frac{\hat{\alpha}\left\{\Gamma\left(1+\hat{k}\right)-1\right\}}{\hat{k}}. \tag{4.18}$$

Remember that $l_1$ is the sample mean, $l_2$ is a measure of scale and $t_3$ is a measure of skewness.

### The Generalised Logistic Distribution

The distribution function for the three-parameter Generalised Logistic distribution (GLO) is

$$F(x) = \left[1 + \left(1 - \frac{k}{\alpha}(x - \xi)\right)^{1/k}\right]^{-1}. \tag{4.19}$$

As with the GEV distribution, $\xi$ is the location parameter, $\alpha$ ($> 0$) is the scale parameter and $k$ is the shape parameter. When $k = 0$ the GLO reduces to the two-parameter Logistic distribution.

The GLO inverse distribution function is

$$x(F) = \xi + \frac{\alpha}{k}\left(1 - \left((1 - F)/F\right)^k\right), \tag{4.20}$$

and the GLO probability density function is

$$f(x) = \frac{\left(1 - \frac{k}{a}(x - \xi)\right)^{1/k-1}}{\alpha\left[1 + \left(1 - \frac{k}{a}(x - \xi)\right)^{1/k}\right]^2}. \tag{4.21}$$

Hosking (1990) showed that point estimates of the parameters of the GLO distribution can be obtained via L-moments by:

$$\hat{k} = -t_3, \tag{4.22}$$

$$\hat{\alpha} = \frac{l_2}{\Gamma(1 + \hat{k})\Gamma(1 - \hat{k})}, \tag{4.23}$$

$$\hat{\xi} = l_1 + \frac{l_2 - \hat{\alpha}}{\hat{k}}. \tag{4.24}$$

### The Lognormal Distribution

The distribution of $X$ is said to be Lognormal if $Z = log(X - \xi)$ is Normally distributed. The distribution function for the three-parameter Lognormal distribution (LN3) is

$$F(x) = \Phi\left(\frac{log\,(x - \xi) - \mu}{\sigma}\right), \tag{4.25}$$

where $x > \xi$ and $\Phi$ is the standard Normal distribution function. The expected value and standard deviation of $Z = log(X - \xi)$ are denoted by $\mu$ and $\sigma$ respectively. Any

change in the value of $\xi$ affects only the location of the distribution. When $\xi = 0$, Equation 4.25 reduces to the two-parameter Lognormal distribution.

The LN3 inverse distribution function is

$$x(F) = \xi + exp\left[\mu + \sigma\Phi^{-1}(F)\right]. \tag{4.26}$$

The LN3 probability density function is

$$f(x) = \left((x-\xi)\sqrt{2\pi}\sigma\right)^{-1} exp\left[-\frac{1}{2}\frac{(log(x-\xi)-\mu)^2}{\sigma^2}\right]. \tag{4.27}$$

At-site point estimates of the parameters of the LN3 distribution are given by Hosking (1990) as:

$$z = \sqrt{(8/3)}\Phi^{-1}\left(\frac{1+t_3}{2}\right), \tag{4.28}$$

$$\hat{\sigma} \approx 0.999281z - 0.006118z^3 + 0.000127z^5, \tag{4.29}$$

$$\hat{\mu} = log\left(\frac{l_2}{erf(\sigma/2)}\right) - \frac{\hat{\sigma}^2}{2}, \tag{4.30}$$

$$\hat{\xi} = l_1 - exp\left(\hat{\mu} + \frac{\hat{\sigma}^2}{2}\right), \tag{4.31}$$

where *erf* is the error function.

Now that we have been introduced to the theory of L-moments and our three candidate distributions, we are ready to estimate flood exceedance quantile levels for the Waimakariri River.

### 4.3.5 Frequentist Estimates of Exceedance Quantiles for the Waimakariri River

The flood distribution of the Waimakariri River has previously been studied by McKerchar and Pearson (1990), Pearson (1993) and Connell and Pearson (2001). McKerchar and Pearson (1990) used PWMs to test if the shape parameter of the GEV distribution was equal to zero at each of 275 New Zealand river locations. Pearson (1993) re-investigated the same problem using L-moments, and concluded that Canterbury rivers have a parent EV2 distribution. Connell and Pearson (2001) applied the Two-Component Extreme Value distribution (a distribution of the maxima of two independent Gumbel distributions) to AMS data from East Coast rivers. They concluded that the rivers could be split into three homogeneous groups: Main

Divide rivers (of which the Waimakariri is one), Northern East Coast rivers (includes rivers from the Ashley to the Rangitata) and Southern East Coast rivers (includes rivers from the Orari to the Hakataramea).

### At-site Estimates of Exceedance Quantiles

The simplest method of quantile estimation involves the researchers selecting a distribution they feel adequately represents the underlying flood frequency distribution, and estimating the characterising parameters of the distribution from the AMS recorded at the site of interest. Point estimates of parameters, and estimates of exceedance quantiles, $Q(0.95)$, $Q(0.98)$, $Q(0.99)$, $Q(0.995)$ and $Q(0.999)$, are found for each of the three candidate distributions.

### Regional Estimates of Exceedance Quantiles

Regional estimates of exceedance quantiles are calculated by pooling data from a number of different, but related, sites. This has the advantage of increasing the number of recorded AMS values. However, the more heterogeneous a region, the less effective data pooling, meaning that we must make a decision between increasing the sample size and increasing the heterogeneity.

It has been shown (Mosley, 1981; McKerchar and Pearson, 1990; Pearson, 1991) that rivers draining on the East Coast of the South Island form reasonably homogeneous flood frequency regions. Mosley (1981) achieved this through cluster analysis, McKerchar and Pearson (1990) by fitting GEV curves to 275 AMS data records and Pearson (1991) identified homogeneous regions by considering the similarity between the L-skewness and L-kurtosis at different sites. The sites considered to be part of the same region as the Waimakariri River are all rivers from the Canterbury region. The rivers are listed in Table 4.2. See Walter (2000) for more detail on the site records.

We shall consider the three different regionalisation techniques introduced in Section 4.3.2: a standard scaled data approach, an index flood approach, and an hierarchical analysis.

| Site | River | $n$ | area | mean | std dev. | $CV$ | skew |
|---|---|---|---|---|---|---|---|
| 60110 | Waihopai | 23 | 764 | 425 | 178 | 0.42 | 0.69 |
| 62103 | Acheron | 41 | 973 | 333 | 179 | 0.54 | 1.92 |
| 62105 | Clarence | 43 | 440 | 193 | 89 | 0.46 | 0.67 |
| 65104 | Hurunui | 45 | 1060 | 531 | 218 | 0.41 | 0.50 |
| 66204 | Ashley | 30 | 472 | 320 | 222 | 0.70 | 1.19 |
| 66401 | Waimakariri | 72 | 3210 | 1485 | 652 | 0.44 | 1.77 |
| 68001 | Selwyn | 38 | 164 | 77 | 66 | 0.85 | 2.13 |
| 68526 | Rakaia | 44 | 2560 | 2419 | 929 | 0.38 | 1.66 |
| 68806 | South Ashburton | 35 | 539 | 102 | 66 | 0.64 | 1.55 |
| 69302 | Rangitata | 43 | 1461 | 1357 | 737 | 0.54 | 1.09 |

**Table 4.2: Rivers used in regional analysis. Record length is measured in years. Mean and standard deviation are measured in cumecs. Area is measured in squared kilometres.**

### Scaled Data Regional Estimates of Exceedance Quantiles

First, we shall undertake a simple process which merely involves scaling each observation so that each observation is part of a 'super-site'. Next, we estimate the parameters of the rescaled data. Finally, we construct and rescale the appropriate density curve. The steps involved in this process are:

1. Rescale each observation by its at-site mean, $x^{'} = x_{ij}/\hat{\mu}_i$, $j = 1, \ldots, n_i$, $i = 1, \ldots, n$. The index $i$ is the site number, and $n_i$ is the number of years of AMS recordings at that site. Each site may be measured over any number of years. The $x_{ij}^{'}$ now form a super-site of size $\sum_{i=1}^{N} n_i$.

2. Estimate parameters of super-site using the method of L-moments.

3. Form density function and rescale it by $\hat{\mu}_i$.

This process was undertaken using each of our candidate distributions. A total of 414 normalised observations were obtained, with values ranging from 0.13 to 4.46. Normalised values from the Waimakariri river ranged from 0.48 to 2.69. Figure 4.2

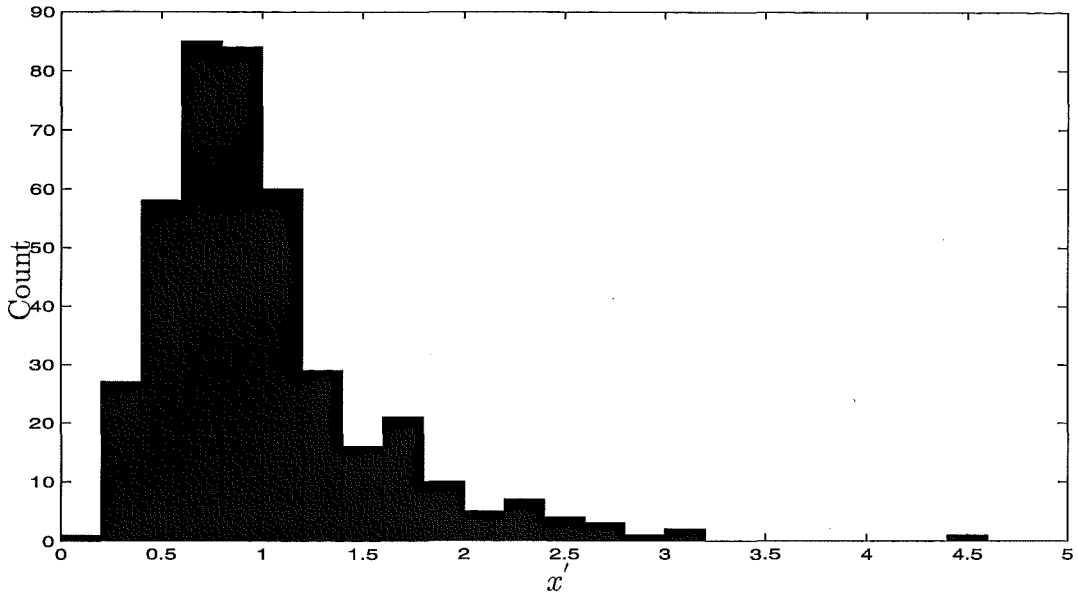


**Figure 4.2: Normalised AMS for Canterbury rivers.**

displays the shape of the normalised observations. Note that the histograms displayed in Figure 4.2 and in the lower panel of Figure 4.1 are approximately the same shape.

### Index Flood Regional Estimates of Exceedance Quantities

We undertake an index flood procedure as outlined in Section 4.3.2. First, scale each site's data by its mean and estimate the characterising L-moments at each site. Using these, estimate the regional L-moments and thus calculate the regional normalised flood frequency distribution. Finally, rescale the distribution and compute the quantiles of interest. This procedure was undertaken for the Waimakariri data.

### Hierarchical Regional Estimates of Exceedance Quantities

Hierarchical regional estimation methods were outlined in Section 4.3.2. A typical hierarchical procedure is to calculate the shape parameter, which controls skewness, from all the sites in a region while calculating the scale and location parameters using at-site data. In practice this involves normalising and pooling the data from all sites in a region. A regional estimate of the shape parameter is calculated from this pooled data. Using the regional estimate of the shape parameter we estimate the scale and location parameters using the at-site data.

### 4.3.6 Results

#### At-site Results

It is a simple matter to estimate GEV parameters for the Waimakariri River using Equations 12–15. Parameter estimates of the at-site frequency distribution are $\hat{k} = -0.25$, $\hat{\alpha} = 355$ and $\hat{\xi} = 1165$. Using these estimates we can plot the shape of the underlying flood frequency density. This is shown as the blue curve in Figure 4.3. These parameter estimates can also be used to estimate exceedance quantiles using the inverse GEV distribution function. The parameter and quantile estimates obtained for all three candidate distributions and shown in Table 4.3 in the row headed "AS". Note that the parameter estimates displayed have been normalised, so they can be easily compared with the parameter estimates obtained through regional procedures. In particular, observe that the estimate of $\xi$ given in Table 4.3 is 0.78, and the at-site mean, from Table 4.2, is $1485m^3/sec$. Multiplying these two values, and discounting rounding errors, gives $\hat{\xi} = 1165$, the at-site estimate. $\hat{Q(0.95)}$ is $2729m^3/sec$. This is interpreted to mean that, in any year, we expect there is a 95% chance that the maximum flow will not exceed $2729m^3/sec$.

The at-site GLO parameter estimates for the Waimakariri River are $\hat{k} = -0.34$, $\hat{\alpha} = 215$ and $\hat{\xi} = 1149$. These parameters lead to the density curve plotted in red in Figure 4.3, and to the exceedance quantiles, measured in cumecs, displayed in Table 4.3.

The at-site LN3 parameter estimates for the Waimakariri River are $\hat{\sigma} = 0.72$, $\hat{\mu} = 6.49$ and $\hat{\xi} = 636$. The estimated LN3 density curve is shown in green in Figure 4.3, and estimated exceedance quantiles are displayed in Table 4.3.

Figure 4.3 shows the estimated GEV, GLO and LN3 densities. Clearly the GLO density is quite different from the other two. Although the GEV and LN3 densities have different modes, they are very similar in the upper tail, where the quantities we are most interested in reside. Figure 4.4, a plot which concentrates on the upper end of the distribution curve for our three candidate distributions, demonstrates this. For example consider the point $Q(0.95)$. Find the point 0.95 on the $F(x)$ axis and look to the right. The first distribution we encounter, at $x = 2238$, is the GLO, represented by the red line. Continuing to the right we cross the blue

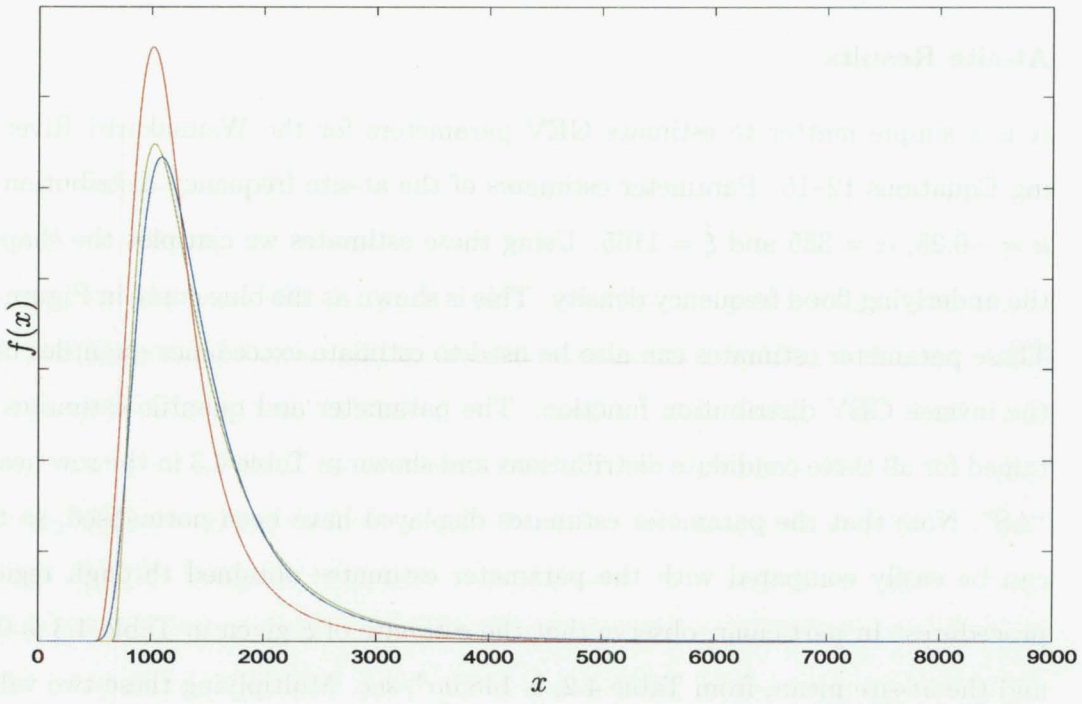


**Figure 4.3: At-site density functions estimated using Waimakariri River AMS. Densities are GEV (blue), GLO (red) and LN3 (green).**

GEV line at $x = 2729$, and then almost immediately cross the green LN3 line at $x = 2771$. There is a difference of $533m^3/sec$ between the smallest and largest estimates of $Q(0.95)$ over the three candidate distributions. This illustrates the importance of assuming an appropriate distribution for the AMS. Figure 4.4 and Table 4.3 show a similar situation exists for higher quantile estimates. The LN3 and GEV exceedance estimates are more similar than the GLO. For a fixed return period exceedance estimates based on the GLO are lowest for $F(x) < 0.998$. The GEV and LN3 estimates are the same at $F(x) \approx 0.975$, below this quantile the GEV is lower, above it the LN3 estimate is the smaller of the two.

### Regional Results

The parameter and quantile estimates obtained for all three candidate distributions are listed in Table 4.3. Scaled data estimates are listed in the row headed "SD", index flood estimates are listed in the row headed "IF" and hierarchical estimates are listed in the row headed "Hi". Remember that the parameter estimates are

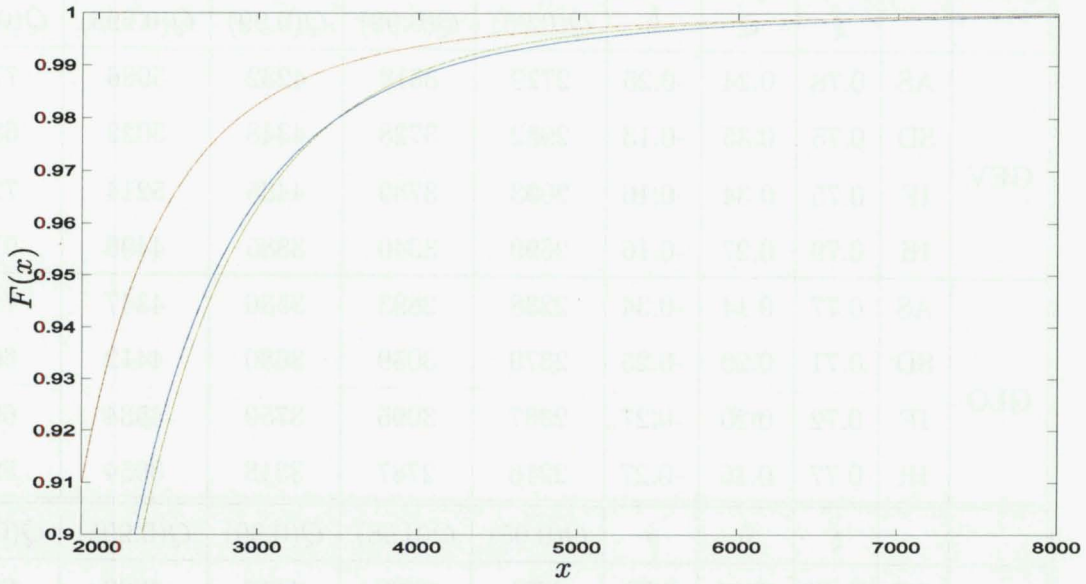


**Figure 4.4: At-site cumulative density functions estimated using Waimakariri River AMS. Distributions are GEV (blue), GLO (red) and LN3 (green).**

based on the normalised regional frequency curve. For each of the three candidate distributions, the three different regional estimates are closer to each other than any of them are to the at-site estimate. In particular there is a considerable difference between the shape parameter estimated from at-site and regional data. For every estimation method the GEV and LN3 quantile estimates are closer to each other than to the GLO estimates, suggesting that the regional estimation methods produce equivalent differences between the distributions, as the at-site methods do.

### 4.3.7 Comparison of Approximation Methods

To this point we have estimated five flood exceedance quantiles for the Waimakariri River, using four estimation methods. How can we judge the worth of these estimates? Conventional measures of the adequacy of a specified distribution are the bias and the root-mean-squared error (RMSE). Bias is a measure of how closely the expected value of an estimate is to the parameter that it is supposed to estimate. A statistic, $T = T(X_1, \ldots, X_n)$, is said to be an unbiased estimator of the parameter $\theta$ if $E(T) = \theta$ for all $\theta$. If random estimator $T$ is unbiased it possesses a distribution

| | | $\hat{\xi}$ | $\hat{\alpha}$ | $\hat{k}$ | $\hat{Q(0.95)}$ | $\hat{Q(0.98)}$ | $\hat{Q(0.99)}$ | $\hat{Q(0.995)}$ | $\hat{Q(0.999)}$ |
|---|---|---|---|---|---|---|---|---|---|
| GEV | AS | 0.78 | 0.24 | -0.25 | 2729 | 3512 | 4232 | 5086 | 7741 |
| | SD | 0.75 | 0.35 | -0.13 | 2982 | 3728 | 4348 | 5022 | 6824 |
| | IF | 0.75 | 0.34 | -0.16 | 2993 | 3789 | 4465 | 5214 | 7278 |
| | Hi | 0.79 | 0.27 | -0.16 | 2699 | 3340 | 3885 | 4490 | 6167 |
| GLO | AS | 0.77 | 0.14 | -0.34 | 2238 | 2893 | 3536 | 4347 | 7153 |
| | SD | 0.71 | 0.20 | -0.25 | 2379 | 3059 | 3680 | 4412 | 6647 |
| | IF | 0.72 | 0.20 | -0.27 | 2387 | 3095 | 3750 | 4534 | 6957 |
| | Hi | 0.77 | 0.16 | -0.27 | 2216 | 2787 | 3318 | 3954 | 5953 |
| | | $\hat{\xi}$ | $\hat{\mu}$ | $\hat{\sigma}$ | $\hat{Q(0.95)}$ | $\hat{Q(0.98)}$ | $\hat{Q(0.99)}$ | $\hat{Q(0.995)}$ | $\hat{Q(0.999)}$ |
| LN3 | AS | 0.43 | -0.81 | 0.72 | 2771 | 3499 | 4117 | 4800 | 6659 |
| | SD | 0.05 | -0.19 | 0.53 | 3008 | 3711 | 4271 | 4859 | 6344 |
| | IF | 0.12 | -0.29 | 0.57 | 3004 | 3686 | 4307 | 4973 | 6633 |
| | Hi | 0.29 | -0.50 | 0.57 | 2717 | 3316 | 3801 | 4316 | 5638 |

**Table 4.3: Parameter and quantile estimates for the Waimakariri River for the three candidate distributions. The letters in column 1 refer to: AS = at-site; SD = scaled data; IF = index flood; Hi = hierarchical. Remember that the parameter estimates are for the (normalised) regional frequency distribution. Exceedance quantiles are estimated in cumecs.**

whose mean is the parameter $\theta$ being estimated.

Unbiasedness alone is not enough on which to base a choice of method, as more than one statistic can be unbiased. If a number of statistics are unbiased we seek to find the one with the minimum variance — this is called the best unbiased estimator. If $T$ is not an unbiased estimator of parameter $\theta$, we judge its merits on the basis of the mean-squared error, defined as $E\left[(t-\theta)^2\right]$, rather than on $V(t)$. It is well known that biased estimators can produced lower mean-squared error than unbiased ones.

Since the true form of the underlying distribution of floods is unknown and unobservable, we use a Monte Carlo approach both to generate our own sequence of AMS data and to assess competing estimation procedures. The Monte Carlo proce-

| $M(CV)$ | $R^*(CV)$ | Site 1 | | | Site 11 | | | Site 21 | | |
|---|---|---|---|---|---|---|---|---|---|---|
| | | $\lambda_1$ | $\lambda_2$ | $k$ | $\lambda_1$ | $\lambda_2$ | $k$ | $\lambda_1$ | $\lambda_2$ | $k$ |
| 0.5 | 0.3 | 2 | 1.15 | -0.17 | 2 | 1 | -0.14 | 2 | 0.85 | -0.11 |
| 0.5 | 0.5 | 2 | 1.25 | -0.17 | 2 | 1 | -0.14 | 2 | 0.75 | -0.11 |
| 1.0 | 0.3 | 1 | 1.15 | -0.17 | 1 | 1 | -0.14 | 1 | 0.85 | -0.11 |
| 1.0 | 0.5 | 1 | 1.25 | -0.17 | 1 | 1 | -0.14 | 1 | 0.75 | -0.11 |

**Table 4.4: Summary of regions used in Monte Carlo experiments.**

dure assumes that the underlying flood distribution exists and is known. With this Monte Carlo approach we can estimate both the accuracy (variance) and precision (bias) of the quantile estimates.

### Data Generation

The Monte Carlo procedure consists of two primary parts. First we generate the data. Then we test the different methods. When generating the data we attempt to produce simulated series that are plausible representations of the real life flood process. Data is simulated from a GEV distribution. A study of the form of Equation 4.11 and Equation 4.24 shows that the two most important measures to represent accurately are the measures of spread and skewness. In both cases the spread and skewness determine the shape of the distribution and the location term only acts to translate the distribution along the $x$-axis.

A region consisting of 21 sites was considered. The region's statistics are summarised in Table 4.4. Population skewness, record length and CV varied by site. Record lengths ranged from 10 years at site 1, to 30 years at site 21, increasing by 1 year per site. Population skewness ranged linearly from $-0.17$ at site 1 to $-0.11$ at site 21. The population skewness was specified to be greatest at the sites with the shortest record lengths, because small catchment areas, which are associated with high at-site estimates of skewness, tend to have been gauged for a shorter time period than bigger catchments.

The distribution of $CV$ over the sites reflects the degree of heterogeneity of the sites within the region. Remember that one of the assumptions of the index

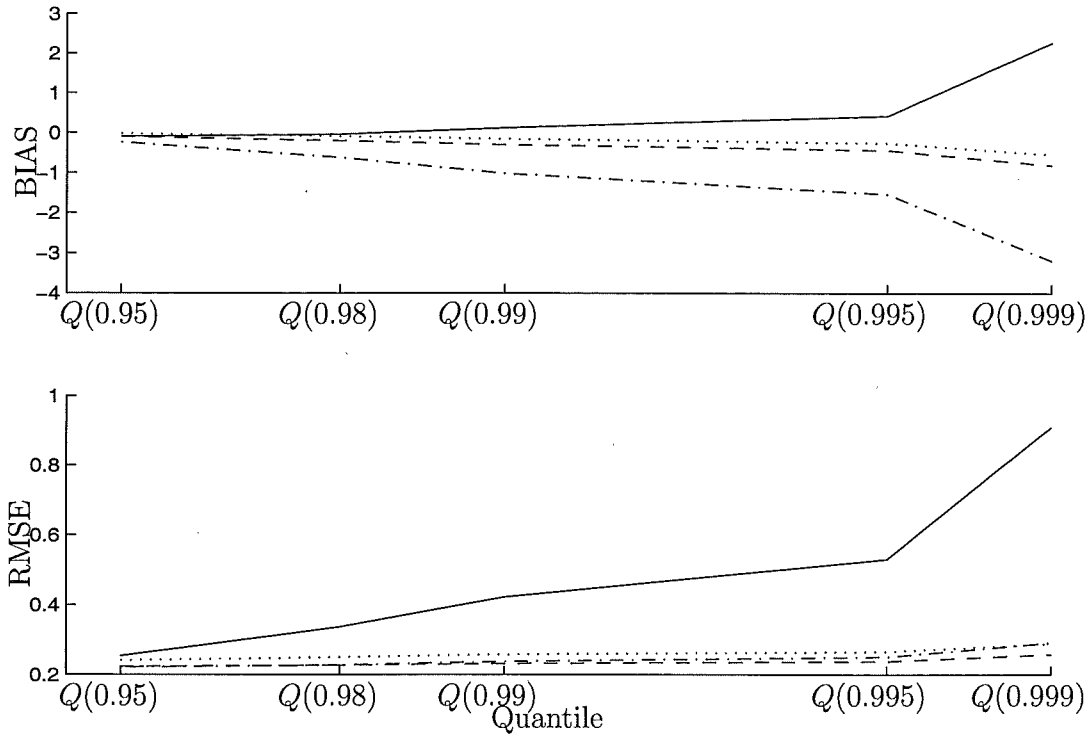


**Figure 4.5: Root-mean-squared error and bias for site 11 of a 21 site region when $M(CV) = 0.5$ and $R^*(CV) = 0.3$. Types of estimation methods are: at-site (—), scaled data (-.-.), index flood (- -) and hierarchical (...).**

flood method is that sites are homogeneous over a region. Thus, as heterogeneity increases, we expect the estimates to be both increasingly inaccurate and have higher variance. $CV$ is defined in terms of the regional median, denoted $M(CV)$, and the range of the $CV$ within a region, denoted $R(CV)$. The regional range is normalised as $R^*(CV) = R(CV)/M(CV)$.

Two different values of $M(CV)$, 0.5 and 1.0, as well as two different values of $R^*(CV)$, 0.3 and 0.5, are considered. These values were selected to mimic the suspected $CV$ values of the region containing the Waimakariri River. If a researcher asserts a GEV distribution to summarise their uncertainty about a sequence of AMS values, it is inevitable that the GEV distribution will have positive mass for $x < 0$, especially for the $(M(CV), R^*(CV))$ combinations under consideration. For example, site 11 of a region with $M(CV) = 0.5$ has approximately an 8% chance of generating a negative value, while site 11 of a region with $M(CV) = 1$ has approximately a 32% chance. Clearly it is impossible to observe a negative

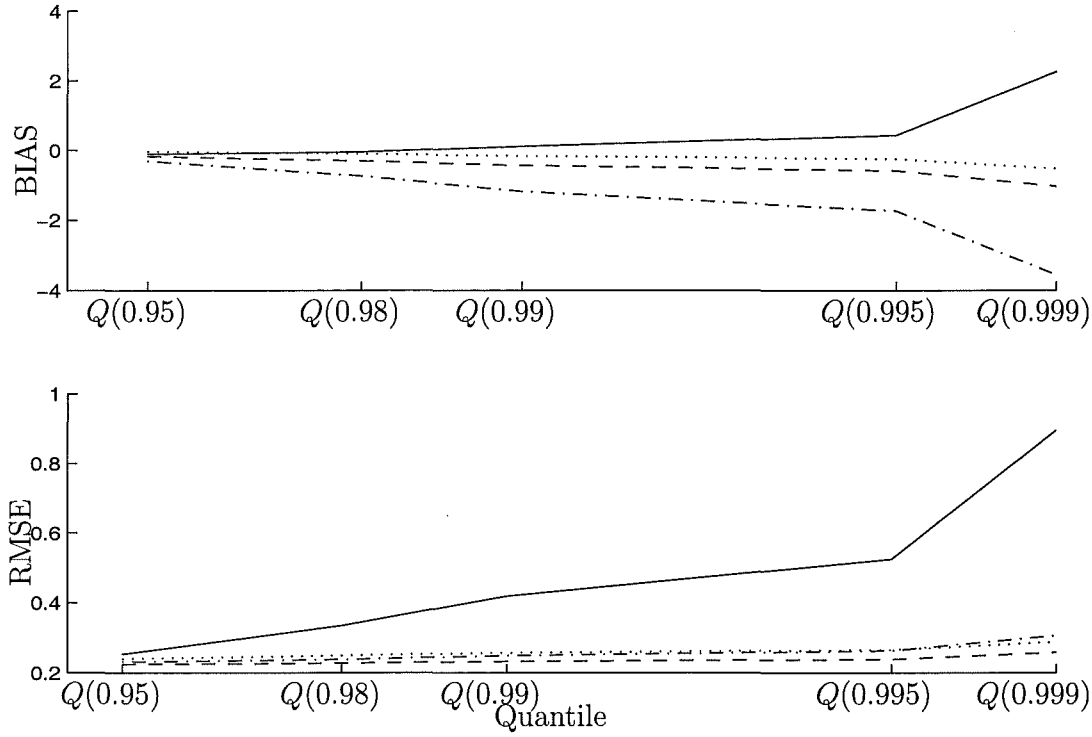


**Figure 4.6: Root-mean-squared error and bias for site 11 of a 21 site region when $M(CV) = 0.5$ and $R^*(CV) = 0.5$. Types of estimation methods are: at-site (—), scaled data (-.-.), index flood (- -) and hierarchical (...).**

river flow. Thus the distribution our simulated regions were generated from was a truncated GEV distribution.

Simulations are run for each of the four $(M(CV), R^*(CV))$ combinations. For each combination the population $CV$ at site 1 was set to $M(CV)(1 + R^*(CV)/2)$ and parameters $\alpha_1$ and $\xi_1$ were determined. The population CV at site 11 was set to $M(CV)$ and parameters $\alpha_{11}$ and $\xi_{11}$ determined. Similarly the population $CV$ at site 21 was set to $M(CV)(1 - R^*(CV)/2)$ and parameters $\alpha_{21}$ and $\xi_{21}$ were determined. The population parameters for the remaining sites were found by linearly interpolating between these three sites. For this experiment 50,000 samples were generated for each $(M(CV), R^*(CV))$ combination. This method of simulating a series of AMS measurements is based on the method implemented by Lettenmaier et al. (1987). The values of $M(CV)$ used in their simulations ranged from 0.5 to 2, while values of $R^*(CV)$ ranged from 0.2 to 0.5. However neither the $\lambda_1$ or $\lambda_2$ values, where $CV = \lambda_2/\lambda_1$, were specified.

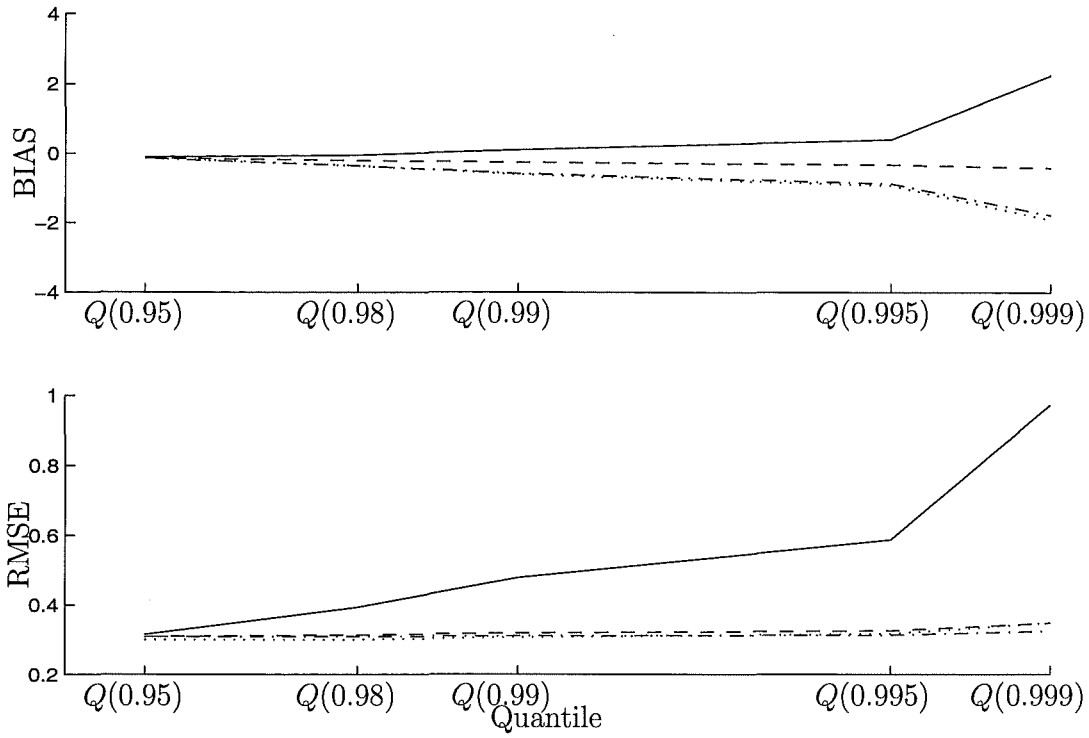


**Figure 4.7: Root-mean-squared error and bias for site 11 of a 21 site region when $M(CV) = 1$ and $R^*(CV) = 0.3$. Types of Estimation methods are: at-site (—), scaled data (-.-.), index flood (- -) and hierarchical (...).**

### Results

Once each of the four data sets has been generated, we use each of the four estimation methods (at-site, regional scaled data, regional index flood, hierarchical) to estimate parameters, and hence return periods, of the (known) underlying flood frequency distribution. The data used for each $(M(CV), R^*(CV))$ combination was generated once, and the different estimation methods were applied to the same data set.

The methods are compared by estimating biases and normalised root-mean-squared errors at each site and for each estimation method. Bias was estimated as

$$\frac{1}{n}\sum_{p=1}^{n}\hat{x}_{pqr} - x_{Tq}, \tag{4.32}$$

where $p$ is the Monte Carlo simulation index, $q$ is the site number, $r$ is the estimation method and $x_{Tq}$ is the true flood quantile at site $q$. Normalised root-mean-squared

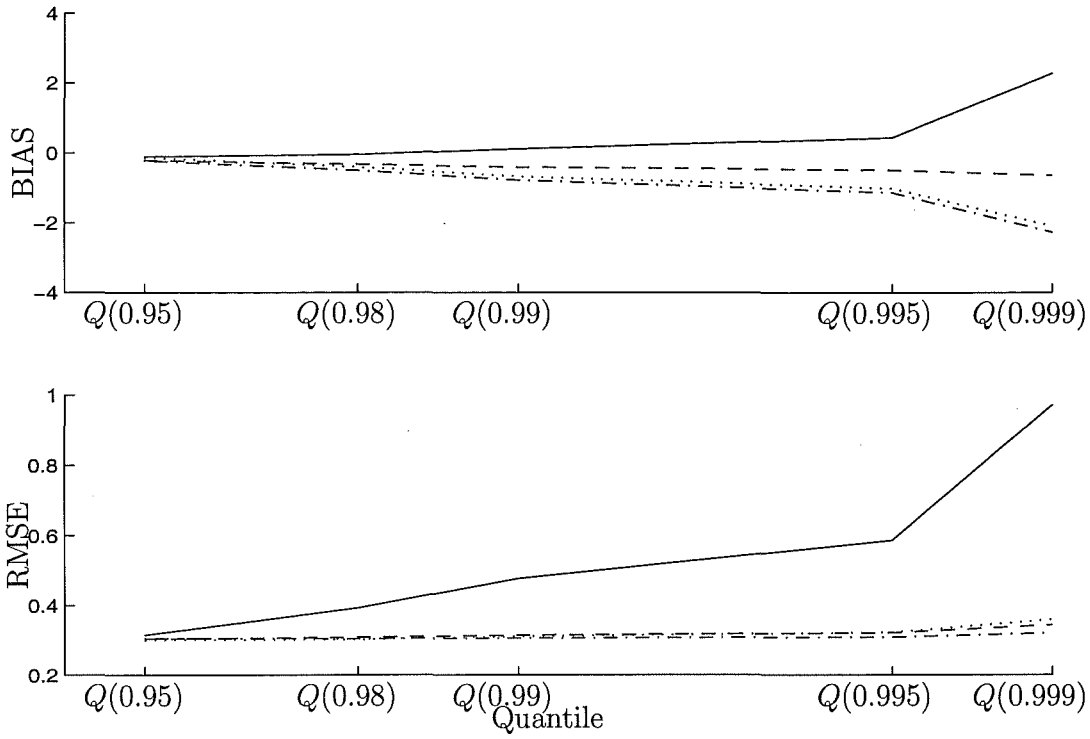


**Figure 4.8: Root-mean-squared error and bias for site 11 of a 21 site region when $M(CV) = 1$ and $R^*(CV) = 0.5$. Types of estimation methods are: at-site (—), scaled data (-.-.), index flood (- -) and hierarchical (...).**

error was estimated as

$$\frac{\left[n^{-1}\sum_{p=1}^{n}\left(\hat{x}_{Tpqr} - x_{Tq}\right)^2\right]^{1/2}}{x_{Tq}}. \tag{4.33}$$

Figures 4.5 to 4.8 show the estimated bias and RMSE, as a function of quantile level, for the 11th site in our 21 site region. Four fitting methods were used: at-site, scaled data, index flood and hierarchical. The median CV is either 0.5 or 1 and the range of regional $CV$ is 0.3 or 0.5. It is clear from the lower panel of each figure that the RMSE of the at-site estimator is much larger than any of the three regional estimators, which are all relatively similar.

The at-site quantile estimates are biased upwards in every case studied. The three regional estimates are all biased downward. Of the three regional estimates the scaled data estimate is the most biased for every combination except $(1, 0.3)$, when the hierarchical is slightly worse. The index flood estimates are consistently the least biased. The hierarchical estimate is the least biased estimate when the median $CV$ is low, but as $CV$ increases it rapidly becomes biased, especially in the

extreme tail (when return period $> 500$).

These results are equivalent to those found by Lettenmaier et al. (1987), who compared a number of at-site and regional estimators all of which used one of the three types of GEV distribution. They found that the GEV distribution gave excessively variable flood quantile estimates when it was used for evaluating quantiles at-site. However, when it was incorporated into a regional estimation scheme it was relatively insensitive to modest regional heterogeneity in the $CV$. The higher the value of the regional mean coefficient of variation, $M(CV)$, the more the advantage of methods that assumed regional homogeneity declined.

## 4.4 Assessing Flood Exceedance Quantiles Using Updated Mixture Mass Functions as Sequential Forecasting Distributions

In Chapter 3 we described in detail a procedure for forecasting the value of various items when the analysis involves sequences of observations that the researcher regards exchangeably, where particular interest centres on the sequence of updated probability mass functions $f(x_{i+1} \mid \mathbf{X_i} = \mathbf{x_i})$. Although the procedure studied dealt specifically with a digitised Normal-Gamma mixture Normal distribution, the updating process can be extended to encompass any number of parameters and to account for any functional form the researcher wishes to specify for the prior distribution and the ITF.

### 4.4.1 Introduction

When studying extreme geologic phenomena the items in which we are most interested are exceedance quantiles. This Section concerns the construction and implementation of a procedure for sequentially updating mixture mass functions. These mass functions are used to forecast exceedance quantiles for the Waimakariri River AMS data. We shall specify densities as approximations of our uncertain knowledge, and then construct exact mass functions by digitising these densities. Before moving on to the mechanics of the updating procedure itself, we consider the functional

form of the density used to assess uncertain knowledge of AMS.

### The Functional Form Of the Information Transfer Function

As discussed previously in Section 4.3.4, there is no consensus about which distribution, if any, can best be used to represent knowledge about the components of the AMS. In Section 4.3.4, three common choices of distribution to represent the form of AMS data were introduced: the Generalised Extreme Value distribution, the Generalised Logistic distribution and the Lognormal distribution. Any one of these three distributions could be digitised and specified as our ITF — although of course our choice of ITF is not limited to one of these three distributions.

After deciding on the form of the ITF we implement the digital updating procedure and obtain as many conditional quantile estimates as desired. The question is then: How can we compare results obtained using ITFs of different functional forms? In particular, does one ITF give 'better' results than the other two? One way we can compare the candidate distributions is by using scoring rules to evaluate our assessment of the form of ITF. We now briefly detour from the task at hand to introduce the notion of scoring rules.

## 4.4.2 Proper Scoring Rules

Scoring rules are used to evaluate states of uncertain knowledge. Scoring rules are comprehensively covered by Lad (1996, Chapter 6). Scoring rules attach a numerical score to any assertion, $K(X)$, about an uncertain but observable quantity, $X$, once that quantity is observed formally. A scoring rule is a function that assigns a real valued number to each possible $(X, K(X))$ combination, where $K(X)$ represents the assertion value. The value of the real number is called the score. A scoring rule is defined so that it achieves its maximum when $K(X) = x$, and is non-increasing as $x$ departs from $K(X)$ for each $K(X)$, and as $K(X)$ departs from $x$ for each $x$.

One desirable feature of a scoring rule is that it should reward researchers for accurately and honestly assessing $K(X)$. A proper scoring rule is one for which the researcher's prevision for the numerical score $S(X, K(X))$ is greatest when they assert $K(X)$ as their assertion of knowledge about $X$. Clearly, under a proper

scoring rule, it is to the researcher's advantage to honestly specify $K(X)$. There are a number of well-known types of proper scoring rules, which can be divided into two main groups: proper scoring rules for previsions and proper scoring rules for distributions.

### Proper Scoring Rules for Distributions

If we assert a probability mass function for a quantity with realm $\mathbf{R}(X) = \{x_1, x_2 \ldots, x_N\}$, then our specification of knowledge about $X$ is denoted by $\mathbf{K}_N(X) = \mathbf{p}_N$, where $\mathbf{p}_N$ represents our assertions of probabilities for the constituents of the partition generated by X. There are a multitude of proper scoring rules for assessing the probability mass function on the basis of observing $X$. In this subsection we shall consider three of them.

### The Quadratic Score of a Distribution

If $X$ is a quantity with realm $\mathbf{R}(X) = \{x_1, x_2 \ldots, x_N\}$, the quadratic score of a distribution is defined as

$$S(X, \mathbf{p}_N) \equiv -\left[\sum_{i=1}^{N} (X = x_i)(1 - p_i)^2 + \sum_{i=1}^{N} (X \neq x_i) p_i^2\right], \tag{4.34}$$

where $\mathbf{p}_N = (p_1, p_2, \ldots, p_N)$ is the vector of probabilities defining the asserted mass function $\mathbf{p}_N$ over the realm values.

Note that the quadratic score of a distribution is the sum of the quadratic scores attained by each of the constituents of the distribution, since $(X = x_i) = 1$ for only one element of the realm, and is zero for the other $(N - 1)$ elements. The largest value the score of a quadratic distribution can attain is 0. This is achieved when the forecaster is sure of the exact value of $X$, asserting the degenerate distribution that associates probability 1 with the event $(X = x_i)$ that occurs. The worst value of a quadratic score for a distribution is $-2$, when a distribution specifies $P(X = x_i) = 1$ and $x_i$ does not occur. All other distributions achieve scores between 0 and $-2$. The quadratic score is sometimes called the Brier Score of the distribution.

Note that quadratic scores are defined so that they are always non-positive. It is always better to have a score closer to 0 than it is to have one farther away from 0. Note also that the quadratic score of prevision $K$, $S(X, K) = -(X - K)^2$,

scores the difference between the asserted and observed values of $X$. Whereas the quadratic score of a distribution scores the difference between the asserted and observed probabilities. Thus any two distributions that have the same assessed probabilities, in any permutation, will have the same score as long as the assert the same probability for $x^*$, where $X = x^*$ is observed.

### The Logarithmic Score of a Distribution

If $X$ is a quantity with realm $\mathbf{R}(X) = \{x_1, x_2 \ldots, x_N\}$, the logarithmic score of a distribution is defined as

$$S(X, \mathbf{p}_N) \equiv \sum_{i=1}^{N} (X = x_i) \, log(p_i) \, . \tag{4.35}$$

The logarithmic score of a distribution is merely the logarithm of your prevision for the event that equals one. Thus two distributions will have the same score as long as they each specify the same probability for the constituent of $X$ that does occur — regardless of how the assessed distributions differ over the remaining $(N-1)$ possibilities. The logarithmic scoring rule is particularly appealing for researchers who believe that the observation gives no information about the other possible values of $X$ that did not occur — no matter how near or far these other possibilities are from $x^*$. All logarithmic scores of distribution are non-positive. The closer the score is to 0 the better.

### The Spherical Score of a Distribution

If $X$ is a quantity with realm $\mathbf{R}(X) = \{x_1, x_2 \ldots, x_N\}$, the spherical score of a distribution is defined as

$$S(X, \mathbf{p}_N) \equiv \frac{\sum_{i=1}^{N} (X = x_i) \, p_i}{\left(\sum_{i=1}^{N} p_i^2\right)^{1/2}}. \tag{4.36}$$

The spherical score of a distribution is the expectation placed on $x^*$ divided by the square root of the sum of the squared probabilities for each constituent of $X$. All spherical scores are non-negative. The minimum achievable score is 0, when a degenerate distribution is specified on a value of $X$ that does not occur. The maximum achievable score is 1, when a degenerate distribution is specified on the

value of $X$ that does occur. When considering the spherical score of a distribution, the higher the score the better.

Scoring rules are a measure of the value of information asserted about $X \in \mathbf{R}(X)$ contained in $\mathbf{p}_N$. In general, the scoring rule we choose should be based on how severely we want to penalise distributions that place substantial probabilities on possible values of $X$ that do not occur, depending on their distance from the distribution that is degenerate on $x^*$. The difference between these three scoring rules is graphically displayed by Lad (1996, pp. 348–349).

### Previsions for Scores of Distributions

As well as being able to score any assessed distribution upon observing $X = x^*$, we can also score our assessed distributions to measure how much information is contained in each asserted distribution. The amount of information asserted about $X \in \mathbf{R}(X)$ contained in $\mathbf{p}_N$ depends on the shape of the assessed distribution. The achieved value of $X$ has no bearing on the information contained by the assessment. Information content is measured by the score a distribution expects to achieve. Two differently assessed distributions may contain the same amount of information, but achieve different scores. We should note how this works for the three scoring rules we have discussed.

### Prevision for Quadratic Distribution Score

The prevision for a quadratic distribution score is

$$P\left(S[X, \mathbf{p}_N]\right) = \sum_{i=1}^{N} p_i^2 - 1. \tag{4.37}$$

Simple calculus shows that this prevision has a maximum value of 0, which occurs whenever the forecaster is sure of the exact value of $X$, asserting a distribution that is degenerate at that value. When this is the case, one element of $\mathbf{p}_N$ equals 1 and the other $(N-1)$ elements all equal 0. Remember that our prevised score does not depend on whether it turns out that the assessment is correct, it only measures how sure the assessor is that a certain outcome will occur.

The minimum value of $P\left(S[X, \mathbf{p}_N]\right)$, $(1/N) - 1$, occurs when all members of the constituent set are specified to have the same probability, that is, when a Uniform

distribution is specified. Anyone who specifies $\mathbf{p}_N$ in this way is saying that they are equally (un)sure about each of the possible outcomes. Naturally this is when an assessment is least precise. The prevision for a quadratic distribution score is always non-positive. The closer $P(S[X, \mathbf{p}_N])$ is to 0 the more information the assessment contains.

#### Prevision for Logarithmic Distribution Score

The prevision for a logarithmic distribution score is

$$P(S[X, \mathbf{p}_N]) = \sum_{i=1}^{N} p_i log(p_i). \tag{4.38}$$

This equals the well-known entropy of the distribution.

#### Prevision for Spherical Distribution Score

The prevision for a spherical distribution score is

$$P(S[X, \mathbf{p}_N]) = \left[\sum_{i=1}^{N} p_i^2\right]^{1/2}. \tag{4.39}$$

This number is the Euclidean length of $\mathbf{p_N}$, our vector of previsions. The larger the prevision for a spherical distribution score, the more information is contained in the assessment. $P(S[X, \mathbf{p}_N])$ has a maximum value of 1 when a degenerate distribution is specified and a minimum value of $N^{-1/2}$ when a Uniform distribution is specified.

### 4.4.3 Digital Updating Procedure

Now we shall assess the flood exceedance quantiles using updated mixture mass functions as sequential forecasting distributions. We know from Chapter 3 that to undertake the computations involved in this assessment we must first construct:

- $\mathbf{R}(X)$, a vector to represent the realm of possible measurement values of $X$.
- $\mathbf{R}(\theta_1), \ldots, \mathbf{R}(\theta_p)$, vectors representing the realms of possible values for parameters $\theta_1, \ldots, \theta_p$.
- $f(x \mid \theta_1, \ldots, \theta_p)$, an array of mass values of size $s_X \times s_{\theta_1} \times \ldots \times s_{\theta_p}$, where $s_{\theta_i}$ is the size of $\mathbf{R}(\theta_i)$. The first dimension of the array corresponds to conditional

probability mass functions for $X$ given every different combination of values for $\theta_1, \ldots, \theta_p$.

- $f(\theta_1 \mid \theta_2, \ldots, \theta_p), \ldots, f(\theta_{p-1} \mid \theta_p)$, arrays of conditional probability mass values. Each array consists of vector $\theta_r$, $1 \leq r \leq p-1$, evaluated over every $(\theta_{r+1}, \ldots, \theta_p)$ combination, for each element of $\theta_r$. Thus the number of (unique) dimensions varies according to the number of conditioning parameters. For example $f(\theta_1 \mid \theta_2, \ldots, \theta_p)$ differs on $p$ dimensions. Each of its component vectors corresponds to a different combination of $(\theta_1, \ldots, \theta_p)$ values. $f(\theta_{p-1} \mid \theta_p)$ differs on two dimensions. It has different component vectors for each $(\theta_{p-1}, \theta_p)$ combination. For computational purposes each array must be the same size as $f(x \mid \theta_1, \ldots, \theta_p)$. Thus each array of conditional probability mass values must be replicated and tiled to form an array with $p+1$ dimensions. Each array has size $s_X \times s_{\theta_1} \times \ldots \times s_{\theta_p}$.

- $f(\theta_p)$, an array of marginal probability mass values. This array is of size $s_X \times s_{\theta_1} \times \ldots \times s_{\theta_p}$ and is identical across all but one dimension.

- $f(\theta_1, \theta_2, \ldots, \theta_p)$, a $p$-dimensional array representing the joint mass function $(\theta_1, \ldots, \theta_p)$. It is formed by element-wise multiplication of arrays $f(\theta_1 \mid \theta_2, \ldots, \theta_p), \ldots, f(\theta_{p-1} \mid \theta_p) f(\theta_p)$.

Once these arrays have been constructed we can implement our procedure for assessing items of interest, in this case exceedance quantiles, in the manner described in Chapter 3. The process we follow is:

1. Observe $X_i = x_i$.

2. Extract the array corresponding to $X_i$ from array $f(x \mid \theta_1, \ldots, \theta_p)$. The extracted array will be of dimension $p$. This is the ITF through $\theta_1, \theta_2, \ldots, \theta_p$ from $X_i = x_i$ to $X_{i+1}$.

3. Implement Bayes' Theorem to update the mixing function $f(\theta_1, \ldots, \theta_p \mid \mathbf{X}_i = \mathbf{x}_i)$. This involves multiplying $p$-dimensional arrays $f(x_i \mid \theta_1, \ldots, \theta_p)$ and $f(\theta_1, \ldots, \theta_p \mid \mathbf{X}_{i-1} = \mathbf{x}_{i-1})$ element-wise, and normalising.

| | GEV | | | GLO | | | | LN3 | | |
|---|---|---|---|---|---|---|---|---|---|---|
| | Min | Inc | Max | Min | Inc | Max | | Min | Inc | Max |
| $X$ | 100 | 10 | 9000 | 100 | 10 | 9000 | $X$ | 100 | 10 | 9000 |
| $\xi$ | 1000 | 12.5 | 1500 | 1000 | 12.5 | 1500 | $\xi$ | 250 | 12.5 | 740 |
| $\alpha$ | 150 | 12.5 | 650 | 150 | 12.5 | 650 | $\mu$ | 3.5 | 0.125 | 8.5 |
| $k$ | -0.498 | 0.012 | -0.03 | -0.498 | 0.012 | -0.03 | $\sigma$ | 0.49 | 0.052 | 1.01 |

**Table 4.5: Elements of realms used in digital computations. "Min" and "Max" denote the smallest and largest elements of the realm. "Inc" denotes the increment between successive elements.**

4. Replicate and tile array $f(\theta_1, \ldots, \theta_p \mid \mathbf{X}_i = \mathbf{x}_i)$ so it has $p+1$ dimensions and is the same size as $f(x_i \mid \theta_1 \ldots \theta_p)$.

5. Calculate $f(x_{i+1} \mid \mathbf{X}_i = \mathbf{x}_i)$, the updated predictive mass function, by multiplying $f(x \mid \theta_1, \ldots, \theta_p)$ and $f(\theta_1, \ldots, \theta_p \mid \mathbf{X}_i = \mathbf{x}_i)$ element-wise, and then summing over $\theta_1, \ldots, \theta_p$.

6. Calculate any items of interest, e.g. conditional expectation, conditional exceedance quantiles.

Repeat this process as many times as required.

This procedure was undertaken with the ITF having three different functional forms. These were digitised GEV, GLO and LN3 densities. The realm of $X$ was defined to range from 100 cumecs to 9000 cumecs at intervals of 10 cumecs. Any further refinement of AMS measures is not of practical use; in particular, treating $X$ as if it is continuous may be useful for calculation purposes (if we could find a conjugate prior) but it adds nothing to our interpretation. Each of the three parameters for each ITF was specified initially to be Uniformally distributed over the components of its realm. These are reasonable, if conservative, prior distributions. Realms of the parameters are listed in Table 4.5. Notice that for each of our three examples the size of each of the four realms is the same: for the GEV and GLO ITF's we have $s_X = 891$, $s_\xi = 41$, $s_\alpha = 41$ and $s_k = 40$, and for the LN3 ITF the realm sizes are $s_X = 891$, $s_\xi = 41$, $s_\mu = 41$ and $s_\sigma = 40$. Thus the size of each four dimensional array is $891 \times 41 \times 41 \times 40$. For simplicity, from here on

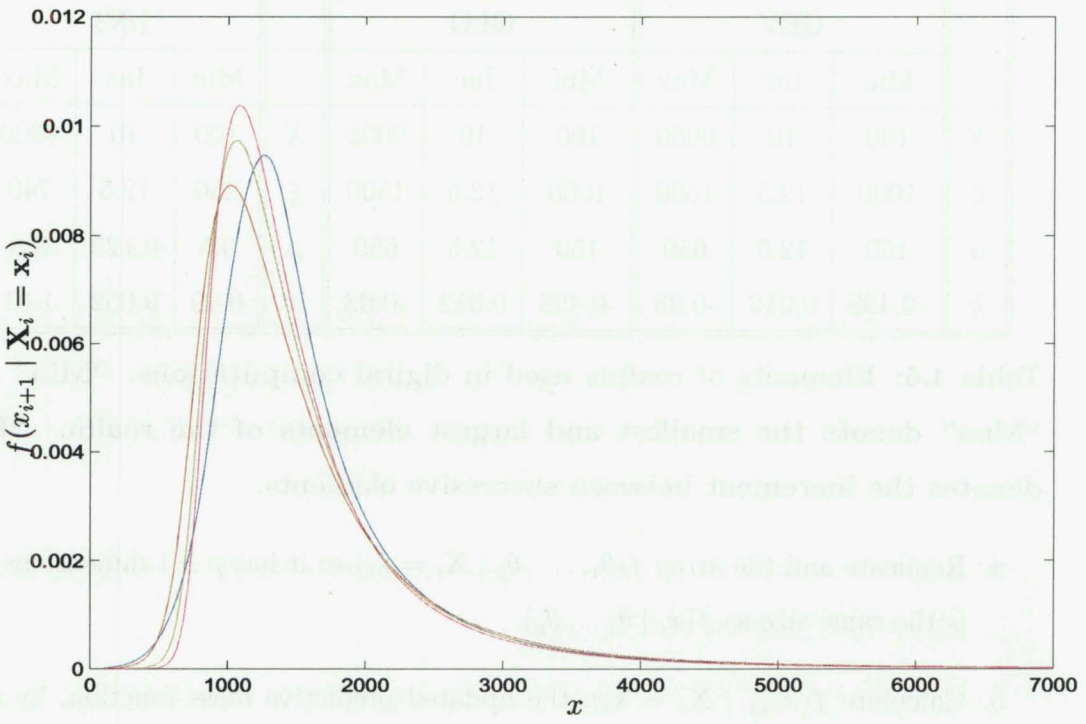


**Figure 4.9: Marginal mass function of $X$ after 0 (blue), 25 (red), 50 (green) and 72 (magenta) recorded observations. The ITF is specified to have a GEV form.**

the characterising parameters of the ITF will be labeled as $\xi$, $\alpha$, and $k$, regardless of the form of the ITF. An array representing the ITF is computed by evaluating $f(x \mid \xi, \alpha, k)$ at each of the 59,910,840 possible $(X, \xi, \alpha, k)$ combinations.

### 4.4.4 Results of the Digital Forecasting Procedure

At any step of our digital computations we can compute any item that is of interest to us. In this case we are particularly interested in the shape of $f(x_{i+1} \mid \mathbf{X_i} = \mathbf{x_i})$, the updated predictive mass function, from which we can compute the value of any conditional exceedance quantile we wish. Figure 4.9 demonstrates the shape of the predictive mass function at different stages during the observation of the 72 AMS measurements from the Waimakariri River, when the ITF is specified to have a GEV form. Notice that the variance of $f(x_{i+1} \mid \mathbf{X_i} = \mathbf{x_i})$ decreases as more observations are processed. As we record more observations $f(x_{i+1} \mid \mathbf{X_i} = \mathbf{x_i})$ becomes more 'peaked'.

| | $Q(0.95)$ | $Q(0.98)$ | $Q(0.99)$ | $Q(0.995)$ | $Q(0.999)$ |
|---|---|---|---|---|---|
| GEV | 2840 | 3500 | 3920 | 4720 | 7000 |
| GLO | 2770 | 3440 | 3890 | 4650 | 6950 |
| LN3 | 2800 | 3390 | 3770 | 4200 | 5950 |

**Table 4.6: Conditional exceedance quantile forecasts for the Waimakariri River when the ITF is assessed to have a particular functional form.**

Conditional exceedance quantile forecasts are shown in Table 4.6. Note the similarity across the three different ITF's. Remember that for the frequentist at-site method the GEV and LN3 estimates were close to one another, but the estimate based on the GLO was significantly smaller for $Q(F) < 0.995$. Comparing the forecasts to the frequentist quantile estimates we see that the values of $Q(0.95)$ are similar, but as the return period increases the distance between the digital forecasts and the frequentist estimates increases.

In Section 4.3.5 we found point estimates for each parameter in the distribution under investigation. Now we can compute a mass function that represents our updated knowledge about the location of each parameter. Figure 4.10 represents these mass functions for the GEV ITF. Remember that by using a frequentist at-site procedure we calculated point estimates of $\hat{\xi} = 1165$, $\hat{\alpha} = 355$ and $\hat{k} = -0.25$. These estimates are marked with a red "$*$" in Figure 4.10. We can see that for the location and spread parameters the frequentist at-site parameter point estimate is close to the mode of the predictive mass function. The mode of shape parameter $k$ is approximately $-0.33$, as opposed to the point estimate of $-0.25$. The shape of the mass functions tells us how sure we are in mixing forecasts over the size of a parameter. In this case, the broadness of the mixing mass functions displays how uncertain we are about the values of the characterising parameters. Compare this to the frequentist procedure, where all that is specified about a parameter is a point estimate. Of the three parameters $k$ is defined in the least-precise manner. This is consistent with the paradigm of the frequentist regional hierarchical estimation method — that we will need more observations to achieve an equivalently good estimate of the shape parameters than we will for the spread parameter or location parameter.

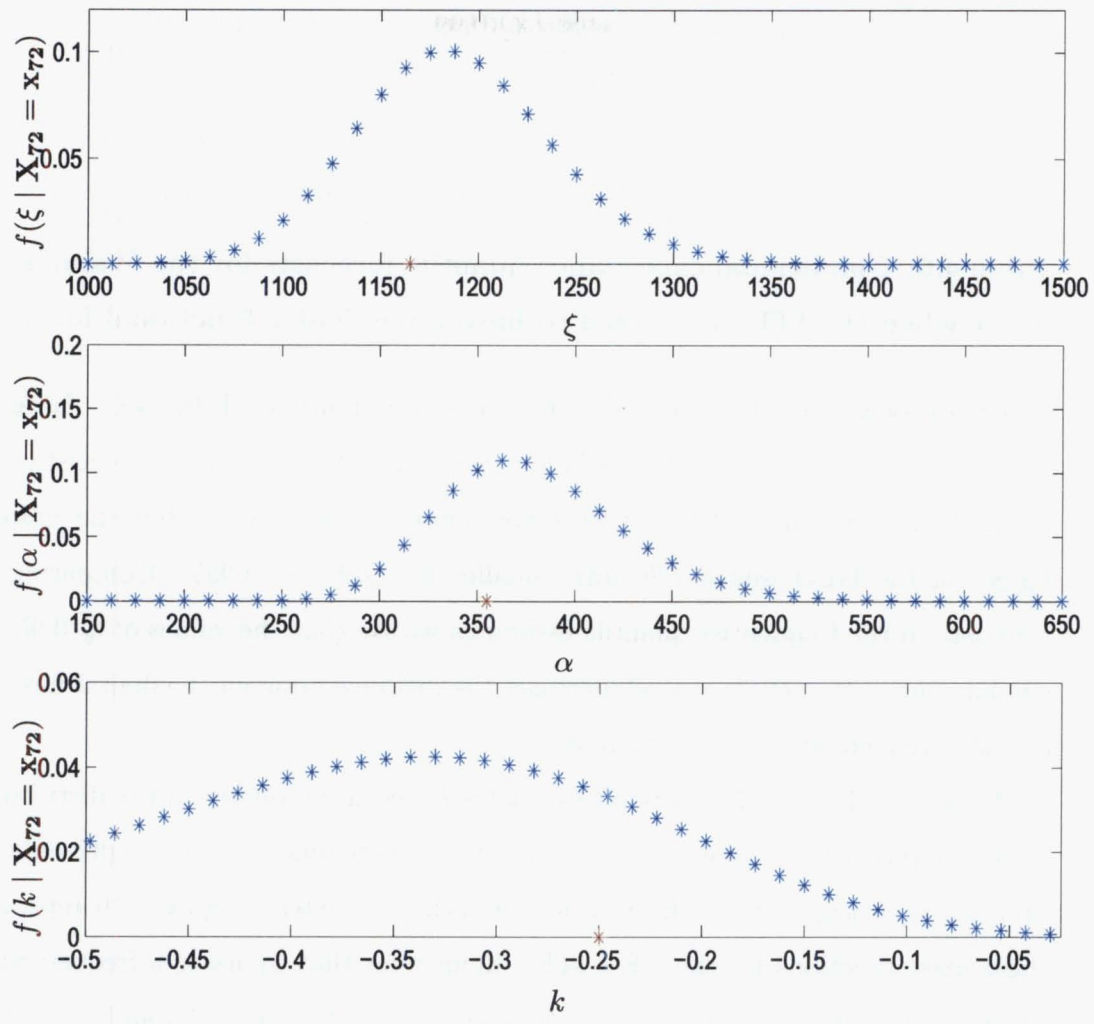


**Figure 4.10: Conditional marginal mass functions for, in descending order, $\xi$, $\alpha$ and $k$, when we specify that the ITF has a GEV form. The frequentist at-site point estimates are marked on the $x$-axis by red "$*$".**

### The Scores of Distributions

We have obtained exceedance quantile forecasts for each of the three forms of specified ITF. To empirically evaluate these three competing theories we will score each of the observations and compare the results. This is called scored sequential forecasting. As well as investigating the difference between the candidate ITFs, we shall use this as an exercise to examine the differences between the quadratic, logarithmic and spherical scoring rules.

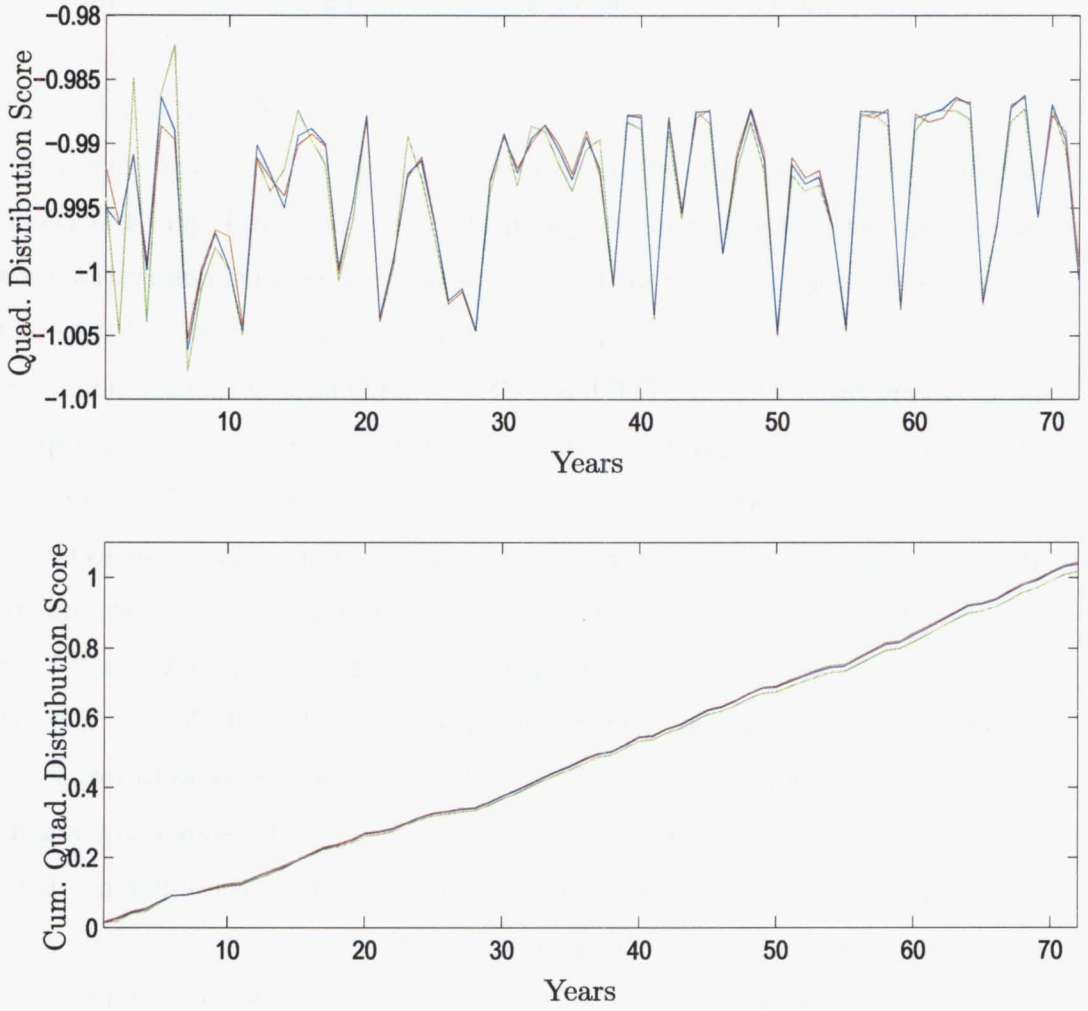


**Figure 4.11: Sequential individual (upper panel) and cumulative (lower panel) quadratic score of a distribution for ITF with functional form: GEV (blue), GLO (red) and LN3 (green).**

### Quadratic Score

The quadratic score is the first scoring rule that we shall consider. Quadratic scores were calculated for each observation, for each of the three forms of ITF. The results are shown in Figure 4.11. The upper panel displays the score of the distribution as each observation is processed. We score the GEV (blue), GLO (red) and LN3 (green) distributions. The lower panel shows the cumulative scores. For clarity the cumulative scores are plotted as the difference between the achieved score and $-1.008$, the minimum value achieved by any of the scores. Plotting cumulative scores in this manner means that the larger the score is, the better.

The scores achieved using ITFs of different functional forms are most different from each other when $i$ is small. The bigger discrepancies in scores appear early on in the analysis because this is when the form of the ITF itself has most effect, because the data has not been recorded for a long enough period to dominate the results. Notice that the first major 'jag' in the upper panel of Figure 4.11 occurs at $i = 7$, which, according to Figure 4.1, is when the first recorded observation differed significantly from the previous sequence of AMS recordings. Notice that, although the scores produced when the ITF has a GEV or GLO form are more similar to each other than to the scores produced when the ITF has a LN3 distribution (especially when $i < 17$), in general the scores associated with the three ITFs are similar. All scores take values within a very narrow range. This is not unexpected when we consider the construction of $S(X, \mathbf{p}_N)$. As Equation 4.34 shows, the quadratic score consists of two parts. The first part of $S(X, \mathbf{p}_N)$ is $\sum_{i=1}^{N} (X = x_i)(1 - p_i)^2$. Remember that $(X = x_i)$ is a vector that contains one "1" and $(N - 1)$ "0"s. There are a large number of elements in the realm of $X$, so the expectation that any single one of them will occur is small. In fact, as Figure 4.9 shows, the maximum expectation that any $X$ will occur is less than 0.01. Thus the difference between alternative potential scores is small for different outcome vectors. Similarly the second part of $S(X, \mathbf{p}_N)$, $\sum_{i=1}^{N} (X \neq x_i) p_i^2$, is the sum of the squares of all the values contained in $\mathbf{p}_N$, excluding the value assigned to the actual outcome. Again, because $\mathbf{R}(X)$ is large and the value assigned to any individual $X$ is small there will only be a small difference over different "unsuccessful" values of $X$. The lower panel shows the LN3 distribution has the minimum (and therefore worst) score. The GEV and GLO scores are very close, with the GLO score being slightly better.

### Logarithmic Score

The logarithmic scores can be interpreted in a similar manner to the quadratic scores. Remember that the logarithmic score is just the logarithm of the probability assigned to the value of $X$ that occurs. Because there is little difference between the various assigned values of $f(x_{i+1} \mid \mathbf{X_i} = \mathbf{x_i})$, the difference of their logarithms will also be small. Thus we can expect the range of scores for individual recorded measurements to be small. For example, the maximum score attained is $-4.36$, for

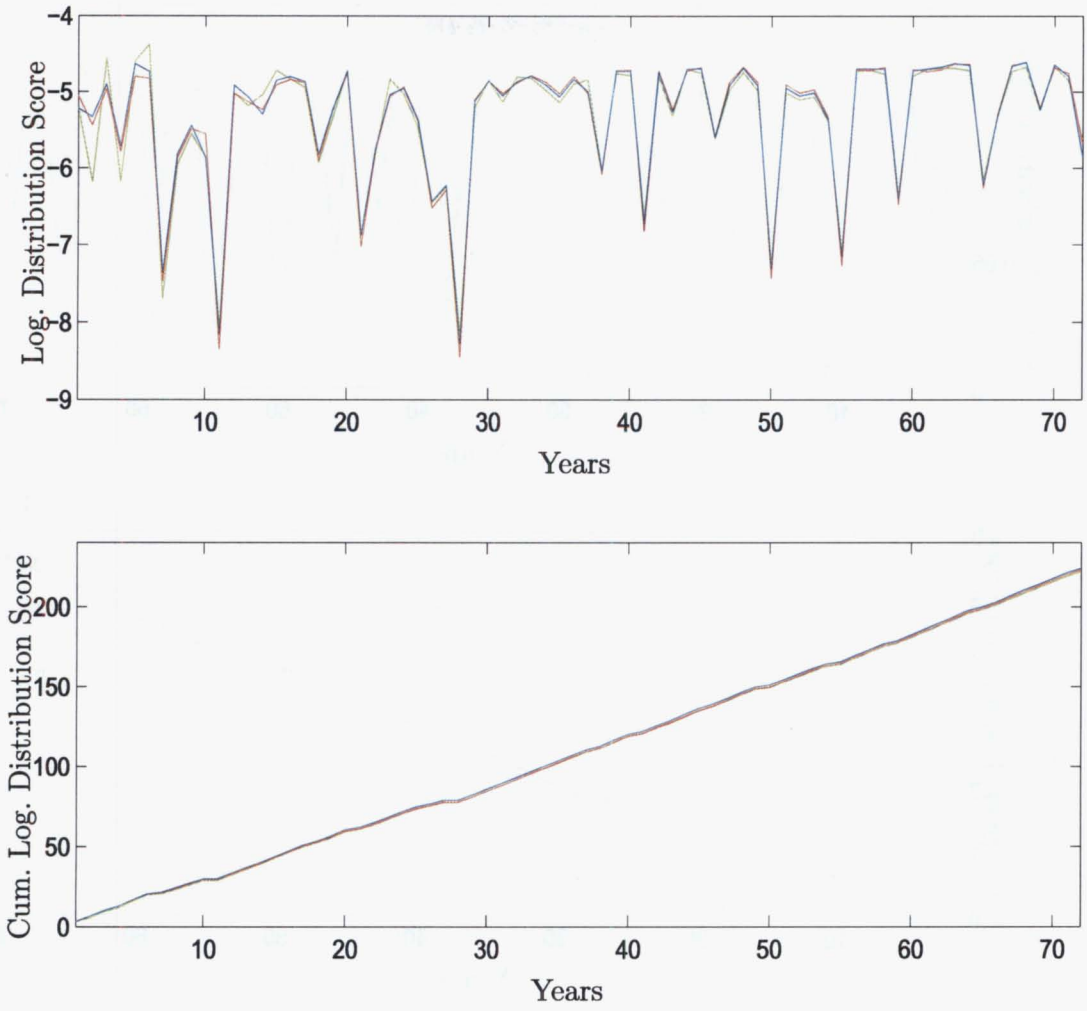


**Figure 4.12: Sequential individual (upper panel) and cumulative (lower panel) logarithmic score of a distribution for ITF with functional form: GEV (blue), GLO (red) and LN3 (green).**

$i = 6$ when the functional form of the ITF is assessed as LN3. The minimum score is $-8.44$ for $i = 28$ when the functional form of the ITF is assessed as GLO. The year corresponding to $i = 28$ is 1963, the year of the largest recorded flow.

Achieved scores are displayed in the upper panel of Figure 4.12. Cumulative scores, which are displayed in the lower panel, are shown as the cumulative difference of the recorded and minimum score. When scores are displayed in this way, the larger the score is the better. The lower plot shows the cumulative sum of Log Scores. The GEV has the maximum score, followed by GLO and LN3. All three scores appear very similar, which is as we expect considering the size of the differences between

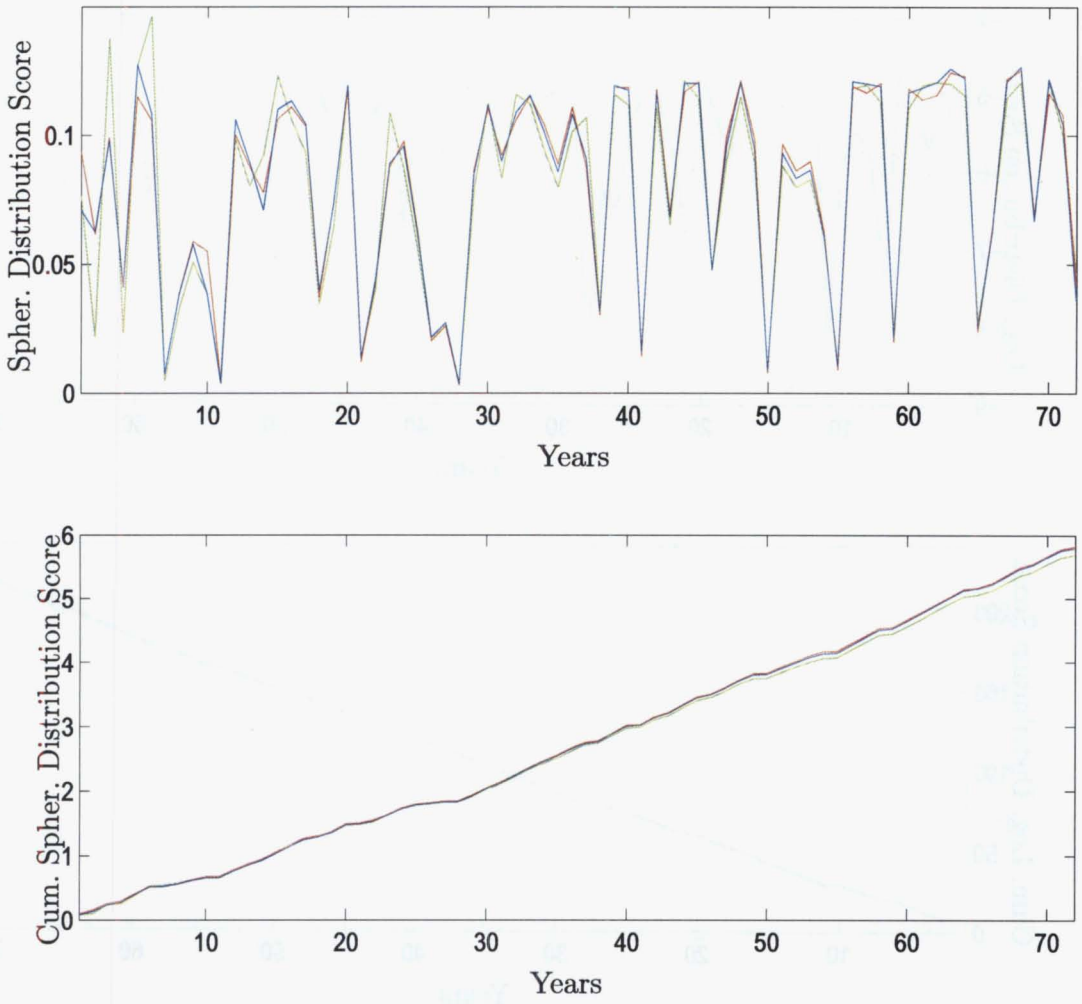


**Figure 4.13: Sequential individual (upper panel) and cumulative (lower panel) spherical score of a distribution for ITF with functional form: GEV (blue), GLO (red) and LN3 (green).**

the different forms of the ITF in the upper panel, and the large scale on the y-axis in the lower panel. .

### Spherical Score

The last scoring method we consider is the spherical score. Remember from Equation 4.36 that the spherical score is the assessment that has been placed on $x^*$ divided by the square root of the sum of each of the asserted probabilities squared. As in the previous two cases we do not expect there to be a large difference between the different scores because of the relative similarity between the mass values attached

to the elements of $\mathbf{R}(X)$

The upper panel of Figure 4.13 shows that the shape of the individual scores is similar to that obtained from the quadratic and logarithmic scores. However there is a relatively large difference between the three forms of ITF, and in particular between the LN3 and the other two, for $i < 17$. As the number of observations increases, each individual observation has less of an impact on the shape of $f(x_{i+1} \mid \mathbf{X}_i = \mathbf{x}_i)$, and consequently there is less of a difference between the scores attained through the three candidate distributions. The lower panel of Figure 4.13 shows the cumulative scores. Remember that, when dealing with spherical scores, the larger the score is the better. Once again the LN3 score is the worst. The GEV and GLO scores are very similar, with the GLO score being slightly better.

Before we leave scoring rules, we shall briefly examine what information the predictive mass functions claim to provide about our current state of uncertain knowledge about $X$.

### Previsions for Scores of Distributions

Previsions for scores of distributions measure how sure the researcher is about the assertions they have made. The most apparent thing about the Previsions of Scores in Figure 4.14 is how similar they look over the three different types of score. Notice that the range of differences between any of the previsions for scores is small, as it was with the scores we discussed in the preceding Section. We start being most sure about assessments when the form of the ITF is specified as LN3. At approximately $i = 30$ the previsions related to the LN3 scores drop until they are slightly below previsions relating to the GEV and GLO forms of ITF. From $i = 30$ onward our assessment of previsions appears to improve to some extent, in all cases exceeding the initial expected score of the first period. Now that we have established a procedure for scoring sequential forecasts created by updating mass functions, we move on to comparing these digital approximations with frequentist estimates.

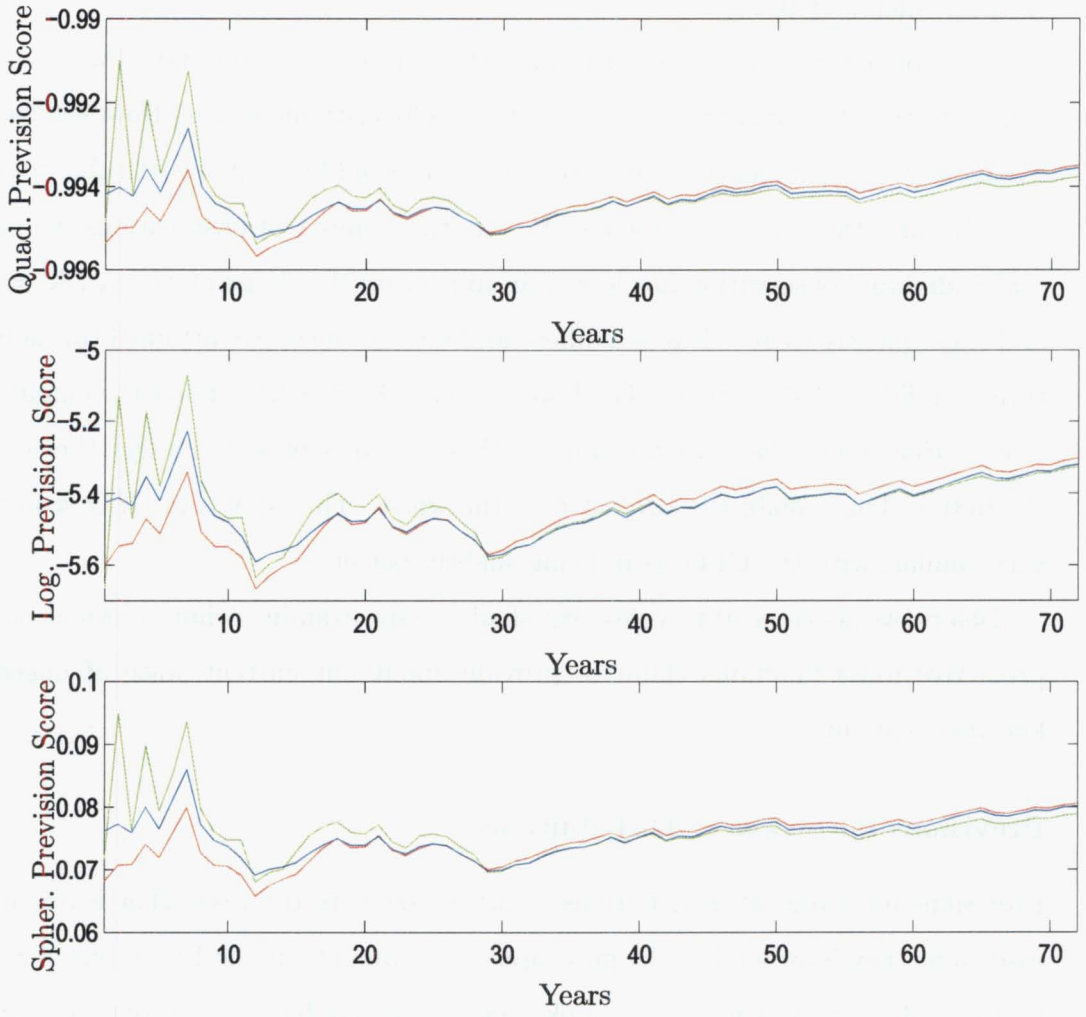


**Figure 4.14: Scores of sequential previsions for ITF with functional form: GEV (blue), GLO (red) and LN3 (green). Scoring rules used are (in descending order) quadratic, logarithmic and spherical.**

## 4.5 Comparing Frequentist Estimates and Digital Forecasts

In Section 4.3 we used conventional frequentist techniques to find point estimates of the characterising parameters of distributions commonly used in the study of flood frequency analysis. These point estimates were then used to estimate flood exceedance quantiles. In Section 4.4 we constructed and implemented a digital updating procedure. This was used to score sequential forecasting methods for an analysis which involved sequences of observations regarded exchangeably. To

conclude this Chapter we shall compare the two approaches. First, we base our comparison on scores obtained with the Waimakariri River AMS data. Second, we shall compare the two procedures using a simulated data set.

Frequentist estimates, calculated by using the method of L-moments, and subjective forecasts, achieved via updated mixture mass functions, are fundamentally different. Thus, no method for comparing the two procedures really makes sense. Subjective theory is not orientated towards estimating parameters (that don't exist) but toward forecasting measurements (which are functions of real historical records). Ultimately, what any statistical method should be able to do is to forecast historical measurements in the context of uncertainty. Thus, we shall score forecasts based on objectivist estimators against real subjectivist sequential forecasts. To conclude this Chapter we shall cater to the objectivist and abuse the subjectivist outlook to measure subjective Bayesian forecasts using frequentist criteria, namely the bias and root mean-squared-error.

Before studying the Waimakariri River AMS data again, we shall take another brief diversion to describe proper scoring rules for expectations and variances.

### 4.5.1 Proper Scoring Rules for Expectations

In Section 4.4.2 we introduced proper scoring rules as measures used to evaluate states of uncertain knowledge. Although our main focus was on proper scoring rules for distributions, we briefly mentioned that we can also score assessments of expectations and variances, which we shall denote $E(X)$ and $V(X)$ respectively.

One proper scoring rule we can use is the quadratic scoring rule. The quadratic score of $K$ is defined as

$$S(X, K(X)) = -(X - K(X))^2, \tag{4.40}$$

where $K(X)$ is some numerical assessment of $X$. This is an analogue of the quadratic scoring rule for distributions given in Equation 4.34. The quadratic scoring function is concave. It's maximum occurs when the prevised value of $X$ is achieved. Notice that the achieved score only depends on the difference between $X$ and $K(X)$, and that $S(X, K(X)) = S(K(X), X)$. The quadratic scoring rule is the only proper scoring rule for which either of these properties holds true. Notice that the quadratic

score is the negative of the squared difference — this is in keeping with our idea that a larger score is better. Remember that the score for a distribution is the difference between asserted and observed probabilities, whereas the score for an expectation is the difference between the asserted and achieved values of $X$.

The quadratic score for the expectation and variance of $X$ can be written as

$$S(X, E(X)) = -(X - E(X))^2 \tag{4.41}$$

$$\text{and} \quad S(X, V(X)) = -((X - E(X))^2 - V(X))^2. \tag{4.42}$$

In the subsequent subsections we shall score the expectation and variance of $X_{i+1} \mid (\mathbf{X}_i = \mathbf{x}_i)$, for various values of $i$.

Our motivation for introducing scoring rules for expectations and variances is because we cannot directly compare the scores of distributions for the frequentist and digital procedures. Remember that the frequentist method of L-moments is used to estimate the characterising parameters of the GEV distribution. These parameters are then used to construct a continuous density function. The continuous density function is an approximation of the predictive mass function of $X$. Scores of approximating continuous probability density functions are found using continuous analogues of Equations 4.34, 4.35 and 4.36. For example, the logarithmic score of a continuous probability density function is

$$S(X, f_X(\cdot)) \equiv log\left(f_X\left(X\right)\right). \tag{4.43}$$

See the text of Lad (1996, pp. 350) for the proper scores of other continuous approximating distributions. This score is not readily comparable to the score of the predictive mass function obtained through updated mixture mass functions. Remember that the predictive mass function, $f(x_{i+1} \mid \mathbf{X}_i = \mathbf{x}_i)$, is a vector whose size is defined by the size of $\mathbf{R}(X)$. Since $f(x_{i+1} \mid \mathbf{X}_i = \mathbf{x}_i)$ is normalised to sum to 1, the size of the mass attached to the observed outcome will depend on the size of $\mathbf{R}(X)$. That is, the more finely delimited $\mathbf{R}(X)$ is, the lower the mass will be at any particular point. Although we can't compare the score of an approximating continuous distribution directly with the score of a mass function, one compromise which allows us to compare the two different procedures is to digitise the approximating continuous density over $\mathbf{R}(X)$.

### 4.5.2 Comparing L-moment Estimates and Updated Mixture Mass Forecasts using Scoring Rules for the Waimakariri River Annual Maxima Series Data

This Section involves using proper scoring rules to sequentially score the frequentist estimates and digital forecasts of exceedance quantiles.

#### Estimating the Conditional Mean and Variance Using the Method of L-moments

In Section 4.3.3 we described how to use the method of L-moments to estimate the parameters of the "underlying distribution" which "generates the series of random outcomes that compose the AMS". We can estimate these parameters at any stage that interests us. The only constraint, when using the method of L-moments to estimate the parameters of the GEV distribution, is that we must have observed at least three values in the sequence, see Equations 4.9 and 4.15. Once L-moment estimates of the parameters of the GEV distribution, $\xi$, $\alpha$ and $k$, are obtained, they can be used to compute $E(X)$ and $V(X)$ using Equation 4.13 and Equation 4.14.

We shall forecast $E(X_{i+1} \mid \mathbf{X}_i = \mathbf{x}_i)$ and $V(X_{i+1} \mid \mathbf{X}_i = \mathbf{x}_i)$ as $E(X_i)$ and $V(X_i)$ respectively, where $E(X_i)$ and $V(X_i)$ are the expectation and variance after $i$ observations. From now on whenever we refer to the "frequentist forecast at stage $i+1$", we will be referring to the statistics estimated after $i$ observations.

#### Forecasting the Conditional Mean and Variance Using Updated Mixture Mass Functions

In Section 4.4 we described how to forecast the value of various items when interest centres on the sequence of updated mass functions $f(x_{i+1} \mid \mathbf{X}_i = \mathbf{x}_i)$. At each successive step the digitally updated predictive mass function is used to assess our expectation and variance for the next $X$ value to be observed. The computational procedure involves generating a digitised prior mixing mass function and digitised ITF and using them, via Bayes' Theorem, to update the posterior mass function, and hence the predictive mass function. The ITF is specified to have a GEV form.

The realm of possible AMS values, $X$, as well as the realms of the characterising

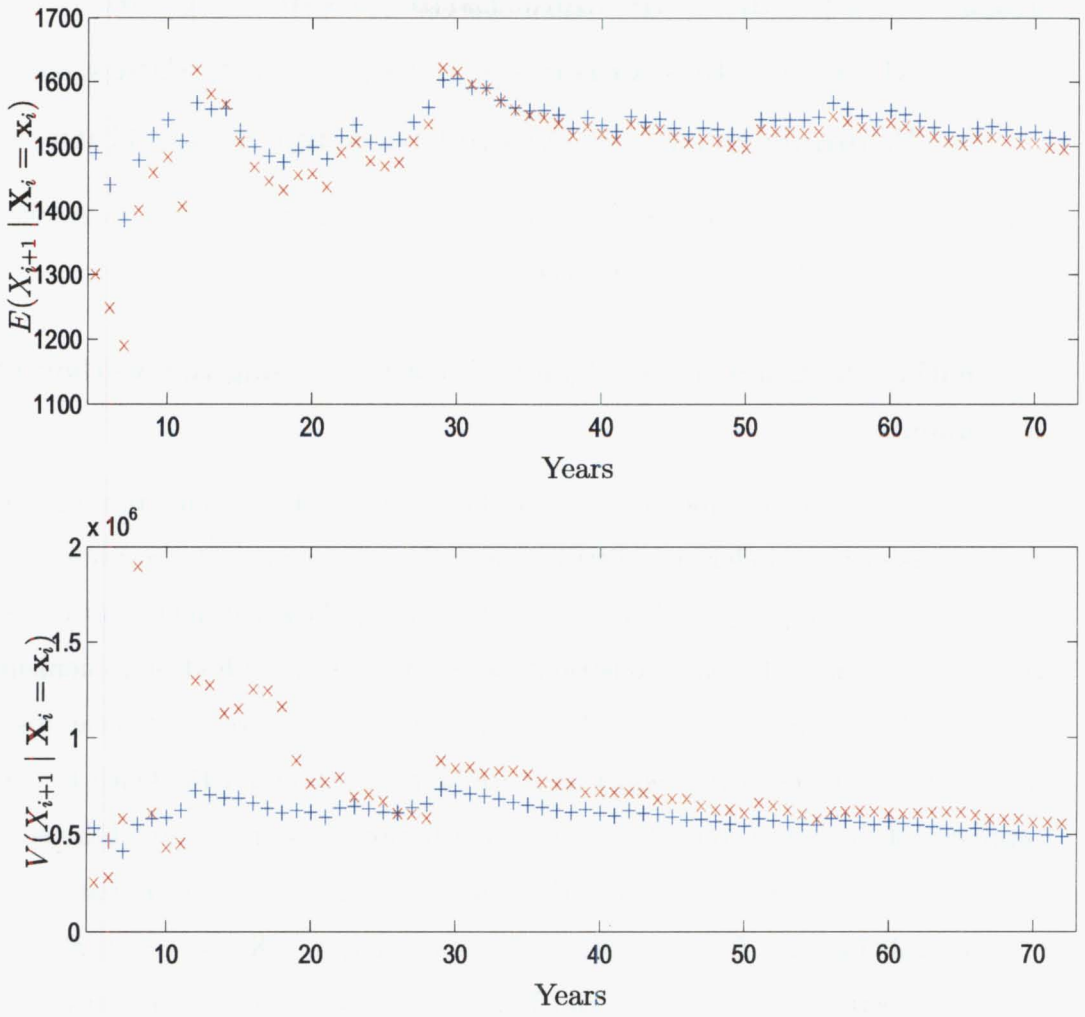


parameters $\xi$, $\alpha$ and $k$, are the same as those defined as in Section 4.4. They are displayed in the column of Table 4.5 headed "GEV". The updated predictive mass function is used to calculate the expectation and variance of $X_{i+1} \mid (\mathbf{X}_i = \mathbf{x}_i)$, as detailed in Section 2.2 of Chapter 3.

**Results**

Forecasts $E(X_{i+1} \mid \mathbf{X}_i = \mathbf{x}_i)$ and $V(X_{i+1} \mid \mathbf{X}_i = \mathbf{x}_i)$ were computed for both the digital and frequentist cases, for $i \geq 4$. In the upper panel of Figure 4.5.2 the sequence of updated conditional expectations are displayed. The subjectivist forecasts are represented by blue "+" and the frequentist forecasts are represented by red "×". The lower panel of Figure 4.5.2 displays the sequence of updated

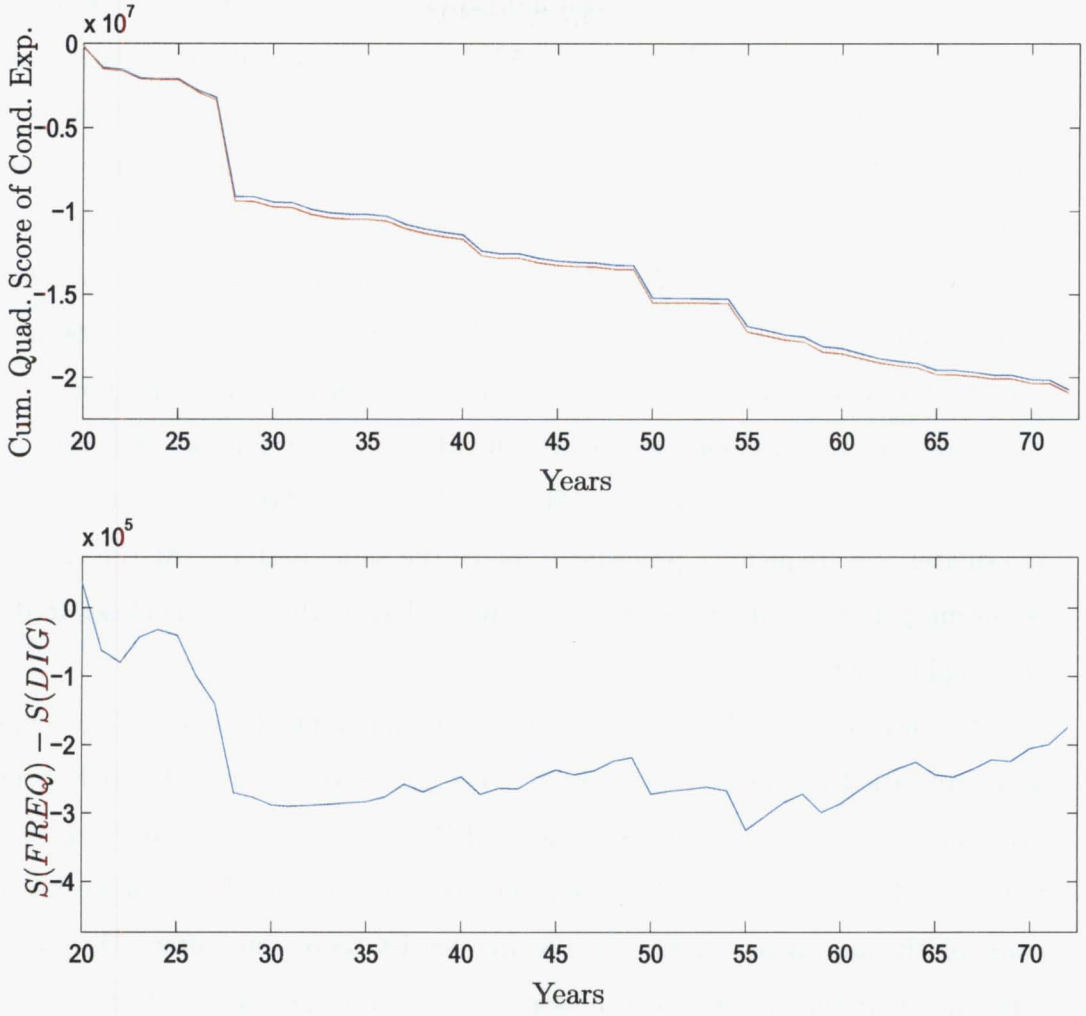


**Figure 4.15: Sequential cumulative quadratic score of the conditional expectation for digital (blue) and frequentist (red) forecasts (upper panel). The lower panel displays the difference between the forecasts.**

conditional variances. Notice that for both items the frequentist estimates are much more varied at the start, when each new observation has a greater influence on the parameter estimates. For example, notice how the frequentist variance increased in the $8th$ year, after being influenced by (what was at that stage) the highest AMS recorded value of $2660m^3/sec$. Forecasts for both procedures stabilise toward the same value, although even after 72 observations they are still noticeably different.

The sequential quadratic scores of the conditional expectation are displayed in Figure 4.15. The upper panel displays the cumulative sum of individual scores, starting at year 20. The digital forecast is displayed in blue and the frequentist

forecast in red. Remember that each individual score is the difference between the assessed expectation and the observed AMS value. By viewing the upper panel of Figure 4.1 and the upper panel of Figure 4.5.2, and squaring the distance between observation $X_{i+1}$ and forecast $E(X_{i+1} \mid \mathbf{X}_i = \mathbf{x}_i)$ we get an idea of the quadratic score for any particular observation. For example, notice there is a big jump in the cumulative score for $E(X_{28} \mid \mathbf{X}_{27} = \mathbf{x}_{27})$. If we look at Figure 4.1 we can see that the observed maximum flow in 1957 (the 28th year on record) is $3990m^3/sec.$ The digital conditional expectation for the instantaneous maximum flow in 1957 was approximately $1560m^3/sec.$ Consequently, the score for the $28th$ year is approximately $-6,000,000$ (from $-(3990-1560)^2$). The scores of the expectations of the digital and frequentist procedures follow the same pattern. At the end of the recording period the digital score is marginally larger, that is, it is closer to 0, and thus slightly better.

The lower panel of Figure 4.15 displays the difference between the cumulative scores recorded by the two procedures. The scores of the digital and frequentist procedures are denoted "S(DIG)" and "S(FREQ)" respectively. We can see that until the $30th$ value of the AMS sequence is recorded, the digital score has been consistently improving relative to the frequentist score, but after this point the difference between the scores stabilises. There is a suggestion that after the $60th$ year the frequentist forecast scores slightly better than the digital forecast.

If we had have started scoring earlier than the $20th$ year, then the difference between the cumulative scores would have been greater, as a study of the forecast expectations in Figure 4.5.2 and the actual outcomes in Figure 4.1 shows.

The sequential quadratic scores of the conditional variance are displayed in Figure 4.16. The upper panel displays the cumulative sum of individual scores, starting in the $20th$ year. The lower panel of Figure 4.16 displays the difference between the cumulative scores. Observe that the scores have approximately the same shape, but the difference between the scores continues to increase as the number of observations increases. Clearly the digital procedure produces a better overall score. The conclusion we can take from Figures 4.15 and 4.16 is that the frequentist and digital procedures do a similar job of assessing conditional expectation, but the digital procedure is much better at assessing conditional variance.

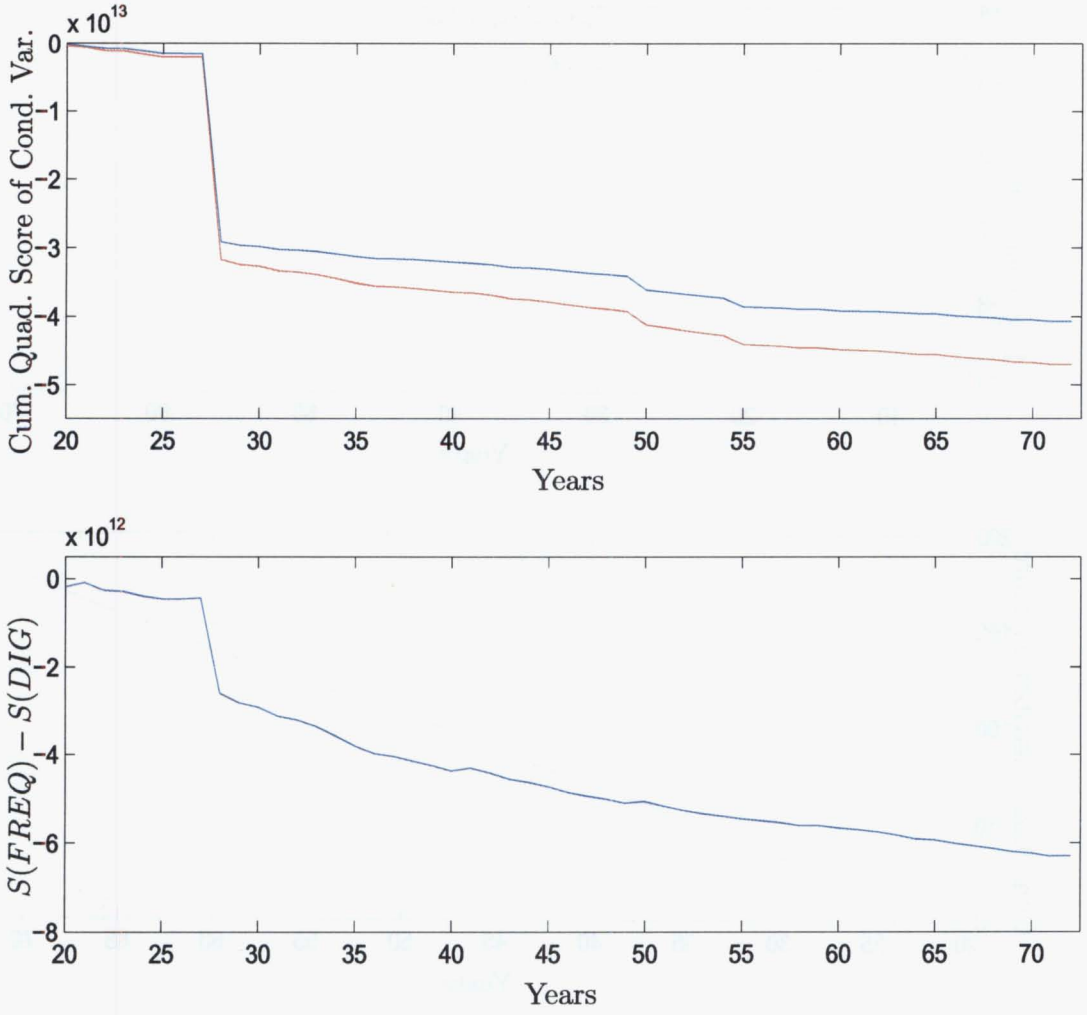


**Figure 4.16: Sequential cumulative quadratic score of the conditional variance for digital (blue) and frequentist (red) forecasts (upper panel). The lower panel displays the difference between the forecasts.**

Now that we have detailed the scores of the conditional expectation and variance, we shall briefly consider the logarithmic score of the forecasting distributions. Remember that after each new observation is recorded, we can use the method of L-moments to re-estimate the parameters of the GEV distribution and thus construct the probability density function. After digitising the density over $\mathbf{R}(X)$, we can find the logarithmic score of the forecasting distribution of $X$ using Equation 4.35.

The logarithmic score for the sequential forecasting distributions are displayed in Figure 4.17. The upper panel displays the individual scores from the $5th$ year

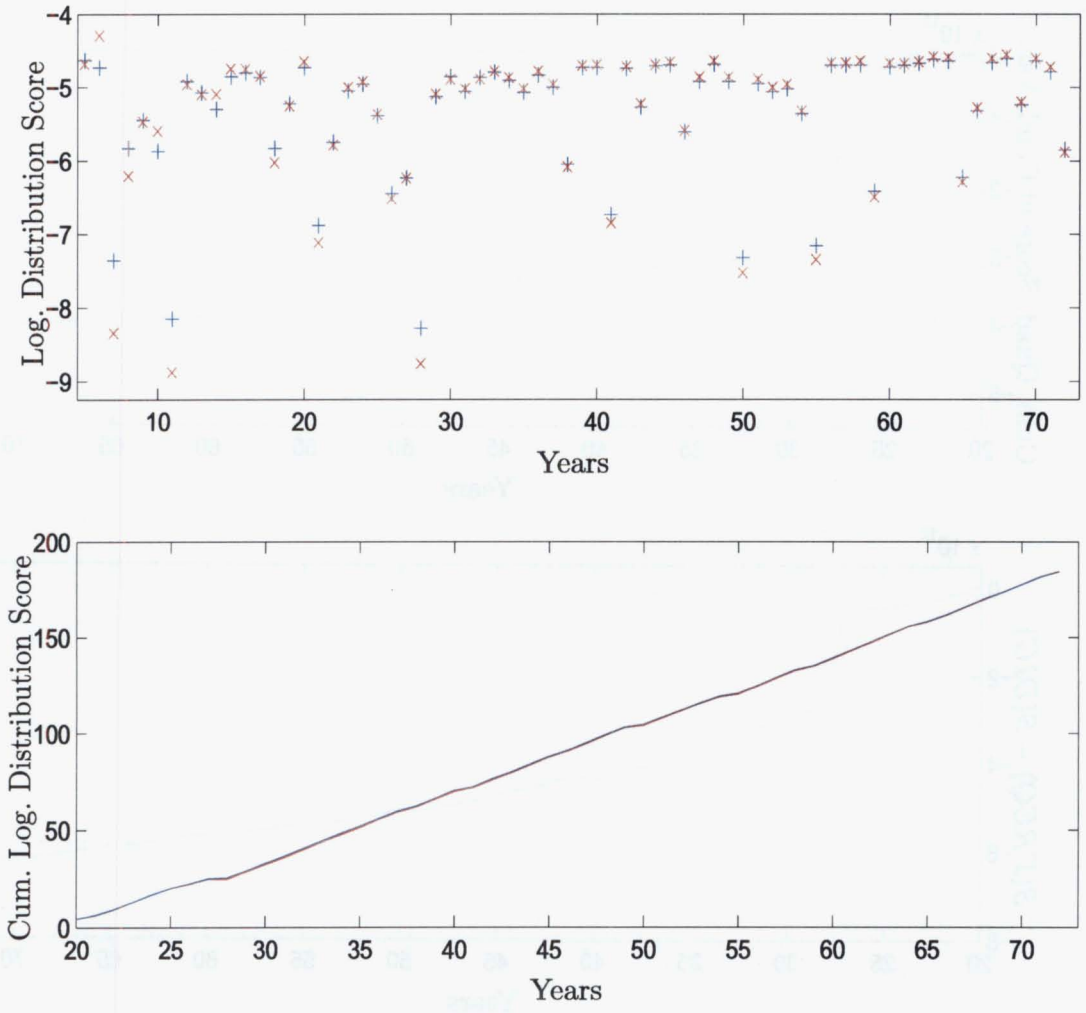


**Figure 4.17: Sequential individual (upper panel) and cumulative (lower panel) logarithmic score of a distribution for digital (blue) and frequentist (red) forecasts. The cumulative scores are almost indistinguishable.**

onwards. The lower panel displays the cumulative scores, where scoring starts in the $20th$ year. In the lower panel the cumulative scores are shown as the difference between the recorded score and $-8.85$, the minimum score achieved by any value after the $20th$ year. Displaying scores in this way means that, as usual, the larger the score is, the better. At this scale the different cumulative scores are indistinguishable.

There is little difference between the cumulative scores, although the updated mixture mass forecasting procedure is slightly better, with a score of 184.5. The frequentist procedure scored 184.2. If we had have started cumulatively scoring earlier, there would be a bigger difference between the scores — in particular see

the individual scores for years 7 and 11.

Now that we have compared scores from a real data set, we shall use a Monte Carlo procedure to compare scores from a simulated data set.

### 4.5.3 Comparing L-moment Estimates and Updated Mixture Mass Forecasts using Scoring Rules for Data Generated from a Generalised Extreme Value Distribution

We shall use a Monte Carlo procedure to compare forecasts made using L-moment estimates against forecasts achieved via updated mixture mass functions. The Monte Carlo procedure consists of two parts. First we simulate AMS data for a large number of sites. Then we score each site's data and analyse the results.

Data was simulated as in Section 4.3.7. The data was generated from a GEV distribution with $E(X) = 2$, $CV = 0.5$ and $k = -0.14$. These are the same conditions that we used in Section 4.3.7 when simulating data from site 11 of a region with median $CV$ of 0.5. We simulate data from 10,000 sites, each of which has 100 years of recorded AMS values.

Forecasts are made using L-moment estimates in the manner described in Section 4.5.2. Forecasts are achieved via updated mixture mass functions as described in Section 4.5.2. The digital forecasting procedure requires that we specify the realm of $X$, and the realms of the characterising parameters of the GEV distribution, $\xi$, $\alpha$ and $k$, before any calculations can take place. The realms we use are listed in the column of Table 4.7 headed "At-site". The conditional mass functions, $f(\xi \mid \alpha, k)$ and $f(\alpha \mid k)$, and the marginal mass function $f(k)$, were defined to be Uniformally distributed over their realm.

Sequential quadratic scores of conditional expectation and variance were calculated for every site, starting at the $20th$ year. The mean of the cumulative scores of the conditional expectation are displayed in the upper panel of Figure 4.18. As usual, the larger the score the better and because the quadratic score is the negative of the squared difference, the closer the score is to 0 the better. The difference between the cumulative scores is displayed in the lower panel of Figure 4.18. It is clear

| $CV$ | | At-site | | | Regional | | | | | |
|---|---|---|---|---|---|---|---|---|---|---|
| | | | | | I | | | II | | |
| | | Min | Inc | Max | Min | Inc | Max | Min | Inc | Max |
| 0.5 | $X$ | 0 | 0.05 | 20 | 0 | 0.05 | 20 | 0 | 0.05 | 20 |
| | $\xi$ | 0.975 | 0.075 | 1.5 | 0.5 | 0.025 | 0.7 | 0.975 | 0.075 | 1.5 |
| | $\alpha$ | 0.75 | 0.1 | 1.45 | 0.4 | 0.025 | 0.6 | 0.75 | 0.1 | 1.45 |
| | $k$ | -0.375 | 0.025 | -0.025 | -0.375 | 0.025 | -0.025 | -0.375 | 0.025 | -0.025 |
| 1 | $X$ | 0 | 0.05 | 20 | 0 | 0.05 | 20 | 0 | 0.05 | 20 |
| | $\xi$ | 0.6 | 0.05 | 1.3 | 0.3 | 0.05 | 0.7 | 0.6 | 0.05 | 1.3 |
| | $\alpha$ | 0.6 | 0.05 | 1.3 | 0.45 | 0.025 | 0.65 | 0.6 | 0.05 | 1.3 |
| | $k$ | -0.375 | 0.025 | -0.025 | -0.375 | 0.025 | -0.025 | -0.375 | 0.025 | -0.025 |

**Table 4.7: Elements of realms used in digital computations. "Min" and "Max" denote the smallest and largest elements of the realm. "Inc" denotes the increment between successive elements. "I" and "II" refer to the two different stages in the regional procedure.**

that as the number of observations increases, the mixture mass forecast is increasingly better than the frequentist forecast, although the rate of increase is slowing. However, after 100 observations the mean difference between the two scores is only just above 4, out of a total score of approximately -320. Thus, although the score achieved by the digital procedure is better, both scores are still relatively similar.

Figure 4.19 demonstrates how the difference between the scores of the conditional expectation for the two forecasting procedures develops as the number of recorded observations increase. The biggest difference between the two scores, at the end of the recording period, is 92.7. For clarity, we have only displayed scores for which $-16 < (S(DIG) - S(FREQ)) < 24$. The top panel displays the difference in cumulative scores after the $20th$ observation. As this is the first observation to be scored, it is hardly surprising that there is little to separate the cumulative scores at this stage. The second panel displays the difference between the cumulative scores after 30 observations. We can see that the digital forecasts are beginning to have better scores. This trend continues in the third and forth panels, which correspond to the difference between the cumulative scores after 50 and 100 observations. As more

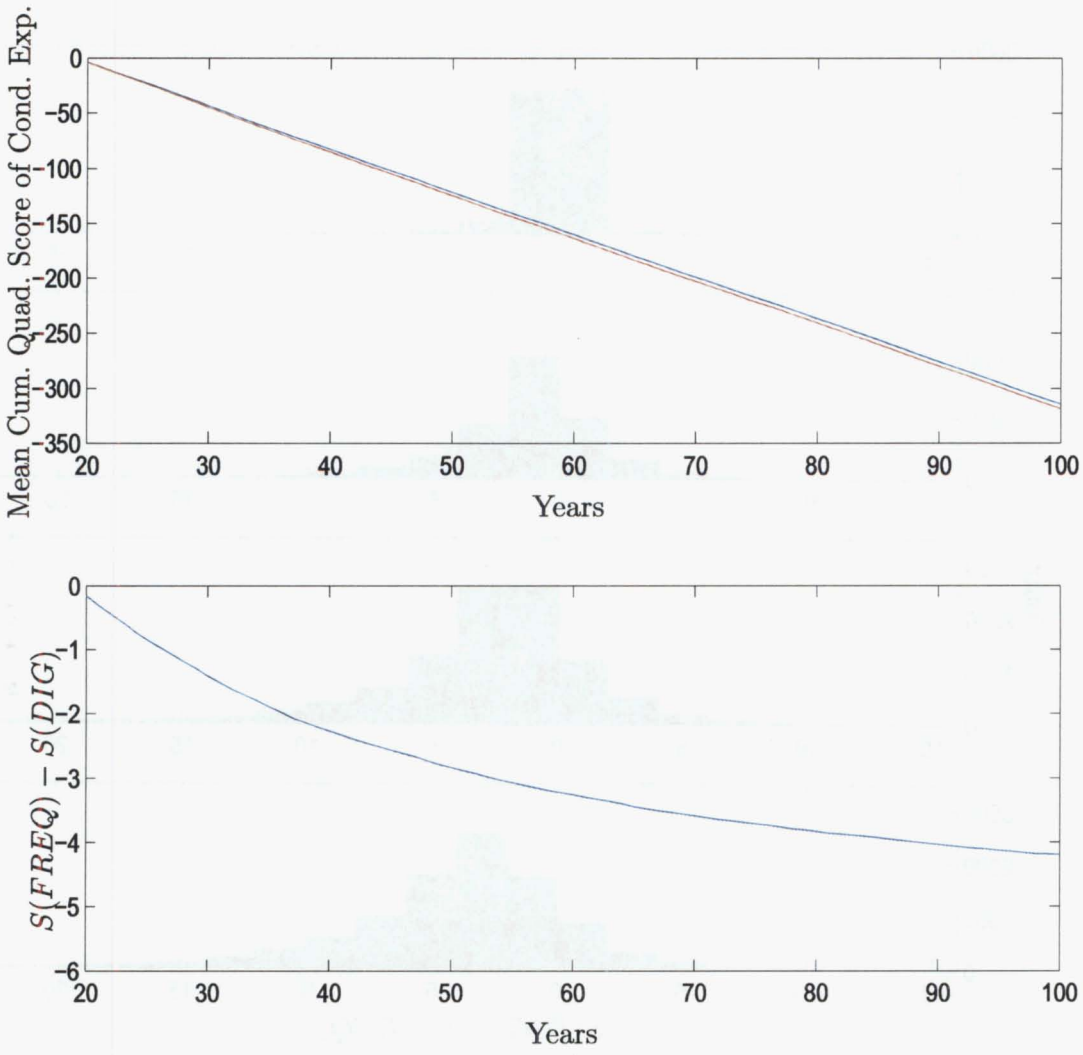


**Figure 4.18: Sequential mean cumulative quadratic score of the conditional expectation for digital (blue) and frequentist (red) forecasts (upper panel). The lower panel displays the difference between the forecasts.**

observations are scored, the average difference between the two procedures continues to increase, reinforcing the conclusion the mixture mass forecast is increasingly better than the frequentist forecast

Figure 4.20 displays the difference between the median cumulative quadratic scores of the conditional variance for the simulated region. The first observation scored was the $20th$. Notice that on this occasion we consider the median cumulative score rather than the mean cumulative score. This is because, as Equation 4.14 shows, one component of the variance of the GEV distribution is $\Gamma(1+2k)$. On rare occasions the L-moment estimate of the shape parameter, $k$, is very close to

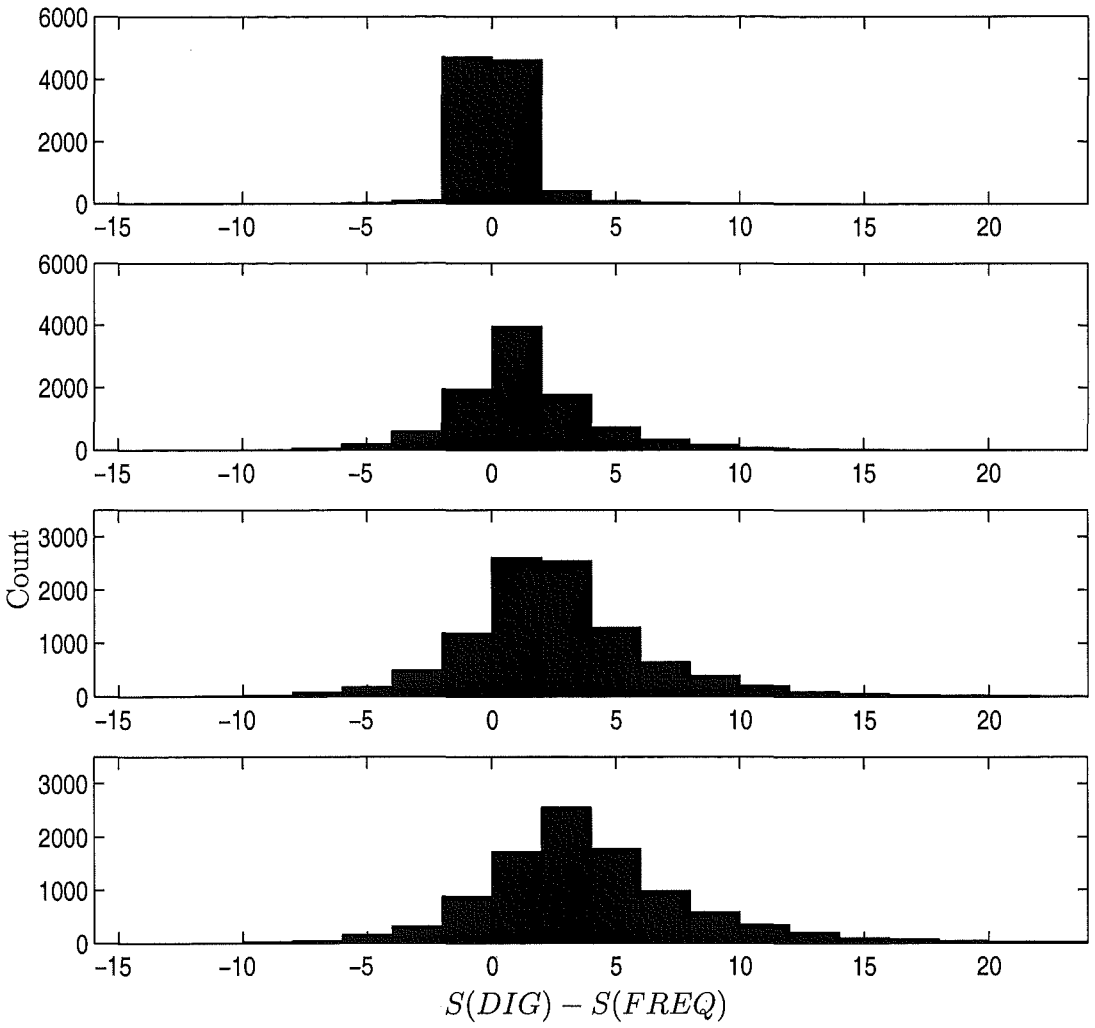


**Figure 4.19: Difference between mean cumulative quadratic scores of the conditional expectation after 20, 30, 50 and 100 observations.**

$-0.5$. When this happens the estimated value of $V(X)$ can become extremely large, since $\Gamma(\theta)$ increases rapidly as $\theta$ gets close to 0. Consequently, in this case it is more appropriate to compare the medians than the means.

The upper panel of Figure 4.20 shows that the digital forecast of the conditional variance scores significantly better than the frequentist forecast. The lower panel shows that the digital forecast continues to improve against the frequentist forecast. As with the Waimakariri River AMS data, both procedures score similarly for their forecasts of conditional expectation, but the updated mixture mass functions are considerably better at assessing conditional variance.

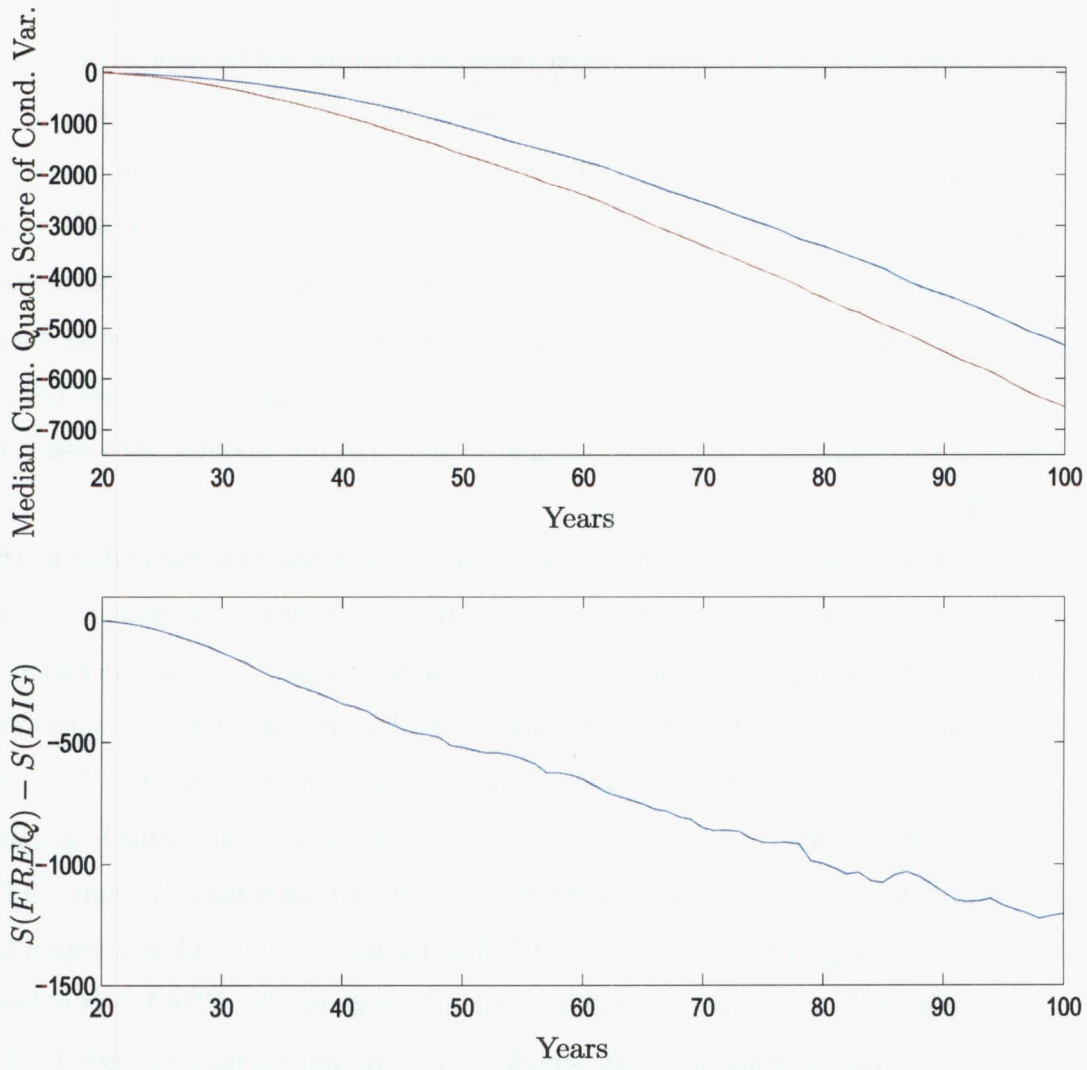


**Figure 4.20: Sequential median cumulative quadratic score of the conditional variance for digital (blue) and frequentist (red) forecasts (upper panel). The lower panel displays the difference between the forecasts.**

### 4.5.4 Comparing L-moment Estimates and Updated Mixture Mass Forecasts using Frequentist Measures for Data Generated from a Generalised Extreme Value Distribution

In Section 4.3 we used conventional frequentist techniques to find point estimates of the characterising parameters of distributions commonly used in the study of flood frequency analysis. These point estimates were then used to estimate flood exceedance quantiles. Estimates were calculated for both at-site and regional cases.

The appropriateness of the frequentist estimates was judged by comparing the bias (a measure of accuracy) and root mean-squared-error (a measure of precision) for a particular site. The site was the 11th site of a 21 site region. The region was simulated to have sites of varying length, skewness and $CV$. Data was generated using a GEV distribution. In Section 4.4 we constructed and implemented a digital updating procedure. This was used to score sequential forecasting methods for an analysis which involved sequences of observations regarded exchangeably. We conclude this Section by comparing frequentist estimates and digitally updated forecasts under objectivist criteria.

We shall compare four quantile approximation methods: two frequentist methods and two digital forecasting methods. A Monte Carlo method was used to compare the four procedures. The comparison consists of two parts: data generation and method testing. The data was generated according to the procedure specified in Section 4.3.7. The same four regions are used, each comprising 21 sites. Site record lengths range from 10 years, at site 1, to 30 years, at site 21. Data is generated from an EV2 distribution. The skewness of the data ranges linearly from $-0.17$ to $-0.11$ depending on the length of record. The median $CV$ of sites in a region is set to be either 0.5 or 1.0. The normalised regional range in $CV$, $R^*(CV)$, is either 0.3 or 0.5. For this experiment 50,000 simulated regions were generated. See Table 4.4 for a summary of the regions used in the Monte Carlo experiments.

Forecasts of exceedance quantiles were obtained using four methods. Frequentist and digital measures were calculated using both at-site and regional procedures. The frequentist at-site method used is described in Section 4.3.5. The frequentist regional method used is the index flood method, which was described in Section 4.3.5. Digital forecasts are also computed at-site and regionally. The at-site digital forecast is found by updating mixture mass functions as sequential forecasting distributions, as detailed in Section 4.4.3. The procedure used to forecast regional digital exceedance forecasts is:

1. Normalise the data from each site in a region by the at-site mean.

2. Pool the normalised data and treat it as a series of observations from a super-site.

3. Calculate the marginal mass function from the observations in the super-site.

4. Forecast the at-site exceedance quantiles, using $f(k)$ as the prior mass function for $k$.

This is essentially a digital version of the hierarchical regionalisation method proposed in Section 4.3.5.

The digital forecasting procedures require that the realms of $X$, $\xi$, $\alpha$ and $k$, are specified before any computations can commence. The specified realms are listed in Table 4.7. The regional updating procedure requires that parameters are defined to have different realms at each of the two stages. This is due to the use of scaled data in the approximation of $f(k)$. $\mathbf{R}(k)$ is the same for both stages. As previously mentioned, scaling the data by its mean has no effect of the distribution's shape. The second stage sees a reversion to the realms used in the at-site updating procedure. This is because we are merely repeating the at-site procedure with an updated $f(k)$ mass function. It eventuates that the ranges of $\mathbf{R}(\xi)$ and $\mathbf{R}(\alpha)$ have little effect on the exceedance quantile forecasts. For both the at-site and regional updating procedure, the conditional mass functions, $f(\xi \mid \alpha, k)$ and $f(\alpha \mid k)$, and the marginal mass function $f(k)$, were defined to be Uniformally distributed over their realm.

The at-site estimates should be the same for any $(M(CV), R^*(CV))$ combination containing the same $M(CV)$ value. For example, at-site estimates of combinations $(0.5, 0.5)$ and $(0.5, 0.3)$ should have the same bias and RMSE. This is because the only data used in an at-site estimate comes from the site itself, in this case Site 11, which is not effected by different $R^*(CV)$ measures. The data at Site 11 is generated from a GEV distribution with parameters $\xi = 1.08$, $\alpha = 1.25$ and $k = -0.14$. The differences in the regional results are due to the effect of heterogeneity in the region.

### Results

The bias and RMSE for the 11th site of the 21 site region for the $(M(CV), R^*(CV))$ combinations $(0.5, 0.5)$ and $(0.5, 0.3)$ are displayed in Figure 4.22. The upper panel displays $(M(CV), R^*(CV)) = (0.5, 0.5)$ and the lower panel displays $(M(CV), R^*(CV)) = (0.5, 0.3)$.

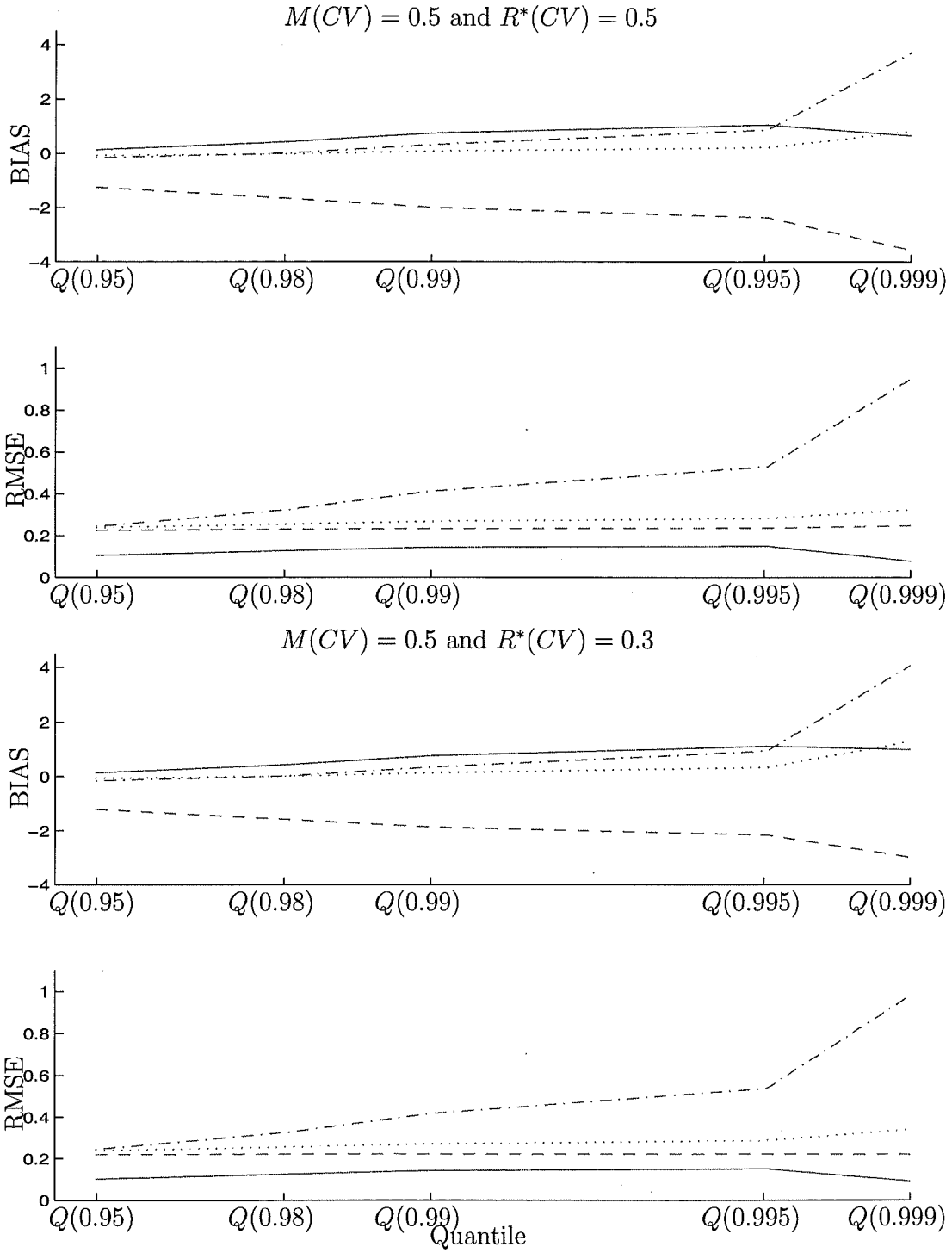


**Figure 4.21: Root-mean-squared error and bias for site 11 of a 21 site region. Methods are digital at-site (—), frequentist at-site (-.-.), digital regional (–) and frequentist regional (...). The upper panel shows $(M(CV), R^*(CV)) = (0.5, 0.5)$, the lower panel shows $(0.5, 0.3)$.**

| $min(\mathbf{R}(k))$ | -0.01 | -0.03 | -0.05 | -0.07 | -0.09 | -0.11 | -0.13 |
|---|---|---|---|---|---|---|---|
| $Q_{20}$ | 5.31 | 5.34 | 5.39 | 5.46 | 5.54 | 5.65 | 5.77 |

**Table 4.8: Estimates of $Q(0.95)$ obtained via the digital regional forecast, for different $\mathbf{R}(k)$. $(M(CV), R^*(CV)) = (0.5, 0.5)$. In each case $max(\mathbf{R}(k)) = -0.35$ and elements increment in steps of 0.02. The experiment is designed to generate data so $Q(0.95) = 5.67$**

The RMSE and bias estimates appear very similar for both different values of $R^*(CV)$. For both cases the digital at-site forecast appears to be the best of the four methods. Despite the sizeable bias values, the root-mean-squared error is considerably lower than for either of the frequentist estimates. The frequentist regional estimate procedure appears relatively unbiased but inefficient. A surprising result is the large negative bias shown by the regional digital forecast. On closer investigation the quantile forecasts obtained through the use of the regional digital procedure are highly dependent on the range of $\mathbf{R}(k)$. Table 4.8 demonstrates that the marginal mass function of $k$ computed in the first stage of the regional procedure places more mass on the smaller elements of $\mathbf{R}(k)$ then expected. It would be interesting to see if this happens for all $(\xi, \alpha)$ values, or whether the estimation improves as $\xi$ or $\alpha$ increase.

The bias and RMSE for the 11th site of the 21 site region for the $(M(CV), R^*(CV))$ combinations, $(1, 0.5)$ and $(1, 0.3)$, are displayed in Figure 4.23. The upper panel displays $(M(CV), R^*(CV)) = (1, 0.5)$ and the lower panel displays $(M(CV), R^*(CV)) = (1, 0.3)$. For both combinations the digital at-site forecast has the lowest bias and lowest RMSE. One possible reason for the improvement of the digital forecasts, relative to the frequentist estimates, is that the distribution the data were generated from is more severely truncated when $M(CV) = 1$ then it is when $M(CV) = 0.5$, consequently the frequentist methods are attempting to fit parameters to a distribution using GEV L-moment estimates, when the distribution does not have a GEV shape at all.

The digital regional forecast still has a large negative bias, but the bias is relatively stable for different return periods, especially compared to the frequentist quantile estimates. In all four cases the digital regional forecast has the second

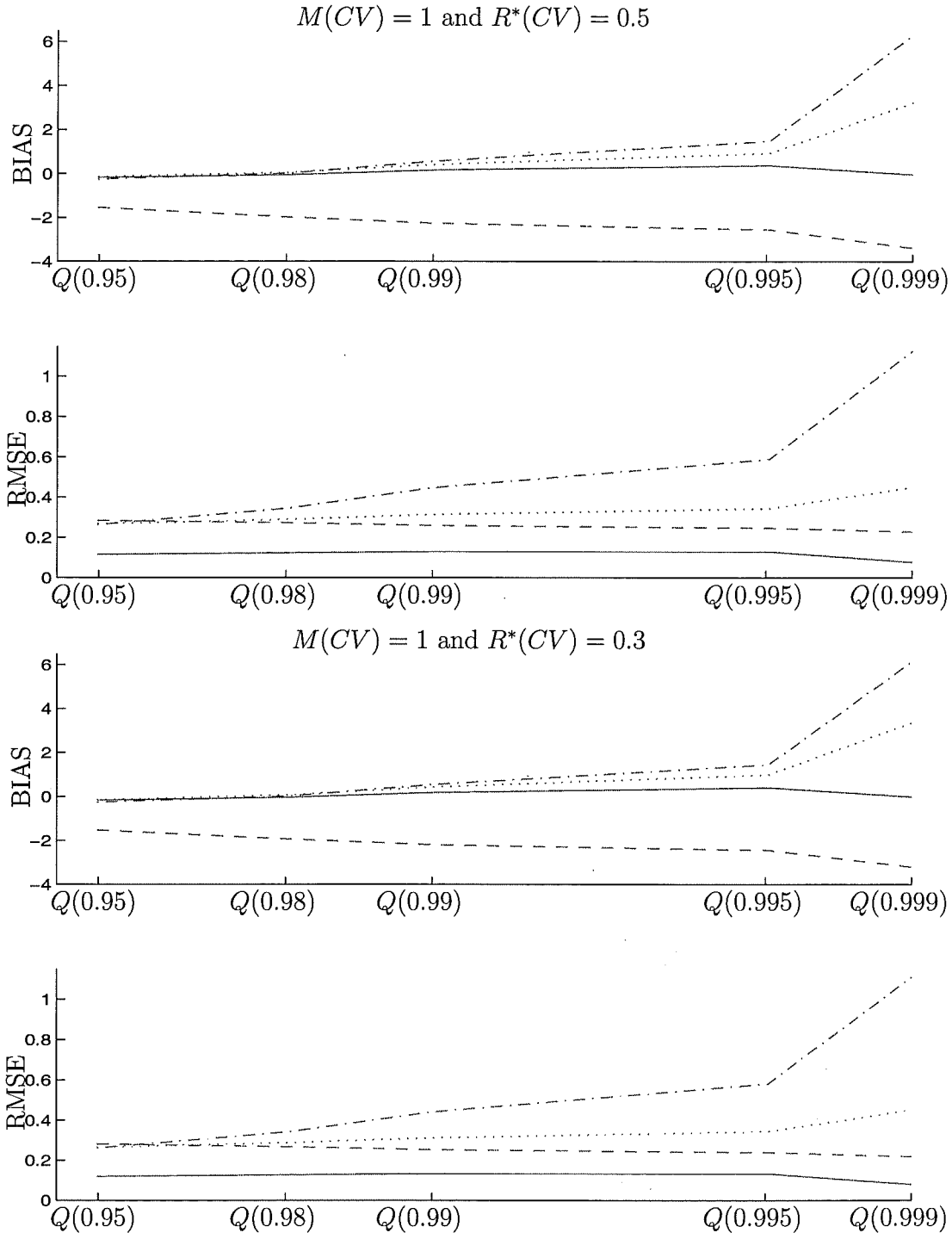


**Figure 4.22: Root-mean-squared error and bias for site 11 of a 21 site region. Methods are digital at-site (—), frequentist at-site (-.-.), digital regional (–) and frequentist regional (...). The upper panel shows $(M(CV), R^*(CV)) = (1, 0.5)$, the lower panel shows $(1, 0.3)$.**

lowest RMSE, suggesting that there could be some way of finding a better performing estimate. Possible alternative procedures for implementing a regional digital updating procedure would be:

- Scale all the data by its at-site mean. Treat these observations as coming from a 'super-site'. Calculate quantile forecasts and rescale.
- Calculate mass functions $f(\xi \mid \alpha, k)$, $f(\alpha \mid k)$ and $f(k)$ at sites 1–10 and 12–21. Combine these mass functions using a weighted average. Consider the new combined mass functions as prior mass functions and conduct the at-site procedure at site 11.

A considerable advantage that the digital procedure has over frequentist measures is that the digital procedure can begin in the first period, and advance sequentially as data is recorded. Conversely, the frequentist estimates rely on gathering a sizeable data set before quantile estimates can be calculated, hence the motivation of regionalisation techniques.

## 4.6 Summary

This Chapter has focussed on flood frequency analysis, and in particular on the estimation of flood quantile levels. Our problem of characterising extreme floods was introduced in Section 2. We described river flow measurement procedures, paying particular interest to the Waimakariri River. In Section 3, conventional frequentist estimates were calculated for the Waimakariri River. A Monte Carlo procedure was used to compare different estimation methods in terms of accuracy and precision, for an experimental data set. In Section 4 a procedure for scoring sequential forecasts using digitised mass functions was developed. This procedure is based on the work developed in Chapter 3. Different scoring rules were examined using a sequence of annual maximum river flows from the Waimakariri River. Finally, we compared the appropriateness of the frequentist and digital procedures using both subjective and objective techniques. The scores of conditional expectations of both procedures were similar, but the score of the conditional variance was much better for the updated mixture forecasts. When objectivist measures were considered, the mixture

distributions computed via the discrete digital method provide forecasts with lower root mean-squared-error. This is despite the fact that when the coefficient of variation is small the digital methods are more biased than the frequentist methods. As the coefficient of variation increases, the accuracy of the digital methods improves rapidly, even reducing the bias.

# Chapter 5

# Summary

This Thesis has detailed three studies of numerical approximation. We began with a brief introduction to recent developments in numerical methods, particularly as applied to Bayesian theory. The importance of evaluating, often analytically intractable, posterior integrals was discussed, underlining the importance of quick and accurate numerical integration techniques. Non-Monte Carlo, non-iterative Monte Carlo and iterative Monte Carlo methods were discussed, and the most important numerical integration methods of each type outlined.

Chapter 2 was concerned with the resolution of a specific electrical engineering problem. Essentially, the problem involved calculating the probability that the sum of the product of variables assessed with a Normal distribution is negative. First the distribution of the product of two Normally distributed variables, $Y = X_1X_2$, was assessed. Craig (1936) was the first to determine the algebraic form of the moment-generating function of the product of two Normally distributed variables. Cornwell et al. (1978) described the numerical evaluation of this product. We found $f(y)$ by outlining a simple numerical integration procedure, which involved the joint distribution of $Y$ and $X_2$. We discovered $f(y, x_2)$ has a simple singularity at $(0, 0)$, and discussed the implications pertaining to the numerical integration. The numerical integration was implemented via MATLAB and Maple subroutines, eliminating the need for evaluation via statistical tables. New graphics were presented to aid understanding of the shape of the distribution $Y$. We undertook a specific analysis of the skewness of the product of two Normally distributed variables when the multiplicands are correlated. The second step of the problem involved assessing the

distribution for the sum of a number of these products of Normally distributed variables, $Z = Y_1 + \ldots + Y_j$. A computational procedure for approximating the required distribution was developed using a numerical evaluation of convolution theory. The mass function resulting from the implementation of this procedure was an approximation of $f(z)$.

Chapter 3 investigated how well continuous conjugate theory approximates real discrete mass functions in various measurement settings. We examined how well digital Normal mass functions and digital parametric mixtures are approximated by continuous Mixture Normal and Normal-Gamma Mixture Normal distributions for such items as $E(X_{i+1} \mid \mathbf{X}_i = \mathbf{x}_i)$ and $V(X_{i+1} \mid \mathbf{X}_i = \mathbf{x}_i)$. Bayes' Theorem was used to compute posterior mass functions; approximating posterior densities were evaluated using continuous conjugate theory. The two sets of results were compared. The main achievement of this Chapter was to formalise a computing strategy that can be applied to problems with prior mixture mass functions and information transfer functions of many functional forms in the context of real discrete measurements. An example of a useful application was presented in Chapter 4.

The problem of estimating the return period of extreme flood events was considered in Chapter 4. The computing strategy detailed in Chapter 3 was adapted for use in the assessment of flood exceedance quantiles using updated mixture mass functions as sequential forecasting distributions. A procedure for scoring these sequential forecasts was developed. Conventional frequentist estimates of exceedance quantiles were obtained. Although the two methods of estimation used are fundamentally different, we compared the results of the two procedures. First, we compared various scores achieved by sequential forecasts. A second comparison was undertaken using objectivist criteria. We compared accuracy and precision using bias and root mean-squared-error. We found the mixture distributions computed via the discrete digital method performed better under both criteria. In particular they provide for a much more realistic assessment of the variance of our uncertain forecasting distribution.

Numerical approximation allows almost unlimited scope for realistic statistical modeling. The rapid advance of computing power allows us to approach problems in ways that have previously only been theorised. The content of this Thesis has

involved constructing tools for use in different numerical approximation scenarios. We have shown that the specific characteristics of the problem define which different method of numerical approximation is appropriate.

# References


Aroian, L. A. (1947). The Probability Function of a Product of Two Normally Distributed Variables. *Ann. Math. Statist.*, 18:265–271.

Aroian, L. A., Taneja, V. S., and Cornwell, L. W. (1978). Mathematical Forms of the Distribution of the Product of Two Normal Variables. *Commun. Statist.-Theor. Meth.*, 7(2):164–172.

Berger, J. O. (2000). Bayesian Analysis: A Look at Today and Thoughts of Tomorrow. *J. Amer. Statist. Assoc.*, 95:1269–1276.

Brooks, S. P. and Roberts, G. (1998). Assessing Convergence of Markov Chain Monte Carlo Algorithms. *Statistics and Computing*, 8:319–335.

Connell, R. J. and Pearson, C. P. (2001). Two-component extreme value distribution applied to Canterbury annual maximum flood peaks. *Journal of Hydrology (NZ)*, 40(2):105–127.

Conradie, W. and Gupta, A. (1987). Quadratic Forms in Complex Normal Variates: Basic Results. *Statistica*, 47:73–84.

Cornwell, W., Aroian, L. A., and Taneja, V. S. (1978). Numerical Evaluation of the Distribution of the Product of Two Normal Variables. *J. Statist. Comput. Simul.*, 7:123–131.

Craig, C. C. (1936). On the Frequency Function of $xy$. *Ann. Math. Statist.*, 7:1–15.

Dalrymple, T. (1960). Flood Frequency Analysis. Technical Report Water Supply Pap., 1543-A, U.S. Geol. Surv.

Fisher, R. A. (1925). *Statistical Methods for Research Workers.* Edinburgh: Oliver and Boyd.

Fisher, R. A. and Tippett, L. H. C. (1928). Limiting Forms of the Frequency Distribution of the Largest r Smallest Member of a Sample. *Proceedings of the Cambridge Philosophical Society*, 24:180–190.

Gabriele, S. and Arnell, N. (1991). A Hierarchical Approach to Regional Flood Frequency Analysis. *Water Resour. Res.*, 27(6):1281–1289.

Gelfand, A. E., Hills, S., Racine-Poon, A., and Smith, A. F. M. (1990). Illustration of Bayesian inference in normal data models using Gibbs sampling. *J. Amer. Statist. Assoc.*, 85:972–982.

Geman, S. and Geman, D. (1984). Stochastic relaxation, Gibbs distributions and the Bayesian restoration of images. *IEEE Trans. Pattern Anal. Mach. Intell.*, 6:721–741.

Gilks, W., Richardson, S., and Spiegelhalter, D., editors (1996). *Markov Chain Monte Carlo in Practice.* Chapman & Hall.

Greenwood, J. A., Landwehr, J. M., Matalas, N. C., and Wallis, J. R. (1979). Probability Weighted Moments: Definition and Relation to Parameters of Several Distributions Expressed in Inverse Form. *Water Resour. Res.*, 15:1049–1054.

Greis, N. P. and Wood, E. F. (1981). Regional Flood Frequency Estimation and Network Design. *Water Resour. Res.*, 17:1167–1177.

Griffin, A. (2000). *Coding CPFSK for differential demodulation.* PhD thesis, University of Canterbury.

Hastings, W. K. (1970). Monte Carlo sampling methods using Markov chains and their applications. *Biometrika*, 57:97–109.

Hosking, J. R. M. (1990). L-moments: Analysis and Estimation of Distributions using Linear Combinations of Order Statistics. *J. R. Statist. Soc. B*, 52(1):105–124.

Hosking, J. R. M. and Wallis, J. R. (1987). Parameter and Quantile Estimation for the Generalised Pareto Distribution. *Technometrics*, 29:339–348.

Hosking, J. R. M. and Wallis, J. R. (1993). Some Statistics Useful in Regional Frequency Analysis. *Water Resour. Res.*, 29(2):271–281.

Hosking, J. R. M., Wallis, J. R., and Wood, E. F. (1985). Estimation of the Generalized Extreme-Value Distribution by the Method of Probability-Weighted Moments. *Technometrics*, 27:251–261.

Hoti, F. J., Sillanpää, M. J., and Holmström, L. (2002). A Note on Estimating the Posterior Density of a Quantitative Trait Locus From a Markov Chain Monte Carlo Sample. *Genetic Epidemiology*, 22:369–376.

Jenkinson, A. F. (1955). The Frequency Distribution of the Annual Maximum (or Minimum) of Meteorological Elements. *Journal of the Royal Meteorological Society*, 81:158–171.

Kjeldsen, T. R., Smithers, J. C., and Schulze, R. E. (2002). Regional flood frequency analysis in the Kagouls – Natal province, South Africa, using the index flood method. *J. Hydroa.*, 255:194–211.

Kroll, C. N. and Vogel, R. M. (2002). Probability distribution of low streamflow series in the United States. *Journal of Hydrologic Engineering*, 7:137–146.

Lad, F. (1996). *Operational Subjective Statistical Methods. A Mathematical, Philosophical and historical Introduction.* Wiley-Interscience.

Landwehr, J. M., Matalas, N. C., and Wallis, J. R. (1979). Probability Weighted Moments compared with some traditional techniques in estimating Gumbel parameters and quantiles. *Water Resour. Res.*, 15:1055–1064.

Lettenmaier, D. and Potter, K. W. (1985). Testing Flood Frequency Estimation Methods using a Regional Flood Generation Model. *Water Resour. Res.*, 21(12):1903–1914.

Lettenmaier, D. P., Wallis, J. R., and Wood, E. F. (1987). Effect of Regional Heterogeneity on Flood Frequency Analysis. *Water Resour. Res.*, 23(2):313–323.

Madsen, H., Pearson, C. P., and Rosbjerg, D. (1997). Comparison of Annual Maximum Series and Partial Duration Series Methods for Modeling Extreme Hydrologic Events. 2 Regional Modeling. *Water Resour. Res.*, 33(4):759–769.

McKerchar, A. I. and Pearson, C. P. (1990). Maps of Flood Statistics for Regional Flood Frequency Analysis in New Zealand. *Hydrological Sciences Journal*, 35(6):609–621.

Metcalfe, A. V. (1997). *Statistics in Civil Engineering.* Arnold.

Metropolis, N., Rosenbluth, A. W., Rosenbluth, M. N., Teller, A. H., and Teller, E. (1953). Equations of state calculations by fast computing machines. *J. Chem. Phys.*, 21:1087–1092.

Metropolis, N. and Ulam, S. (1949). The Monte Carlo method. *J. Amer. Statist. Assoc.*, 44:335–341.

Monahan, J. and Genz, A. (1996). A Comparison of Omnibus Methods for Bayesian Computation. *Computing Science and Statistics*, 27:471–480.

Mosley, M. P. (1981). Delimitation of New Zealand Hydrologic Regions. *J. Hydrol.*, 49:173–192.

Müller, P. (1993). *A generic approach to posterior integration and Gibbs sampling.* PhD thesis, Purdue University, West Lafayette, Indiana.

National Environment Research Council (1975). *Flood Studies Report, vol. 1.* London, U.K.

Park, J. S., Jung, H. S., Kim, R. S., and Oh, J. H. (2001). Modelling summer extreme rainfall over the Korean peninsula using Wakeby distribution. *Int. J. Climatol.*, 6(5):1371–1384.

Pearson, C. P. (1991). Regional Flood Frequency Analysis for Small New Zealand Basins. *Journal of Hydrology (N.Z.)*, 30(2):77–92.

Pearson, C. P. (1993). Application of L Moments to Maximum River Flows. *New Zealand Statistician*, 28(1):2–10.

Rand Corporation (1955). *A Million Random Digits with* 100,000 *Normal Deviates.* The Free Press, Glencoe, Ill., U.S.A.

Robert, C. P. (2001). *The Bayesian Choice: Second Edition.* Springer.

Robert, C. P. and Casella, G. (1999). *Monte Carlo Statistical Methods.* Springer.

Scott, D. W. (1985). Averaged shifted histograms: effective nonparametric density estimators in several dimensions. *Annals of Statistics*, 13:1024–1040.

Scott, D. W. (1992). *Multivariate density estimation.* New York: John Wiley and Sons.

Smith, J. A. (1989). Regional Flood Frequency Analysis Using Extreme Order Statistics of the Annual Peak Record. *Water Resour. Res.*, 25:313–317.

Stedinger, J. R. (1983). Estimating a regional flood frequency distribution. *Water Resour. Res.*, 19(2):503–510.

Stedinger, J. R. and Lu, L. H. (1995). Appraisal of Regional and Index Flood Quantile Estimators. *Stochastic Hydrology and Hydraulics*, 9(1):49–75.

Tanner, M. and Wong, W. H. (1987). The calculation of posterior distributions by data augmentation. *J. Amer. Statist. Assoc.*, 82:528–550.

von Neumann, J. (1951). Various techniques used in connection with random digits. *J. Resources of the National Bureau of Standards - Applied Mathematics Series*, 12:36–38.

Walter, K. (2000). Index to hydrological recording sites in New Zealand. Technical Report 73, NIWA, Wellington, N.Z.

# Appendix A

# The Moment-Generating Function of the Product of Two Correlated Normally Distributed Variables

Assume $X_1 \sim N(\mu_1, \sigma_1^2)$, $X_2 \sim N(\mu_2, \sigma_2^2)$ and that $X_1$ and $X_2$ have correlation $\rho$. If we define $X_1 = X_0 + Z_1$ and $X_2 = X_0 + Z_2$, where

$$\begin{bmatrix} X_0 \\ Z_1 \\ Z_2 \end{bmatrix} \sim N\left( \begin{bmatrix} 0 \\ \mu_1 \\ \mu_2 \end{bmatrix}, \begin{bmatrix} \rho\sigma_1\sigma_2 & 0 & 0 \\ 0 & \sigma_1^2 - \rho\sigma_1\sigma_2 & 0 \\ 0 & 0 & \sigma_2^2 - \rho\sigma_1\sigma_2 \end{bmatrix} \right).$$

We have decomposed $X_1$ and $X_2$ into independent summands of which one is shared between them.

To find the moment-generating function of $Y = X_1X_2 = (X_0 + Z_1)(X_0 + Z_2)$, we know that

$$\begin{aligned} M_Y(t) &= \int_{-\infty}^{\infty} e^{ty} f(y) dy \\ &= \int_{-\infty}^{\infty}\int_{-\infty}^{\infty}\int_{-\infty}^{\infty} e^{t(x_0+z_1)(x_0+z_2)} f(x_0, z_1, z_2) dx_0 dz_1 dz_2 \\ &= \frac{1}{\sqrt{2\pi\rho\sigma_1\sigma_2}} \frac{1}{\sqrt{2\pi\left(\sigma_1^2 - \rho\sigma_1\sigma_2\right)}} \frac{1}{\sqrt{2\pi\left(\sigma_2^2 - \rho\sigma_1\sigma_2\right)}} \\ &\quad \int_{-\infty}^{\infty}\int_{-\infty}^{\infty}\int_{-\infty}^{\infty} e^{t(x_0+z_1)(x_0+z_2) - \frac{1}{2}\frac{(x_0-0)^2}{\rho\sigma_1\sigma_2} - \frac{1}{2}\frac{(z_1-\mu_1)^2}{\sigma_1^2-\rho\sigma_1\sigma_2} - \frac{1}{2}\frac{(z_2-\mu_2)^2}{\sigma_2^2-\rho\sigma_1\sigma_2}} dx_0 dz_1 dz_2 \end{aligned} \quad \text{(A.1)}$$

To undertake the triple integration in Equation A.1, we will need to reorganise the exponent of the exponential term. Let

$$q_1 = t\left(x_0 + z_1\right)\left(x_0 + z_2\right) - \frac{1}{2}\left(\frac{\left(x_0 - 0\right)^2}{\rho\sigma_1\sigma_2} - \frac{\left(z_1 - \mu_1\right)^2}{\sigma_1^2 - \rho\sigma_1\sigma_2} - \frac{\left(z_2 - \mu_2\right)^2}{\sigma_2^2 - \rho\sigma_1\sigma_2}\right). \quad \text{(A.2)}$$

If we define

$$q_2 = -\frac{1}{2}\left(\frac{x_0 - c_1\left(z_1 + z_2\right) - c_2}{c_3}\right)^2 - \frac{1}{2}\left(\frac{z_1 - c_4 z_2 - c_5}{c_6}\right)^2 - \frac{1}{2}\left(\frac{z_2 - c_7}{c_8}\right)^2 + c_9, \quad \text{(A.3)}$$

we can rewrite $q_1$ in the form of $q_2$ by equating terms $c_1$ to $c_9$ with some part of $q_1$. The moment-generating function of $Y$ can then be written in the form

$$M_Y(t) = \frac{1}{\sqrt{\rho\sigma_1\sigma_2}}\frac{1}{\sqrt{\sigma_1^2 - \rho\sigma_1\sigma_2}}\frac{1}{\sqrt{\sigma_2^2 - \rho\sigma_1\sigma_2}} c_3 c_6 c_8 e^{c_9}. \quad \text{(A.4)}$$

By rewriting $q_1$ and $q_2$ as

$$\begin{aligned} q_1 &= x_0^2\left(t - \frac{1}{2\rho\sigma_1\sigma_2}\right) + x_0\left(z_1 + z_2\right)(t) + x_0(0) + z_1^2\left(-\frac{1}{2(\sigma_1^2 - \rho\sigma_1\sigma_2)}\right) \\ &\quad + z_1\left(\frac{\mu_1}{\sigma_1^2 - \rho\sigma_1\sigma_2}\right) + z_2^2\left(-\frac{1}{2(\sigma_2^2 - \rho\sigma_1\sigma_2)}\right) + z_2\left(\frac{\mu_2}{\sigma_2^2 - \rho\sigma_1\sigma_2}\right) + z_1 z_2(t) \\ &\quad + \left(-\frac{\mu_1^2}{2(\sigma_1^2 - \rho\sigma_1\sigma_2)} - \frac{\mu_2^2}{2(\sigma_2^2 - \rho\sigma_1\sigma_2)}\right) \end{aligned} \quad \text{(A.5)}$$

and

$$\begin{aligned} q_2 &= x_0^2\left(-\frac{1}{2c_3^2}\right) + x_0\left(z_1 + z_2\right)\left(\frac{c_1}{c_3^2}\right) + x_0\left(\frac{c_2}{c_3^2}\right) + z_1^2\left(-\frac{c_1^2}{2c_3^2} - \frac{1}{2c_6^2}\right) \\ &\quad + z_1\left(-\frac{c_1 c_2}{c_3^2} + \frac{c_5}{c_6^2}\right) + z_2^2\left(-\frac{c_1}{2c_3^2} - \frac{c_4}{2c_6^2} - \frac{1}{2c_8^2}\right) + z_2\left(-\frac{c_1 c_2}{c_3^2} - \frac{c_4 c_5}{c_6^2} + \frac{c_7}{c_8^2}\right) \\ &\quad + z_1 z_2\left(-\frac{c_1^2}{c_3^2} + \frac{c_4}{c_6^2}\right) + \left(-\frac{c_2^2}{2c_3^2} - \frac{c_5^2}{2c_6^2} - \frac{c_7^2}{2c_8^2} + c_9\right), \end{aligned} \quad \text{(A.6)}$$

and then solving on Maple, we get the results:

$$\begin{aligned} c_1 &= \frac{t\rho}{1 - 2t\rho\sigma_1\sigma_2}, \\ c_2 &= 0, \\ c_3 &= \sqrt{\frac{\rho}{1 - 2t\rho\sigma_1\sigma_2}}, \\ c_4 &= \frac{t\sigma_1(t\rho\sigma_1\sigma_2 - 1)(\sigma_1 - \rho\sigma_2)}{t^2\rho\sigma_1^3\sigma_2 - (t\rho\sigma_1\sigma_2 - 1)^2}, \\ c_5 &= \frac{\mu_1(2t\rho\sigma_1\sigma_2 - 1)}{t^2\rho\sigma_1^3\sigma_2 - (t\rho\sigma_1\sigma_2 - 1)^2}, \end{aligned}$$

$$
\begin{aligned}
c_6 &= \sqrt{\frac{2t\rho\sigma_1^2\sigma_2\left(\sigma_1-\rho\sigma_2^2\right)-\sigma_1\left(\sigma_1+\rho\sigma_2\right)}{t^2\rho\sigma_1^3\sigma_2-\left(t\rho\sigma_1\sigma_2-1\right)^2}},\\
c_7 &= \frac{t\rho\sigma_1\sigma_2\left(t\rho\sigma_1\sigma_2\left(\mu_1+\mu_2\right)-t\left(\mu_1\sigma_2^2+\mu_2\sigma_1^2\right)-\mu_1-2\mu_2\right)+t\mu_1\sigma_2^2+\mu_2}{\left(t\rho\sigma_1\sigma_2-1\right)^2-t^2\sigma_1^2\sigma_2^2},\\
c_8 &= \sqrt{\frac{t^2\rho^2\sigma_1^2\sigma_2^2\left(\sigma_1^2-\rho\sigma_1\sigma_2+\sigma_2^2\right)+t\rho\sigma_1\sigma_2^2\left(2\rho\sigma_1-t\sigma_1^2\sigma_2-2\sigma_2\right)+\sigma_2\left(\sigma_2-\rho\sigma_1\right)}{\left(t\rho\sigma_1\sigma_2-1\right)^2-t^2\sigma_1^2\sigma_2^2}},\\
c_9 &= \frac{t^2\left(\mu_1^2\sigma_2^2+\mu_2^2\sigma_1^2-2\mu_1\mu_2\sigma_1\sigma_2\rho\right)+2t\mu_1\mu_2}{2\left(\left(t\rho\sigma_1\sigma_2-1\right)^2-t^2\sigma_1^2\sigma_2^2\right)}.
\end{aligned}
$$

Also

$$
c_3c_6c_8=\sqrt{\frac{\rho\sigma_1\sigma_2\left(\sigma_1^2-\rho\sigma_1\sigma_2\right)\left(\sigma_2^2-\rho\sigma_1\sigma_2\right)}{\left(t\rho\sigma_1\sigma_2-1\right)^2-t^2\sigma_1^2\sigma_2^2}}. \tag{A.7}
$$

To find the moment-generating function of $Y$, substitute $c_3$, $c_6$, $c_8$ and $c_9$ into Equation A.4,

$$
\begin{aligned}
M_Y(t) &= \frac{1}{\sqrt{\rho\sigma_1\sigma_2\left(\sigma_1^2-\rho\sigma_1\sigma_2\right)\left(\sigma_2^2-\rho\sigma_1\sigma_2\right)}}\sqrt{\frac{\rho\sigma_1\sigma_2(\sigma_1^2-\rho\sigma_1\sigma_2)(\sigma_2^2-\rho\sigma_1\sigma_2)}{\left(t\rho\sigma_1\sigma_2-1\right)^2-t^2\sigma_1^2\sigma_2^2}}\\
&\qquad e^{\frac{t^2\left(\mu_1^2\sigma_2^2+\mu_2^2\sigma_1^2-2\mu_1\mu_2\sigma_1\sigma_2\rho\right)+2t\mu_1\mu_2}{2\left(\left(t\rho\sigma_1\sigma_2-1\right)^2-t^2\sigma_1^2\sigma_2^2\right)}}\\
&= \left(\sqrt{\left(t\rho\sigma_1\sigma_2-1\right)^2-t^2\sigma_1^2\sigma_2^2}\right)^{-1} e^{\frac{\mu_1\mu_2t+\frac{1}{2}\left(\mu_1^2\sigma_2^2+\mu_2^2\sigma_1^2-2\rho\mu_1\mu_2\sigma_1\sigma_2\right)t^2}{(1-t\rho\sigma_1\sigma_2)^2-\sigma_1^2\sigma_2^2t^2}}.
\end{aligned} \tag{A.8}
$$

## A.1 Moments

The moment-generating function can be used to find moments about the origin of $Y$. By differentiating $M_Y(t)$ and evaluating at $t=0$ we can find as many moments as required. These moments can be used to calculate the mean, variance and skewness of the product of two correlated Normal variables. Using Maple we find that

$$
\begin{aligned}
M_Y(0) &= 1,\\
M_Y'(0) &= \mu_1\mu_2+\rho\sigma_1\sigma_2,\\
M_Y''(0) &= \left(\mu_1^2+\sigma_1^2\right)\left(\mu_2^2+\sigma_2^2\right)+4\mu_1\mu_2\rho\sigma_1\sigma_2+2\rho^2\sigma_1^2\sigma_2^2,\\
M_Y'''(0) &= \left(\mu_1^3+3\mu_1\sigma_1^2\right)\left(\mu_2^3+3\mu_2\sigma_2^2\right)+9\rho\sigma_1\sigma_2\left(\mu_1^2+\sigma_1^2\right)\left(\mu_2^2+\sigma_2^2\right)\\
&\qquad +6\rho^2\sigma_1^2\sigma_2^2\left(\rho\sigma_1\sigma_2+3\mu_1\mu_2\right).
\end{aligned}
$$

Thus

$$
E(Y) = \mu_1\mu_2+\rho, \tag{A.9}
$$

$$V(Y) = \mu_1^2\sigma_2^2 + \mu_2^2\sigma_1^2 + \sigma_1^2\sigma_2^2 + 2\mu_1\mu_2\rho\sigma_1\sigma_2 + \rho^2\sigma_1^2\sigma_2^2, \tag{A.10}$$

$$\alpha_3(Y) = \frac{6\sigma_1\sigma_2\left(\mu_1\mu_2\sigma_1\sigma_2\left(\rho^2+1\right) + \rho\left(\mu_1^2\sigma_2^2 + \mu_2^2\sigma_1^2\right)\right) + 2\rho\sigma_1^3\sigma_2^3\left(3+\rho^2\right)}{\left(\mu_1^2\sigma_2^2 + \mu_2^2\sigma_1^2 + \sigma_1^2\sigma_2^2\left(1+\rho^2\right) + 2\rho\mu_1\mu_2\sigma_1\sigma_2\right)^{3/2}} \tag{A.11}$$